ASSESSMENT OF ATMOSPHERIC PRESSURE LOADING ON THE INTERNATIONAL GNSS REPRO1 SOLUTIONS PERIODIC SIGNATURES

JAMES DANIEL MTAMAKAYA

October 2012

ASSESSMENT OF ATMOSPHERIC PRESSURE LOADING ON THE INTERNATIONAL GNSS REPRO1 SOLUTIONS PERIODIC SIGNATURES

James Daniel Mtamakaya

Department of Geodesy and Geomatics Engineering
University of New Brunswick
P.O. Box 4400
Fredericton, N.B.
Canada
E3B 5A3

October, 2012

PREFACE

This technical report is a reproduction of a dissertation submitted in partial fulfillment of the requirements for the Doctor of Philosophy in the Department of Geodesy and Geomatics Engineering, October, 2012. The research was supervised by Dr. Marcelo Santos, and support was provided by the Government of the United Republic of Tanzania.

As with any copyrighted material, permission to reprint or quote extensively from this report must be received from the author. The citation to this work should appear as follows:

ABSTRACT

Unambiguous, consistent and homogeneous GPS station coordinates are the fundamental requirement in the appropriate determination of geodetic velocities that are often used to derive geodetic and geophysical models for different applications. As for that, there have been significant efforts in the past decade to improve the modeling and parameterization of GPS solutions. Recently, the International GNSS Service (IGNSS) has generated REPRO1 solutions by reprocessing the historical GPS data from 1994 to March, 2010. REPRO1 solutions adopted the new absolute antenna phase center variations models along with most of the recent model parameters available by then and they are the first solutions to be consistently represented in one reference frame, IGS05.

Based on the availability of REPRO1 solutions, this research has two objectives. The primary objective is to identify the remaining periodic signatures in the International GNSS REPRO1 solutions. These signatures are the impacts of short and long term mismodeled and unmodeled effects from both known and unknown phenomena. As a parallel activity, this research will try to explain the signatures by correlating them with different effects that have either not been modeled or modeled differently with a specific attention to the atmospheric pressure loading (APL). The secondary objective of this study is to perform the harmonic analysis investigation of weekly time series in position and residual domain of REPRO1 solution using Least Squares Spectral Analysis (LSSA) and Least Squares Coherent Analysis (LSCA) with and without APL corrections. Based on the resulting least squares spectra, the impact (benefits) of APL corrections in the present solutions have been assessed as a basis of formulating recommendations in future similar reprocessing campaigns. In order to

accomplish the research objectives, a set of twenty nine (29) stations (part of the present IGNSS network) were selected in a manner which would portray the global overview. Thereafter, the selected stations analyzed using Least Squares Spectral Analysis (LSSA) and Least Squares Coherent Analysis (LSCA) frequency domain multiplications with and without the impact of APL from GGFC model. The investigations were carried out at both REPRO1 positions and residuals domains.

Based on the LS spectra results, it is evident that periodic signatures are still present in the REPRO1 solutions for most of the stations under study and they appear as spectral peaks. Furthermore, the observed signatures appear to be consistent around the first to fourth draconitic harmonics with respective periods of 351.2, 175.6, 117.1 and 87.8 days, within a range of ± 14 days (±0.04 CPY). It was also observed that, there is a slight improvement to spectral peaks that may result into slight improvement of coordinate repeatability if APL were included in the processing. However, the pattern was neither clear nor consistent at different harmonic levels of the same station as well as from one station to another. Furthermore, it was also observed that, the APL does not cause any significant reduction in spectral peaks that are still present in the REPRO1 solutions. This suggest that most of the remaining signatures could be attributed to other un-modeled displacements such as non tidal loading displacement, high order ionosphere terms and mismodeling effect in GPS attitude models. To ascertain the findings, independent solutions for YELL and NRC1 were generated (1995-2010) using Bernese v5.0 software in a baseline mode, in conjunction with latest IERS models. The computed solutions were verified to be compatible with present solutions within a range of ±2.5 cm. Thereafter the computed solutions were analyzed with and without the impact of APL using LSSA and LSCA as a basis of recommendations and future work.

PREFACE

This technical report is a reproduction of a dissertation submitted in partial fulfillment of the requirements for the Doctor of Philosophy in Geomatics Engineering in the Department of Geodesy and Geomatics Engineering at the University of New Brunswick Canada, October, 2012. The research was supervised by Dr. Marcelo Santos, and support was provided by the Government of the United Republic of Tanzania.

As with any copyrighted material, permission to reprint or quote extensively from this report must be received from the author. The citation to this work should appear as follows:

Mtamakaya, J(2012). *Assessment of Atmospheric Pressure Loading on the International GNSS REPRO1 Solutions Periodic Signatures.* Ph.D. dissertation, Department of Geodesy and Geomatics Engineering, Technical Report No. 282, University of New Brunswick, Fredericton, New Brunswick, Canada, 208 pp.

ACKNOWLEDGMENTS

I wish to express my sincere gratitude to the Government of Tanzania through the Ministry of Lands and Human Settlement Developments and the Department of Land Surveys and Mapping for offering me a scholarship to undertake my PhD studies in Geomatics Engineering at the University of New Brunswick, Fredericton, Canada.

I would also like to give my heartfelt thanks and sincere appreciations to my supervisor, Prof. Marcelo Santos for his fatherly guidance, generosity, persevering support and tremendous opportunities he offered me. His patience as well as tireless and meticulous efforts in reviewing my manuscripts is gratefully appreciated. He is truly the quintessential supervisor and I was very fortunate to have him as my mentor.

I also thank the members of my Examination Board (Dr. John Neville, Dr. James Watmough, Dr. Peter Dare, Dr. Yevgen Biletskiy and Dr. John Henton). Their constructive comments and recommendations, together with those from the members of my Advisory committee (Dr. Richard Langley and Dr. D. Kim), are greatly appreciated.

My special thanks go to the head of Geodesy and Geomatics Engineering Professor Sue Nichols. Her encouragement and support at times of difficulties were very valuable and inspired me to feel UNB-Fredericton as my second home away from home.

Lastly but certainly not the least, I would like to express my deep heartfelt thanks to my wife Josephine and my children Mike, Agnes, Fredrick and Geoffrey. I really admire their sincere love, calmness and strong encouragement during the difficult time of my long stay away from them when I was doing this research. It simply would not have been possible without their sacrifice and unfailing support and understanding for so many years. I owe them a huge debt of gratitude and I dedicate this thesis to them.

TABLE OF CONTENTS

List of Tables

List of Figures

LIST OF ACRONYMS

AAC   Associate Analysis Center.

AC   Analysis Center.

AIUB   Astronomical Institute of the University of Berne, Switzerland.

CDDIS   Crustal Dynamics Data Information System, USA.

CEO   Celestial Ephemeris Origin.

CIP   Celestial Intermediate Pole.

CODE   Center for Orbit Determination in Europe, Astronomical Institute,

University of Berne, Switzerland.

CRS   Celestial Reference System.

ECMWF   European Centre for Medium-Range Weather Forecasts.

EMR   Energy, Mines, and Resources; now Natural Resources Canada (NRCan).

EOP   Earth orientation parameter.

ERP   Earth rotation parameters.

ESA   European Space Agency.

ESOC   European Space Operations Centre of ESA, Darmstadt, Germany.

GCRS   Geocentric Celestial Reference System.

GFZ   GeoForschungsZentrum/Potsdam, Germany.

GGFC   Global Geophysical Fluid Center.

GMF   Global Mapping Function.

GNAAC   Global Network Associate Analysis Center.

GNSS	Global Navigation Satellite System
GPT	Global Pressure and Temperature model.
GSD	Geodetic Survey Division, Canada.
GSFC	Goddard Space Flight Center, USA.
IAAC	Ionosphere Associate Analysis Centers.
IACC	Ionosphere Associate Combination Center.
ICRF	International Celestial Reference Frame.
IDS	International DORIS Service.
IERS	International Earth Rotation and Reference Systems Service.
IGG	Institute of Geodesy and Geophysics, Vienna University of Technology, Austria.
IGN	Institut Géographique National, France.
IGP	IGS predicted (orbit).
IGR	IGS rapid (orbit).
IGNSS	International Global Navigational Satellite Service, formerly the International GPS Service (IGS).
ILRS	The International Laser Ranging Service.
ITRF	International Terrestrial Reference Frame.
ITRS	International Terrestrial Reference System.
IVS	International VLBI Service for Geodesy and Astrometry.
JPL	Jet Propulsion Laboratory, Pasadena, California, U.S.A.
LOD	Length of day.

MIT	Massachusetts Institute of Technology, USA.
NCEP	National Centers for Environmental Prediction
NEQ	Normal equation.
NGS	National Geodetic Survey, USA.
NRCan	Natural Resources Canada.
NUVEL-NNR	Northwestern University velocity model, no net rotation.
PDR	GeoForschungsZentrum/Potsdam & Technical University of Dresden, Germany.
PM	Polar Motion.
RINEX	Receiver-Independent Exchange format.
RNAAC	Regional Network Associate Analysis Center.
SIO	Scripps Institution of Oceanography, USA.
SSC	Set of Station Coordinates.
TEC	Total electron content.
TEO	Terrestrial Ephemeris Origin.
TRS	Terrestrial Reference System.
ULR	University of La Rochelle, France.
UPC	Polytechnical University of Catalonia, Barcelona, Spain.
VMF1	Vienna Mapping Function1.
WRMS	Weighted root mean square.
ZTD	Zenith Topographic Delay.

1. INTRODUCTION

This chapter presents the introduction of the different research activities that have been accomplished and is organized in six different sections starting with the statement of the problem describing the basis of implementation of this research. A brief summary of past and most recent similar studies are covered in the second part. The research objectives describing the reason for this study as well the scope of this research are covered in section three. The contributions of this research are summarized in section four and the different tools and types of research data used have been presented in section five. The last part of this chapter presents the organization of the remaining chapters in this dissertation.

1.1 Statement of the Problem

The International GNSS Service (IGS) first reprocessing (REPRO1) solutions are IGS solutions obtained by reanalyzing the full history of GPS data collected by the IGS global network since January 1994 until March 2010. The IGS REPRO1 solutions have been available since April, 2010 [Gent and Ferland, 2010]. They were generated based on the most current set of standards available at that time, most of them as prescribed in the 2003 Conventions [McCarthy and Petit, 2003] published by the International Earth Rotation and Reference Systems Service (IERS). This herculean

effort generated a set of IGS products, such as weekly station coordinates and residuals, in the IGS05 frame, which is closely aligned with the ITRF2005 frame [Claudius, 2009].

The first IGS reprocessing campaign had four major goals. The first and primary goal was to adopt the use of an absolute antenna phase center variation model (IGS05.atx), which was one of the most profound changes in the various IGS Analysis Centers (ACs) processing strategies since the start of the IGS in 1994. The second objective was to generate homogeneous and consistent long time series of combined REPRO1 solution with the full implementation of up-to-date models and standards, most as prescribed in the 2003 IERS Conventions [McCarthy and Petit, 2003]. The third objective was to provide input for the realization of the ITRF2008 and the fourth objective was to establish the basis of further future improvements. Based on Ray [2009], examples of future improvements includes the generation of new absolute satellite antenna calibrations, use of an updated geopotential model and improving the satellite attitude model. Other improvements include relativity corrections, new troposphere propagation model, higher-order ionosphere effects[1], modeling station displacements due to the diurnal (S_1) and semi-diurnal (S_2) atmosphere pressure tidal variations, thermal expansion of monuments and nearby bedrock. It also includes the use of new coefficients determining the position of the Earth rotation axis [Mtamakaya et al., 2011].

The REPRO1 solutions were generated based on a series of models, and it is conceived to be more consistent and homogenous than the ones used to generate past IGS solutions. However, there are still a few challenges that need to be addressed.

---

[1] Higher-Order Ionosphere effects were not applied by most of the IGS Analysis Centers during the REPRO1 generation process.

a)   Like other IGS solutions, REPRO1 solutions were generated based on a series of model parameters derived from past estimated parameters that remain constant in time. However, the GPS satellite constellation is constantly evolving as satellites are commissioned and decommissioned, or removed from the solution due to satellite eclipse or maneuver [King and Watson, 2010].

b)   There exist temporal changes in the observation geometry[2] due site specific obstructions, such as vegetation or man-made structures, which are changes with time and thus affect the least squares design matrices used to generate the GPS solutions. Consequently, the resulting systematic errors will also be affected and will likely produce temporal variations in the propagated signals.

c)   As pointed out above, there exist a number of known and unknown limitations in the present model parameters used to generate the REPRO1 solutions, such as exclusion of high order ionosphere terms in the adjustment procedures. Furthermore, a number of error sources, such as atmospheric loading, were not modeled because the International Earth Rotation and Reference Systems Service (IERS) is yet to recommend appropriate models. Please refer to discussions in section 3.2 for details.

d)   The final weekly REPRO1 solutions were generated based on weekly normal equations from the individual IGS Analysis Centers (ACs) using procedures that have

---

[2] Observation geometry is defined by the receiver location, satellite constellation and local obstructions.

been outlined in section 3.3. However, this approach is challenged by the existence of short discontinuities in the cumulative solutions of the IGS station(s) coordinates which are sometimes hardly detectable. Since they are not well documented in the station logs [Ferland and Piraszewski, 2009]. They could be wrongly interpreted as short term anomalies and vice versa. Furthermore, the present approach of scaling the covariance information from different Analysis Centers is still faced with limitations as it is based on unrealistic assumptions that the past ACs solutions are independent and error free.

Based on the above challenges and many others that have not been addressed, the REPRO1 solution is not perfect as a consequence of various sources of errors that are either mismodeled or unmodeled altogether. If such uncertainties are suitably large, then the ensuing systematic error will likely bias the REPRO1 solutions significantly. Because of that, they may also affect the resulting interpretation of geophysical signals such as tectonic velocity, glacial isostatic adjustment, vertical motion of tide gauges or seasonal geophysical loading signals. Furthermore, such errors would degrade the GPS contribution to the International Terrestrial Reference Frame [Altamimi et al., 2007]. Spectral studies on REPRO1 solutions will help the IGS community to learn and understand different things from their spectra. Our investigation uses the latest IERS error models [Petit and Luzum, 2010] and other models which were not implemented in REPRO1 solutions. From the residual domain we can learn about mismodeled or unmodeled errors. From the position domain we can learn more about actual station motions, such as the ones due to plate tectonics, and other existing features such as

variations at the first, second, third and fourth draconitic[3] harmonics with respective periods of 351.2, 175.6, 117.1 and 87.8 days.

Some of the mismodeled or unmodeled effects are periodic in nature and will appear as spectral peaks when positions and residuals are represented in frequency domain. However, the extent of their contributions in the present REPRO1 solutions can sometimes be hardly quantified as the effects are sometimes embedded in one another. For example, improvements in geopotential model parameters as recognized by IERS conventions 2010 [Petit and Luzum, 2010, pp. 69] suggests the use of the new values for the C_{21} and S_{21} coefficients to describe the position of the Earth's figure axis, which are different from the old values used in the generation of REPRO1 solutions [McCarthy and Petit, 2003, pp.57]. The use of new values will impact mostly the orbit estimations, but they may also affect the resulting estimated parameters such as the coordinate solutions and residuals, Earth rotational parameters, as well as zenith tropospheric path delay estimates, as they are adjusted together. The differences between the old and new C_{21} and S_{21} coefficients values are illustrated in Figures 1.1 and 1.2 respectively, in which the vertical axes are the variations in milliarcseconds and the horizontal axes presents time in days of the year. In both figures, the top panels are the respective variations of the C_{21} and S_{21} coefficients based on IERS 2010, which use the EGM2008 [Pavlis et al., 2008] as the conventional geopotential model. The bottom panels show the C_{21} and S_{21}

---

[3] Draconitic year is the interval of 1.040 ± 0.008 cycles per year (351.2 ± 2.8 days) needed for the Sun to return to the same point in space relative to the GPS orbital nodes (as viewed from the Earth).

variations based on IERS 2003 parameters, that use the EGM1996 [Lemoine et al., 1998] as the conventional geopotential model. The REPRO1 solutions adopted EGM 1996.
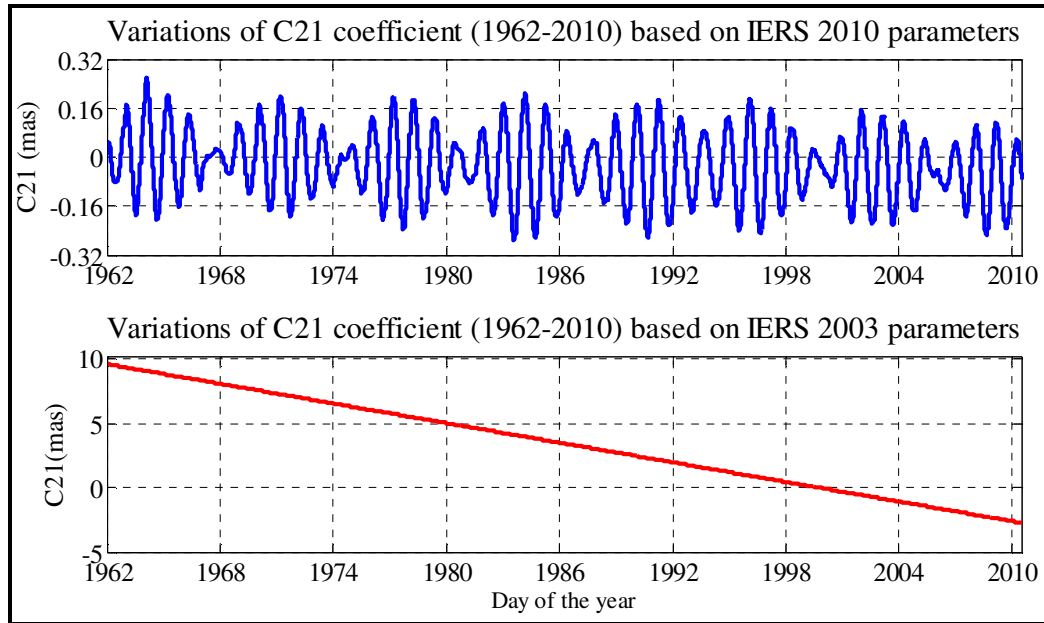
Figure 1.1 Variations of C_{21} coefficient describing the position of the Earth's figure axis.
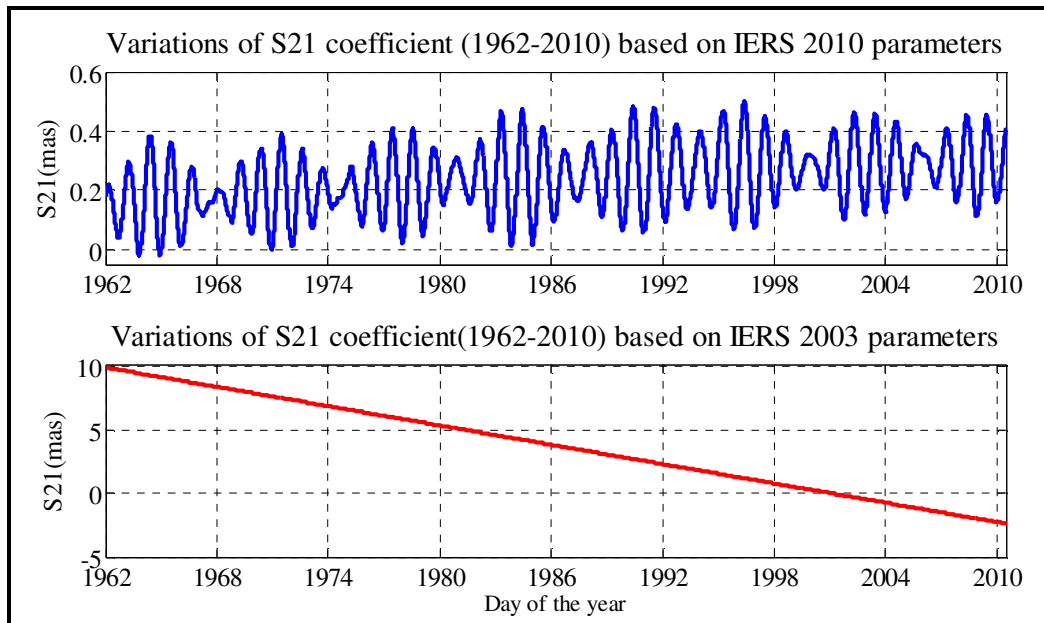
Figure 1.2 Variations of S_{21} coefficient describing the position of the Earth's figure axis.

A more clear cut assessment can be made on site-specific effects such as multipath, antenna imaging (changes in the antenna phase pattern induced by conducting material in the vicinity of the antenna) [Georgiadou and Kleusberg, 1988] and the atmospheric pressure loading (APL). In this research, we are assessing the impact of atmospheric pressure loading, which is one of the site-specific effects that have not been considered in the generation of REPRO1 solution. APL could be either accounted for at the observation level using corrections for the diurnal (S_1) and semi-diurnal (S_2) variations in the APL tides, or at the positional level using time-averaged corrections from a geophysical model to the weekly estimates of station coordinates. At the positional level we can also solve for regression factors between station displacements and the local pressure values. In this study, we are accounting for the APL at the position level using corrections from the Global Geophysical Fluids Center and assessing their impact using Least Squares Spectral Analysis (LSSA) and Least Squares Coherent Analysis (LSCA).

1.2 Overview on Power Spectra Studies on GPS solutions

Power spectra studies of GPS solution time series (mostly based on the assessment of the linear motions) have been underway for a considerable period since their availability. Such studies have identified seasonal signals (annual and semi-annual

signals as well as low and higher order harmonics) caused by apparent positional displacements. Most of the observed signals (some of which are insidious in nature) have been attributed to two primary mechanisms. The first mechanism is comprised of different limitations in the functional and stochastic models that are used to model the observed parameters. It follows that the partial mitigated geophysical phenomena such as unmodeled tidal signals (near semidiurnal and diurnal periods) in the geodetic observation processing could be propagated into longer-period signals [Penna and Stewart, 2003; Penna et al., 2007]. In a similar way King et al. [2008] showed that un-modeled (subdaily) solid earth tides and ocean tide loading displacements could as well substantially propagate into annual and semi-annual signals on the observed GPS coordinate series. Similarly, annual and semi-annual repeating signals have also been attributed to hydrological and atmospheric loading and could cause a significant bias in the annual estimated coordinate velocities if left unaccounted for [Van Dam et al., 2001; Blewitt and Lavallee, 2002]. A similar study by Dong et al. [2002] estimated that only 40 percent of the observed GPS seasonal power can be explained by redistributions of geophysical fluid mass loads. The second primary mechanism is based on all aspects related to un-modeled long-period signals, such as satellite antenna modeling errors that propagate differently as the satellite constellation changes. Examples of them are the signals due to mismodeling of GPS orbits, solar declination and elliptical waves [Collilieux et al., 2007] and the systematic errors related to the draconitic year [Agnew and Larson, 2007]. However, much of the residual variations are likely caused by still-to-be-identified GPS technique errors and analysis artifacts [King and Watson, 2010].

Since the availability of official coordinate time series consistently expressed in a single reference frame, such as ITRF2005, a few similar studies have been done. They include a spectral study by Collilieux et al. [2007] that has shown the existence of significant spectral power near frequencies of 1.00, 2.00, 3.12, and 4.16 cycles per year and attributed these to both motions of Earth's crust and systematic modeling errors. Spectral study by Ray et al. [2008] has revealed the existence of significant powers close to the frequency of the 1.04 ± 0.008 cycles per year (about 351.2 ± 2.8 days). This period is close to the time required for the satellite constellation to complete a full solar revolution in inertial space, an interval which is very close to the GPS year with a period of 351.4 days (about 1.039 cycles per year). This study attributed the position displacements to systematic errors related to modeling defects of the satellite orbits and aliasing of site-dependent positioning biases, such as the multipath effect as modulated by the varying satellite geometry as a result of sun-satellite interaction. A similar finding was made in a previous study by Hugentobler [2005]. A study by Fritsche et al. [2009] indicated the existence of annual and semi-annual displacements of the center of mass of the Earth and therefore the successive displacements of GPS positions. This study attributed the annual and semi-annual displacements to and mismodeled errors due to solar radiation pressure and higher order ionosphere correction terms that were ignored by most IGS Analysis Centers in the process of the generation of REPRO1 solutions.

1.3 Research Objectives

This research has two objectives.

a) The first and primary objective of this research is to identify the remaining spectral peaks in the first IGS reprocessed solutions (REPRO1) and try to explain them by correlating with known effects not modeled or modeled differently, with a specific attention to the atmospheric pressure loading (APL).

b) The second objective of this study is to perform a harmonic analysis investigation of weekly time series in position and residual domains of REPRO1 solutions using Least Squares Spectral Analysis (LSSA) and Least Squares Coherent Analysis (LSCA) with and without APL corrections. Based on the resulting Least Squares spectra, the impact of the atmospheric pressure loading based on the corrections from the Global Geophysical Fluids Center (GGFC) model in both positional and residual domains of the REPRO1 solutions will be quantified.

1.3.1 Scope of this research

To accomplish the research objectives, a sub-set of twenty seven (27) IGS stations, as shown in Figure 1.3, were selected based on geographical locations that would portray the global continental coverage. Furthermore, some of the stations were close by in order to establish any possible common trend that may possibly exist between them. The statistical information of the selected stations has been tabulated in Table1.1.
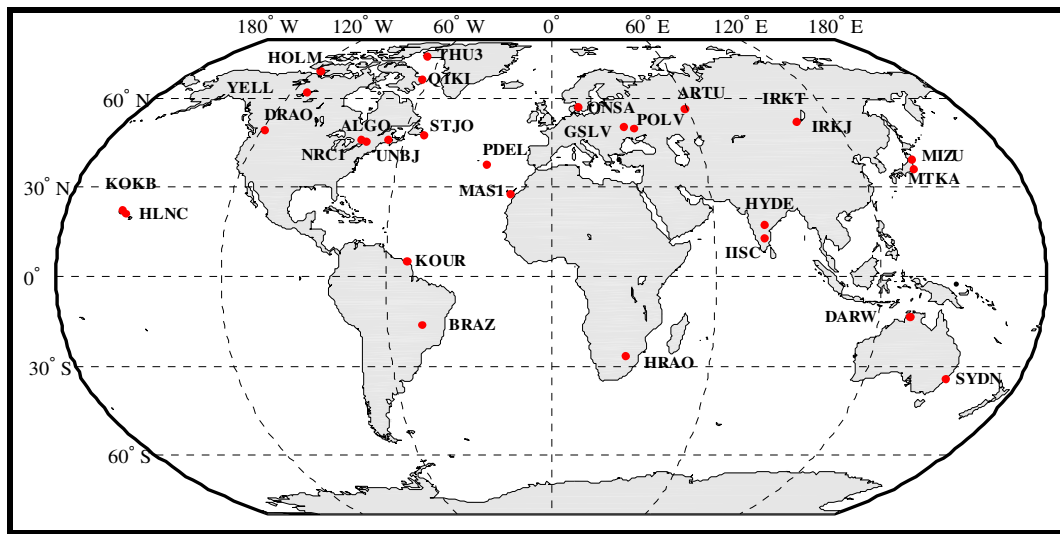
Figure 1.3 A subset of IGS stations used in the harmonic analysis study.

In Table1.1, the second column shows the station names, the third and fourth columns indicate the respective beginning and end dates of the reprocessed data. The fifth column gives the number of weekly solutions that have been generated by the IGS based on the available observational data. Columns six and seven give the respective information on the length of data span in days and years for each station under study. Based on Table 1.1, stations ALGO, DRAO, KOKB, KOUR, ONSA, STJO and YELL

have the longest time series (16 years); SYDN and QIKI have the shortest time series (5 years). Furthermore, the time series of REPRO1 positions and residuals for station DRAO have been illustrated in Figures 1.4 to 1.7.

Table 1.1 Statistical Data of the selected IGS Stations

No.	Station	Start date (dd/mm/yyyy)	End date (dd/mm/yyyy)	Number of weekly solutions	Data span	
					days	year
1	ALGO	05/01/1994	14/01/2010	824	5854	16.04
2	ARTU	06/08/1999	07/01/2010	517	3807	10.43
3	BRAZ	05/03/1995	13/01/2010	686	5429	14.87
4	DARW	22/10/1994	13/01/2010	629	5563	15.24
5	DRAO	06/01/1994	14/01/2010	833	5853	16.04
6	GSLV	27/02/1998	14/01/2010	616	4340	11.89
7	HLNC	19/06/1997	14/01/2010	631	4593	12.58
8	HOLM	30/08/2001	13/01/2010	432	3049	8.35
9	HRAO	27/09/1996	14/01/2010	608	4858	13.31
10	HYDE	31/10/2002	13/01/2010	372	2632	7.21
11	IISC	15/01/1995	13/01/2010	706	5496	15.06
12	IRKJ	12/06/2002	13/01/2010	367	2773	7.60
13	IRKT	22/09/1995	14/01/2010	729	5229	14.33
14	JAB1	08/08/1997	27/08/2008	406	4038	11.06
15	KOKB	06/01/1994	13/01/2010	813	5852	16.03
16	KOUR	06/01/1994	14/01/2010	786	5853	16.04
17	MAS1	05/06/1994	13/01/2010	790	5702	15.62
18	MIZU	21/03/2002	14/01/2010	382	2857	7.83
19	MTKA	06/01/1999	14/01/2010	557	4027	11.03
20	NRC1	11/06/1994	14/01/2010	764	5697	15.61
21	ONSA	06/01/1994	14/01/2010	836	5853	16.04
22	PDEL	20/04/2000	14/01/2010	495	3557	9.75
23	POLV	21/06/2001	14/01/2010	448	3130	8.58
24	QIKI	18/07/2004	14/01/2010	266	2007	5.50
25	STJO	07/01/1994	13/01/2010	830	5791	15.87
26	SYDN	24/11/2004	13/01/2010	269	1877	5.14
27	THU3	13/11/1998	14/01/2010	573	4081	11.18
28	UNBJ	21/07/2001	13/01/2010	328	3098	8.49
29	YELL	07/01/1994	13/01/2010	819	5851	16.03
NB: The weekly solutions have different length because of different operation start dates and observation breaks outs which can be verified from the site log files.						

Figure 1.4 below is the plot of the weekly reprocessed solutions in geodetic coordinate system for station DRAO for the period 1994-2010. Top panel is the plot of geodetic latitude in degrees, minutes and seconds (vertical axis). The middle panel is the plot of geodetic longitude in degrees, minutes and seconds (vertical axis). The bottom panel is the plot of geodetic heights whereby the vertical axis corresponds to height in meters. In all three panels the horizontal axis represents time in day of the year (DOY).
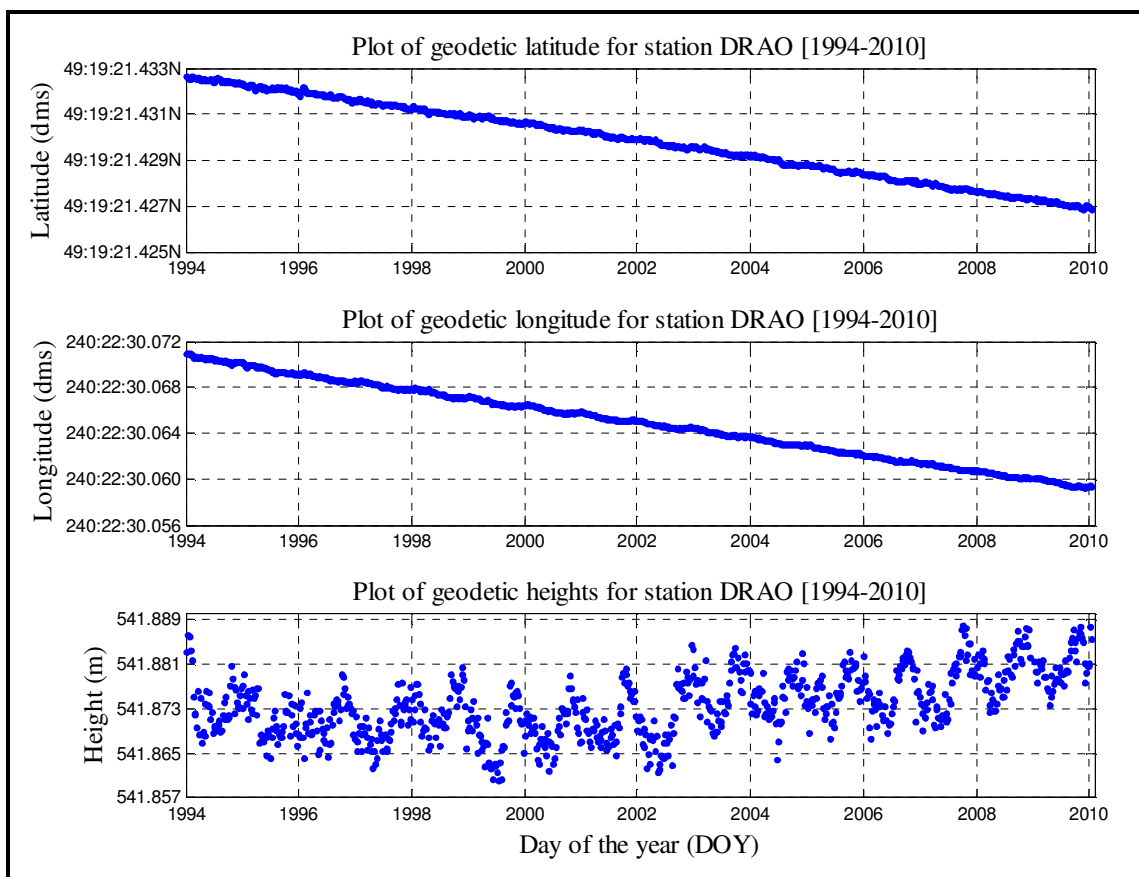
Figure 1.4 Plot of weekly IGS REPRO1 positions in geodetic coordinate system for station Penticton (DRAO) 1994-2010.

Figure 1.5 below is the plot of the weekly REPRO1 positions in Cartesian coordinate system for station Penticton (DRAO) for the period 1994-2010. The top panel is the plot of X coordinate in meters (vertical axis). The middle panel is the plot of Y coordinate in meters (vertical axis). The bottom panel is the plot of Z coordinates in meters (vertical axis). In all panels the horizontal axis represents time in day of the year (DOY).
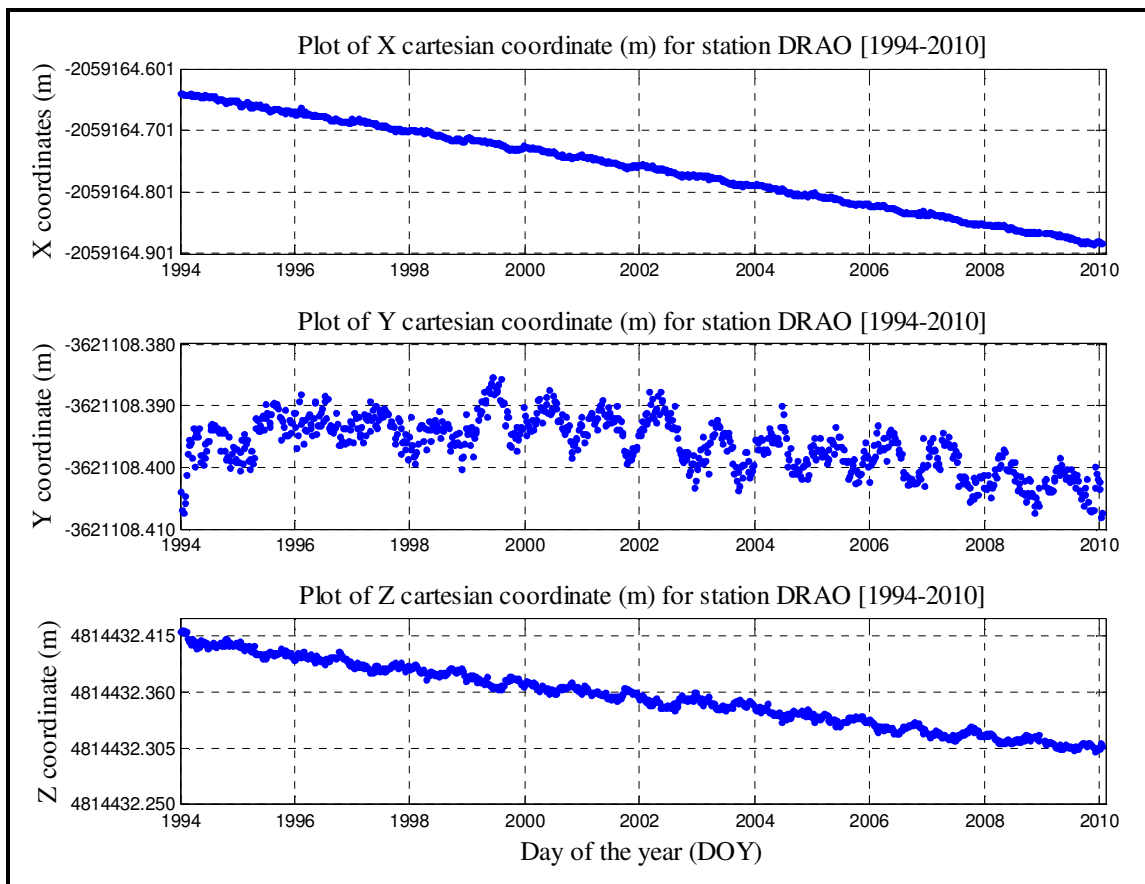
Figure 1.5 Plot of weekly reprocessed positions in Cartesian coordinate system for station Penticton (DRAO) for the period 1994-2010.

Figure 1.6 is the plot of the REPRO1 weekly residuals in geodetic coordinate system for station DRAO (1994-2010). The top panel is the plot of geodetic latitude residuals in milliarcseconds (vertical axis), the middle panel represents the geodetic longitude residuals in milliarcseconds (vertical axis) and the bottom panel is the plot of geodetic height residuals in millimeters (vertical axis). In all three panels the horizontal axis represents time in day of the year (DOY).
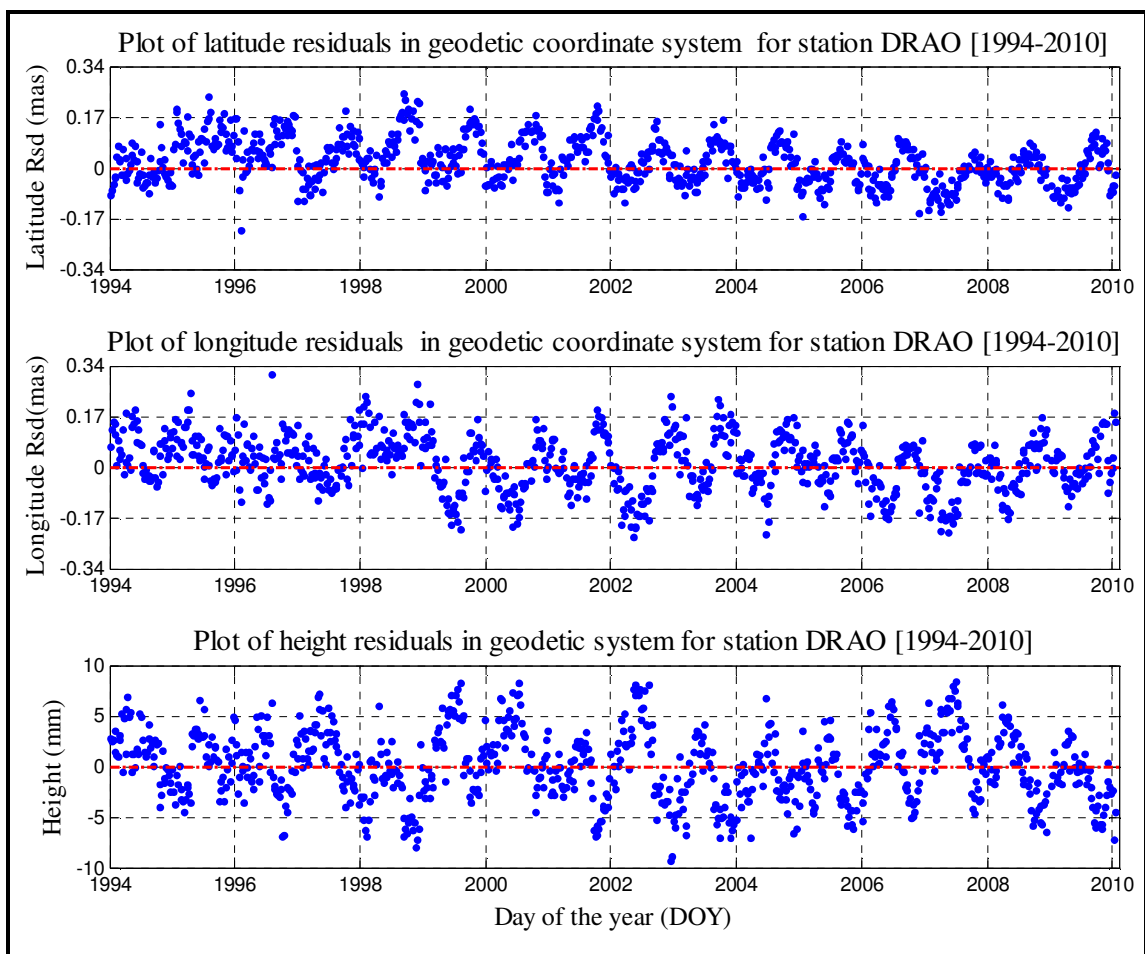
Figure 1.6 Plot of weekly REPRO1 residuals in geodetic coordinate system for station Penticton (DRAO) for the period of 1994-210.

Figure 1.7 below is the plot of the weekly residuals in Cartesian coordinate system for station DRAO for the period 1994-2010. The top panel is the plot of X residuals in millimeters (vertical axis). The middle panel is the plot of Y residuals in millimeters (vertical axis). The bottom panel is the plot of Z residuals in millimeters (vertical axis). In all three panels the horizontal axis corresponds to time in day of the year (DOY).
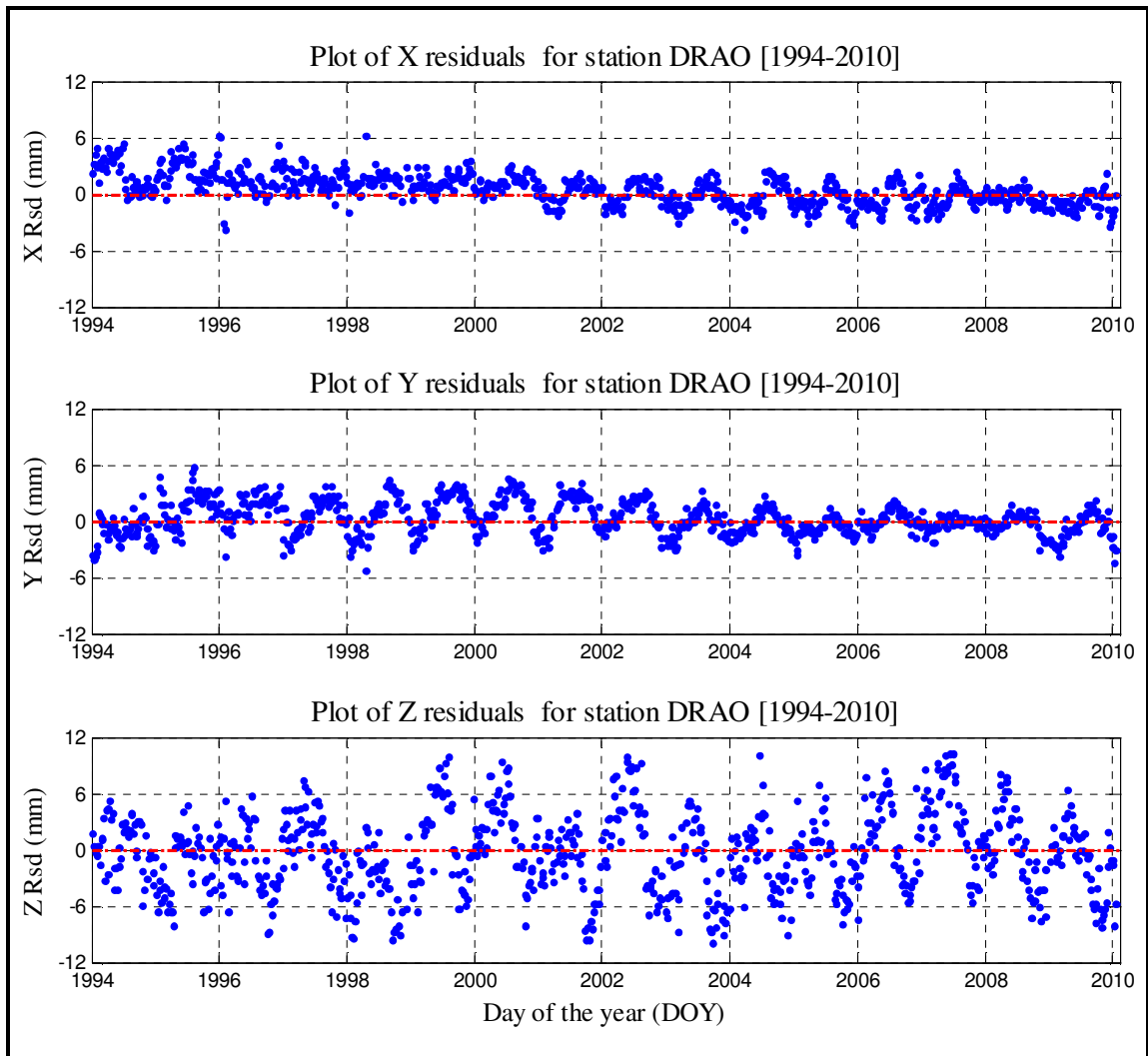
Figure 1.7 Plot of weekly reprocessed residuals in Cartesian coordinate system for station Penticton (DRAO) for the period of 1994-2010.

1.4 Research Contributions

The contributions (expected benefits) from this research include the assessment of the lack of APL in REPRO1 solutions, implementation of Least Squares Coherent Analysis (LSCA); provide a summary of REPRO1 processing options and providing the recommendations to the IGS community. The contributions are briefly explained in the following subsections.

1.4.1 Assessment of the lack of APL in REPRO1 solutions

APL displacement is one of the geophysical phenomena that have not been taken into account in the generation of REPRO1 solutions. This study will help to provide the IGS community with a clear cut assessment on the lack of APL in REPRO1 using a frequency domain multiplication process and establish whether there is a need of using them in future similar campaigns. As parallel activity, this research has been able to demonstrate that, with few exceptions the APL corrections from the presently available geophysical models based on National Centers for Environmental Prediction products have similar impacts at the position level at both six hours and weekly sampling rates.

1.4.2 Implementation of Least Squares Coherent Analysis (LSCA)

The present LSSA software has been designed to handle one dimensional data only. This research has been able to implement both LSSA and LSCA in the scope of multidimensional data analysis of long-term coordinate and residual series. The dual implementation has been done through code developments which allow LSSA spectra multiplication in the frequency domain. Thereafter the common peaks from two or more Least Squares spectra under consideration are extracted in a rigorous way. Multiplication of two or more spectra segments in the frequency domain is equivalent to convolution (filtering) in the time domain. Therefore the common spectral peaks are amplified while the non-common ones are attenuated. The codes will be made available and can as well be improved for more robust future analysis regarding geodetic applications.

1.4.3 Provide a summary of REPRO1 processing options

Like other IGS solutions, REPRO1 solutions were generated by combining weekly solutions from different IGS Analysis Centers as detailed in chapter three. Each of them used different software and different processing strategies and in some cases different model parameters were used for similar applications in contrast to the initial requirements of IERS. However, besides the Analysis Center processing summaries which are subject to regular updates based on the availability of new processing model,

there exists no official documentation regarding the processing details. This research has developed a comprehensive summary of all the processing models parameters and other options as implemented by all IGS Analysis Centers that were involved in the REPRO1 generation process. Such a summary is vital for independent research activities that would require mimicking similar procedures such as the one illustrated in section 4.4.

1.4.4 Recommendations to the IGS community

Based on research finding, a few recommendations will be formulated to the IGS community regarding the lack of atmospheric pressure loading displacements, as part of the artifacts still remaining in REPRO1 solutions. It is believed such recommendations will be vital as the IGS is looking forward for a second reprocessing campaign that will include a number of new models. Examples include the ITRF 2008, new antenna calibrations based on REPRO1 solutions, new geopotential model, and higher order ionosphere terms, and new model for albedo accelerations [Griffiths et al., 2009].

1.5 Research Tools and Data

Tools that have been used in this study are the Least Squares Spectral Analysis and Least Squares Coherent Analysis, Bernese v5.0 GPS software and Matlab software. Data used for this research has been obtained from IGS and Global Geophysical Fluids Center; and all of them are explained in the following subsections.

1.5.1 Least Squares Spectral Analysis (LSSA) software

LSSA is the main tool which has been used to identify periodic signatures in the reprocessed coordinates and residuals. LSSA is based on the developments by Vaníček [1969; 1971], Wells et al. [1985] and Pagiatakis [1999]. Recently it has been extended to Least-Squares (LS) self-coherency Analysis by Pagiatakis et al. [2007]. LSSA allows analysis of data time series with known and unknown apriori variance factors, and the data may be correlated or uncorrelated. LSSA can handle unevenly spaced time series without a pre-processing requirement, rigorous analysis of systematic noise without shifts in the spectral peaks. Chapter two provide a comprehensive overview of the LSSA.

1.5.2 Bernese v5.0 GPS software

The Bernese v5.0 Software [Dach et al., 2007], is a sophisticated tool capable of meeting quality specifications of geodetic applications using IGNSS measurements. It can also process data related to kinematic and dynamic precise orbit determination for low earth orbiters and satellite laser ranging measurements. It has been used to ascertain the research findings by reprocessing a few selected baselines using a processing strategy and clean datasets as close as possible to those used in the generation of REPRO1 solutions. It includes the implementation of IERS2003 conventions [McCarthy and Petit, 2003)], absolute antenna model and the IGS05 terrestrial frame.

1.5.3 Matlab software

Matlab has been widely used in this reasearch. A number of different codes and functions have been developed and used in three different ways starting with the preparation of inputs in LSSA and LS coherent analysis. It is worth mentioning that, IGS products that have been used in this research are provided in Cartesian and UTM formats whereas this research has been done using curvelinear coordinates. It was therefore necessary to make appropriate conversions. Likewise, it is worth reminding that, the current global atmospheric pressure loading corrections for most geodetic applications are based on geophysical models and they are provided at a six hours

interval. Concatenation into weekly values to input into the LSSA procedure was done using Matlab; for details and illustrations the reader is referred to chapter four. The second part of this research involved processing using the Bernese software which use seven different data types; these data sets are archived in compressed formats in two different ftp servers. They are daily precise orbits in IGS05 frame, daily IGS clock files, Earth rotation parameter files and daily observation files as archived by the CDDIS ftp server. Others are the differential code bias files, satellite information files and the daily atmospheric mapping files as archived by Center for Orbit Determination in Europe ftp server at the Astronomical Institute, University of Berne, Switzerland. A Matlab code with different functions was developed to perform file downloads, unzip and change them into Bernese format before adding them into appropriate Bernese subdirectories. The software has also been extensively used in the preparation of different types of research deliverables in graphical form for a better perception of the results.

1.5.4 Data from IGS and Global Geophysical Fluids Center(GGFC)

Soon after the release of the IGS REPRO1 solutions [Gendt and Ferland, 2010], data were obtained them from IGS via the then IGS Reference Frame Coordinator (RF) at Natural Resources Canada (NRCan). NRCan is one of the IGS Analysis Centers that participated in the generation of REPRO1 solutions. This research has adopted APL corrections from the Global Geophysical Fluids Center (GGFC) model.

1.6   Organization of this research

This dissertation is organized into five different chapters. Chapter one covers the general introduction including an overview of the basic concepts of REPRO1 solutions studies followed by a literature review on past and present similar spectral studies on GPS solutions. A discussion on the research objectives and the research contributions has also been included in this chapter. To conclude the chapter, discussions on different research data and software tools that have been adopted has also been made.

Chapter two of this thesis provides an overview of the two analysis tools used in this research: Least Squares Spectral Analysis (LSSA) and Least-Squares (LS) self-Coherency for harmonic analysis and the Bernese 5.0 GPS software for data processing. The LSSA overview includes a brief summary of the software applications, the test of statistically significant spectral peaks and multivariate data analysis by LS self-coherency analysis. The later is based on the product of the Least-Squares spectra segments of the analyzed data series to establish a new confidence level for detecting significant peaks rigorously. The overview on Bernese summarizes the recommended software updates on the present UNB software version (12-Feb-2005 release) so as to allow the Bernese Processing Engine (BPE) match with the processing requirements and the input data in the context of IGS05, which is the terrestrial frame used to generate IGS REPRO1 solutions. To conclude the chapter, the adopted processing summary along with different models that have been used in the processing has been discussed.

Chapter three of this dissertation gives a review on the generation of IGS first reprocessed (REPRO1) solutions and the role of antenna phase centre corrections. The chapter provides an insight into the different IGS products with their accuracies and latencies followed by the discussions of different activities associated with the process of REPRO1 generation. Examples are the different types of measurement models used, different types of force modes used in the solution of the satellite equations of motion, and the transformation between the celestial and the terrestrial reference frames. A summary of the strategy used by IERS to combine the REPRO1 daily terrestrial reference frame parameters into official weekly parameters has been discussed. The chapter concludes with an overview of the satellite and receiver antenna phase center offset and phase center variations, the summary of their role in the process of generation of REPRO1 solutions as well as the advantages of their adoption.

Chapter four of this dissertation presents the research results and is divided into three sections. The first section provides the results of Least Squares Spectral Analysis and Least Squares Coherent Analysis on positions and residual domain without APL corrections. The second part presents the results of the comparison of the APL correction from the geophysical models based on the NCEP data. Also presented in section two, are the LSSA and LS coherent Analysis on position and residuals with APL corrections from the Global Geophysical Fluids Center model. The section part of this chapter presents the results of Bernese processing for stations NRC1 and YELL.

Chapter five of this dissertation provides the assessment of the results followed by concluding remarks and other observations for a possible future work.

2. TOOLS FOR HARMONIC ANALYSIS AND DATA PROCESSING

This chapter presents an overview of the two analysis tools used in this research; they are Least Squares Spectral Analysis (LSSA) and least-squares (LS) self-coherency for harmonic analysis and Bernese 5.0 GPS software for data processing. The chapter is organized into two main sections. The first section provides an overview of LSSA which includes a brief summary of the software applications, the test of statistically significant spectral peaks and multivariate data analysis by LS self-coherency analysis. The later is based on the product of the least-squares spectra segments of the analyzed data series to establish a new confidence level for detecting significant peaks rigorously.

Section two provides an overview on Bernese v 5.0 GPS software in context of this research. The first part summarizes the recommended software upgrade procedures on the Bernese Processing Engine for efficient switch from relative to absolute PCVs. This is because the software has been improved fifteen times from its first release (24-May-2004) to the current version of 11-May-2011. The UNB software version (12-Feb-2005 release) had to be updated to the current version, which allows processing using antenna absolute phase center variations. The second part presents different models used and the processing summary. Some of processing features which are of much interest to this research are not available in the present Bernese 5.0 software[4]; efforts were made to request the use of the academic version for this research to no avail [Datch, 2011].

---

[4] Bernese software is currently being upgraded to enhance its processing capabilities and new features will also be available. Examples of them are the processing of the S1 and S2 atmospheric tidal loading and the FODITS option (find outliers and discontinuities in time series)

2.1 Harmonic Analysis

Harmonic analysis can be conceived as the mathematical approach of representing functions or signals as a superposition of basic waves. As a general principle, the study is accomplished through the decomposition of the main function (data series) from time domain into finite (possibly infinite) smaller periodic functions or periodic signals in the frequency domain. A variety of approaches with different capabilities are presently available such as Fast Fourier transformation (FFT), Frequency Analysis Mapping On Unusual Sampling (FAMOUS) and least squares spectral analysis (LSSA[5]). However, all of them use a set of base functions made up of sine and cosine functions in the decomposition process to generate a frequency spectrum.

Harmonic analysis studies based on the frequency spectrum have proven to be useful in diverse fields such as geodesy, astronomy, signal and image processing and optics. Different things can be learnt from the analyses or from the diverse fields depending on the nature of the analyzed data series. This research is based on the IGS REPRO1 position and residual series which are analyzed using the present available LSSA software version 5.02, in order to study the harmonic nature of the periodic signals that may be still existing in them. A summary of the software overview along with its capacities are summarized in the following sections.

---

[5] LSSA software was developed in the Department of Geodesy and Geomatics Engineering at the University of New Brunswick

2.1.1 Overview of the least squares spectral analysis (LSSA)

Least squares spectral analysis (LSSA) is the main tool which has been used to analyze and identify periodic signatures in the reprocessed coordinates and residuals with and without the impact of atmospheric loading (APL) displacements. LSSA is based on the developments by Vaníček [1969; 1971], Wells et al. [1985] and Pagiatakis [1999; 2007]. It was developed as an alternative to bypass the limitations and stringent requirements present in the classical Fourier methods. These limitations include the need for long records, constant sampling rate, equally weighted data values, no presence of gaps or datum shifts all of which render the experimental series strongly non stationary. In contrast to the classical Fourier analysis, LSSA can analyze data time series with known and unknown apriori variance factors, and the data may be correlated or uncorrelated. LSSA can analyze short data series and unevenly spaced time series without prior windowing of the data or a pre-processing requirement such as de-gapping, de-trending and de-spiking. LSSA allows rigorous analysis of systematic noise without shifts in the spectral peaks as well as testing their statistical significance.

Consider a time series $f(t)$ in a Hilbert space[6] [Pagiatakis, 1999] observed at discrete intervals $t_i, i = 1, 2, 3..., m$ not necessarily equally spaced, with a fully populated covariance matrix C_f. The first primary objective of LSSA is to detect

---

[6] A Hilbert space is an abstract vector space possessing the structure of an inner product (real or complex) that allows length and angle to be measured. Hilbert spaces are required to be complete, a property that provides enough limits in the space to allow the techniques of calculus to be used.

periodic signals in the input data series $f(t)$, especially when it contains both, random and systematic noise. The objective is achieved by using the projection theorem[7] to model the input series by its orthogonal function $g = \Phi x$ onto a plane in the Hilbert space whereas $x^T = [x_s \,|\, x_n]^T$ is a vector of unknown parameters comprised of signal s and noise n. The projection as illustrated in Figure 2.1, use a Vendermonde matrix $\Phi = [\Phi_s \,|\, \Phi_n]$, made of cosine and sine base functions at frequencies ω_i and coefficients $\hat{c}_{1i}, \hat{c}_{2i}$ estimated in a LSSA procedure. In Figure 2.1 f is a known vector to be approximated in LSSA procedure, not necessarily equal spaced observations, $S(\omega_i)$ is the collection of spectral values that can be properly modeled by its orthogonal projection $g = \Phi x$ and, $r = f - g$ are the residuals.
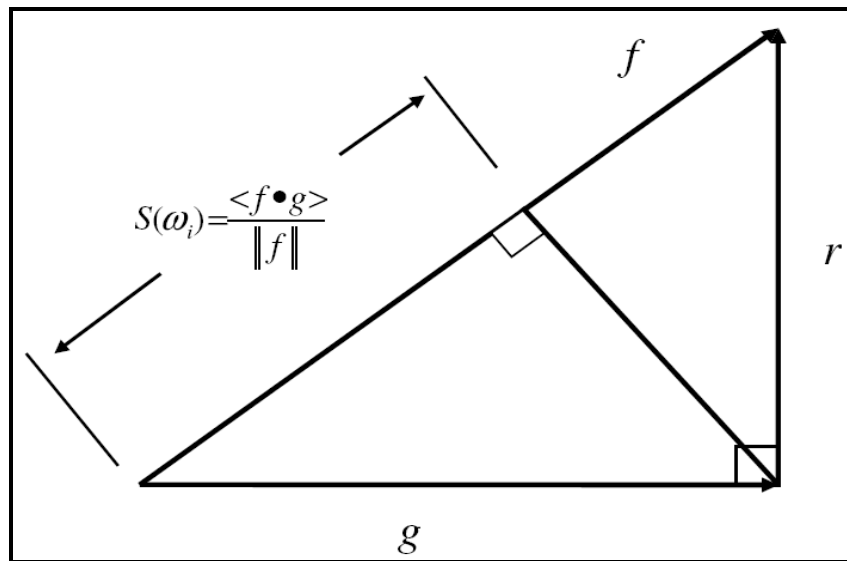
Figure 2.1 Orthogonal projection of the input data series, $f(t)$ onto $g = \Phi x$.

---

[7] The shortest distance between an element (vector) of Hilbert space and a (plane) manifold of Hilbert space is the perpendicular from the point to the plane. The theorem guarantees the uniqueness of the closest point and orthogonality of the residual. it also provides a formula for computation of both.

$$\hat{g}(\omega_i) = \hat{c}_{1i}\cos(\omega_i) + \hat{c}_{2i}\sin(\omega_i) \tag{2.1}$$

After some developments (not part of this discussion), the least squares spectral value[8]

$S(\omega_i)$ of the function $f(t)$ at a frequency ω_i is described in percentage as the ratio of

the norm of the orthogonal projection to the norm of the time series:

$$S(\omega_i) = \frac{f^T C_f^{-1}\hat{g}(\omega_i)}{f^T C_f^{-1} f}, \in (0,1). \tag{2.2}$$

The probability density function of LS spectrum follows the (standard) beta distribution[9]

defined by two parameters $\alpha = 1$ and $\beta = 0.5(m-u-2)$; where m is the number of data

points and u is the number of unknown parameters estimated by the LS procedure.

The second objective of LSSA is to establish the statistically significant spectral

peaks. To achieve this objective, the probability distribution function from Equation 2.2

is decomposed into two statistically independent components of signal and noise

regardless the nature of the covariance matrices (diagonal or fully populated) as follows:

$$S(\omega) = \left[1 + \frac{f^T C_f^{-1}(I-J)f}{f^T C_f^{-1} Jf}\right]^{-1} = \left[1 + \frac{Q_n}{Q_s}\right]^{-1}. \tag{2.3}$$

In Equation 2.3, I is identity matrix and J is an idempotent matrix[10] given as

follows:

---

[8] A collection of least squares spectral values for all frequencies, $S(\omega) = \{S(\omega_j); j = 1:nsv\}$ constitutes a least squares spectrum, where nsv is the number of spectral values in a band.

[9] A family of continuous population distributions defined on the interval [0, 1] parameterized by two positive shape parameters, denoted by α and β, that appear as exponents of the random variable and control the shape of the distribution.

[10] Idempotent matrix is a square matrix which, when multiplied by itself, yields itself.

$$J = \Phi \, (\Phi^T C_f^{-1} \Phi)^{-1} \Phi^T C_f^{-1} \tag{2.4}$$

Extraction of significant spectral peaks are then extracted rigorously using Fischer distribution, significance parameters α, degrees of freedom[11] υ, dimensionality of the problem d and the expansion factor EF as in Equation 2.5;

$$S(\omega_i) \geq \left[1 + \frac{\upsilon}{d} F_{(\upsilon,d,\alpha)} \right]^{-1} . \tag{2.5}$$

Expansion factors (EF)[12] for unknown and known a-priori variance are respectively computed using Fischer and Chi-Squared χ^2 distributions as per respective Equations 2.6 and 2.7;

$$EF^2 = d F_{(\upsilon,d,\alpha)} , \tag{2.6}$$

$$EF^2 = \xi_{\chi_\upsilon^2}, 1 - \alpha . \tag{2.7}$$

---

[11] Is the number of independent values of data being used in to make calculation; the more degrees of freedom, the more certain we can be that we have accurately sampled the entire population.

[12] More discussions about expansion factors can be found in Mikhail (1976).

2.1.2 The basics of working with least squares spectral analysis

The basic approach in working with LSSA is done in three steps and they are illustrated by means of Figure 2.2. The first step is the pre-processing (pre-analysis) of the data series under analysis so as to provide the general knowledge of the time series under investigation; this avoids aliasing in the spectral peaks. The pre-analysis steps (indicated in light blue) include the removal of linear trends, auto regression process, the impact of the random walk process and the filtering of the time series based on the processing requirements and data sampling rate. The second step in LSSA is the appropriate definition of the input characteristics of the data series under analysis. Examples of these include length[13], units, datum shifts, datum biases, presence of linear trends, presence of random walk and periodic signals to be enforced. Others are apriori variance factor, the number of spectral bands, number of spectral values in a band (spectrum resolution), largest and smallest period and the critical level for determining the spectral peaks. The third step is the LS analysis of the data series at a confidence level of interest. However, it is strongly recommended that this process should be preceded with data scaling when dealing with data series which vary within a millimetre level accuracy. Based on the experience gained during this research, the present software version cannot detect any periodic signals in larger data values which vary within millimetre level without appropriate scaling. As an example when station

---

[13] LSSA software version 5.02 has been set to analyze 10,000 values. The size arrays of the arrays can be modified accordingly based on the length of the analyzed series and the computer system used.

coordinates are subject to atmospheric loading (APL) corrections, the input data have to be scaled for the software to respond properly. Under the basic approach, the LS spectrum for each data series under analysis is first determined without removing (enforcing) any periodic constituents. Significant peaks from the initial spectra are then identified and removed in subsequent spectra determinations until all statistically significant peaks are identified. The enforcement (removal) of significant peaks at each analysis stage should be done in a meaningful way by observing the significant reduction of the χ^2 test on the variance, quadratic norm of the residuals and Chi-Squared χ^2 goodness-of-fit test of the residual histogram.
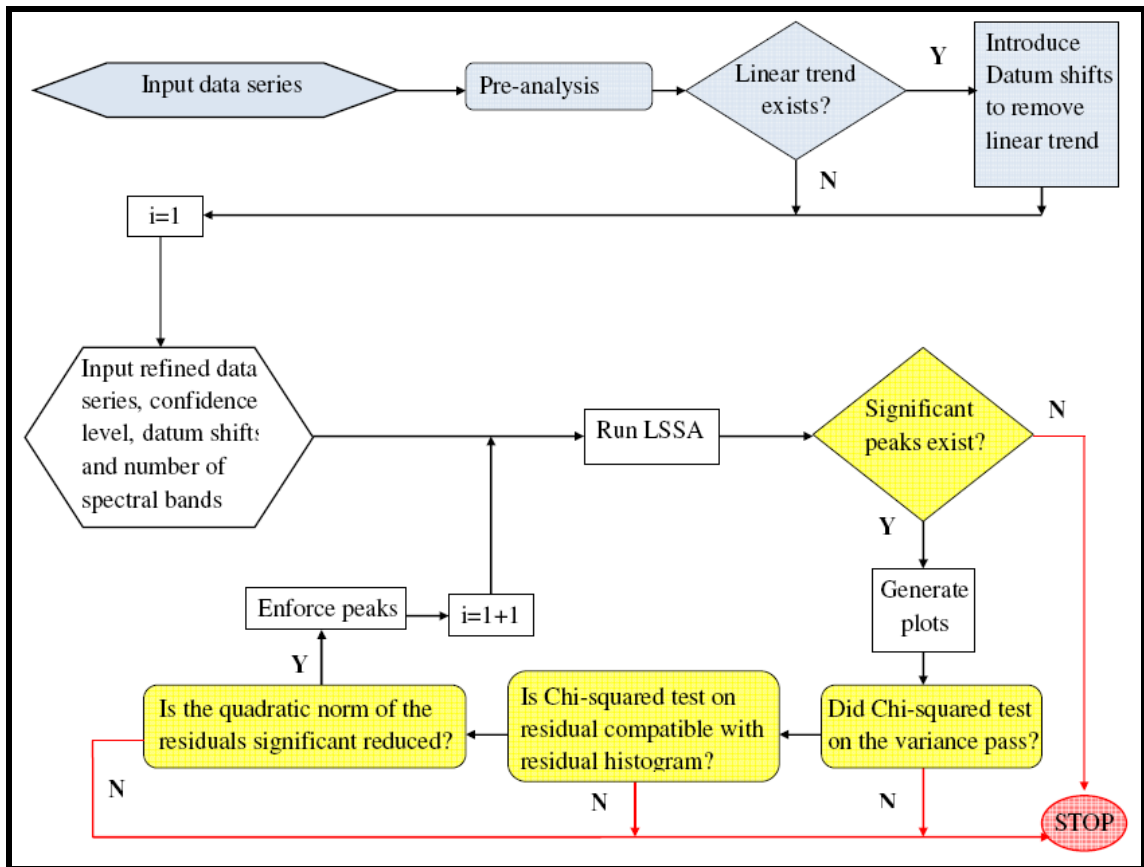
Figure 2.2 Overview of the basic LSSA implementation procedure

2.1.3 Least Squares self coherent analysis (LSCA)

In this research, Least-squares (LS) product spectrum theorem [14] has been effectively used to generate new LS spectra known as the LS self-coherent spectrum [15] with a new probability distribution function and new confidence level based on two or more LS spectra of the data series under consideration. The new probability distribution function amplifies the common peaks while attenuating the non-common ones [Pagiatakis et al., 2007]. Spectral peaks which are significant and common in the LS spectra of the data series under consideration are thereafter extracted in a rigorous way followed by the analysis of the product spectrum herein after known as LS self-coherent analysis. The LS spectra segments of the analyzed time series do not necessarily need to have the same sampling rate but rather the same number of spectral values in their bands.

Based on the theoretical overview of the new theorem, a product spectrum can be conceived as a multiplication operation in the frequency domain to generate a new spectrum, which gets the common peaks between the components of the input spectra while suppressing the non-common ones. That is, multiplying the two spectra together (multiplication in the frequency domain) is equivalent to convolution (filtering) in the time domain. The individual spectrum for each data series follows the beta distribution $(x_i; \alpha, \beta)$ such that $\alpha = 1$ and β depends on the degrees of freedom, it

---

[14] The logarithm of the product LS spectrum $\ln H_n$ is a maximum probability and maximum likelihood estimator that follows approximately the log-normal distribution.

[15] LS coherent spectrum is generated from the product of two or more LSSA spectra segments of data series under consideration.

follows that the product spectrum will also follow a beta distribution. It follows that the population distribution function of a product spectrum can as well be derived based on the central limit theorem[16] [e.g. Hogg and Craig, 2005]. This is through the definition of a new random variable z, based on the natural logarithm of the percentage variance of the individual spectra X_i, as shown in Equation 2.7:

$$z = \sum_{i=1}^{n} \ln (X_i). \tag{2.7}$$

In Equation 2.7, each of the individual spectra X_i, is being considered as a random variable distributed as beta $(x_i; \alpha, \beta)$, with respective finite first (μ_i) and second (σ_i^2) moments as per Equations 2.8 and 2.9:

$$\mu_i = \frac{2}{m_i - u_i}, \tag{2.8}$$

$$\sigma_i^2 = \frac{4(m_i - u_i - 2)}{(m_i - u_i + 2)(m_i - u_i)^2}. \tag{2.9}$$

In equations 2.8 and 2.9, m_i and u_i are, respectively, the number of data points and unknown parameters estimated by the LS procedure. Parameter β_i is given as:

$$\beta_i = \frac{(m_i - u_i - 2)}{2}. \tag{2.10}$$

Based on Pagiatakis et al. [2007], the new random variable z approximately follows the normal distribution under the assumptions of the central limit theorem. After some

---

[16] The distribution of sample means taken from a large population each with finite mean and variance will approximately approach a normal (Gaussian) curve.

developments (not part of this discussion), a new population distribution function based on two (for easy illustration) individual spectra segments are given as follows:

$$f(z) = \int_z^0 [\beta_1 \beta_2 e^z (1 - e^{z-s_2})^{\beta_1 - 1} (1 - e^{s_2})^{\beta_2 - 1}] dz_2 . \tag{2.11}$$

The new population distribution function is defined by its mean and variance as per respective Equations 2.12 and 2.13 in which k is the number of individual spectra and β is defined as per Equation 2.9. The two moments are obtained through derivation and developments involving Beta integration and logarithmic factorial functions[17] (details not part of this discussion) in a two steps process. The first step is the projection of the variable z into a set $A(x)$ such that $0 < x < 1$. The second step is the definition of a transformation[18] $z = v(x) = \ln x$ between sets A and $B(z)$ such that $-\infty < z < 0$, as well as the Jacobian of the transformation $J = \dfrac{dx}{dz} = e^z$.

$$\mu_z = -\sum_{k=0}^{\infty} \left(\frac{1}{k+1} - \frac{1}{k+1+\beta} \right), \tag{2.12}$$

$$\sigma^2_z = \sum_{k=0}^{\infty} \left(\frac{1}{(k+1)^2} - \frac{1}{(k+1+\beta)^2} \right). \tag{2.13}$$

Based on the normal distribution property of LS product spectrum, the significant spectral peaks in the LS coherent spectrum have the maximum probability estimates as well as maximum likelihood estimates. This property makes the LS self coherent

---

[17] Illustration and examples regarding integrations involving Beta functions and logarithmic factorial functions can be referred from Gradshteyn and Ryzhik [1965, p.538-541].

[18] The approach is based on descriptions by Hogg and Craig [1995, Section 4.3].

spectrum a best liner unbiased estimator (BLUE). This research has adopted the least squares (LS) self coherency analysis approach in the identification of the common spectral peaks from different analysed time series using the following steps:

a) Different spectra are produced for each component of the data series under investigation (e.g., positions, residuals, atmospheric pressure loading) using the LSSA software v5.02 and each of them had 2000 spectral values[19] in their bands.

b) Different spectra were imported into matlab followed by the appropriate rearrangements of the input files. Thereafter, the natural logarithms of different spectra are taken and used to generate a LS coherent spectrum at the 99% confidence levels. The resulting probability density function is used to identify the significant peaks rigorously using a matlab function that was generated for this task.

c) Significant peaks in the product spectrum must as well be statistically significant in the individual spectra under analysis.

d) Generation of final plots are of the least squares (LS) coherent spectrum as required based on the research objectives

e) It should be noted that, estimates of their amplitudes and phases of the common significant peaks are obtained suppressing them in each of the individual LS spectra.

---

[19] Number of spectral values in each band (max 5000) specifies the resolution of the output LS spectrum. However, large values slow down the execution time of LSSA especially with longer data series. Usually 250-2000 spectral values give good spectral representation, at least at the diagnostic level.

2.2 Bernese 5.0 Software Upgrades and Processing Models

This section presents an overview of the Bernese v5.0 GPS Software [20] necessary upgrade procedures to allow data processing compatible with the ITRF and new absolute variation mode. Bernese software has adopted in this research to generate weekly solutions for stations YELL and NRC1 for the period of 1995 to 2010 in a baseline mode. The software upgrades were necessary prior to the processing activities because the present UNB software version (12-Feb-2005 release) is not compatible with the above requirements and it was therefore necessary to upgrade to the most recent version presently available (11-May-2011 release) in two steps process. The first step is run the software update utility, using "perl bsw50updater.pm"[21] from a command line.

The second step is to update the Bernese Processing Engine (BPE) which is a powerful tool primarily designed for automatic processing large amounts of data from permanent GPS networks. BPE can as well be used to run more than one task at a time on different CPUs, and can even divide a single task across different CPUs as well as perform conditional forward and backward jumps using both sequentially and parallel processing modes. BPE can be run in interactive mode (with the graphical user interface) as in this research as well as in non-interactive mode from the command line. However, while it is true that the BPE allows automatic and consistent processing of data, it also requires the user to predefine many processing options in the program input

---

[20] Installation requirements, campaign set ups and other details on processing information can be referred from the Bernese user manual [Dach et al., 2007].

[21] The update utility should be installed in %X%\EXE directory along with all update files.

files based on the accuracy requirements. This should be done in conjunction with the appropriate definition of a set of standard and user-made process control files (PCFs) and auto-processing menu variables before analyzing the data, all of which requires knowledge of Perl scripting as well as the BPE and Bernese processing software. Based on that, a number of programs input parameters in PCF[22] as well as the menu variables[23] had to be changed to match with the processing requirements and the input data in the context of IGS05, which is the terrestrial frame used to generate IGS REPRO1 solutions. IGS05 is based on the absolute phase center variation models (PSV) and therefore a switch must be made from relative to absolute PCVs to make the BPE efficient and compatible to REPRO1 processing procedures through a two steps process.

The first step is to download the appropriate files to be updated from the URL ftp://ftp.unibe.ch/aiub/BSWUSER50/GEN (also known as Bernese general files). They are the satellite information (SATELLIT.I05), ANTEX file (I05.ATX) and the satellite phase center variation files (PHAS_COD.I05). The first two files have to be put in the $X/GEN directory (%X%\GEN for windows) and I05.ATX file should be in the OUT directory. The second step is to change the input panels which can be done using the BPE variable V_PCV for the file extensions. This will change the names of the satellite information file in all program panels of the option directories ($U/OPT and $X/OPT) from SATELLIT. to SATELLIT. $(PCV). Likewise all the Bernese relative phase center

---

[22] PCF is a list of scripts which have to be run sequentially or in parallel by the Bernese Processing Engine PCF defines which scripts should run and in what order they should be executed. They define which scripts must wait or run in parallel as well as the parameters that are to be passed into the next scripts.

[23] BPE use three different types of variables for auto-processing which are environment variables, client variables and user-defined server variables.

variation files named PHAS_IGS.REL (or PHAS_ccc.REL) will as well be changed to respective absolute file with names PHAS_IGS.$(PCV) (or PHAS_ccc.$(PCV)); where "ccc" identifies the institution providing the files. Alternatively, the manual option can be used either to change the relative files (satellite, phase center variation and antenna) to absolute in appropriate program panels, or you can also use menu Configure>Change general options for the input files in the ${U}/OPT/ and ${U}/PAN/ panel directories. To conclude the BPE update procedures, the JPL DE200/DE405 planetary ephemeris[24] should be installed along with the manual editing of the DATUM file. These two activities are not part of the automated updating process and both files are located is in the BERNE50/GPS/GEN directory. In the editing process, new datum parameters of the IGS05 and ITRF05 which were used to generate IGS REPRO1 solutions were added. The two frames are compatible with the new absolute phase center variation models.

2.2.1 Overview of the adopted Bernese processing strategy

Bernese processing strategy is a set of user predefined process control files (PCF) and ordered instructions which enable the Bernese Processing Engine (BPE) to process the data in questions based on its nature and accuracy requirements. Bernese Processing Engine (BPE) can be run in different ways using one of the standard process

---

[24] JPL ephemeris account for the gravitational attraction of Sun, Moon and the major planets (Jupiter, Venus, and Mars), and consider general relativistic corrections [Dach et al., 2007, pp.92].

control files[25] as well as user predefined set of process control files. However, most geodetic institutions prefer to generate a particular (user) processing strategy based on a selected set of process control files, in order to achieve desired processing requirement based on practical experiences. Under this approach, system users compiles standard programs and may add user interfaces as well as write additional user-made scripts using the Practical Extraction and Report Language (PERL) software so as to meet the desired processing needs of interest based on accuracy, and data archiving mechanisms.

This thesis adopted the user-defined PCF approach by taking advantage of the expertise obtained from a study visit to NRCan. Under my approach, the BPE (Appendix B) processing is preceded with Matlab pre-processing activities[26]. Bernese users are strongly recommended to check for regular updates of different input file types as they are regularly updated based on the availability of new models and modernization aspects as recommended by the IERS. The work flow of the (created) BPE steps are enumerated below and summarized in Figure 2.3 whereas different processing models that have been used are illustrated on the processing summary provided in Tables 2.1.

1) Generate a-priori coordinates using the COOVEL program to the computation date using station velocities information based on nuvel-1a plate motion model as defined in the user campaign STN directory of the processing campaign.

---

[25] The present software version has five standard process control files which are BASTST.PCF, CLKDET.PCF, PPP.PCF, RNX2SNX.PCF and SUPERBPE.

[26] Includes campaign set ups and downloads of the IGS final orbits, IGS clock files, observation files in RINEX and Earth rotational parameters from the URL ftp://cddis.gsfc.nasa.gov/pub/gps/data/ . ANTEX files and station information files, atmospheric files and differential code bias files for both receiver and satellite are retrieved from the URL ftp://ftp.unibe.ch/aiub/ .

2) Verify the RINEX observations using the RXOBV3 program for station names, antenna and receiver names and numbers before importing or rejecting them into Bernese system based on the information on the IGS station information list.

3) Write the Earth orientation information in Bernese format from the IERS/IGS standard format information file using the POLUPD program.

4) Transform the IGS precise orbits from the terrestrial into the celestial reference frame using the PRETAB program.

5) Create the Bernese so-called standard orbits from tabular orbits from step 4 and solve for the satellite equations of motion using the ORBGEN program. As the inputs are selected as precise files, the program uses the satellite positions as pseudo-observations in an orbit determination process (one such process per arc and satellite) [Dach et al., 2007, pp.92].

6) Receiver and satellite clocks are synchronized to generate clock corrections to be used in LS adjustment, using code observables and the CODSPP program based on second degree polynomial interpolations at 12 hours intervals.

7) Baselines creation comprised of Bernese zero difference and single difference baselines using the SNGDIF program using a pre-defined baseline.

8) Preprocessing of the Phase Baseline to repair cycle-slips, followed by the generation ionosphere free (L3) observations using the MAUPRP program.

9) Parameter estimation through LS adjustment using the GPSEST program and generates residuals which are then extracted using the RESRMS program. As a

parallel activity, bad satellites are marked and removed from the processing

procedures using the SATMRK program.

10) Iterative double-difference phase residual screening (if the a-posterior RMS

errors in step 9 are beyond the expected error magnitudes of about 1.0-1.5 mm).

11) Generate float solution and atmospheric parameters based on unresolved

ambiguities using the GPSEST program.

12) Ambiguity resolution using Quasi Ionosphere Free (QIF) approach using the

GPSEST program in baseline mode using a baseline correlation strategy.

13) Final network solutions are generated using the GPEST program in session mode

and constrained to the reference station. Normal equations and final atmospheric

parameters are stored at this stage.

14) Add the normal equations from step 13 using the ADDNEQ2 program and

generate the final daily solution in the SINEX format.
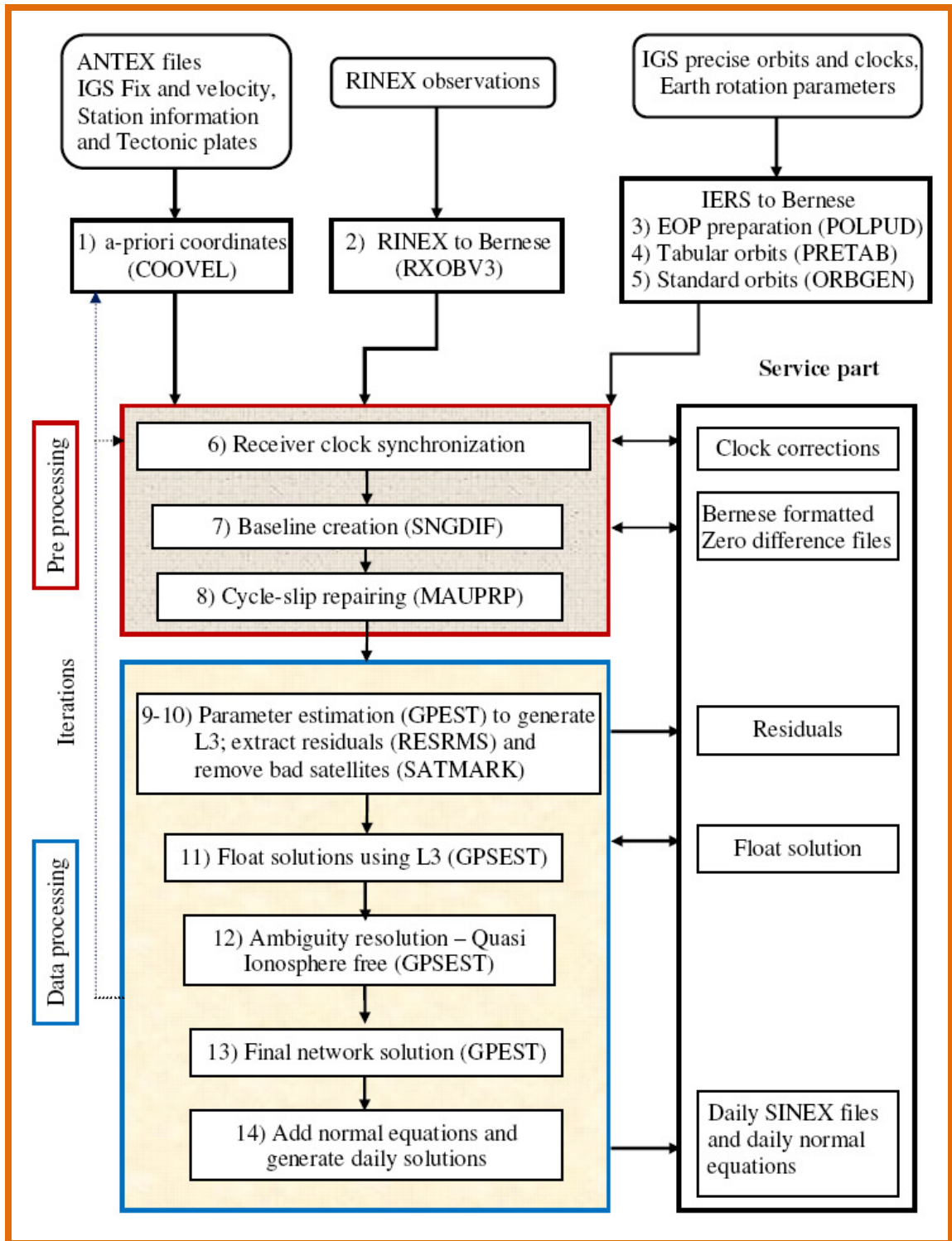
Figure 2.3 Functional flow diagram of the adopted Bernese processing strategy

Table 2.1 below presents a processing summary that show different models that have been used in different Bernese processing activities presented in column one and the description of the processing models used been illustrated on column two.

Table 2.1 Research processing strategy

Research processing strategy summary (IGS template version 2.0, 5 January, 2012)	
Preprocessing	Phase pre-processing in a baseline by baseline mode using double differences; cycle slips are simultaneously fixed through different linear combinations of L1 and L2. Bad data points are removed or new ambiguities are estimated if the cycle slips repair is unreliable.
Basic observable	GPS Carrier phase observations; code observations only used for synchronization of receiver clock and ambiguity resolution
	Elevation angle cut off: 10 degrees sampling rate: 30 sec Elevation-dependent weighting function : 1/cos (z) Code biases: P1P2 and P1C1 from ftp://ftp.unibe.ch/aiub/CODE/
Observables	Double differences, ionosphere free linear combination
RHC phase rotation	Polarization effect applied: Geometrical
Phase center variation models	Ground antenna : IGS05 phase center variation model from ftp://ftp.unibe.ch/aiub/BSWUSER50/GEN/
	Satellite antenna : IGS05 PCV model applied (block specific)
Antenna radome	Calibration applied as per the antenna file IGS05.atx
Troposphere a priori model	zenith delay: "dry" Niell
	Mapping function: Wet Niell Mapping Function
	gradient model: tilting once per 2 hours
Plate motions	IGS05 station velocities
Tidal displacements	1. Solid earth tide: IERS 2003
	2. Ocean tidal loading: FES2004 (by the Bos & Scherneck website http://www.oso.chalmers.se/~loading/)
	3. Solid earth pole tides: IERS 2003
	4. Permanent earth tides: Not applied
	5. Ocean pole tides: Not applied
	6. Atmosphere tides: corrections for S1 & S2 tidal pressure loading not applied (no IERS model available yet)

Table 2.1 Research processing strategy -continued

Non-tidal loading	Not applied : (Atmospheric pressure, ocean bottom up and surface hydrology and other effects)
Earth orientation parameters (EOP)*	Sub daily ERPs : IERS 2000
	Nutation : IAU2000
Geopotential*	JGM3 model up to degree and order 12 as well as the use of the C21 and S21 coefficients for fixing the Earth pole axis
	Geocentric gravitational constant (GM) = 398600.4415 km^3/sec^2
	Equatorial radius of the Earth (AE) = 6378.1363 km
Third body effect*	Sun, Moon, Jupiter, Venus, and Mars are regarded as point masses based on JPL DE200.EPH ephemeris.
Tidal variations in geopotential model *	Solid earth tides:TIDE2000 (IERS 2000)
	Solid earth pole tides: Not applied
	Ocean tides: OT_CSRC.TID
	Ocean pole tides: Not applied
Solar radiation pressure model*	a priori: ROCK4 and ROCK42 approximations version T (including thermal re-radiation, also called T10 and T20)
	Earth albedo: None
	Earth and Moon shadow model: umbra and penumbra
Relativitic effects	Dynamic effect applied as per IERS 2003
Numerical integration*	Based on polynomial of degree 10 for 1 hour
	integration step: 1 hour with no special starter procedure required
	arc length: 24 hours
Adjustment method	Sequential least-squares adjustment
Station coordinates (datum definition)	STJO is used as reference (based on IGS05) with horizontal deviation < 10 mm and vertical deviation < 30
	▪ 3 no-net translation and 3 no-net rotation conditions ▪ geocenter coordinates constrained nominally to zero values
Satellite and receiver clock corrections	Computed using code observations based on the double-difference orbit, Earth rotation parameters, coordinates, troposphere solutions and differential code bias. Computations use LS adjustment at confidence interval of 5 in F*SIGMA

Table 2.1 Research processing strategy-continued

Orbital parameters*	6 Keplerian elements plus 9 solar radiation parameters (RPR) are estimated at start of arc. RPR are based on Beutler et al. (1994). ▪ Constants in D (sun), Y (solar-panel axis) and X-directions ▪ Periodic terms in D,Y and X (towards the Earth) direction
Troposphere	Zenith delay parameters and pairs of horizontal delay gradient parameters are estimated for each station at respective intervals of 2 hours and 24 hours with no a priori constraints applied.
Ionosphere corrections	First-order effect (not modeled) eliminated by forming the ionosphere-free linear combination of L1 and L2
	Second and third order effect: not applied
Ambiguities	Baseline-by-baseline using Quasi-Ionosphere-Free approach
Time argument	GPS time as given by observation epochs, which is offset by only a fixed constant/ leap seconds (approx.) from TT/TDT
Inertial*	Geocentric mean equator and equinox of 2000 Jan 1.5 (J2000.0)
Terrestrial*	IGS05 station coordinates and velocities
Interconnection*	Precession: 2000 Precession theory
	Nutation: 2000 Precession theory

Note: In Table 2.1, the activities with an asterisk (*) notation at the end are used in steps three (3) to five (5) of the processing summary, which deals with treatment of the input precise orbits.

3. GENERATION OF IGS REPRO1 SOLUTIONS AND THE ROLE OF PHASE CENTER VARIATIONS (PCV)

REPRO1 solutions are IGS solutions obtained by reanalyzing the full history of GPS data collected by the IGS global network since January 1994 to March 2010. REPRO1 campaign had three major goals. The first goal was to adopt an absolute antenna phase center model (IGS05.atx) which was one of the most profound changes in the strategy of the various IGS Analysis Centers since the start of the IGS in 1994. The second objective was to generate homogeneous and consistent long time series of combined REPRO1 solutions based on IGS05 reference frame, with the full implementation of up-to-date models and standards [McCarthy and Petit, 2003]. The third objective was to provide input for the realization of ITRF2008 and establish the basis of the generation of new satellite antenna phase center variation model.

This chapter is divided into four sections. The first section provides an overview of different IGS products with their accuracies and latencies. The second part discusses different activities in the process of REPRO1 generation. They include the definition of the measurement models used in the processing, the solution of the satellite equations of motion, and the transformation between the Celestial and the Terrestrial Reference frames. The third part provides the summary of the combining the REPRO1 daily terrestrial reference frame parameters into official weekly parameters. The fourth part provides an overview of the satellite and receiver phase center offset and phase center variations and the summary of their role and advantages of IGS05 phase center variations model in the generation of REPRO1.

3.1 Overview of IGS Products

The International Global Navigation Satellite System Service (IGS), formerly the International GPS Service, is a voluntary federation of worldwide agencies that collects, archives, and distributes GPS and GLONASS observation data from permanent tracking stations. The stations are equipped with continuously operating dual-frequency GPS receivers and the collected data is formatted in a RINEX format (upon verification) prior to their transfer to the Regional or Global Data Centers. The IGS Analysis Centers access and analyze them using one of the six, independent geodetic software packages presented in Table 3.1 in which the first column are the Analysis Centers and the second column provide the software information.

Table 3.1 IGS Analysis Centers processing software

Analysis center	Software
Center for Orbit Determination in Europe, Switzerland (CODE)	Bernese (Dach et al., 2007).
Natural Resources Canada, Canada (EMR)	GIPSY (Lichten et al., 1995).
European Space Operations Centre, Germany (ESA)	NAPEOS (Dow et al., 1999)
GeoForschungsZentrum/Potsdam, Germany (GFZ)	EPOS (Gendt et al., 1999).
Jet Propulsion Laboratory, USA (JPL)	GIPSY (Lichten et al., 1995).
Massachusetts Institute of Technology, USA (MIT)	GAMIT (King and Bock, 1999).
GeoForschungsZentrum/Potsdam & Technical University of Dresden, Germany (PDR)	Bernese (Dach et al., 2007).
Scripps Institution of Oceanography, USA (SIO)	GAMIT (Lichten et al., 1995).
National Geodetic Survey, NOAA, USA (NGS)	PAGE (Schenewerk et al., 1999)
University of La Rochelle, France (ULR)	GAMIT (Lichten et al., 1995).

These software suites are used to generate seven (7) different IGS products under two main categories of products with different accuracies and latencies. The first category is comprised of the final products with components involving the terrestrial reference frame, including the satellite ephemerides, Earth rotation parameters, apparent geocenter positions, IGS tracking station coordinates and velocities, GPS satellite and IGS tracking station clock information. These are produced by the IGS Reference Frame Coordinator by combining their respective weekly SINEX file submissions from the ACs using rigorous mathematical methods based on scale factors and satellite weights. Under the current procedures, the Analysis Center Coordinator use combined results from the Reference Frame Coordinator to form the IGS final orbits and clock products in a way that maintains a high level of overall internal consistency. The second category consists of the zenith tropospheric path delay estimates, daily TEC maps with 2 hours resolution and differential code bias values in IONEX format. The weekly solutions are generated by the Ionosphere Associate Analysis Centers and then submitted to the Ionosphere Associate Combination Center for the generation of the combined IGS products. The different IGS products are summarized in the following subsections.

3.1.1 Earth rotation parameters (ERP)

The present weekly IGS SINEX combination procedure includes the estimates of the daily Earth Rotational Parameters (ERP), length of the day (LOD), pole positions and pole rates. Under the current procedures they are provided at noon on a daily basis, and only the ERPs for the week of interest are combined. However, the combination of the UT parameter is currently not considered in the IGS weekly combinations. This is because of their linear dependency with the right ascension of the ascending node of the satellite orbits a problem that requires some special attention. Based on Ferland and Piraszewski (2009), the present Analysis Center (AC) LOD estimates are subject to biases and have to be removed prior to the combination process. Currently, the AC LOD biases are estimated using the differences between the past LOD and their respect values provided in the IERS Bulletin A, based on a twenty one (21) days sliding window. ERP estimates that cannot be repaired are excluded from the combination. As a measure of quality assurance the final combined products are compared to the values from the Global Network Associate Analysis Center (GNNAC) and IERS Bulletin A. Based on those comparisons, it is conceived that the final differences (biases) in the pole positions, pole rates and LOD are about ±0.05 mas, ±0.10 mas/day and 10µs respectively.

3.1.2 GPS satellite ephemerides and station clocks

The GPS satellite ephemerides (IGS combined orbit and IGS combined clocks) are the IGS primary product and they are available in various flavors such as Ultra-Rapid (IGU), Rapid (IGR), and Final (IGS) as provided in Table 3.2. Ultra-Rapid became officially available on November 5, 2000 (GPS Week 1087) to replace the former IGS predicted (IGP) orbit products [Weber, 2001]. The main difference between the different flavours of the IGS GPS satellite ephemerides is their varying latency, accuracy and the extent of the tracking network used for their computations.

The IGS Ultra-rapid (IGU) products are based on both observations and prediction models and they are released four times per day, at 03:00, 09:00, 15:00, and 21:00 UTC. The IGS Ultra-rapid orbit files contain 48 hours of tabulated orbital ephemerides, and the start/stop epochs continuously shift by 6 hours with each update. The IGS Rapid products (IGR) are made available once a day at about 17:00 UTC. In principle they have a quality nearly comparable to that of the Final products and for that reasons no significant differences can be noticed between them and the IGS Final for most applications concerning non-geodetic users. Examples of such applications include property surveys, topographical surveys, navigation surveys as well as mining surveys. In principle the IGS Final products have the highest quality and internal consistency as compared to all IGS products and they the basis for the IGS reference frame. Usually, they are made available on Thursday after every 12 to 18 days and are intended for those applications demanding high consistency and quality. Table 3.2 provides a summary of different flavors of IGS ephemerides which are currently

generated. Column one provide the information on the type of IGS ephemerid, column two provide the accuracy of the product and the information on the product latency is provided in column three. Column four give the information on how often the products are updated and their respective sampling rates are in column five. Column six provides the information on the present archive places.

Table 3.2 GPS satellite ephemeris (satellite and station clocks)

Ephemerides		Accuracy	Latency	Updates	Sample Interval	Archive locations by March, 2012
Ultra-Rapid (predicted half)	orbits	~5cm	real time	at 03, 09, 15, 21 UTC	15 min	CDDIS(US-MD) IGS CB(US-CA) SOPAC(US-CA) IGN(FR)
	Sat. clocks	~3 ns RMS ~1.5 ns SDev				
Ultra-Rapid (observed half)	orbits	~3cm	3 - 9 hours	at 03, 09, 15, 21 UTC	15 min	CDDIS(US-MD) IGS CB(US-CA) SOPAC(US-CA) IGN(FR)
	Sat. clocks	~150 ps RMS ~50 ps SDev				
Rapid	orbits	~2.5cm	17 - 41 hours	at 17 UTC daily	5 min	CDDIS(US-MD) IGS CB(US-CA) SOPAC(US-CA) IGN(FR),
	Sat. clocks	~75 ps RMS ~25 ps SDev				
Final	orbits	~2.5cm	12 - 18 days	every Thursday	Sat.: 30s Stn.:5min	CDDIS(US-MD) IGS CB(US-CA) SOPAC(US-CA) IGN(FR)
	Sat. clocks	~75 ps RMS ~20 ps SDev				

3.1.3 Geocentric station coordinates and velocities

Geocentric station coordinates and velocities are part of the final IGS products as computed by the IGS reference frame coordinator based on combined weekly solutions from the IGS analysis centers. Nowadays, the IGS generates about 350 sets of station coordinates (SSC) and their velocities on weekly basis, Table 3.3, based on the worldwide IGS tracking network. In Table 3.3, the first column gives the information on the type of the final product and column two is accuracy information of the product. Column three show the latency information and column four gives information on how often the product is updated. Column five is the solution sampling rate and the archive information is provided in column six. However, the IGS solutions computing procedures and the final solution combination procedures by the IGS Reference frame coordinator are often subject to changes in steps and techniques based on software upgrades and availability of new processing models.

Table 3.3 Geocentric coordinates of IGS tracking stations

Coordinate solutions (SSC)		Accuracy	Latency	Updates	Sample Interval	Archive locations by December, 2011
Final positions	horizontal	3 mm	11 - 17 days	every Wednesday	weekly	CDDIS(US-MD) SOPAC(US-CA) IGN(FR)
	vertical	6 mm				
Final velocities	horizontal	2 mm/yr	11 - 17 days	every Wednesday	weekly	CDDIS(US-MD) SOPAC(US-CA) IGN(FR)
	vertical	3 mm/yr				

3.1.4 Apparent geocenter

Based on the satellite dynamics, the attraction from Earth's mass (solid, liquid and atmosphere) is the main force acting on the GNSS satellites. It follows that the estimation of the movement of the Earth's center of mass could be done based on the satellite orbits with a reasonable accuracy. However, this ability is mainly limited by the accuracy of different models used to model the impact of the other forces acting on the satellite (e.g. radiation pressure, third body effects). The label "apparent geocenter" is used to reflect this limitation. By convention, the ACs apparent geocenter, as sensed by the satellite orbits, is implicitly at the origin of the station coordinates and the estimates are provided in the SINEX products along with their uncertainties with respect to the reference frame used to generate the solutions.

3.1.5 Final atmospheric parameters

Presently there are two types of IGS combined atmospheric products as presented in Table 3.4. These are the Final and Ultra-Rapid Troposphere zenith path delay as well as the Final and Rapid Total Electron Content (TEC) grid. Based on Feltens (2003), these products are generated by Ionosphere Associate Combination Center (IACC) in IONEX format on weekly basis. The combination is based on daily TEC maps from the five IGS Ionosphere Associate Analysis Centers (CODE, ESA, JPL, NRCAN and UPC). In Table 3.4, the first column provides the types of generated atmospheric product, column two is the product accuracy information and the latency information is presented in column three. The product updates information is presented in column four and the product sampling rate is provided in column five.

Table 3.4 IGS combined atmosphere products

Atmospheric Parameters	Accuracy	Latency	Updates	Sample Interval
Final troposphere zenith path delay	4 mm	< 4 weeks	weekly	2 hours
Ultra-Rapid troposphere zenith path delay	6 mm	2-3 hours	every 3 hours	1 hour
Final ionosphere TEC grid	2-8 TECU	~11 days	weekly	2 hours; 5° (longitude) x 2.5^o (latitude)
Rapid ionosphere TEC grid	2-9 TECU	<24 hours	daily	2 hours; 5° (longitude) x 2.5^o (latitude)

3.2 Procedure to Generate REPRO1 Solutions by Each AC

In order to get desired and consistent REPRO1 results from all IGS analysis centers, the IGS Central Bureau defined a processing strategy prior to the generation of the final products, comprised of different stages and activities. The first stage is the definition of measurement models which includes the estimation models, different types of a-priori values and other constraints, definition of the orbit models, as well as the definition of the reference frame to be used. Usually, the estimation models are derived using observations from all available core stations (about 135) plus observations from a few other IGS tracking stations chosen mostly to strengthen the network geometry [Ray and Griffiths, 2008]. The estimation models are used to solve for the satellite equations of motion in the Celestial reference frame (CRF). The celestial reference frame[27]is defined by the geocentric mean equator and equinox of 2000 January 1.5 Terrestrial Time (TT). The third stage involves the transformations of the solution from the Celestial to Terrestrial Reference frame (TRF) where the products are used. In the generation of REPRO1 solutions, the transformations adopted the IAU2000 precession-nutation model. The last stage involves the combination of individual weekly solutions from the eleven IGS Analysis centers, which are merged into official IGS solution by the IGS Analysis Center Coordinator (ACC). However, for the purpose of efficiency, the ACC only combines of the IGS final orbits and clock products but the rest of the combination activities are shared.

---

[27] Realized by adopting the mean right ascension of 23 radio sources in a group of catalogs compiled by fixing the right ascension of the quasar 3C 273B to the conventional FK5 value (Kaplan et al., 1982)

3.2.1 IGS analysis centers data usage

In order to achieve consistency in the first reprocessing activities, the IGS defined a wide range of processing parameters to be used. They include data types used for pre-processing and processing and models used for parameter[28] estimation. There is a wide variation in processing parameters as well as processing modes and approaches used by different ACs. This is verified by details of their respective processing summaries which are Schaer et al. (2008) for CODE, Donahue et al. (2008) for EMR, Enderle and Springer (2011) for ESOC and Gendt and Brandt (2011) for GFZ. Others are, Desai et al. (2008) for JPL, Herring et al. (2008) for MIT, Dulaney et al. (2006) for NGS, Steigenberger et al. (2006) for GFZ, Bock et al. (2005) for PDR, Rudenko et al. (2008) for GTZ and Bouin et al. (2007) for URL.

Table 3.5 below summarizes different data types used by different IGS ACs, column one, in the pre-processing and processing activities. The summary is based on AC processing summaries and a similar study by Ray and Griffiths (2008). Based on information in column two, all ACs adopted either differenced or un-differenced carrier phase observables in the processing. In both cases, they were later on used for forming ionosphere free combinations. Code observations were only used for cycle slip repair, clock synchronization and ambiguity resolution using different approaches. Column three present different data rates deployed whereas column four are the different elevation cutoff angles adopted in the processing. Column five present the information on different observation weights used in the computation procedures.

---

[28] Estimated parameters are the IGS station coordinates and velocities, atmosphere delays and initial satellite conditions.

Table 3.5 Comparison of IGS analysis centers (AC) data usage

AC	Observation type	Data rate	Elevation cutoff	Observation weights
CODE	Double difference phase observables; cycle slips are repaired at different linear combinations of L1 and L2	3 min	3 deg	$1/\cos^2(z)$
EMR	Un-differenced phase observables; cycle slips detected and fixed using cc2noncc based on code observables	5 min	10 deg	none
ESA	Un-differenced phase observables; cycle slips are fixed by code observables	5 min	10 deg	$1/\sin^2(e)$
GFZ	Un-differenced phase observables; cycle slips detected and fixed using cc2noncc based on code observables	5 min	7 deg	$1/2\sin(e)$ for e < 30 deg
JPL	Un-differenced phase observables; cycle slips detected and fixed using smoothed carrier phase observables	5 min	15 deg	none
MIT	Double difference phase observables; cycle slips are repaired at different linear combinations of L1 and L2	2 min	10 deg	$a^2 + (b^2/\sin^2(e))$ a, b are from site residuals
NGS	Double difference phase observables; pre-data screening and cycle slips repair are done using TEQC metrics	30 s	10 deg	$[5+(2/\sin(e))\ cm]^2$
PDR	Double difference phase observables; cycle slips are repaired at different linear combinations of L1 and L2	3 min	3 deg	$1/\cos^2(z)$
SIO	Double difference phase observables. Ambiguity: resolved by code ranges	2 min	10 deg	$a^2 + (b^2/\sin^2(e))$ a, b are from site residuals
ULR	Double difference phase observables. Ambiguity: resolved by code ranges	3 min	10 deg	None

3.2.2 Modeling the neutral atmospheric delays

In the generation of REPRO1 solutions, different IGS analysis centers adopted different approaches to model the neutral atmosphere propagation delays, which is about 2.3 m at sea level, and is divided into hydrostatic and wet components. However, the IGS recommended the use of an updated formula based on Saastamoinen (1972) as given by Davis et al. (1985) as the basic model for the a priori hydrostatic delay in the zenith direction using surface pressure as follows:

$$D_{hz} = \frac{[(0.0022786 \pm 0.0000005)]P_o}{1 - 0.00266 \cos\phi - 0.00000028\ H}.$$ 3.1

In equation 3.1, D_{hz}, P_o, H and ϕ are respectively the zenith hydrostatic delay (in meters), the total atmospheric pressure at the antenna phase center, the geodetic height (in meters) and the geodetic latitude (in degrees). In addition, the IGS as well recommended the use of two more approaches for modeling the neutral atmosphere delay. They are the use VMF1 (Boehm et al., 2006a) values provided by the Technical University of Vienna as well as a priori zenith delay consisting of both the hydrostatic and wet components using surface temperature values from Global Pressure and Temperature model (GPT) . The IGS recommended that [Petit and Luzum, 2010, pp. 120] computations of wet delays should be made using the location and season dependent Global Mapping Function model (Boehm et al., 2006b). A summary of the different neutral atmospheric model used by different are presented in Tables 3.6. Column one presents the names of the AC, Column two presents different a priori models whereas the different mapping functions and zenith parameters are

presented in columns three and four respectively and column five present the gradient

parameters.

Table 3.6 Comparison of the IGS AC troposphere measurement models

AC	a priori meteorological data for zenith delay	A priori model		Estimated parameters	
		Zenith Delay	Mapping Function	Zenith parameters	Gradient parameters
CODE	Global Pressure and Temperature (GPT) model	Saastamoinen (dry)	Global mapping function (GMF)	estimated at 2 hours intervals	N-S and E-W solved once every 24 hour
EMR	ECMWF via VMF1	VMF1 (dry + wet)	GMF	5min stochastic Zenith Topo Delay	5-min stochastic
ESA	GPT model	Saastamoinen + GMF (dry)	GMF – dry	GMF-wet at 2 hours intervals	None
GFZ	GPT model	Saastamoinen 'dry' + 'wet'	GMF	GMF-wet at 1 hour intervals	None
JPL	GPT model	dry= scaled (height based) wet=0.1 m	GMF	5min stochastic Zenith Topo Delay	5-min stochastic
MIT	GPT model	Saastamoinen 'dry'+ 'wet'	GMF 'wet'+ 'dry'	GMF-wet at 2 hours interval	N-S and E-W solved twice per 24 hours
NGS	GPT model	Saastamoinen 'dry' +' wet'	GMF 'wet'+ 'dry'	GMF-wet at 1 hour interval	N-S and E-W vary linearly
PDR	Berg (1948)	Saastamoinen dry	Wet-Niell	Wet-Niell at 2 hours intervals	N-S and E-W solved once per 24 hours
SIO	GPT model	Saastamoinen 'dry' + 'wet'	GMF 'wet'+ 'dry'	GMF-wet at 2 hours intervals	N-S and E-W vary linearly
ULR	GPT model	Saastamoinen 'dry' + 'wet'	VMF1 (wet)	Wet-Niell at 1 hour intervals	N-S and E-W solved once per 24 hours

3.2.3 Modeling the tidal loading forces

Instantaneous GNSS observed positions at epoch t, $\vec{X}(t)$ has to be regularized to their equivalent position $\vec{X}_R(t)$ by removing the high-frequency time variations $\sum_i \Delta \vec{X}_i(t)$, resulting into positional displacements. The variations are the impact of both tidal and non tidal loading forces, and have to be modeled as follows:

$$\vec{X}_R(t) = \vec{X}(t) - \sum_i \Delta \vec{X}_i(t).$$ 3.2

Based on that, different IGS solutions have been modeled for those effects as soon as the appropriate models are available and REPRO1 solutions are not an exception. As one of the basic requirements, the IGS REPRO1 generation process included the tidal loading corrections based on IERS 2003 [McCarthy and Petit, 2003]. The tidal forces to be considered were solid earth tides, earth pole tides, ocean loading, ocean pole tides, and sub-daily variations of the Earth Orientation Parameters (EOPs). Likewise, the atmospheric pressure loading, ocean bottom pressure and surface hydrology were to be considered for the non-tidal forces. Based on the summaries of the Analysis Centers processing strategies it was realized that none of the centers applied corrections due to ocean pole tide as well any of the non-tidal loading effects. This is because the IERS was yet to recommend any model for those loading types by the time of the first reprocessing campaign. Table 3.7 provides a summary of the different tidal loading models applied by the IGS ACs, column one. Column two and three are the respective solid Earth and Earth pole tidal models whereas different ocean tidal models are in column four. Column five present model for sub-daily EOPs.

Table 3.7 Comparison of the IGS analysis centers tidal models

Analysis Center	Solid Earth tide	Earth pole tide	Ocean tide loading	Sub daily EOPs
CODE	IERS 2003	IERS 2003	FES2004 [Lyard et al.,2006]	Based on IERS 2003 [McCarthy and Petit, 2003] and IAU 2000 Nutation theory.
EMR	IERS 2003	IERS 2003	FES2004	Based on IERS 1996 without nutation effect
ESA	IERS 2003	IERS 2003	FES2004	Based on IERS 2003 and PMsdnut.for
GFZ	IERS 1992	IERS 2003	FES2004	Based on IERS 2003 and sub-daily Nutation
JPL	IERS 2003	IERS 2003	FES2004	Based on IERS 1996 without nutation effect
MIT	IERS 2003	IERS 2003	FES2004	Based on IERS 2003 and PMsdnut.for
NGS	IERS 2003	IERS 2003	FES2004	Based on IERS 2003 and PMsdnut.for
PDR	IERS 2003	fixed mean pole	GOT00.2 [Ray, 1999].	Based on IERS 1996 without nutation effect
SIO	IERS 2003	IERS 2003	FES2004	Based on IERS 2003
URL	IERS 2003	IERS 2003	FES2004	Based on IERS 2003 and IAU 2000 Nutation theory.

3.2.4 Solution of the satellite Equation of motion

Like in other IGS solutions, the second step in the generation of REPRO1 solutions required the solution of a second order differential equation of satellite motion in the Inertial Celestial Reference Frame (ICRF), and all Analysis Centers are consistent on that. ICRF is the realization of the Celestial Reference System (CRS) which is defined by the geocentric mean equator and equinox of 2000 January 1.5 Terrestrial Time (TT) [Julian Date 2451545.0 TT]. Based on Langley [2007], the solution of the satellite equation of motion generates a set of six osculating parameters as well as a set of model parameters at the initial epoch as follows:

$$\ddot{\vec{r}} = -\frac{GM}{r^3}\vec{r} + \ddot{\vec{P}}(t, \vec{r}, \dot{\vec{r}}, p_0, p_1, p_2, ...),\qquad(3.3)$$

where $\ddot{\vec{r}}$ is the acceleration vector of the satellite, GM is the gravitational constants for the Earth , $\vec{r}$ is the magnitude of the position vector and r is the satellite altitude, $\ddot{\vec{P}}$ is the perturbing acceleration acting on the satellite, and $p_0, p_1, p_2, ...,$ are the parameters of the perturbing accelerations which are not sufficiently known and have to be determined. In GNSS satellites, these parameters are usually associated with the solar radiation pressure and the impact of the third body effects (point masses) from Sun, Moon, Mercury, Venus, Mars, Jupiter, Saturn, Uranus, and Neptune. In Equation 3.3, the first term on the right hand side describes the Keplerian satellite motion[29] in a field influenced by the central part of the earth's gravitational field. The second term represents the sum of other non-central accelerations acting on

---

[29] The satellite motion is usually referred to as prograde (direct) if the satellite is moving from west to east and the orbit is termed as retrograde (indirect) if the satellite is moving from east to west.

the satellite such as solar radiation pressure (direct and indirect effects), tidal forces and relativistic effect. These forces act on the satellite in the radial, along-track and out-of-plane directions and deviates the satellite motion from a pure Keplerian orbit.

The solution of the Equation 3.3 can be obtained by analytical methods or numerical integration, based on the assumption that the gravitational field is conservative. This implies, both the mechanical energy of the satellite and its angular momentum is conserved [Langley, 2007]. The solution by the analytical method uses Langrange equations and is solved by means of variation equations. The disadvantages of this approach are the high computational demands and difficulty of incorporating various kinds of force models. The numerical integration can be done in different ways using different starter procedure, integration steps and orbit arc lengths requirements. However, all numerical integration approaches are based on the known initial conditions of the satellite state vector (position vector $r(t_0) = [X_0, Y_0, Z_0]^T$ and velocity vector $v(t_0) = [\dot{X}_0, \dot{Y}_0, \dot{Z}_0]^T$) at the initial epoch t_0. The initial conditions can also be provided using the Keplerian elements $K(t_0) = [a_0, e_0, i_0, \omega_0, \Omega_0, f_0]^T$ in the right ascension system [Vaníček and Krakiwski, 1986]. The numerical integration approaches are modeling the disturbing accelerations using variation equations which are the partial derivatives of the state vector with respect to the deterministic model parameters at time t, $K(t) = [a(t), e(t), i(t), \omega(t), \Omega(t), p_0, p_1, p_2, ...]^T$ as follows:

$$r_K(t) = \frac{\partial r(t)}{\partial K} \; , \tag{3.4}$$

$$v_K(t) = \frac{\partial v(t)}{dK} . \tag{3.5}$$

Based on Santos et al. [1996], the solution of the satellite equations of motion in the Inertial Celestial Reference Frame is subject to errors in the computation procedures from different sources which include:

1)   The numerical integration technique, reflecting the stability of the integrator as well as the size of the integration steps.

2)   The force model used in the computations.

3)   The accuracy of the initial conditions as a small inaccuracy may result into an error of thousands of meters after the integration.

3.2.5 IGS analysis centers gravity (geopotential) models

In the of generation REPRO1 solution, the IERS recommended the use of EGM96 (Lemoine et al., 1998), model as the conventional model along with the values for the C_{21} and S_{21} coefficients to describe the position of the Earth's figure axis. However, the IGS accepted use of other geopotential models such as the GRIM5-C1 (Gruber et al., 2000) and JGM-3 (Tapley et al., 1996), to degree and order 12, as they could as well achieve similar accuracy in the processing. Table 3.9 presents different gravity models used IGS analysis centers, column one, as well as different options of tidal forces used to model for the gravity field variations. Column two presents the gravity field models whereas Earth tidal model, Earth pole tides, Ocean tides models and Ocean pole tide modes are presented in columns three, four, five and six respectively. Models for the relativistic effects are in column seven.

Table 3.8 Comparison of the IGS analysis centers gravity (geopotential) models

AC	Gravity field (geopotential model)	Tidal variation to the gravity models				Relativity effects
		Earth tides	Earth pole tides	Ocean tides	Ocean pole tides	
CODE	JGM3; + C21, +S21 due to polar motion	IERS 2003	IERS 2003	CSR 3.0	none	Applied based on IERS 2003
EMR	JGM3; + C21, +S21 due to polar motion	IERS 2003	IERS 2003	CSR	IERS 2003	Not applied
ESA	EIGEN; + C21, S21 due to polar motion (PM)	IERS 2003	IERS 2003	IERS 2003	Not applied	Applied based on IERS 2003
GFZ	EIGEN-GLO4S1 +C21, S21 due to polar motion	IERS 2003	GFZ model	GEM-T1	Not applied	Dynamic corrections and bending applied
JPL	GGM02C; +C21, S21 due to polar motion	IERS 2003	IERS 2003	FES2004	Not applied	Dynamic corrections and bending applied
MIT	EGM96; +C21, S21 due to PM	IERS 1992	None	None	None	No dynamic corrections and bending applied
NGS	GEM-T3; +C21, S21 due to PM	IERS 1992	None	None	None	No dynamic corrections and bending applied
PDR	JGM3; +C21, S21 due to PM	IERS 2003	IERS96; fixed pole	CSR 3.0	none	Dynamic corrections and bending applied
SIO	EGM96; +C21, S21 due to PM	IERS 1992	none	none	none	Applied based on IERS 1996
ULR	EGM96; +C21, S21 due to PM	IERS 1992	none	none	none	Dynamic corrections not applied

Table 3.9 Comparison of the IGS analysis centers satellite force models

AC	Third body effect	Solar radiation	Numerical Integration
CODE	Sun and Moon as point masses based on DE405 ephemeris	CODE-RPR model coefficients (of 2007)	Method: Based on Beutler et al.[2005]
			Starter procedure: None
			Integration steps: 1 hour
			Arc length: 72 hours
EMR	Point masses: Moon, Sun, Mercury, Venus, Mars, Jupiter, Saturn, Uranus and Neptune based on DE405	GSPM_EPS model of Bar-Sever	Method: Adams predictor-corrector
			Integration steps : variable
			Starter procedure : Runge-Kutta
			Arc length: 24 hours.
ESA	Point masses: Moon, Sun, Mercury, Mars, Venus, Jupiter, Saturn, Uranus and Neptune based on DE405	No a priori model	Method :Adams-Moulton prediction;
			Integration steps: 120
			Runge-Kutta
			Arc length: 24 hours
GFZ	Point masses: Moon, Sun, Mercury, Mars, Venus, Jupiter, Saturn, Uranus and Neptune based on DE405	No a priori model	Method : Everhart integrator
			Integration steps: variable
			none
			Arc length: 24 hours
JPL	Point masses: Moon, Sun, Mercury, Venus, Mars, Jupiter, Saturn, Uranus, Neptune based on DE405 ephemeris.	JPL empirical SRP model, GSPM-04, Bar-Sever and Kuang, (2004)	Method: Adams predictor-corrector
			Integration steps : variable
			Starter procedure : Runge-Kutta
			Arc length: 30 hours.

Table 3.9 Comparison of the IGS ACs satellite force models-continued

AC	Third-body effect	Solar radiation	Numerical Integration
MIT	Point masses: Sun and Moon based on MIT PEP Ephemeris	corrections to D, Y, B-axes, + 1/rev-terms are estimated	Method: Adams-Moulton fixed-step, 11-pt predictor-corrector
			Integration steps : 75s
			Starter procedure : Runge-Kutta
			Arc length: 24 hours.
NGS	Point masses: Moon, Sun, Mercury, Venus, Mars, Jupiter, Saturn, Uranus, Neptune based on MIT PEP Ephemeris	Berne 9-parameter SRP model with D,Y, B scales + 1/rev-terms	Method: Adams predictor-corrector
			Integration steps : variable
			Starter procedure : Runge-Kutta
			Arc length: 24 hours.
PDR	Sun, Moon, Venus, Mars and Jupiter as point masses based on DE405 ephemeris.	A priori: ROCK4 and ROCK42 approximations	Method: Representation of the orbit by a polynomial of degree 10
			Integration steps : 1 hour
			Starter procedure: none
			Arc length: 72 hours.
SIO	Sun and Moon as point masses. Ephemeris none	corrections to D,Y,B-axes, +1/rev-terms are estimated	Method: Adams-Moulton fixed-step, 11-pt predictor-corrector
			Integration steps : 75s
			Starter procedure : Runge-Kutta
			Arc length: 24 hours.
ULR	Point masses: Moon and Sun. Ephemeris are generated from the MIT PEP program	Berne 9-parameter SRP model with D,Y, B scales + 1/rev-terms	Method: Adams-Moulton fixed-step, 11-pt predictor-corrector
			Integration steps : 75s
			Starter procedure : Runge-Kutta
			Arc length: 24 hours.

3.2.6 Transformation between the celestial and terrestrial systems

The generation of REPRO1 solutions involves the transformation of the solutions of the satellite equations of motion (orbits and other IGS products[30]) from the Celestial Reference System (CRS) to the Terrestrial Reference System (TRS). The TRF is earth-fixed with its origin at the center of mass of the whole Earth, its Z axis points towards the Conventional International Origin (CIO) and the X-axis towards the Greenwich meridian. Both systems have a non-rotating origin (NRO) and they are respectively designed as Celestial Ephemeris Origin (CEO) and the Terrestrial Ephemeris Origin (TEO). The transformation between the CRS and TRS is specified by the position of the Celestial Intermediate Pole (CIP) in the Geocentric Celestial Reference System (GCRS) in the International Terrestrial Reference System, and the Earth rotation angle [McCarthy and Petit, 2003, pp.33] using Equation 3.7 as follows:

$$[CRS] = Q(t)R(t)W(t)[TRS]. \tag{3.7}$$

In equation 3.7, $Q(t), R(t)$ and $W(t)$ are the respective transformation matrices arising from the motion of the celestial pole in the celestial system (precession and nutation effects), from the rotation of the Earth around the axis of the pole and from polar motion. The frame as realized from the [TRS] by applying the transformations $W(t)$ and then $R(t)$ will be called "the intermediate reference frame of epoch t".

---

[30] IGS products are used in the Terrestrial Reference Frame in different ways to support Earth science research , multidisciplinary applications and education.

The $Q(t)$ matrix is defined as follows:

$$Q(t) = \begin{pmatrix} 1 - aX^2 & -aXY & X \\ -aXY & 1 - aY^2 & Y \\ -X & -Y & 1 - a(X^2 + Y^2) \end{pmatrix} . R_3(s),$$

<div align="right">3.8</div>

where:

$$a = \frac{1}{2} + \frac{1}{8}(X^2 + Y^2),$$

<div align="right">3.9</div>

$$s(t) = \frac{1}{2}[X(t)Y(t) - X(t_0)Y(t_0)] + \int_{t_0}^{t_1} \dot{X}(t)Y(t)dt - (\sigma_0 N_0 - \Sigma_0 N_0).$$

<div align="right">3.10</div>

And the terrestrial time:

$$TT = TAI + 32.184s.$$

<div align="right">3.11</div>

$$t = \frac{TT - 2000\, January\ 1.5\ TT}{36525} \text{ (in days).}$$

<div align="right">3.12</div>

In equations 3.8 to 3.12, X, Y are the coordinates of the Celestial Intermediate Pole (CIP) in the Geocentric Celestial Reference System (GCRS) based on the IAU2000A Precession-Nutation model. σ_0, Σ_0 are the positions of the CEO at J2000.0 and the x-axis of the Geocentric Celestial Reference System (GCRS) and N_0 is the ascending node of the equator at J2000.0 in the equator of the GCRS.

The $R(t)$ matrix is defined as follows:

$$R(t) = R_3(-\theta) .$$

<div align="right">3.13</div>

The Earth rotation angle θ is measured along the equator of the Celestial Intermediate Pole between the Celestial Ephemeris and Terrestrial Ephemeris Origins.

The $W(t)$ matrix is defined as follows:

$$W(t) = R_3(-s^{'}).R_2(x_p).R_1(y_p),$$ 3.14

where:

$$s'(t) = \frac{1}{2}\int_{t_0}^{t_1}(x_P\dot{y}_P - \dot{x}_Py_P)dt,$$ 3.15

In equations 3.14 and 3.15 x_p and y_p are the polar coordinates of the Celestial Intermediate Pole (CIP) in the Terrestrial Reference Frame, whereas, $\dot{x}_p$ and $\dot{y}_p$ are their respective changes with time; s' provides the position of the Terrestrial Ephemeris Origin in the equator of Celestial Intermediate Pole.

In order to ensure consistency in the solution of the satellite equations of motion, the IGS Analysis Centers had to define the reference frames in use as well as the interconnection between them prior to the actual generation and the transformation of the process. For the generation of REPRO1 solutions, the IERS recommended the use of Geocentric mean equator and equinox of J2000.0 as the inertial frame and all ACs complied with this requirement. The IGS05, which is closely aligned to ITRF[31] 2005, was recommended for the terrestrial transformations. Likewise the IAU 2000 precession and nutation model was recommended for the interconnection between the CRS and the TRS. However, not all the GS Analysis Centers used the recommended IAU 2000 precession and nutation models. Also a few of them used ITRF 2000 instead as a terrestrial reference frame instead of IGS05 and this aspect may have resulted into variations in the final results. Table 3.12 illustrates different

---

[31] ITRF is the realization of the International Terrestrial Reference System using the space geodesy techniques of IVS, GNSS, ILRS and DORIS. Based on model updates, there are different ITRS realizations.

frames and precession nutation models used by different ACs, column one in the transformation process. Column two shows the time system used whereas the terrestrial reference frames are presented in column three whereas precession and nutation models are shown in column five.

Table 3.10 Comparison of IGS analysis centers reference frames

AC	Time	Terrestrial	Interconnection
CODE	GPS time	IGS05 coordinates and velocities	Precession: IAU 2000
			Nutation: IAU 2000
EMR	GPS time	ITRF 2005 coordinates and velocities	Precession: IAU 1976
			Nutation: IAU 1980
ESA	GPS time	ITRF 2005 coordinates and velocities	Precession: IAU 2000A
			Nutation: IAU2000A
GFZ	GPS time	ITRF 2005 coordinates and velocities	Precession: IAU 2000A
			Nutation: IAU 2000A
JPL	GPS time	IGS05 coordinates and velocities	Precession: IAU 1976
			Nutation: IAU1980
MIT	GPS time	ITRF 2005 coordinates and velocities	Precession: IAU 1976
			Nutation: IAU 2000A
PDR	GPS time	ITRF 2000 coordinates and velocities	Precession: IAU 1976
			Nutation: IAU 2000A
SIO	-	ITRF 2000 coordinates and velocities	Precession: IAU 1976
			Nutation: IAU 1980
NGS	GPS time	ITRF 2005 coordinates and velocities	Precession: IAU 1976
			Nutation: IAU 1980
GTZ	GPS time	ITRF 2005 coordinates and velocities	Precession: IAU 2000A
			Nutation: IAU 2000A
URL	GPS time	ITRF 2005 coordinates and velocities	Precession: IAU 1976
			Nutation: IAU 2000

3.2.7 IGS Analysis centers final solutions

The IGS REPRO1 generation activities explained in sections 3.2.1 to 3.2.6 resulted into daily products for each of the Analysis centers which are categorized into two groups. The first category is consisted of the GPS orbits in SP3C format and satellite clocks in clock RINEX format based on GPS timescale. These, were submitted to the IGS ACC who generates the main official IGS combined products presented in part 3.2. In the process of generating REPRO1 solutions, the ACC functions were performed by the GFZ Department 1 in Potsdam, Germany. As a general overview, the final IGS REPRO1 orbit combination process (details not part of this research) was done directly in the ITRF05 without any alignment to the Bulletin B EOP series using the weighted average software [Springer and Beutler, 1993]. The combination, involved small rotations to the ACs orbit and ERP values to align them to the IGS05. The combined satellite clocks were corrected for the periodical relativistic effects based on the inertial state and velocity vectors.

The second category is made up of the daily IGS reference frame products (station coordinates with full variance-covariance matrix in SINEX format and ERPs). Each of the IGS ACs generated combined weekly products based on their daily solutions (normal equations and coordinates) are thereafter submit them to the IGS Reference Frame Coordinator (RF). During the time of generation of REPRO1 solutions, NRCan was assuming the role of the RF and was responsible in combining the weekly terrestrial products from individual IGS Analysis Centers into final IGS weekly solutions; details of the combination procedures is discussed in section 3.3.

3.3 Combination of the Terrestrial Reference Frame parameters

The daily IGS reference frame products[32] (solutions) generated by each of the IGS Analysis Centers had to be combined into individual weekly solutions using their respective processing software (Table 3.1) based on the daily solution and normal equations. The ACs weekly solutions are thereafter submitted to the IGS RF for their combination to generate the IGS final weekly REPRO1 solutions. Table 3.11 gives a summary of the submissions to the RF in which the first column presents the IGS ACs, the second column presents the span of the submitted data and the third column gives the number of station solutions submitted by each of the ACs.

Table 3.11 IGS analysis centers data in the generation of REPRO1 solutions

Analysis center	Data span	Number of stations
CODE	1994.0-2010.0	322
EMR	1995.0-2010.0	229
ESA	1995.0-2010.0	418
GFZ	1994.0-2010.0	299
JPL	1996.0-2010.0	413
MIT	1998.0-2010.0	700
PDR	1994.0-2008.0	201
SIO	1994.0-2010.0	422
NGS	1995.0-2010.0	436
GTZ	1994.0-2010.0	299
ULR	1996.0-2007.0	275

The primary objective of the combination process was to determine the best possible solution estimates for the parameters as expressed in the IGS05 frame. Based on Kouba [2009] such combinations typically result in more robust, precise and more

---

[32] Terrestrial reference frame products are station coordinates and velocities with full variance-covariance matrix in SINEX format, ERPs in IGS ERP format and apparent geocenter.

consistent solutions. This is because the space technique solutions are quite complex, involving different approaches and modeling that typically generates a random-like noise which is then averaged out within the combination process. The combination of AC solutions to generate the REPRO1 solution estimates was accomplished in a two step process using the GSD SINEX software [Ferland and Piraszewski, 2009]. The first step is the pre-combination to check for inconsistencies to produce unconstrained solutions. The second part is the generation of the final IGS combined solution using a standard LS adjustment. In the process, the contributing solutions are compared to remove outliers and ensure a high level of consistency of the estimated parameters.

3.3.1 Pre-combination process of the REPRO1 solutions

This is the process of removing any existing inconsistencies in the individual ACs weekly solutions and consists of the following six steps as follows:

a) Verify if the ACs solutions are in the agreed SINEX format.

b) Verify if constraints used in each AC solutions are removed.

c) Verify the correctness of local offsets and station name inconsistencies.

d) Verify is solutions are augmented with explicit apparent geocenter.

e) Verify if the individual AC solutions have been combined using the summation of normal equations to give a single (weekly) combined solution.

f) Verify if the solutions are properly rescaled (covariance information) by the weighted root mean square of the residuals (WRMS) in a meaningful way.

3.3.2 Combination of weekly ACs Solutions by LS adjustment

The second step in the combination process to generate the REPRO1 solutions in SINEX format was accomplished after the removal of the inconsistencies and outliers (previous step). In this process the best solution estimates are determined through LS adjustment based on two basic assumptions as follows:

1) The inputs (known) are the solutions the K IGS ACs which are conceived as a priory Terrestrial Reference Frames (TRF) comprised of the following:

   ▪ A network of N points: $X_0^i, Y_0^i, Z_0^i, \dot{X}_0^i, \dot{Y}_0^i, \dot{Z}_0^i, \quad i = 1,..., N.$

   ▪ A set of S solutions points and each of which is comprised of the following:

   a) Station positions and velocities: $X_s^i, Y_s^i, Z_s^i, \dot{X}_s^i, \dot{Y}_s^i, \dot{Z}_s^i \quad t_s^i \quad s = 1,..., S.$

   b) Polar motion: X_s^p, Y_s^p, UT_s and their daily rates $\dot{X}_s^p, \dot{Y}_s^p, LOD_s$.

   c) A full variance covariance matrix C_s .

2) The output (unknown) is a combined reference frame at epoch t_o comprised of :

   a) Station positions and velocities at epoch t_o: $X^i, Y^i, Z^i, \dot{X}^i, \dot{Y}^i, \dot{Z}^i.$

   b)   Polar motion: X^p, Y^p, UT and their daily rates $\dot{X}^p, \dot{Y}^p, LOD$.

   c) The seven transformation parameters at t_k with their time derivatives between individual frames, TRF K with the combined frame.

The individual TRF and the combined TRF are related by the seven transformation parameters, resulting on a non linear combined model as in Equation 3.16 for the positions and velocity and Equation 3.17 for the polar motion parameters:

$$\begin{cases} \begin{pmatrix} X_s^i \\ Y_s^i \\ Z_s^i \end{pmatrix} = \begin{pmatrix} X^i \\ Y^i \\ Z^i \end{pmatrix} + (t_s^i - t_0)*\begin{pmatrix} \dot{X}^i \\ \dot{Y}^i \\ \dot{Z}^i \end{pmatrix} + T_k + D_k\begin{pmatrix} X^i \\ Y^i \\ Z^i \end{pmatrix} + R_k\begin{pmatrix} X^i \\ Y^i \\ Z^i \end{pmatrix} + (t_s^i - t_k)\left[\dot{T}_k + \dot{D}_k\begin{pmatrix} X^i \\ Y^i \\ Z^i \end{pmatrix} + \dot{R}_k\begin{pmatrix} X^i \\ Y^i \\ Z^i \end{pmatrix}\right] \\ \\ \begin{pmatrix} \dot{X}_s^i \\ \dot{Y}_s^i \\ \dot{Z}_s^i \end{pmatrix} = \begin{pmatrix} \dot{X}_s^i \\ \dot{Y}_s^i \\ \dot{Z}_s^i \end{pmatrix} + \dot{T}_k + \dot{D}_k\begin{pmatrix} X^i \\ Y^i \\ Z^i \end{pmatrix} + \dot{R}_k\begin{pmatrix} X^i \\ Y^i \\ Z^i \end{pmatrix} \end{cases}$$

3.16

$$\begin{cases} X_s^p = X^p + R2_k \\ Y_s^p = Y^p + R1_k \\ UT_s = UT - \dfrac{1}{f}R3_k \\ \dot{X}_s^p = \dot{X}^p + \dot{R}2_k \\ \dot{Y}_s^p = \dot{Y}^P + \dot{R}1_k \\ LOD_s = LOD + \dfrac{1}{f}\dot{R}3_k \end{cases}$$

3.17

For a LS adjustment, the non-linear combined model in Equations 3.16 and 3.17 has to be linearized by taking the partial derivatives with respect to time (variation equations) and generate observations equations for each solution. Observation equations for positions and velocity for each solution are as follows:

$$\begin{cases} X_s^i = X^i + \partial t_s^i \dot{X}_i T1_k + X^i D_k 10^{-6} - cR3_k Y^i + cR2_k Z^i + \partial t_k^i[\dot{T}1_k + X^i \dot{D}_k 10^{-6} - c\dot{R}3_k Y^i + c\dot{R}2_k Z^i \\ \\ Y_s^i = Y^i + \partial t_s^i \dot{Y}_i T2_k + Y^i D_k 10^{-6} + cR3_k X^i - cR1_k Z^i + \partial t_k^i[\dot{T}2_k + Y^i \dot{D}_k 10^{-6} + c\dot{R}3_k X^i - c\dot{R}1_k Z^i \\ \\ Z_s^i = Z^i + \partial t_s^i YZ_i T3_k + Z^i D_k 10^{-6} + cR1_k Y^i - cR2_k X^i + \partial t_k^i[\dot{T}3_k + Z^i \dot{D}_k 10^{-6} + c\dot{R}1_k Y^i - c\dot{R}2_k X^i \\ \\ \dot{X}_s^i = \dot{X}^i + \dot{T}1_k + X^i \dot{D}_k 10^{-6} - c\dot{R}3_k Y^i + c\dot{R}2_k Z^i \\ \\ \dot{Y}_s^i = \dot{Y}^i + \dot{T}2_k + Y^i \dot{D}_k 10^{-6} + c\dot{R}3_k X^i - c\dot{R}1_k Z^i \\ \\ \dot{Z}_s^i = \dot{Z}^i + \dot{T}3_k + Z^i \dot{D}_k 10^{-6} + c\dot{R}1_k Y^i - c\dot{R}2_k X^i{}_k \end{cases}$$

3.18

Likewise, the observation equations for the polar motion parameters are as follows:

$$
\begin{cases}
X_s^p(t_p) = X^p(t_p) + (R2_k + \partial t_k^p \dfrac{R2_k}{yr}) * 1000 \\[2mm]
Y_s^p(t_p) = Y^p(t_p) + (R1_k + \partial t_k^p \dfrac{R1_k}{yr}) * 1000 \\[2mm]
UT_s(t_p) = UT(t_p) - \dfrac{1}{f}(R3_k + \partial t_k^p \dfrac{R3_k}{yr}) * 1000 \\[2mm]
\dot{X}_s^p = \dot{X}^p + \dfrac{\dot{R2}_k}{yr} * 1000 \\[2mm]
\dot{Y}_s^p = \dot{Y}^P + \dfrac{\dot{R1}_k}{yr} * 1000 \\[2mm]
LOD_s = LOD + \dfrac{1}{f}\dfrac{\dot{R3}_k}{yr} * 1000
\end{cases}
\tag{3.19}
$$

In Equations 3.18 and 3.19, y_r =365.25, f =1.00273790950795, c =pi/32,400. The observation equations 3.18 and 3.19 for each solution i can as well be written in matrix form as follows:

$$
\begin{pmatrix} A1_s & A2_s \end{pmatrix} \begin{pmatrix} \delta X_s \\ \delta T_k \end{pmatrix} + B_s = v_s
\tag{3.20}
$$

The resulting normal equations of the observation equations are as follows:

$$
\begin{pmatrix} A1_s^T C_s^{-1} A1_s & A1_s^T C_s^{-1} A2_s \\ A2_s^T C_s^{-1} A1_s & A2_s^T C_s^{-1} A2_s \end{pmatrix} \begin{pmatrix} \delta X_s \\ \delta T_k \end{pmatrix} + \begin{pmatrix} A1_s^T C_s^{-1} B_s \\ A2_s^T C_s^{-1} B_s \end{pmatrix} = 0
\tag{3.21}
$$

In Equations 3.20 and 3.21, δX_s and δT_{ks} are the respective linearized solution in a combined frame and the 7 parameters of transformation (unknowns) whereas B_s and v_s are the respective constant matrix and residual vectors; I is identity matrix, $A1_s$ and $A2_{ks}$ are the respective design matrices which are defined as follows:

$$
A1_s = \begin{pmatrix} I & (t_s^i - t_0).I \\ 0 & I \end{pmatrix}
\tag{3.22}
$$

$$A2_s = \begin{pmatrix} A_s^i & (t_s^i - t_0).A_s^i \\ 0 & A_s^i \end{pmatrix}$$

3.23

$$A_s^i = \begin{pmatrix} 1 & 0 & 0 & 10^{-6}*X_0^i & 0 & c*Z_0^i & -c*Y_0^i \\ 0 & 1 & 0 & 10^{-6}*Y_0^i & -c*Z_0^i & 0 & c*X_0^i \\ 0 & 0 & 1 & 10^{-6}*Z_0^i & c*Y_0^i & -c*X_0^i & 0 \end{pmatrix}$$

3.24

The normal equations of the individual solutions as in Equations 3.21 in the combined frame are stacked together to generate a system of combined normal equations and thereafter used to solve for the unknown parameters in an interactive process.

In the combination (LS adjustment) process, constraints were imposed to detect potential inconsistencies (bias and outliers) in the solution estimates and consequently, have a best defined TRF with better internal consistency (minimum or no distortion). Based on Ferland and Piraszewski [2009], the outlier detection thresholds were set at 5 sigma for the statistical component and 5 cm for absolute component. The procedures for removing bias and outlier detection are as follows:

a) Comparison with the Reference Frame realization is necessary to avoid biases.

b) Comparison among AC contributing solutions.

c) Comparison with the weekly combined solution of the previous week as a method of detecting short and long term abnormal coordinate variations.

d) Compare with cumulative combination [33] of the previous week to detect abnormal coordinate variations and minimise bias from unrealistic covariance matrices.

---

[33] Coordinate time series are also known as cumulative combination.

The outlier detection and rejection process is based on reference frame realization, other contributing solutions and previous weekly combined solution which are assumed to be correct on the basis of previous validations. Therefore, any large discrepancies are likely to be from the current solutions and as for that they are removed from the current individual AC solutions and the combination repeated from the beginning. One of major challenges in the present outlier detection process is the availability of discontinuities in station coordinate series as they tend to make the interpretation of GPS results problematic. Large discontinuities are easily be detected in the cumulative solutions. However, smaller discontinuities[34] are hardly detectable and could be wrongly interpreted as short term anomaly and vice versa. Currently this problem is minimized by rescaling and combining the covariance information provided by the ACs and the Global Network Associate Analysis Center (GNAAC) in a meaningful way based on the scale factors. Based on Ferland and Piraszewski [2009], the scale factors $(= \sqrt{Variance\ Factor})$, ranges from approximately 1.5 to about 35 and they are determined by comparing the input solutions with the cumulative solution. In this process the scale factors from previous weeks are used as initial approximations for the current week in an iterative refining process which is expected to converge within two to three iterations of normal procedure. Usually a week to week variations of the scale factor for a particular AC ranges within 10–15 percent and it is such that the expected combined solution estimates based on appropriate rescaled covariance matrices will achieve a formal sigma within a factor 2 between the comparable AC parameters.

---

[34] Most of the discontinuities observed from the GPS station coordinate time series could be attributed to equipment changes and/or earthquakes but unfortunately some still remains unknown.

3.4 The role of Phase Centers in the Generation of IGS Products

The phase centers of both the GNSS satellite and the receiver antenna are important in GPS data processing as they serve as the end points of the measured distance between the GNSS satellite and the GPS antenna on the ground. If the antenna phase center corrections are ignored they may lead to height errors of up to 10 cm [Rotacher et. al., 1995; Schmid et al., 2007]. Likewise they may result into incorrect scale factors up to 0.015 ppm [Dach et. al., 2007, pp. 327] with mixed antenna baselines for long distances, because the antennas see the same satellite under different elevation angles. Therefore, their exact position were modeled by a consistent set of phase center offset (PCO) and variations (PCVs) values in the generation of REPRO1 solutions and other related IGS products.

3.4.1 Satellite antenna phase center offset and phase center variation

With reference to Figure 3.1, the GPS satellite center of mass (white dot) is the theoretical position at which the entire weight of the aircraft is assumed to be concentrated in relation to the body. GPS satellite antenna phase center (green dot) is the antenna position from which the measurements of GPS orbit ephemerides in the broadcast navigation message are made. Based on Kouba (2009), satellites antenna phase centers are subject to Z axis (nadir) dependent phase center variations as well

as offsets from the satellite center of mass in *Z* coordinate direction (to some satellites also in *X* coordinate direction) with respect to the spacecraft-fixed reference system.
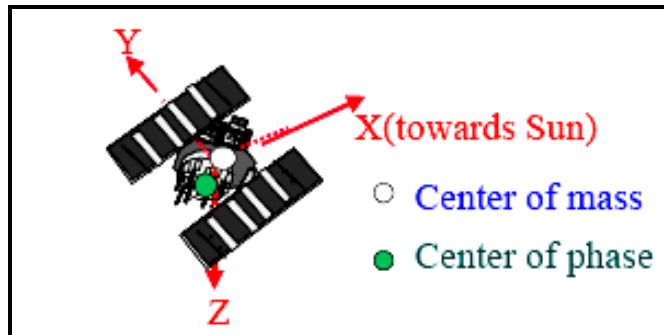
Figure 3.1 Satellite antenna phase center in body fixed reference frame [Kouba, 2009]

However, the satellite antenna phase center is not the most natural point of reference for accurately describing the motion of an Earth-orbiting satellite in the spacecraft-fixed reference system[35] and its response to the various forces that perturb its motion (refer to section 3.2.4). The satellite's center of mass is a more appropriate position to describe the force models that are used for satellite orbit modeling, and the generation of the IGS products. Therefore, to both generate and use these ephemerides in GPS data processing, the offset between the center of mass and the satellite's antenna phase center (phase center offsets, PCO) and their variations (PCVs) must be accurately known and modeled. This is necessary for monitoring the orientation of the offset vector in space as the satellite orbits the Earth.

---

[35] The system origin is the satellite's center of mass, the y-axis points along the nominal rotation axis of the solar panels, the z-axis points along the navigation antenna bore-sight toward the center of the Earth, and the x-axis points toward the hemisphere containing the Sun completes the right-hand system.

3.4.2 Modelling of (GPS) satellite antenna PCO and PCVs

Up to November 4, 2006, the IGS Analysis Centers processing strategies presumed that the phase center offsets and phase center variations for GPS satellites were block-specific. It was also conceived that, Block IIR (IIR-A, IIR-B, IIR-M), satellite antennas phase center Z-offsets were much closer to zero with negligible phase center variations [Kouba, 2009]. Therefore, blocks II and IIA phase centers offsets were corrected with respect to Block IIR phase centers, using block-specific values of 0.279 m, 0.000 and 1.023 m for the X, Y and Z components respectively. However, it was later realized that the corrections were not sufficient due to significant differences in the phase center behavior between certain subgroups of the satellite blocks and individual satellites [Ge and Gendt, 2005; Schmid et al., 2005].

Starting November 5, 2006, the IGS processing procedures attempted to adopt the absolute phase center offsets and non-zero PCVs for the satellite antennas. However, by the time of processing REPRO1 solutions, only the absolute variation models for GPS receiver antennas were available [IGSMAIL 5444, 18 Oct 2006]. The absolute variation model for GPS satellites were not yet available because of the modelling difficulties and as for that they were not used. One of the major problems in this context is the high correlation between several parameters, namely clock biases, tropospheric delays, as well as phase center offsets and variations of both the receiver and the satellite antennas [Schmitz et al., 2008]. Currently there are different approaches that are used to generate satellite antenna phase center variations [Schmid and Rothacher 2003; Schmid et al. 2007].

3.4.3 Receiver antenna phase center and phase center variations

Receiver phase center is the apparent center of GPS signal reception at an antenna. However, the receiver phase center is neither a physical point nor a stable point for any given GPS antenna as it is always changing based on the direction of the signal from a satellite. Because of that, antenna calibrations are necessary to yield the mean phase center as shown on Figure 3.2 [Langley, 2007]. The antenna reference point (ARP) is an antenna point where the GNSS measurements are referred to, being different from the phase center. The vector between the antenna reference point and the mean phase center is known as the phase center offset and has to be modeled for accurate GPS positioning (both precise point positing and relative positioning).
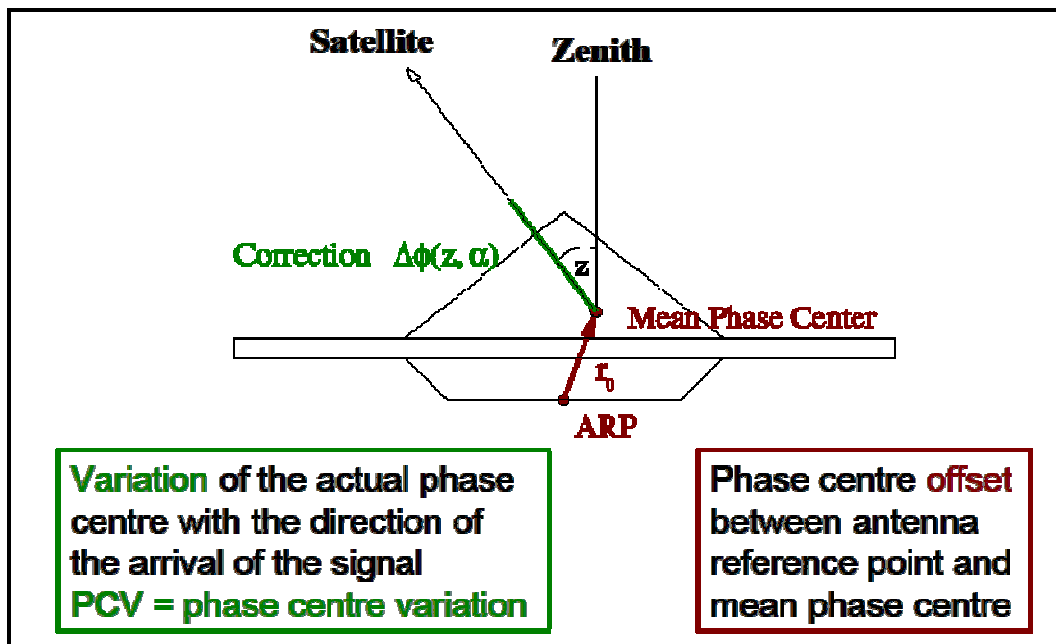
Figure 3.2 GPS receiver antenna phase centers from Schmid et al. [2005]

3.4.4 Modelling of GPS antenna PCO and PCVs

Prior to November 5, 2006, most of the IGS analysis centers applied the receiver antenna phase center corrections in a conventional way to allow a non-spherical phase response of the tracking antennas [Dow et al., 2005]. The corrections comprised of mean offsets of the electrical antenna phase center compared to the physical antenna reference point (ARP) and the phase center variations as a function of the elevation angle. The correction values were derived from the GPS data collected on a short baseline with the reference antenna AOAD/M T at one end of the baseline and the antenna to be calibrated on the other end. It was assumed that the reference antenna had zero PCV and was free of other limitations. This assumption was proved to be wrong as it caused systematic errors over a large terrestrial scale causing change of about 15 ppb in global GPS solutions [Schmid et al., 2005; 2007]. The current modeling approach uses robotic field measurements by Geo++ GmbH for GPS or anechoic chambers and the concept can be conceived using Figure 3.3 below.

Figure 3.3 Modelling of receiver phase centers offsets (left) and receiver nadir dependent phase center variation (right) from Schimid et al. [2005]

In Figure 3.3 above (to Equation 3.17) α and z are respectively the azimuth and nadir angle of the original GPS antenna pha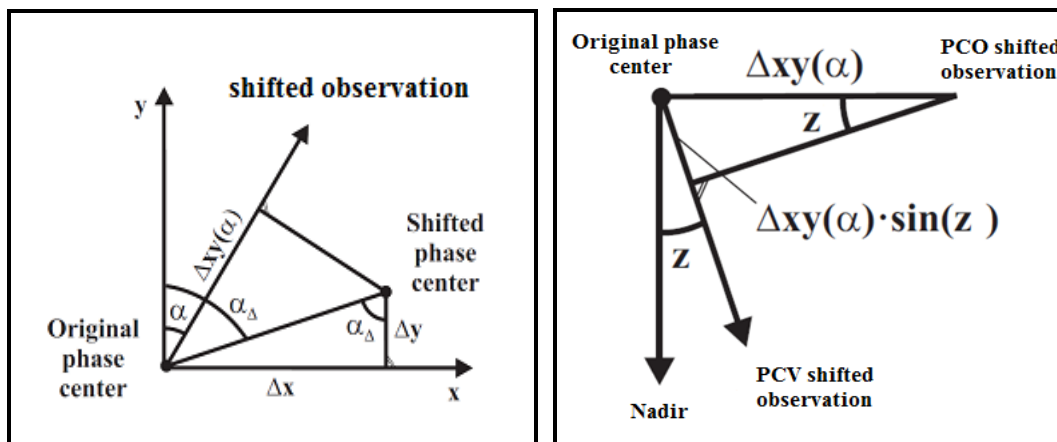se center whereas α_Δ is the azimuth angle of the shifted phase center as seen from the original phase center. Also, Δx and Δy are the respective horizontal phase center offsets in the X and Y axis directions from its original position. An observation in the azimuth direction α, will be affected by amount $\Delta xy \, (\alpha)$, due to PCO as follows:

$$\Delta xy \, (\alpha) = \sqrt{\Delta x^2 + \Delta y^2} * \cos \, (\alpha_\Delta - \alpha). \qquad 3.16$$

Likewise, an observation will be shifted by $\Delta \phi \, (z, \alpha)$, due to PCV as follows:

$$\Delta \phi \, (z, \alpha) = \sqrt{\Delta x^2 + \Delta y^2} * \cos \, (\alpha_\Delta - \alpha) * \sin \, z. \qquad 3.17$$

The impact of the nadir angle z (Equation 3.17) in the phase center variations is zero in the nadir direction and has a maximum effect at $z_{max} \approx 14.3^0$ [Schimid et al., 2005]. Alternatively, the absolute phase center corrections can be derived from relative values using the corrected values of the reference antenna [Schmid et al., 2007].

$$PCO_{abs} = PCO_{rel} + [PCO_{abs} \, (AOAD/M\_T) - PCO_{rel} \, (AOAD/M\_T)], \qquad 3.18$$

$$PSV_{abs} = PSV_{rel} + [PSV_{abs} (AOAD/M\_T)]. \qquad 3.19$$

In equations above PCO_{abs}, PCO_{rel} are the respective relative and absolute PCO of the calibrated antenna whereas $PCO_{abs} \, (AOAD/M\_T)$, $PCO_{rel} \, (AOAD/M\_T)$ are the respective absolute and relative PCO of the reference antenna. Also, PSV_{abs}, and PSV_{rel}, are the respective absolute and relative PCV of the antenna to be calibrated whereas $PSV_{abs} (AOAD/M\_T)$ is the absolute PCV of the reference antenna.

3.4.5 Advantages of GPS receiver absolute phase center model

Past studies on regional and global networks to quantify the impact of azimuth and elevation dependent phase center biases have shown that the use of absolute phase centers is GPS processing is inevitable. Studies by Ge et al. [2005], Schmid et al.[2005; 2007] just to name a few, have demonstrated that the use of absolute phase centers have many advantages when mixing results derived by GPS data processed with different receiver and satellite antenna calibration models especially over long baselines. Examples of them include the following:

1. Absolute antenna model avoids systematic errors over long baselines

2. Repair of the discontinuities in the GPS weekly time series (e.g. GPS week 1400). Discontinuities tend to be problematic in rescaling the covariance information and make a proper interpretation of the results during the IGS solutions combination process [Ferland and Piraszewski, 2009].

3. Allows antenna calibrations below 10° elevation and therefore low elevation GPS data can be used with less error impact on both height and scale

4. Reduce/eliminate the dependence of reference antenna and its coordinates

5. Separates the multipath effect from PVCs; the two are correlated

6. At global solutions it reduce the scale drift of between GPS and ITRF solutions (~ 15 ppb) and provide better consistency in orbit and reference frames solutions [Dach et. al., 2007, pp. 327].

4. SUMMARIES OF PROCESSING RESULTS

This chapter presents the results of different research activities and is divided into four main sections. The first section presents the LSSA and LS coherent analysis results in both position and residuals domain for the selected stations without considering the impact of atmospheric pressure loading (APL) corrections.

The second part covers the discussion on different types of APL results. It starts with the general overview of APL impact on the Earth crustal deformation followed by discussions about the different types of APL models and sources of corrections that are presently available. Thereafter, comparison results between the two geophysical APL models that use parameters from the NCEP are presented. This comparison forms the basis of the adoption of the APL corrections from the GGFC model for this research.

The third section presents the LSSA spectra results of both position and residuals with and without the impact of APL corrections. Based on the results on sections two and three, two baselines were selected and processed using Bernese software v5.0.

The fourth section covers the results on Bernese processing starting with a brief summary of the fifteen years daily solutions based on the selected baselines. The daily solutions were generated using models and clean datasets as close as possible to the ones used by the IGS Analysis Centers. Also in this section, is the comparison results between the computed weekly solutions and the IGS REPRO1 weekly solutions have been presented. To conclude the chapter, the results of LSSA and LS coherent analysis of the computed positions with and without APL corrections are presented.

4. 1 LSSA Results on REPRO1 Data without APL

This section presents the results of the LSSA and least squares (LS) coherent analysis based on position and residuals domains for all stations under study without APL corrections. Figures 4.1 and 4.2 below present the respective position and residuals logarithmic plots of the LS coherent spectrum for station DRAO (1994-2010). In both plots, the top plot panels present the respective vertical component spectra and the bottom plot panels present the respective horizontal spectra component. In both figures, the vertical axis is the logarithm of percentage variance and the horizontal axis is number of cycles per year and CL stands for confidence level.
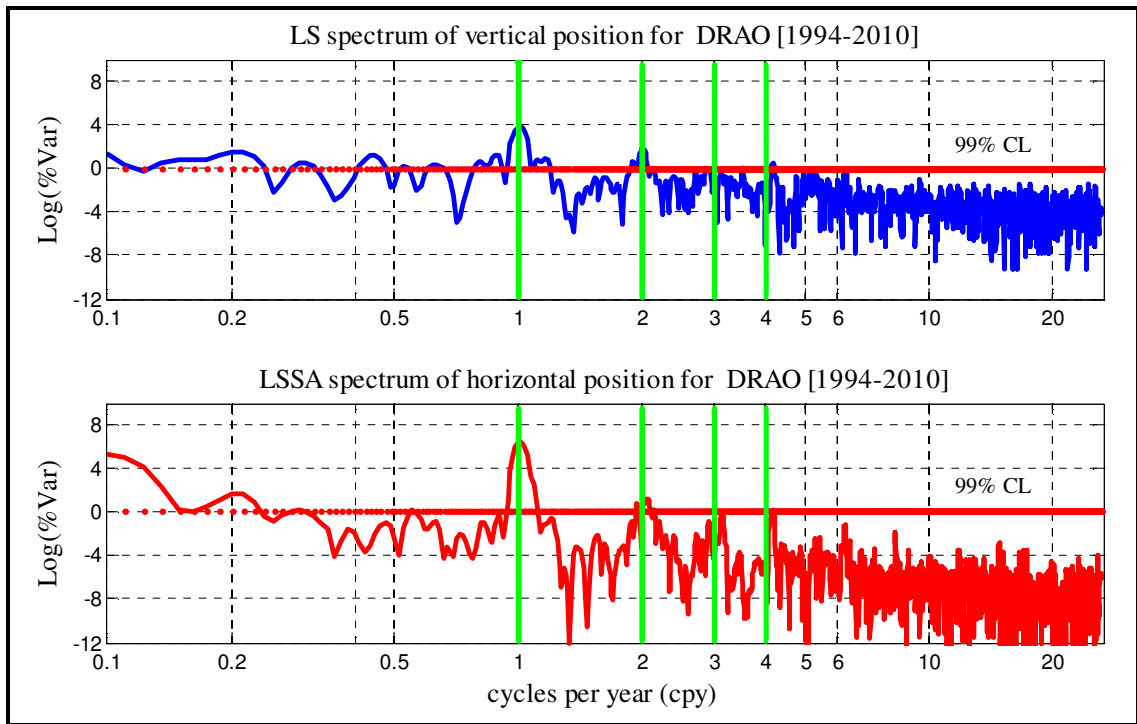
Figure 4.1 LS Spectra of Horizontal and vertical positions of station DRAO
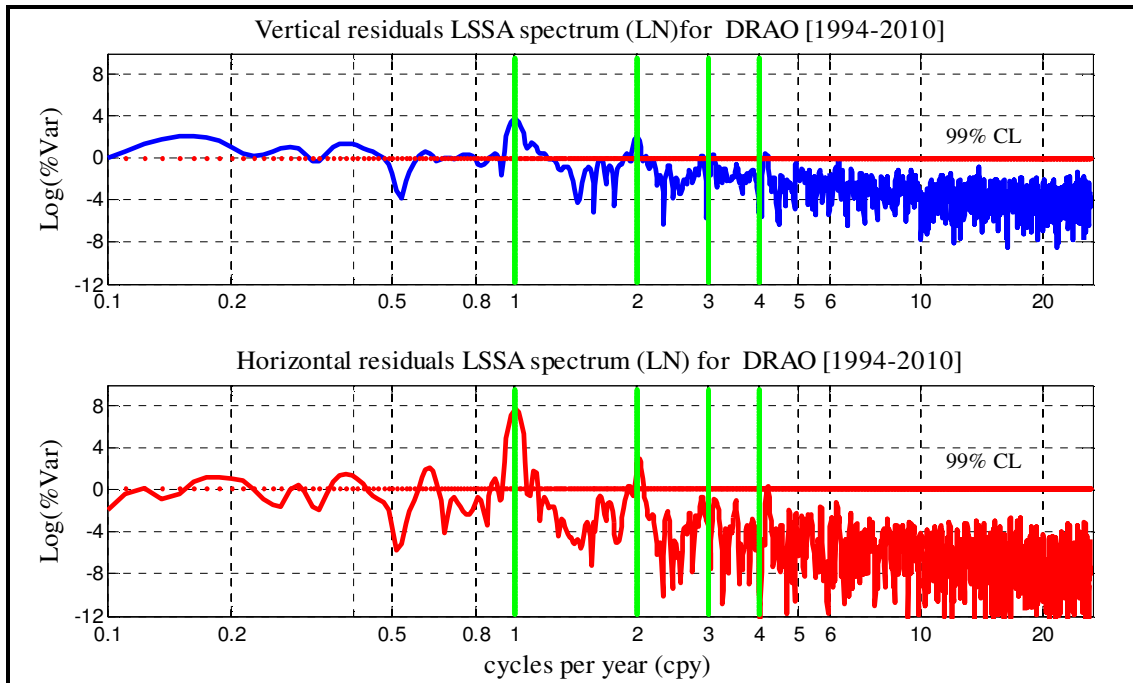
Figure 4.2 LS Spectra of Horizontal and vertical residual of station DRAO

From the LS spectra results shown in Figures 4.1 and 4.2 above, the existence of spectral peaks in both position and residuals domain of station DRAO is evident. A similar finding was made in respect of all twenty seven (27) stations under study, and most of them are predominant around the first to fourth draconitic harmonic level with respective periods of 1, 2, 3 and 4 cycles per year. Based on this finding, the spectral peaks at the first to fourth harmonics were thereafter extracted rigorously from the LS coherent spectra of the positions and residuals. Furthermore, the statistical data of the extracted peaks (percentage variance) in both vertical positions and residuals have been summarized in Figures 4.3 and 4.4 respectively. Figure 4.5 presents the results for the horizontal positions. In Figures 4.3, 4.4 and 4.5, the vertical axis is the percentage variance and the horizontal axes represent the first to the fourth dracotinic harmonics for each station, and they are indicated in different colors for easy clarification.

Figure 4.3 Spectral peaks in the vertical positions without APL at first harmonic (H1), second harmonic (H2), third harmonic (H3) and fourth harmonic (H4) . The vertical axis is the percentage variance and the horizontal axis represents the stations.

Figure 4.4 Spectral peaks in the vertical residuals without APL at first harmonic (H1), second harmonic (H2), third harmonic (H3) and fourth harmonic (H4). The vertical axis is the percentage variance and the horizontal axis represents the station.
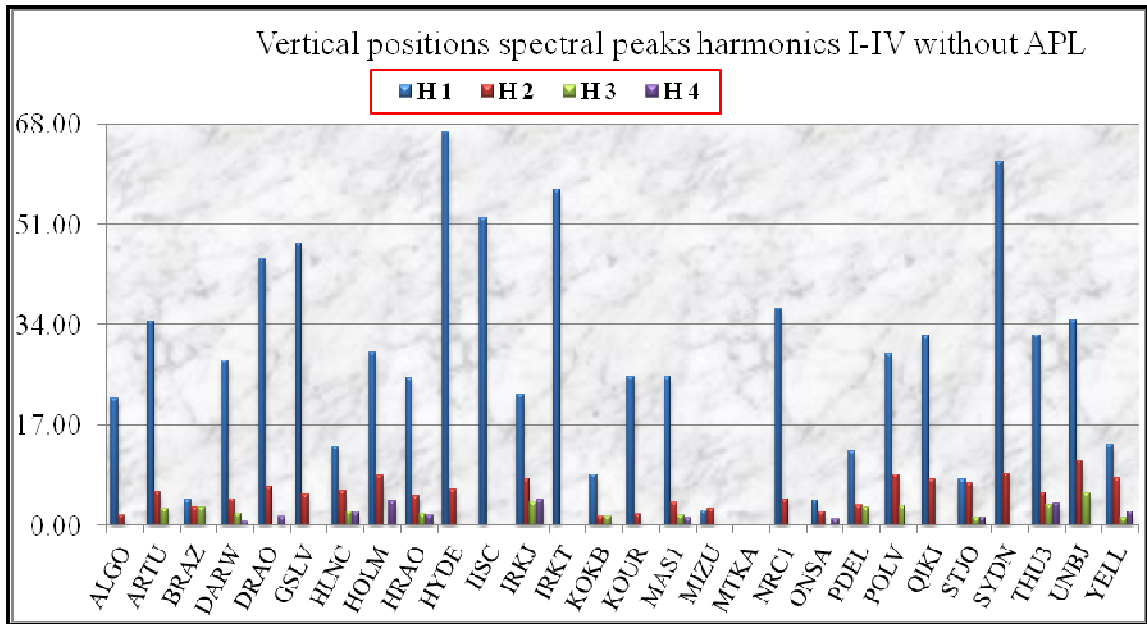
91

Figure 4.5 Spectral peaks in the horizontal positions without APL at first harmonic (H1), second harmonic (H2), third harmonic (H3) and fourth harmonic (H4) . The vertical axis is the percentage variance and the horizontal axis represents the stations.
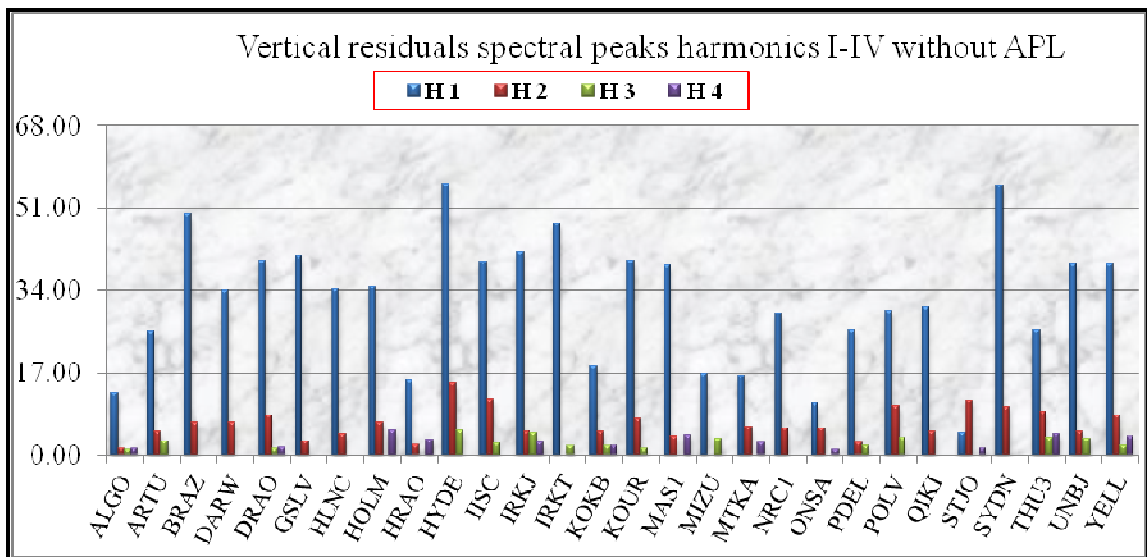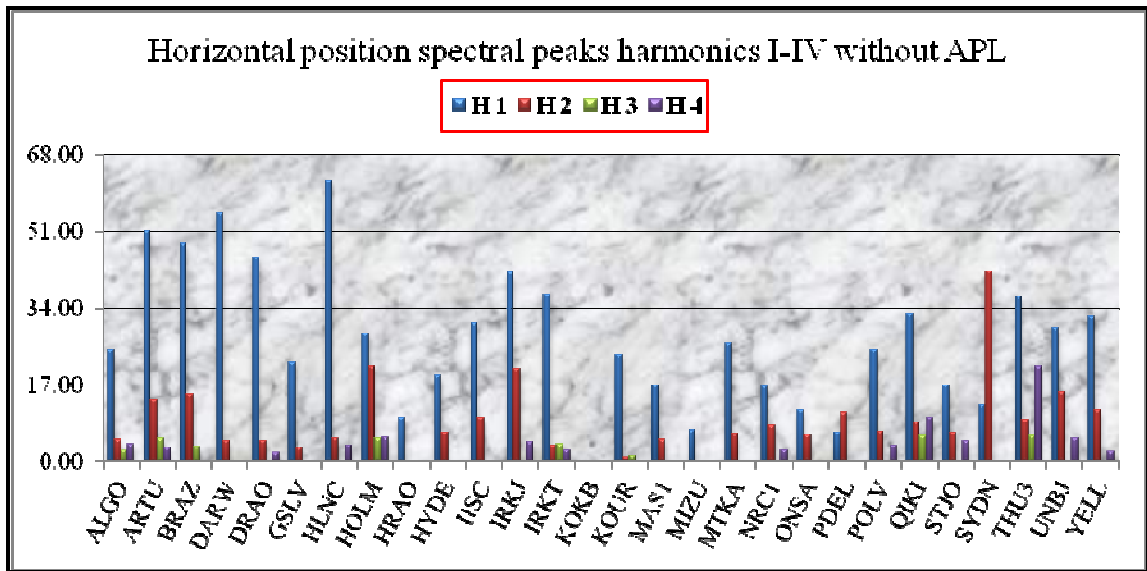
4.1.1 Observations on LS spectral results of REPRO1 solutions

Based on the LS spectral results, we have observed the existence of spectral peaks in both vertical and horizontal positions as well as residuals, that are statistically significant at the 99 percent confidence level; and they have different strengths from one station to the other. Overall, the peaks in the vertical positions and residuals are much stronger as compared to the peaks in the horizontal positions and residuals. Furthermore, the peaks in the position domain appear to be stronger as compared to signals in the residual domain and as expected the spectral peaks first harmonic are generally the strongest as compared to others. The annual spectral peaks in vertical position for HYDE, IRKT, SYDN, GSLV and DRAO appear to be comparatively the strongest.

The presence of spectral peaks in the position domain suggests the existence of un-quantified amount of apparent station motions, which are harmonic in nature for most of the stations under study. The motions could be attributed to the real motion of the ground and the impacts of un-modelled and miss modelled (to some extent) geophysical phenomena in the present REPRO1 solutions. Likewise, the presence of spectral peaks in the residual domain could be largely attributed to the miss modelled effects; that is, different limitations in the functional and stochastic models that are used to model the observed parameters in the REPRO1 solutions generation process. Consequently, the partial mitigated geophysical phenomena such as un-modeled tidal signals and miss-modelled GPS orbits may be propagated into longer-period signals. Similar observations were made by Penna and Stewart [2003], Penna et al. [2007],

Collilieux et al. [2007] and King et al. [2008]. Examples of the phenomena include the following:

a)   The impacts of geopotential model miss modelling effects. The present REPRO1 solutions adopted EGM1996 [Lemoine et al., 1998] as the conventional geopotential model along with the respective values of C_{20}, C_{21} and S_{21} (and their time derivatives) to describe the position of Earth's rotational axis. These model parameters are known to have some limitations and therefore they have been revised as per chapter six of the IERS 2010 conventions [Petit and Luzum, 2010]. For that reason the IGS has recently adopted EGM2008 as the conventional geopotential model along with new model parameters and therefore the orbit estimation process will also be impacted. However, the orbits and the resulting estimated parameters such as the GPS station coordinates and residuals are presently adjusted together in the IGS solution generation process. It follows that some of the miss modelled effect will be embedded in the estimated solutions and may cause apparent positional displacements and they may likely appear as part of the observed spectral peaks in the positional domain.

b)   The impact of the miss modelled effects of antenna phase center variation model. The REPRO1 solutions adopted the IGS05.ATX as the absolute center variation model, though the level of consistency between the IGS05 frame and IGS05.atx were yet to be properly determined [Ray, 2009]. Moreover, some of the station receivers used in the processing were still based on relative phase center offsets and variations. Furthermore, no absolute model was available for the azimuthal satellite corrections. Such anomalies

are likely to affect the estimated parameters and they may as well appear as part of the observed positional spectral peaks at different harmonic levels.

c)   The impact of un-modelled tidal loading displacements. There exist a number of both tidal and non-tidal loading forces that are known to impact GPS solutions. Examples of them are the S_1 and S_2 atmospheric tides and ocean pole tides for the tidal forces as well as the atmospheric pressure loading, ocean bottom pressure and surface hydrology for the non-tidal forces. However, they were not considered in the REPRO1 generation process because the IERS was yet to recommend any model for those loading types by the time of the first reprocessing campaign. Such omission will likely cause un-quantified amount of apparent position displacements and may appear as part of the spectral peaks in the LSSA spectra of the position domain.

d)   The impact of the IGS solution combinations process. Like other IGS solutions, REPRO1 solutions were generated based on weekly normal equations from the individual IGS Analysis Centers using the SINEX software[36] based on procedures outlined in section 3.3. However, this approach is based on scaling of the covariance information from different Analysis Centers under the un-realistic assumptions that the past ACs solutions are independent and error free. Furthermore, the current approach to impose constraints for detecting outliers and discontinuities is not very efficient. Therefore, the discontinuities in the cumulative solutions of the IGS station(s)

---

[36]   The IGS is currently developing the next-generation IGS product combination system (ACC2.0) which will be capable of finding outliers and discontinuities in the time series in a more robust way.

coordinates, which are sometimes hardly detectable especially when they are short, are not well documented in the station logs [Ferland and Piraszewski, 2009]. Such inconsistencies are likely to cause un-quantified amount of apparent motion in the final GPS positions that could appear as the positional domain spectral peaks. Such peaks could therefore be wrongly interpreted as short term anomaly and vice versa.

e)   The impact of high-order ionosphere effects. In the REPRO1 generation process. The IGS Analysis Centers did not model ionosphere effects; instead they eliminated the first-order effect by forming the ionosphere-free linear combination of L1 and L2. Furthermore, no attempt was made to deal with the second and the third order effects which are likely to impact the resulting solutions and may as well appear as part of the spectral peaks in both positional and residual domain.

f)   The impact of the miss modelling effect in GPS attitude models. It is known that the horizontal satellite antenna offsets are highly correlated with the orbital elements depending on the position of the Sun with respect to the orbital plane [Schmid et al., 2005; 2007]. It follows that the accuracy of the estimated horizontal offsets as well as the IGS products will as also depend on the behaviour of the attitude control of the GPS satellites and the orientation of the orbital planes with respect to the elevation of the sun. Furthermore, the secular precession of the ascending node $\dot{\Omega}$ of a satellite orbit is directly related to its inclination [Montenbruck and Gill, 2000]; [Langley, 2007]. This is illustrated by Equation 4.1 below in which T, a, i, R_e and J_2 are respectively the orbital period, semi-major axis, inclination, radius of the Earth and the oblateness.

$$\dot{\Omega} = -3\pi \frac{J_2}{T} \left(\frac{R_e}{a}\right)^2 .\cos \; i.$$ 4.1

It follows that, the secular precession of the ascending node (as per Equation 4.1) will cause a drift of the GPS node in space by about -14.16^0 per year, primarily because of the oblateness effect. Consequently, this effect will make the time period T_R between the same orientations of the orbital planes with respect to the Sun shorter than one year; this period is also known as the GPS "draconitic" year is and illustrated in Equation 4.2 below:

$$T_R = \frac{2\pi}{2\pi - \dot{\Omega}_{GPS} .1 year} 365.25 \, days \approx 351.51 \, days .$$ 4.2

It follows that the periods of $T_R, T_{R/n}, n = 2,....,6$ respectively correspond to 351.51, 175.76, 117.17, 87.88, 70.30 and 58.59 days. Within a range of ± 14 days (±0.04 CPY), the above draconitic periods are highly correlating to the average spectral periods of 364.93, 181.51, 119.43 and 88.35 days that have been observed in this research at the first to sixth harmonics for most of the stations understudy. This observation is in a close agreement to previous spectral studies by Collilieux et al. [2007] and Ray et al. [2008]. The strong correlation between the observed and the draconitic periods suggests that some of this effect may be embedded in final solutions and show up as the apparent positional displacements and may appear as spectral peaks of the positional domain at the said harmonics levels. Likewise, they may as well show up as spectral peaks in the residual domain spectra as part of the miss modelled satellite effect.

4.2 Atmospheric Pressure Loading on REPRO1 Position and Residuals

Atmospheric pressure loading (APL) is the deformation of the earth's crust as a result of the temporal variations of pressure systems over the Earth caused by air mass movements between the continents and ocean, as well as basin-wide air pressure signals. Studies by Rabbel and Zschau [1985], Rabbel and Schuh [1986], Van Dam and Wahr [1987], and Manabe et al. [1991] have shown that, the surface deformations due to the observed synoptic pressure systems have greater impact on higher latitude sites as compared to mid-latitude sites, low latitudes and locations within 500 km of the sea or ocean. This variation is a result of more intensive weather systems on higher latitude sites. Based on the above studies, the maximum vertical displacement is about 25 mm whereas the maximum horizontal displacement is about one third of the former. Figure 4.6 illustrate the maximum vertical and horizontal APL positional displacements on IGS stations under study from 1994 to 2010, based on the GGFC model.
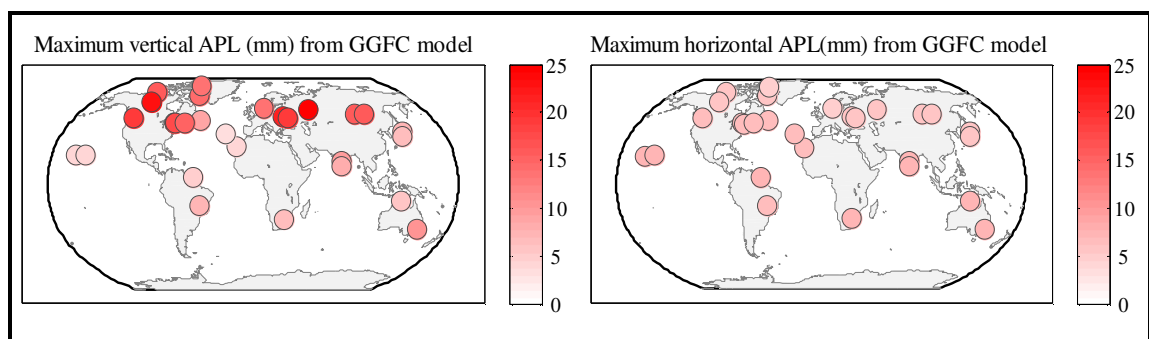

Figure 4.6 Left panel presents the maximum vertical APL displacements; right panel are the maximum horizontal APL displacements in millimetres (1994-2010) for the selected stations. The APL displacements are based on the GGFC model.

Darwin [1982] was the first who realized that APL can cause station deformation to the level of several centimeters, and based on that he proposed a simple model for its computation. However, despite this earlier finding and further illustrations, the impact of atmospheric pressure loading were still thought to be insignificant and have been ignored in the processing procedures of GPS positions along with other types of loading, such as snow, soil moisture and ground water, as well as ocean bottom pressure despite the knowledge of their existence. Following increase in precision of space geodetic techniques, recent different studies have demonstrated that GNSS position time series can show considerable sensitivity to the station displacement due to atmospheric pressure loading [Van Dam et al., 1994; 2001; Petrov and Boy, 2004; Tregoning and Watson, 2009; Van Dam et al., 2010]. However, despite the above observations and many others regarding the impact of APL on GNSS positions, the present REPRO1 solutions do not account for APL displacements because the IERS was yet to recommend any APL processing model at the time of their generation. Moreover, the IERS was yet to establish a particular approach on how these surface displacements should be accounted for. So far, the possible approaches are correction (reduction) at the time of making observations (observational level) or applying time-averaged values corrections to the coordinates after the analysis of the observations as well as solving of regression factors between station displacements and the local pressure values. The last two approaches are implemented at the positional level. Likewise, the hydrological surface loads, the ocean bottom pressure, snow and soil moistures were not applied due to lack of sufficient models [Blewitt et al., 2002; McCarthy and Petit, 2003].

4.2.1 Sources of APL corrections

In recent years, the computation of atmospheric loading corrections with respect to the center of mass of the total Earth (solid Earth, oceans and atmosphere) are done by different institutions using different approaches. The computed corrections can be applied directly on station coordinates, at position-level during data analysis or used for solving the regression factors between the local pressure and the station displacement have been applied so far. Based on McCarthy and Petit [2003, pp. 85), the there are three basic methods for computing APL corrections to geodetic data. The first approach use geophysical models or simple approximations derived from these models based on data from numerical weather models and the second approach use empirical models based on site-dependent data. The third approach is based on hybrid models, which are the combination of first two models. The three approaches are summarized as follows:

4.2.2 APL corrections from geophysical models

Currently, the estimation process of the vertical and horizontal APL corrections using standard geophysical model is the most reliable method and can be computed in a standardized way for any point on the Earth's surface more or less instantaneously. Under this approach, the computation of the APL corrections is done using different atmospheric models that are developed based on data from numerical weather models determined by various institutions. For that reason they have different spatial resolutions

depending on which model and hypotheses have been adopted. Currently there are three models that are based on the geophysical approach. They are NASA Goddard Space Flight Center Space Geodesy Branch (GSFC) model [Petrov and Boy, 2004], the IERS Global Geophysical Fluids Center (GGFC) model [Van Dam et al., 2002] and the Institute of Geodesy and Geophysics (IGG) model [Wijaya et al., 2010]. The APL computations from the first two models are based on numerical whether model from the National Center for Environmental Prediction (NCEP) operational pressure data sets for the inverted barometer and the non-inverted barometer ocean models. The IGG model is based on data from European Center for Medium-Range Weather Forecasts (ECMWF). The APL corrections estimation process using the standard geophysical models are done as the convolution process of an appropriate Farrell's (1972) Greens function with the global surface pressure field from NCEP or ECMWF. The NCEP surface pressure fields are usually provided grid files (2.5^o x 2.5^o) with six (6) hour time resolution. Likewise, the ECMWF surface pressure fields are also provided in grid files (2.0^o x 2.5) every six (6) hours. Based on illustrations by Petrov and Boy [2004], the vertical displacement u_r and horizontal displacement u_h at a station with coordinates $\vec{r}$ induced by surface pressure variations $\Delta P(\vec{r}',t)$ at epoch t are given as follows:

$$u_r(\vec{r},t) = \iint \Delta P(\vec{r}',t) G_R(\phi) \cos\varphi \, d\lambda d\varphi, \qquad\qquad 3.1$$

$$u_h(\vec{r},t) = \iint \vec{q}(\vec{r},\vec{r}') \Delta P(\vec{r}',t) G_H(\phi) \cos\varphi \, d\lambda d\varphi. \qquad\qquad 3.2$$

In equations 3.1 and 3.2, G_R, G_H are the respective vertical and horizontal Green functions, φ, λ are the respective geocentric latitude and longitude whereas ϕ is the angular distance between the station and the pressure source with coordinates $\vec{r}'$.

Usually the vertical and horizontal Green functions used for the estimation process in Equations 3.1 and 3.2, are based on Love numbers up to a high spherical harmonic degree (such as $n = 9000$). Such computations use a spherically symmetric, non-rotating, elastic and isotropic Earth model based on Preliminary Reference Earth Model (PREM) elastic parameters [Petrov and Boy, 2004]. However, the downside of this approach includes the requirement of a global pressure data set with short sampling intervals, low pressure data resolution and the uncertainties in the Green's functions and uncertainties in the ocean response model [McCarthy and Petit, 2003, pp.85].

4.2.3 APL corrections from empirical models

In this approach, crustal motion due to atmospheric loading are computed based on the reliable site-dependent pre-determined regression coefficients. The site-dependent coefficients are obtained from fitting the local pressure variations to geodetic observations over a prolonged period. Because of that, this approach should be expected to produce better results compared to the geophysical approach. However, this approach has a number of limitations. Examples of them includes the inability to extrapolate the regression coefficients to a new site (for which no data exist), and the regression coefficient can only be used for vertical crustal motions. For more limitations of this approach the reader is referred to McCarthy and Petit [2003, pp. 85].

4.2.4 APL correction from hybrid approach

This approach computes the loading displacements by the use of regression coefficients as is the case with the empirical approach. However, this approach attempts to overcome the limitations on lack of site-dependent local geodetic pressure observations. It does so by using the geophysical model to compute the regression coefficients for station displacement. Under this approach, the vertical deformation caused by the change in pressure, can be given in terms of a local pressure anomaly and thereafter used to compute the regression coefficients. The down side of this approach is the uncertainty in the Green's function and the quality of the air pressure data affect the quality of the determined regression [McCarthy and Petit 2003, pp. 85-86].

4.2.5 APL corrections adopted for this research

This research has adopted APL correction from the Global Geophysical Fluids Center model. Presently there are two sets of APL corrections that are based on NCEP parameters and all of them are provided at six hours sampling rate. It was therefore necessary to compare the GSFC and the GGFC models at six hours sampling rate for all stations under study as a basis of selection of one APL source that would be the appropriate in the study. It is also worth mentioning that, the IGS REPRO1 values that have been used in this study are provided in weekly values. In order to assess the impact of APL it was therefore necessary to concatenate the APL datasets into weekly mean

APL values. Thereafter, a comparison APL values between the GGFC and GSFC models were as well done at weekly (7 days) sampling rate in respect all stations under study. Figures 4.7 to 4.9 below present respective illustrations of the comparison results between the two models for station STJO (Up component), HYDE (North component) and STJO (East). The three stations have the maximum differences in the indicated APL components, amongst the stations under study. In each plot, the top panel corresponds to comparisons at six (6) hours sampling rate and the bottom panel corresponds to the comparisons of the mean weekly comparisons. The mean weekly APL values were concatenated from the six hours APL.

Figure 4.7 Top is the difference in the vertical APL between the GSFC and GGFC models at six hours rate for STJO. Bottom plot is the respective weekly differences

Figure 4.8 Top is the difference in the North APL between the GSFC and GGFC models

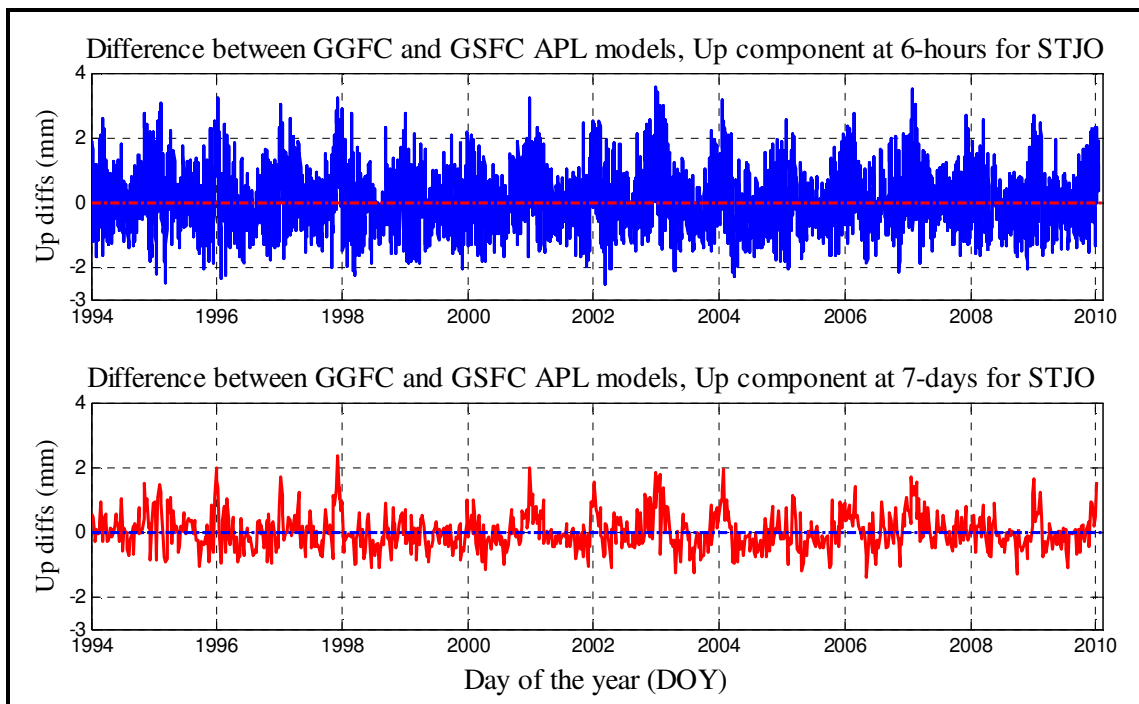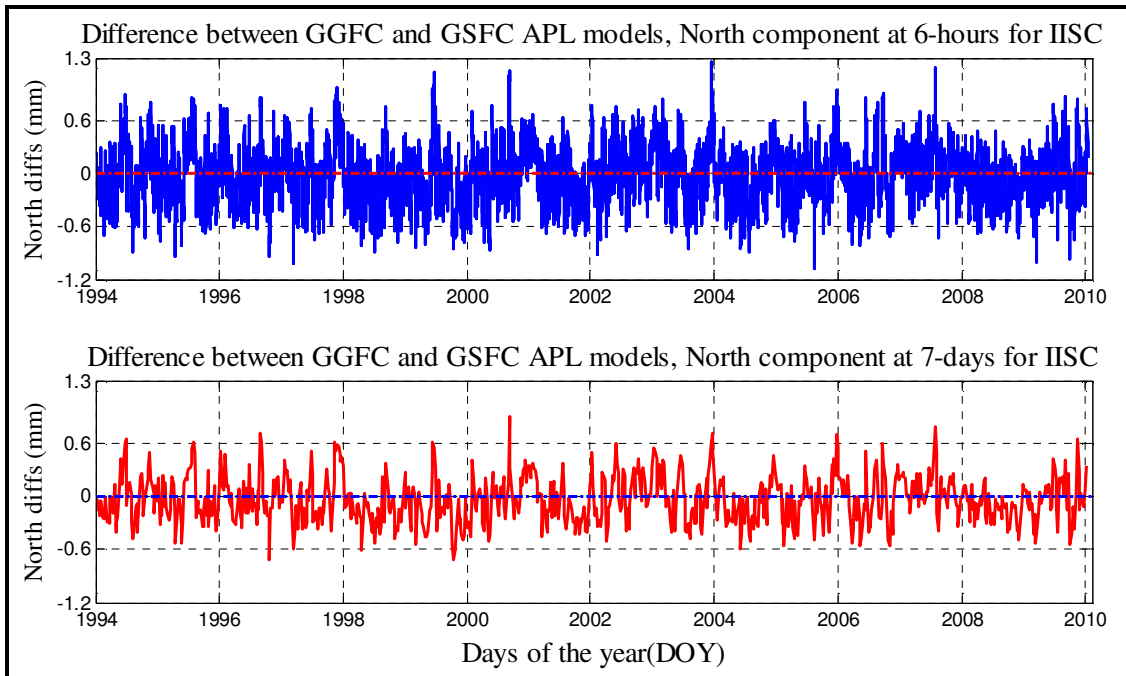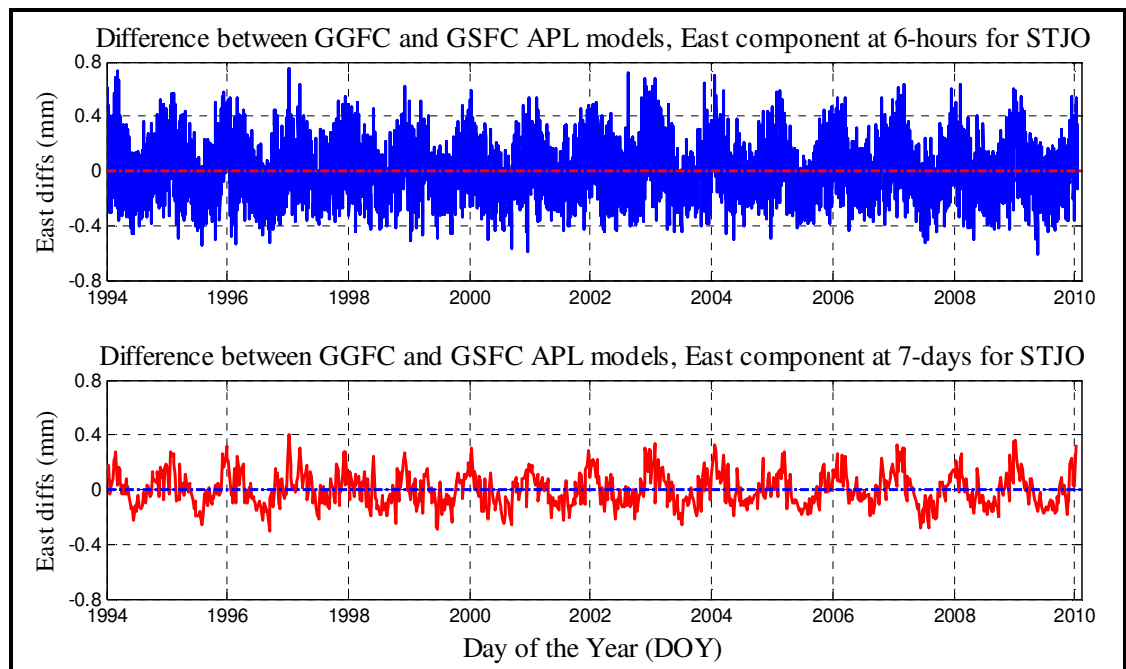at six hours sampling rate for HYDE. Bottom plot is the respective weekly differences

Figure 4.9 Top is the difference in the East APL between the GSFC and GGFC models

at six hours sampling rate for STJO. Bottom plot is the respective weekly differences

It was observed that, the difference between the two models is too small to have any significant impact in the choice of APL modelling for most of the twenty seven (27) stations under study; similar observation was made by van Dam et al. [2003]. The only significant differences at six hours sampling rate were observed at stations STJO in Canada and HYDE in India; with respective maximum differences in the Up and North components of 3.566457 mm and 1.254189 mm. Station STJO was also found to have the maximum difference in East component of 0.746316 mm. Furthermore, we found and removed outlier in Up APL components from stations measurements on 20 August, 2002 for stations HYDE and IISC in India with respective values of 3.789439 mm and 3.130496 mm. The Global overview of the maximum differences between the GGFC and GSFC models and other statistical information of the differences is provided in Figures 4.10-4.18. Tables 4.1 and 4.2 tabulate the differences and the statistical information of the differences between the two models for all stations under study.

Figure 4.10 Plot of the maximum differences in the vertical APL between the GSFC and GGFC models 1994-2010. Blue bars are the maximum differences at six hours rate whereas red bars are the maximum differences seven days (weekly) sampling rate .

106

Figure 4.11 Plot of the maximum differences in the north APL between the GSFC and GGFC models 1994-2010. Blue bars are the maximum differences at six hours rate whereas red bars are the maximum differences seven days (weekly) sampling rate .
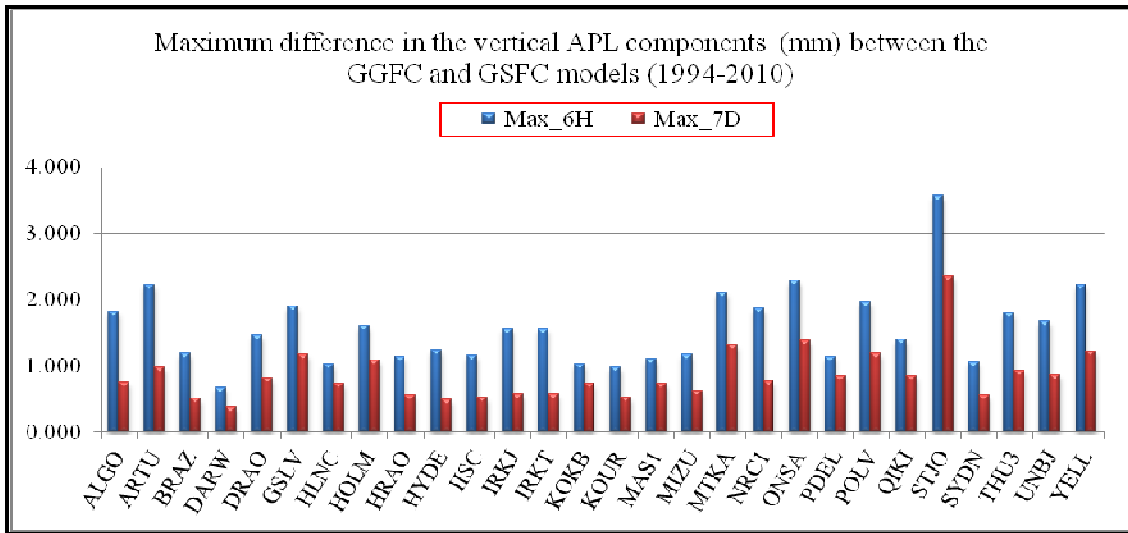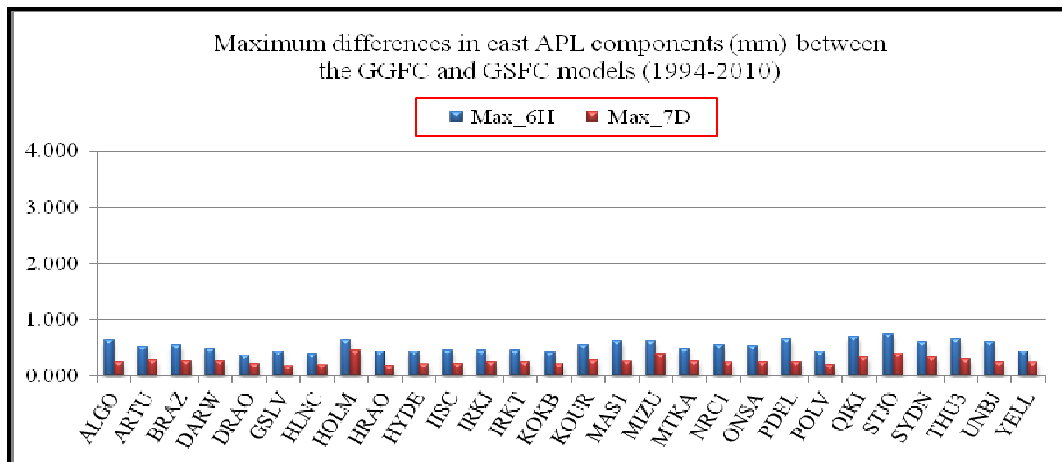

Figure 4.12 Plot of the maximum differences in the east APL between the GSFC and GGFC models 1994-2010. Blue bars are the maximum differences at six hours rate whereas red bars are the maximum differences seven days (weekly) sampling rate .
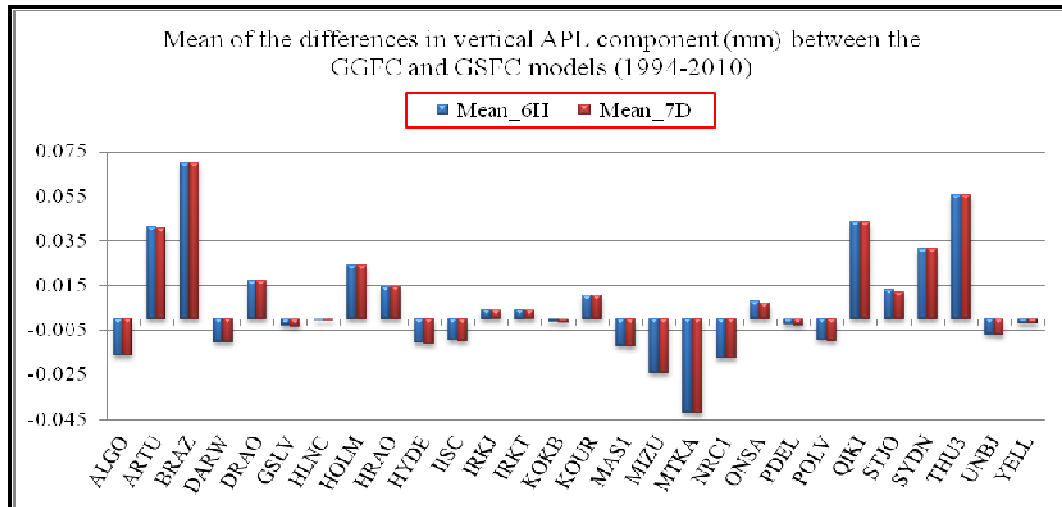
Figure 4.13 Plot of mean of the differences in the vertical APL between the GSFC and GGFC models 1994-2010. Blue bars are the mean of the differences at six hours rate whereas red bars are the mean of the differences weekly sampling rate.
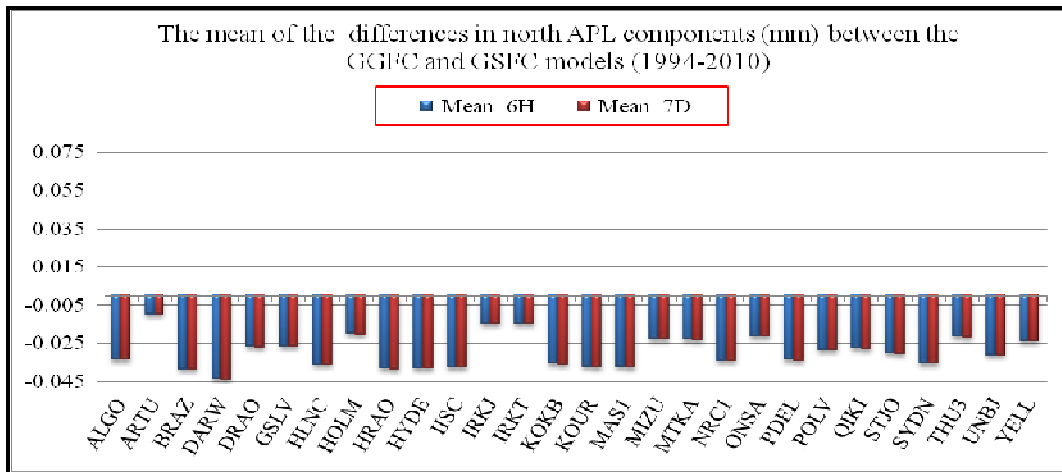
Figure 4.14 Plot of mean of the differences in the north APL between the GSFC and GGFC models 1994-2010. Blue bars are the mean of the differences at six hours rate whereas red bars are the mean of the differences weekly sampling rate.
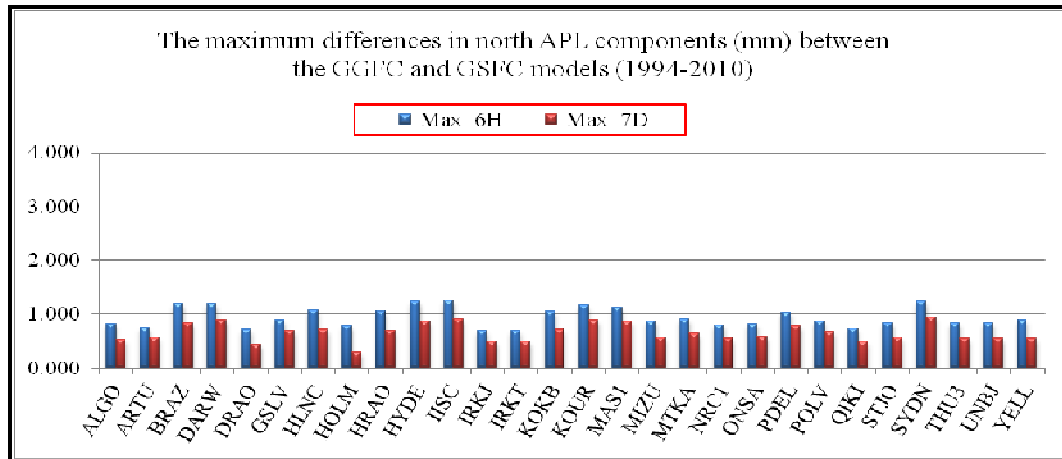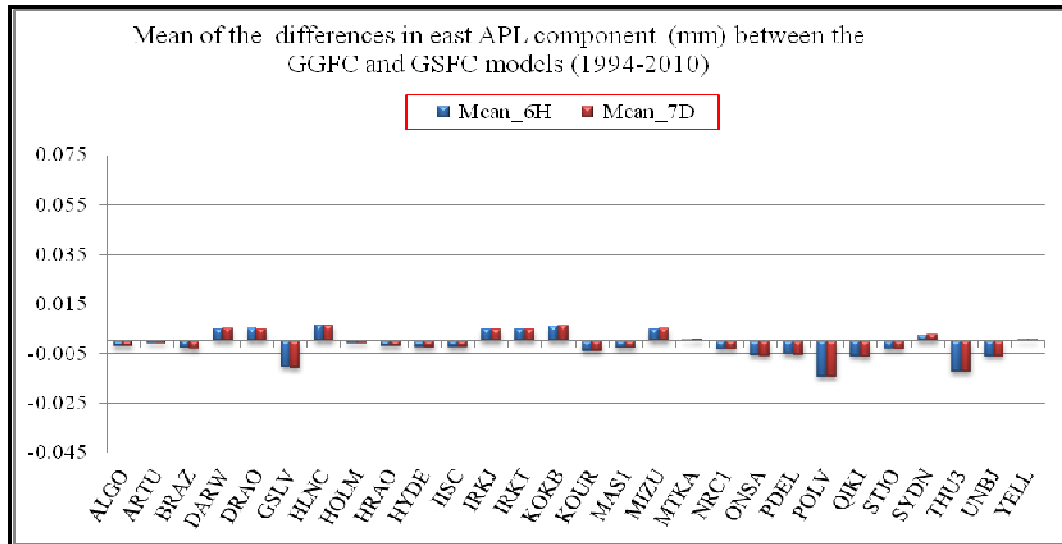
Figure 4.15 Plot of mean of the differences in the east APL between the GSFC and GGFC models (1994-2010). Blue bars are the mean of the differences at six hours sampling rate whereas red bars are the mean of the differences weekly rate.

Figure 4.16 Plot of the standard deviation of the differences in the vertical APL between the GSFC and GGFC models (1994-2010). Blue bars are the six hours standard deviations whereas red bars are the standard deviations at weekly rate.

Figure 4.17 Plot of the standard deviation of the differences in the north APL between the GSFC and GGFC models (1994-2010). Blue bars are the six hours standard deviations whereas red bars are the standard deviations at weekly sampling rate.
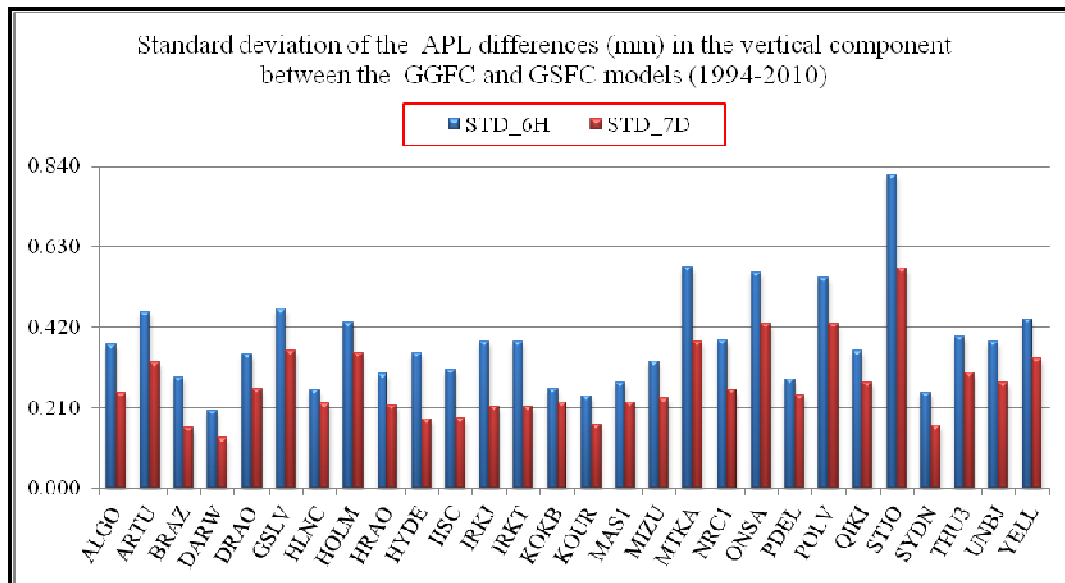

Figure 4.18 Plot of the standard deviation of the differences in the east APL between the GSFC and GGFC models (1994-2010). Blue bars are the six hours standard deviations whereas red bars are the standard deviations at weekly sampling rate.
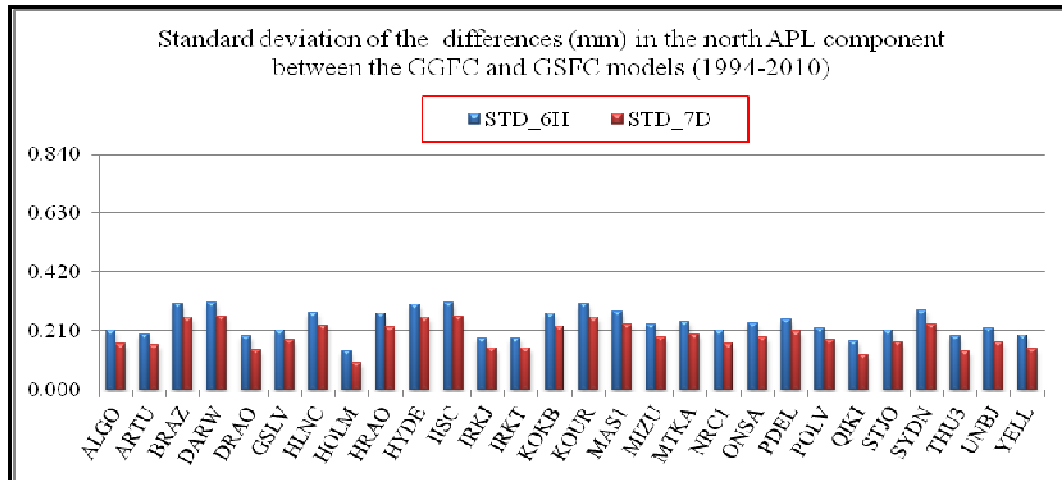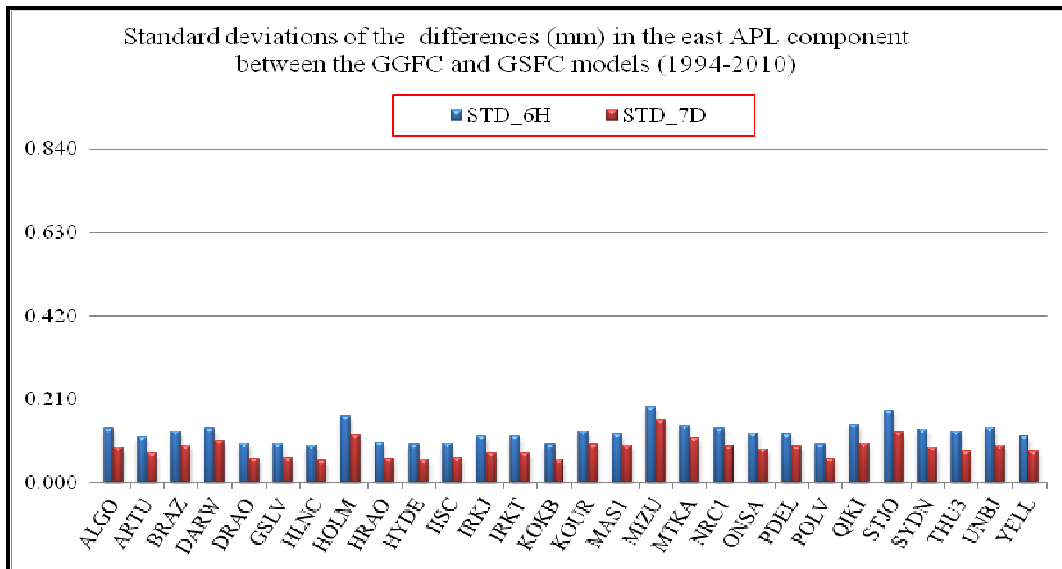
Tables 4.1 and 4.2 below, provide the tabulated summary of the differences and the statistical information of differences between the GGFC and the GSFC models for all stations under study at six hours and weekly (7 days) sampling rates, respectively for the 1994 to 2010 period. In both tables, column one gives the station names and column two shows the APL components in which U stands for vertical component, N is the north component and E is the east component. Column three and four show the respective maximum and minimum differences between the two models in millimeters. Column four provides the mean of the differences whereas column five provides the standard deviations of the differences and all of them are in millimeters.

Table 4.1 Six hours APL comparison between GSFC and GGFC models (1994–2010)

Station	APL	Maximum (mm)	Minimum (mm)	Mean(mm)	St. Dev(mm)
ALGO	U	1.821900	-1.579749	-0.016393	0.374309
	N	0.817522	-0.781231	-0.033509	0.212718
	E	0.639020	-0.488474	-0.001849	0.134852
ARTU	U	2.224578	-2.446426	0.041385	0.460501
	N	0.750959	-0.761781	-0.009940	0.198685
	E	0.515897	-0.463993	-0.000863	0.115057
BRAZ	U	1.186109	-1.198854	0.069945	0.290887
	N	1.197150	-1.065937	-0.038472	0.308178
	E	0.549714	-0.460016	-0.003024	0.128420
DARW	U	0.665311	-0.802182	-0.010392	0.201588
	N	1.203462	-1.087635	-0.043901	0.310763
	E	0.487511	-0.637796	0.004824	0.136531
DRAO	U	1.465623	-1.359115	0.017165	0.350291
	N	0.714971	-0.753111	-0.026645	0.191269
	E	0.360943	-0.408377	0.004945	0.099164
GSLV	U	1.906520	-1.688374	-0.002866	0.467990
	N	0.883522	-0.872216	-0.026545	0.214927
	E	0.428909	-0.394369	-0.010616	0.097979
HLNC	U	1.025225	-0.936075	-0.000701	0.257825
	N	1.062585	-0.949123	-0.036036	0.276674
	E	0.393784	-0.379709	0.006347	0.092990

Table 4.1 Six hours APL comparison between GSFC and GGFC models - continued

HOLM	U	1.613310	-1.470140	0.023975	0.433204
	N	0.773566	-0.597676	-0.020079	0.140336
	E	0.647110	-0.741161	-0.000940	0.165803
HRAO	U	1.138193	-1.010779	0.014564	0.299239
	N	1.047887	-0.969744	-0.038207	0.273084
	E	0.437405	-0.409738	-0.001918	0.100202
HYDE	U	1.230242	-1.556740	-0.010735	0.352710
	N	1.235980	-1.052485	-0.038033	0.305053
	E	0.440165	-0.453831	-0.002519	0.096430
IISC	U	1.162065	-1.444332	-0.009524	0.309571
	N	1.254189	-1.078272	-0.037562	0.310893
	E	0.456225	-0.415454	-0.002377	0.098571
IRKJ	U	1.555759	-1.449710	0.004095	0.383593
	N	0.696396	-0.659594	-0.015007	0.186310
	E	0.450778	-0.519408	0.004808	0.117674
IRKT	U	1.555759	-1.449710	0.004095	0.383593
	N	0.696396	-0.659594	-0.015007	0.186310
	E	0.450778	-0.519408	0.004808	0.117674
KOKB	U	1.033297	-0.939165	-0.001244	0.259691
	N	1.056925	-0.946884	-0.035745	0.274103
	E	0.413983	-0.372745	0.006062	0.094798
KOUR	U	0.981001	-0.991606	0.010666	0.240773
	N	1.164503	-1.100358	-0.037110	0.309466
	E	0.548618	-0.490953	-0.003843	0.128469
MAS1	U	1.101161	-0.977941	-0.011900	0.276099
	N	1.126992	-0.971414	-0.037233	0.280831
	E	0.624941	-0.412113	-0.002873	0.122626
MIZU	U	1.165741	-1.639759	-0.024049	0.331266
	N	0.872490	-0.870705	-0.022751	0.232883
	E	0.622271	-0.733611	0.004855	0.190992
MTKA	U	2.105336	-3.134811	-0.042087	0.576037
	N	0.899996	-0.882882	-0.023173	0.243221
	E	0.485077	-0.682821	0.000399	0.143481
NRC1	U	1.869790	-1.440533	-0.017543	0.384556
	N	0.793201	-0.812524	-0.033989	0.211999
	E	0.562188	-0.543768	-0.003390	0.136989
ONSA	U	2.293477	-2.099710	0.007777	0.563173
	N	0.809215	-1.039350	-0.021217	0.238426
	E	0.538232	-0.509667	-0.005733	0.122993
PDEL	U	1.133474	-0.933800	-0.002587	0.285050
	N	1.034951	-0.864250	-0.033637	0.251101
	E	0.661407	-0.423030	-0.005320	0.121501

Table 4.1 Six hours APL comparison between GSFC and GGFC models - continued

POLV	U	1.966298	-1.937414	-0.009579	0.549944
	N	0.865351	-0.800905	-0.028304	0.218485
	E	0.432523	-0.480369	-0.014294	0.095896
QIKI	U	1.399427	-1.297380	0.043578	0.357547
	N	0.728948	-0.658429	-0.027731	0.173389
	E	0.694022	-0.519378	-0.006229	0.144385
STJO	U	3.566457	-2.542907	0.013000	0.817845
	N	0.835960	-0.813017	-0.030164	0.213727
	E	0.746316	-0.609196	-0.003156	0.181079
SYDN	U	1.057375	-1.310753	0.031409	0.248848
	N	1.234093	-0.947567	-0.035428	0.284454
	E	0.607780	-0.735095	0.002484	0.134343
THU3	U	1.798613	-1.324036	0.055681	0.396330
	N	0.841465	-0.843909	-0.021577	0.191478
	E	0.662890	-0.551646	-0.012584	0.127948
UNBJ	U	1.667870	-1.448748	-0.006956	0.382715
	N	0.827391	-0.897711	-0.031044	0.218682
	E	0.612824	-0.526169	-0.006135	0.138018
YELL	U	2.214260	-1.701263	-0.001925	0.440750
	N	0.891123	-0.800064	-0.023795	0.197313
	E	0.444212	-0.434671	0.000519	0.116384
NB: Results are in six decimal places to conform to the original data format.					

Table 4.2 Weekly APL comparison between GSFC and GGFC models (1994–2010)

Station	APL	Max (mm)	Min (mm)	Mean (mm)	St. Dev (mm)
ALGO	U	0.748267	-0.682339	-0.016581	0.248779
	N	0.534669	-0.512438	-0.033705	0.163970
	E	0.258554	-0.279248	-0.001855	0.087951
ARTU	U	0.976525	-0.947515	0.040868	0.328941
	N	0.571801	-0.484213	-0.009973	0.162137
	E	0.284049	-0.246697	-0.000885	0.075238
BRAZ	U	0.502041	-0.357535	0.069805	0.158204
	N	0.835120	-0.730292	-0.038805	0.259507
	E	0.276257	-0.268673	-0.003140	0.094442
DARW	U	0.377385	-0.394372	-0.010501	0.131619
	N	0.883850	-0.749027	-0.044253	0.260923
	E	0.274228	-0.301592	0.004955	0.105846
DRAO	U	0.823370	-0.648914	0.016919	0.258335
	N	0.436768	-0.456744	-0.026883	0.144514
	E	0.222354	-0.155725	0.004912	0.060787
GSLV	U	1.176444	-1.158772	-0.003364	0.358482
	N	0.690623	-0.529966	-0.026632	0.178085
	E	0.177255	-0.181386	-0.010756	0.061677
HLNC	U	0.727283	-0.617392	-0.000998	0.222296
	N	0.717473	-0.685978	-0.036356	0.229740
	E	0.195844	-0.163403	0.006427	0.056131
HOLM	U	1.089498	-1.008642	0.023721	0.351451
	N	0.299180	-0.351907	-0.020291	0.098979
	E	0.449231	-0.332342	-0.001021	0.119863
HRAO	U	0.554622	-0.504731	0.014353	0.215330
	N	0.684207	-0.681056	-0.038528	0.223953
	E	0.188051	-0.202390	-0.001990	0.060698
HYDE	U	0.494548	-0.573457	-0.010971	0.179117
	N	0.877069	-0.688844	-0.038349	0.258169
	E	0.210878	-0.223373	-0.002545	0.058719
IISC	U	0.517564	-0.598786	-0.009783	0.184232
	N	0.900387	-0.711456	-0.037872	0.262298
	E	0.224161	-0.230002	-0.002385	0.063417
IRKJ	U	0.579867	-0.701013	0.003949	0.213911
	N	0.494704	-0.406775	-0.015130	0.149609
	E	0.255566	-0.245932	0.004825	0.074835
IRKT	U	0.579867	-0.701013	0.003949	0.213911
	N	0.494704	-0.406775	-0.015130	0.149609
	E	0.255566	-0.245932	0.004825	0.074835
KOKB	U	0.733789	-0.619100	-0.001544	0.223958
	N	0.707638	-0.678578	-0.036062	0.227349
	E	0.209605	-0.165329	0.006154	0.058652

Table 4.2 Weekly APL comparison between GSFC and GGFC models - continued

KOUR	U	0.527022	-0.517312	0.010456	0.167028
	N	0.890337	-0.755985	-0.037447	0.259047
	E	0.283066	-0.270621	-0.003926	0.096499
MAS1	U	0.739155	-0.656666	-0.012314	0.225316
	N	0.866812	-0.665112	-0.037473	0.235309
	E	0.262785	-0.240168	-0.003027	0.092633
MIZU	U	0.629529	-0.723102	-0.024267	0.234604
	N	0.569390	-0.579594	-0.023010	0.189037
	E	0.388866	-0.412895	0.005032	0.157492
MTKA	U	1.317409	-1.041326	-0.042362	0.381515
	N	0.643406	-0.601857	-0.023424	0.199492
	E	0.268755	-0.317745	0.000595	0.113448
NRC1	U	0.774454	-0.713948	-0.017755	0.257587
	N	0.540095	-0.519501	-0.034190	0.165399
	E	0.246457	-0.270613	-0.003401	0.091196
ONSA	U	1.388137	-1.419273	0.006928	0.430512
	N	0.585505	-0.606430	-0.021425	0.189635
	E	0.253603	-0.213801	-0.005874	0.083183
PDEL	U	0.854670	-0.695077	-0.003012	0.244593
	N	0.778871	-0.609315	-0.033847	0.208255
	E	0.258044	-0.242112	-0.005446	0.090322
POLV	U	1.181824	-1.311352	-0.009924	0.430714
	N	0.668914	-0.509722	-0.028384	0.178826
	E	0.202873	-0.192269	-0.014410	0.060586
QIKI	U	0.851046	-0.606720	0.043202	0.276070
	N	0.490323	-0.401803	-0.027907	0.127205
	E	0.342210	-0.272718	-0.006261	0.099121
STJO	U	2.356153	-1.389889	0.011763	0.573164
	N	0.572397	-0.523715	-0.030403	0.170096
	E	0.397437	-0.309760	-0.003352	0.125996
SYDN	U	0.556990	-0.429009	0.031306	0.163432
	N	0.950081	-0.706696	-0.035679	0.235112
	E	0.331801	-0.221688	0.002577	0.088931
THU3	U	0.926257	-0.744152	0.055349	0.300653
	N	0.545231	-0.462014	-0.021759	0.141287
	E	0.303942	-0.257313	-0.012551	0.079550
UNBJ	U	0.863868	-0.748216	-0.007229	0.276899
	N	0.546741	-0.553951	-0.031239	0.170607
	E	0.253204	-0.286144	-0.006125	0.093829
YELL	U	1.221289	-1.118835	-0.002012	0.337884
	N	0.555724	-0.447129	-0.024069	0.147646
	E	0.249266	-0.212516	0.000494	0.078459
NB: Results are in six decimal places to conform to the original data format.					

4.2.6 APL spectra

The present APL corrections based on geophysical models such as GGFC model are given at six hours sampling rate as illustrated on Figure 4.19 showing the APL corrections in millimeters (mm) for station HRAO. In Figure 4.19, the top panel presents the Up APL corrections, the middle panel present the North APL corrections and the bottom panel show the East APL corrections. In all three panels, the vertical axes present the APL corrections and the bottom panel present the period in days of the year.
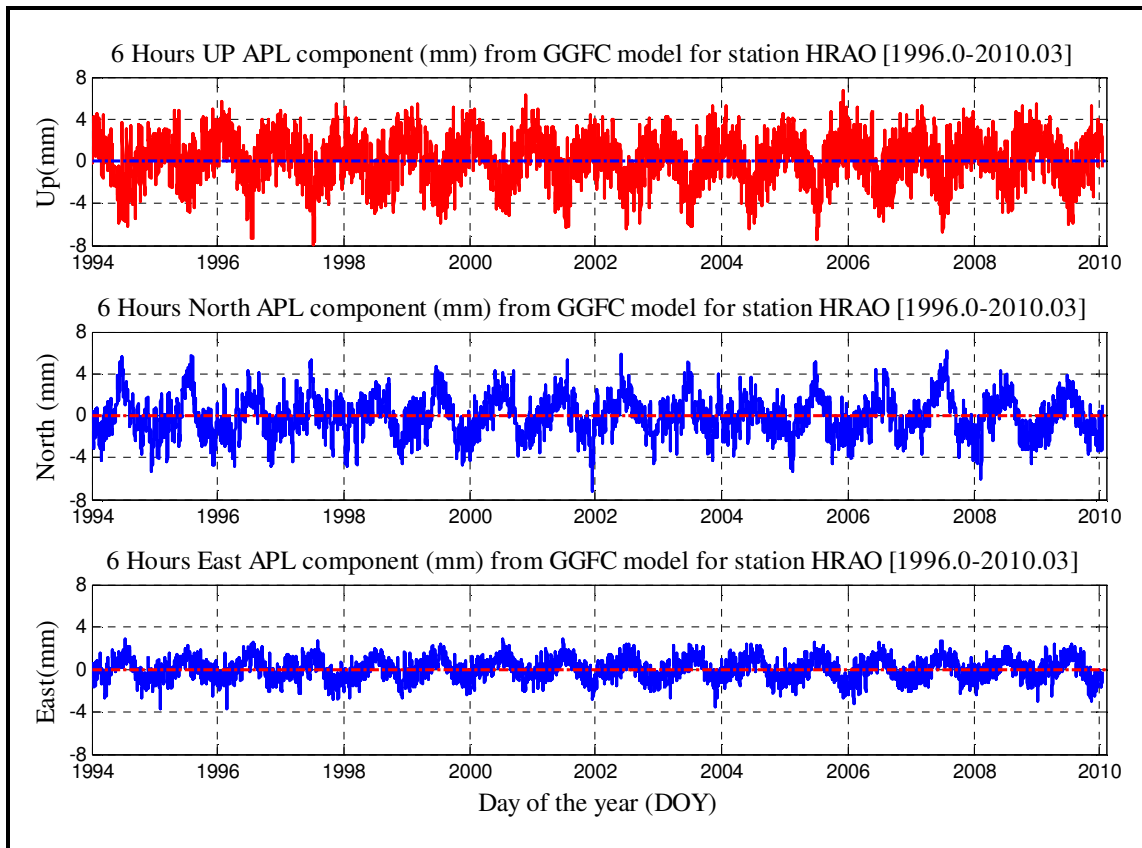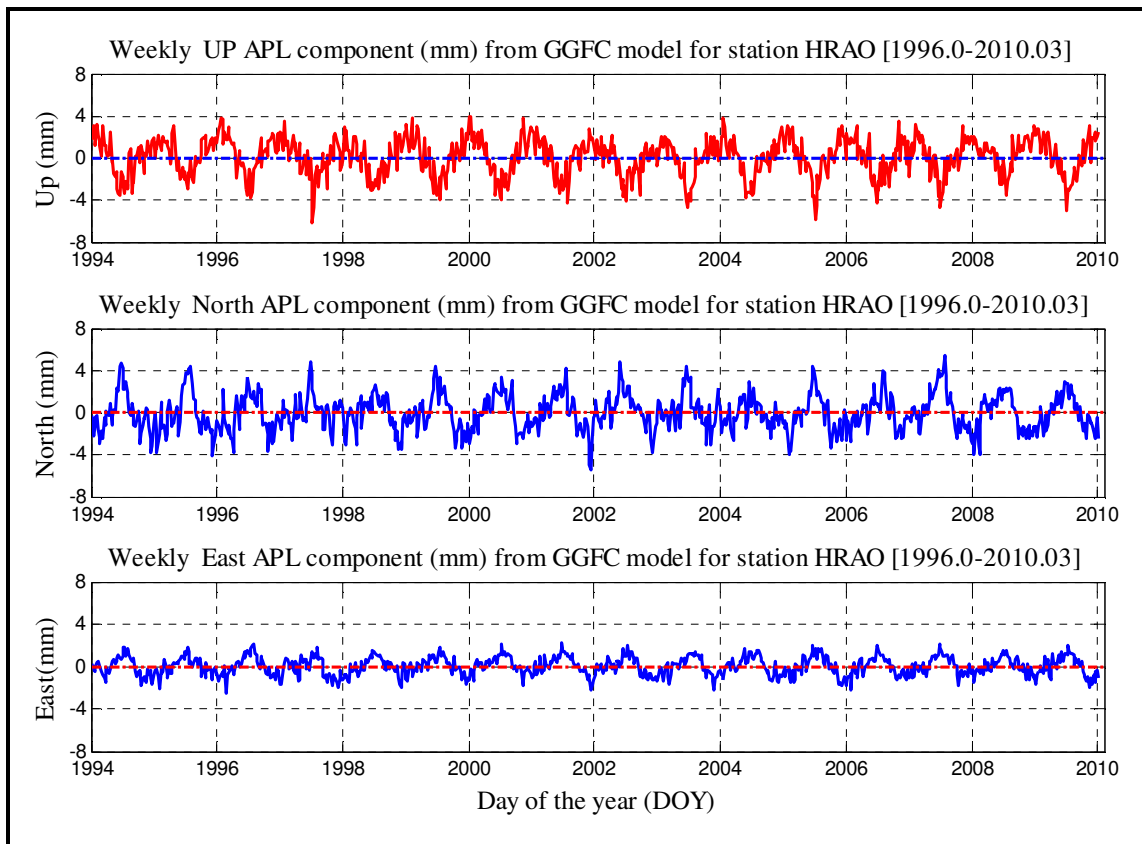

Figure 4.19 6 hours APL corrections in millimeters (mm) for station HRAO (1994-2010) based on GGFC model. The top panel corresponds to the Up APL corrections, the middle panel corresponds to the North APL corrections and the bottom panel correspond to the East APL corrections.

When a LS Spectrum is generated based on them, annual and semi-annual signals become evident as illustrated in Figure 4.20 for the station HRAO.
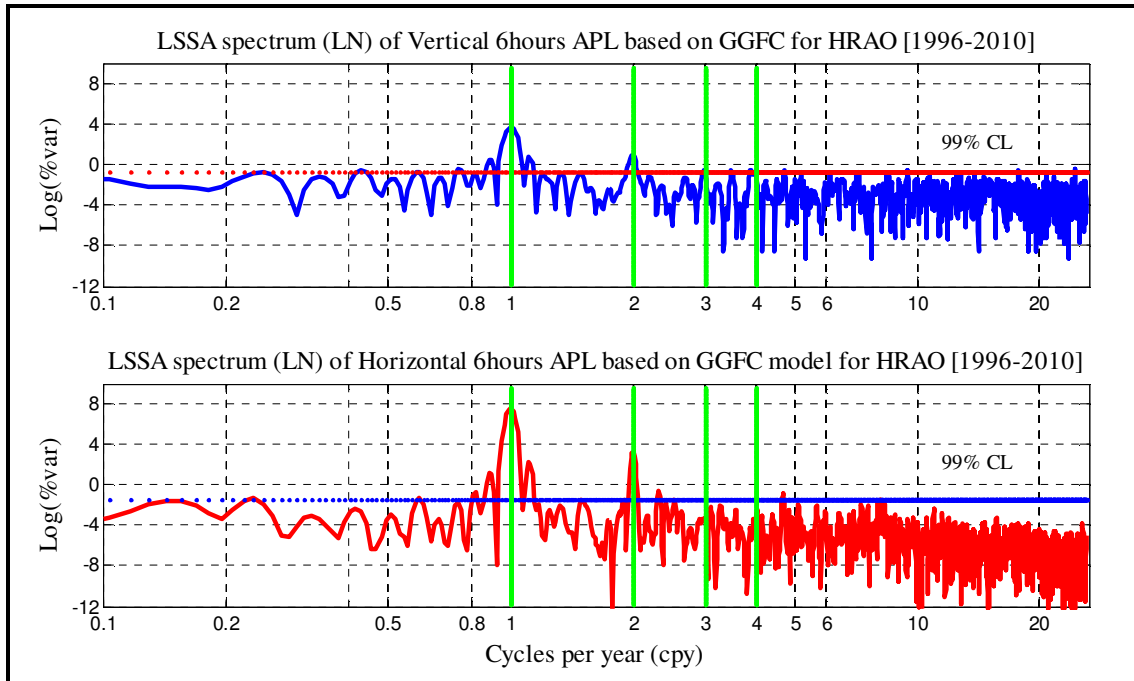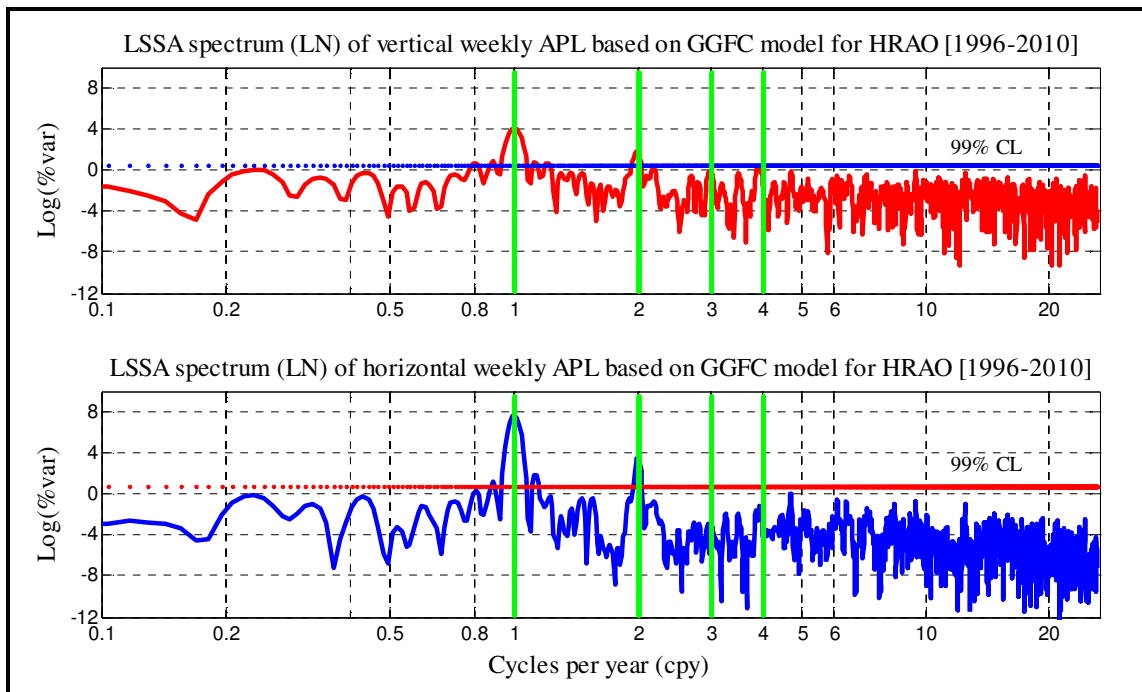

Figure 4.20 LSSA spectra of 6-hour APL correction values from GGFC model for station HRAO for 1996-2010. Top panel is the spectrum of the vertical APL corrections whereas bottom panel is the spectrum of the horizontal component APL corrections.

Thereafter, the six hours APL corrections were concatenated into mean weekly corrections in millimeters (mm) to synchronize them with the REPRO1 solutions as illustrated in Figure 4.21. In Figure 4.21 the top panel presents the mean (weekly) Up APL, the middle panel present the mean (weekly) North APL and the bottom panel show the mean (weekly) East APL corrections. In all three panels, the vertical axes present the APL corrections and the horizontal axes show the period in days of the year.

Figure 4.21 Mean (weekly) APL corrections in millimeters (mm) for station HRAO (1994-2010) based on GGFC model. The top panel corresponds to the mean (weekly) Up APL corrections, the middle panel corresponds to the mean (weekly) North APL corrections and the bottom panel correspond to the East APL corrections.

Likewise, a LS Spectrum was generated based on the concatenated weekly mean values and it was realized that, the annual and semi-annual periodic signals still remains evident as illustrated in as in Figure 4.22. Furthermore, the observed weekly signals show a close similarity to the ones observed in six hours APL spectra presented in Figure 4.20. A similar observation was made by Blewitt and Lavallee [2002], Penna and Stewart [2003] and Stewart et al. [2005]. We can conclude that the effect of APL variation within 24 hours may be significant as compared with the magnitude of the resulting daily positional displacements; a similar observation was made by Böhm et al. [2009]. Therefore, we can simply apply the APL corrections on station the weekly GPS coordinate solutions and improve coordinate repeatability.

Figure 4.22 LSSA spectra of weekly APL corrections from GGFC model for HRAO for 1996-2010. Top panel is the spectrum of the weekly vertical APL correction whereas bottom panel is the spectrum of the weekly horizontal component APL corrections.

4. 3 LSSA Results on REPRO1 Positions and Residuals with APL

This part presents an analysis on the impact of APL displacements on REPRO1 positions and residuals which was accomplished in a two steps process. We first generated the LSSA spectra of both REPRO1 positions and residuals based on the selected IGS stations without considering the impact of APL. This process was followed by analysis using the LS frequency domain multiplication of the obtained LSSA spectra segments to generate LS self-coherency spectrum based on both REPRO1 position and residuals. To complete the process, the common significant peaks were identified and extracted in a rigorous way from the LS self-coherency spectra so generated and the results have been illustrated in section 4.1 for all stations under study.

Secondly, we applied weekly mean APL corrections from the GGFC model to both REPRO1 positions and residuals followed by the generation of LSSA spectra and LS coherent spectra. To achieve this objective, the 6 hours APL corrections were first concatenated into weekly mean values to synchronize them with weekly REPRO1 values prior to their application, as discussed in section 3.2. However, it is worth mentioning that, like other IGS weekly solutions, the REPRO1 weekly coordinates and residuals are provided in geocentric Cartesian coordinate system. For the purpose of this study it was therefore necessary to transform them into equivalent geodetic values in an iterative approach based on predefined thresholds prior to LSSA. Likewise, their respective standard deviations were transformed into their equivalent geodetic values using appropriate rotational matrices. On the other hand; the up, north and east APL corrections were conceived to be respective coordinate displacement in the local

geodetic coordinate system as Δh, $\Delta \phi$ and $\Delta \lambda$ in metric units, and therefore had to be transformed to their equivalent curvilinear geodetic values before their application. The vertical displacements Δh were presumed to be normal to the reference ellipsoid and needed no transformation. The north and east displacements were transformed to their respective values $d\phi$ and $d\lambda$ in the curvilinear geodetic coordinate system as in Equations 4.1 and 4.2 using the radius of curvature in the prime meridian, M and the radius prime vertical N, prior to be applied to the REPRO1 solutions.

$$d\phi = \frac{\Delta \phi}{M},$$

4.1

$$d\lambda = \frac{\Delta \lambda}{N \cos \phi},$$

4.2

The final results of the LSSA spectra and LS coherent spectra for station UNBJ have been illustrated in Figures 4.23 and 4.24 whereas Figures 4.25 and 4.26 present the results for station HRAO. In all four plots, the top panels correspond to the plots of the vertical position spectra and the bottom panel are the spectra plots for the horizontal positions. Also, the spectra results without APL corrections (red plots) and spectra results with APL correction (blue plots) have been plotted together for easy reference with the 99 percent confidence level (CL) being shown using a red horizontal line. The vertical green lines represents the first, second, third and fourth draconitic harmonics. Furthermore, the plots have been produced using a logarithmic scale in order to have a better overview of the results in a single plot.
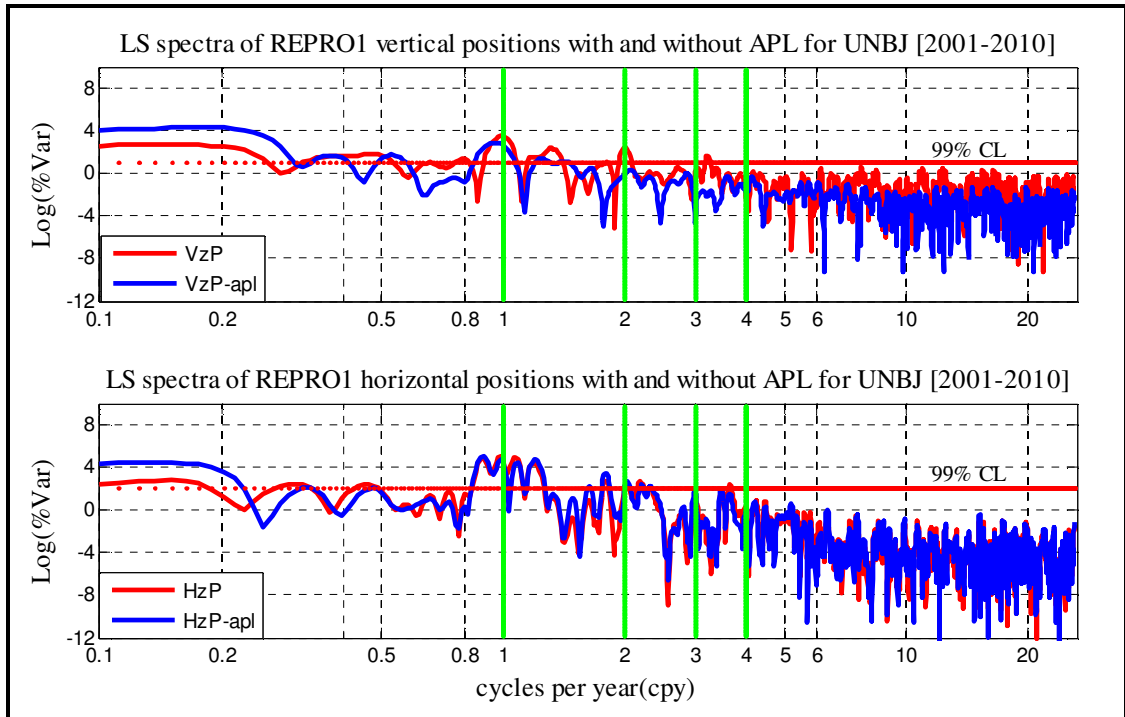
Figure 4.23 Least squares coherent spectra of REPRO1 positions with (blue) and without (red) APL for UNBJ (2001-2010).
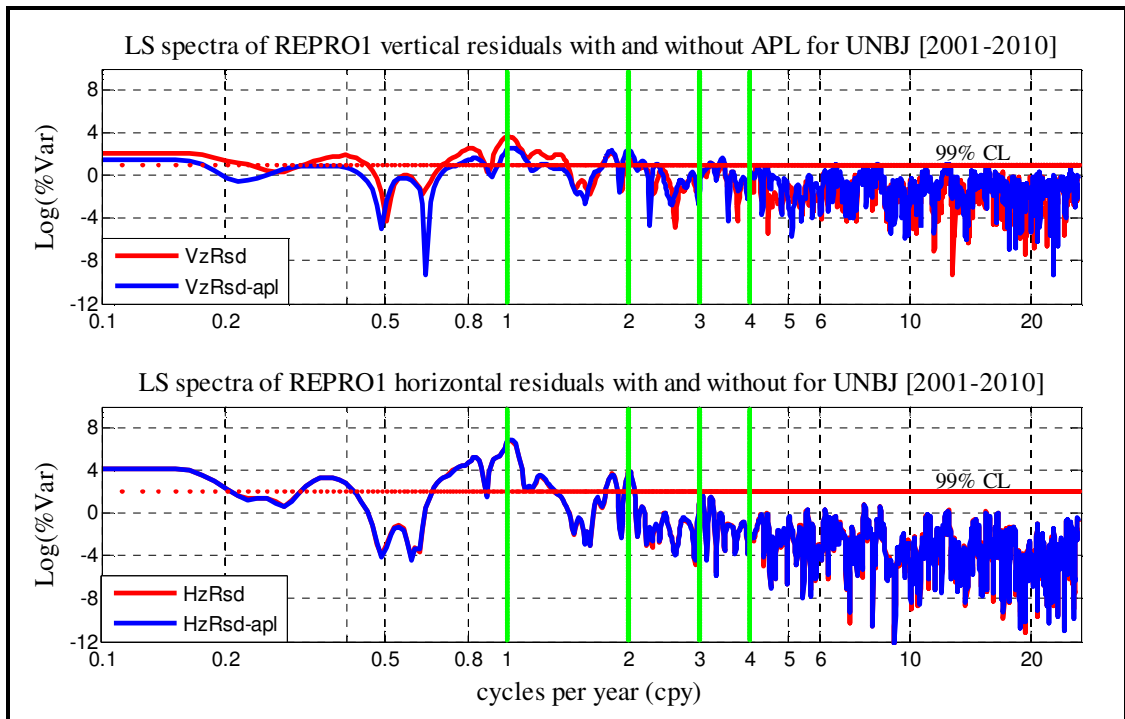

Figure 4.24 Least squares coherent spectra of REPRO1 residuals with (blue) and without (red) APL for UNBJ (2001-2010).
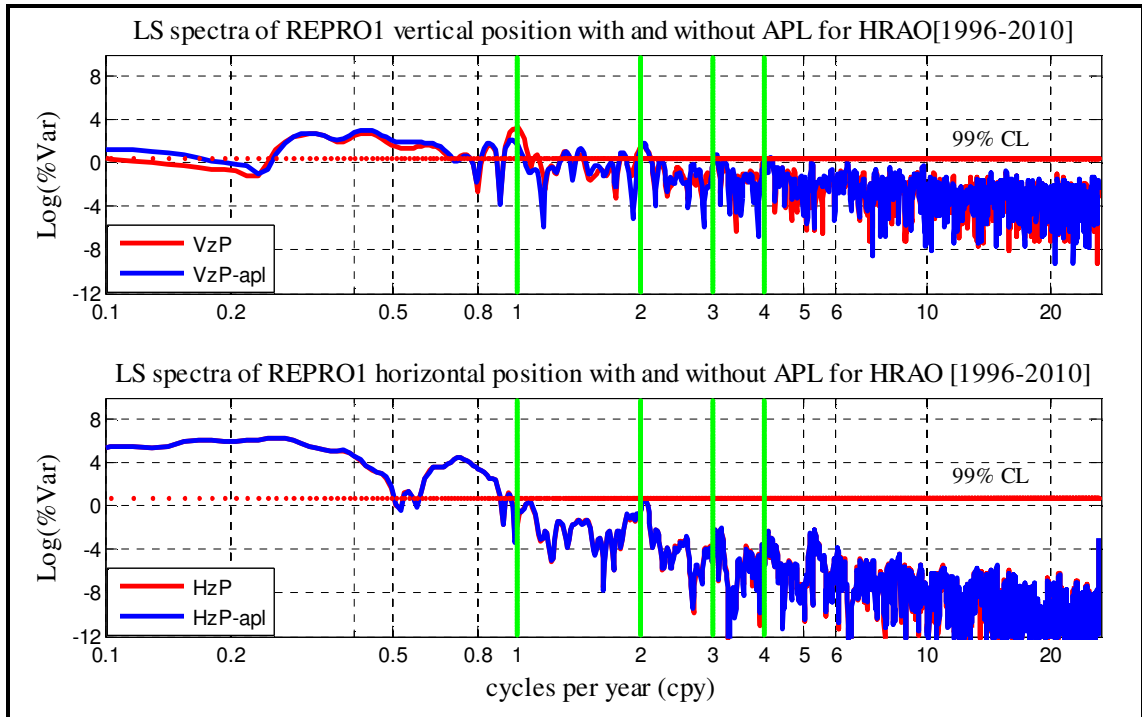
Figure 4.25 Least coherent squares spectra of REPRO1 position with (blue) and without (red) APL for HRAO (1996-2010).
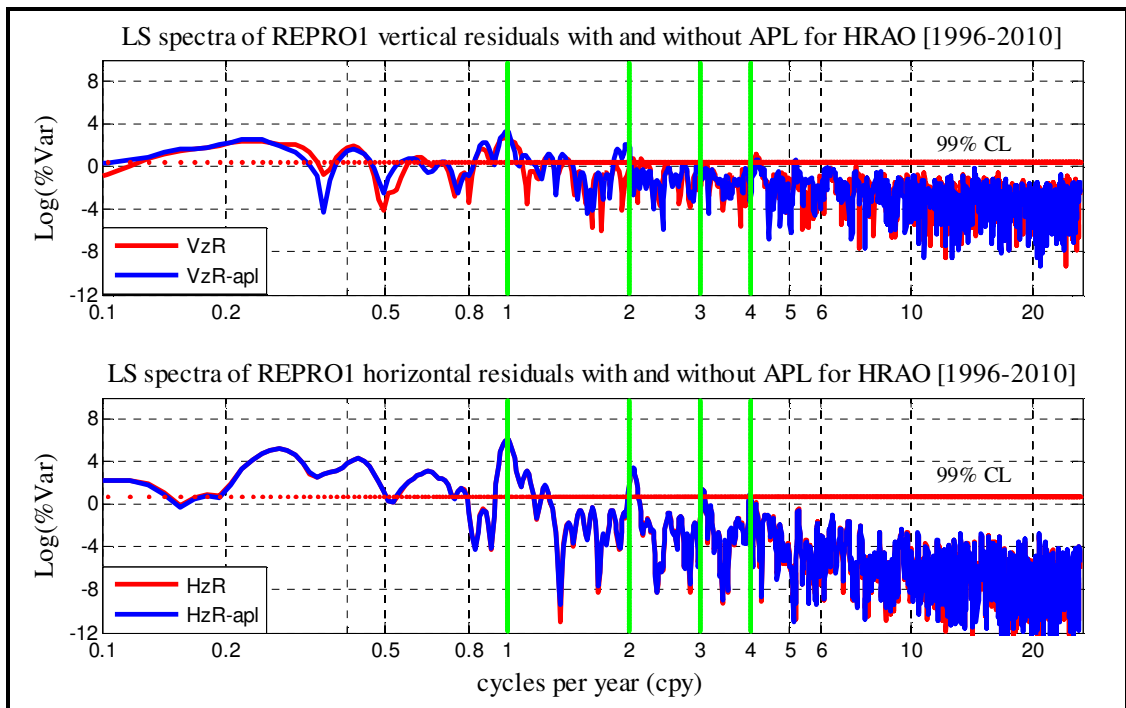

Figure 4.26 Least coherent squares spectra of REPRO1 residuals with (blue) and without (red) APL for HRAO (1996-2010).

Based on the spectra results as presented in Figures 4.23 to 4.26, we have three observations. The first observation is that, the existence of strong insidious (most likely) periodic signatures is evident in the spectra of both REPRO1 positions and residuals. The observed signals have different spectral power strength and different periodicities; however, most of them appear to be consistent around the first through to the fourth harmonics and they have been indicated using green vertical lines. The statistical data of the observed position and residual harmonics have been respectively summarized in Tables A1 and A2 in appendix A, along with the information of other IGS stations under study. Furthermore, not all stations show all peaks the four harmonics. Secondly, we have observed that, there exists reduction in the size of the spectral peaks in response to the APL corrections and as expected, they are more significant in the vertical components compared to the horizontal components. Furthermore, we have also noted that in some cases we had a negative impact for reasons which cannot be well explained and sometimes the APL had no impacts in the spectra peaks. Thirdly, we have observed that there is no correlation in the reduction or increase of the sizes of the spectral peaks at different harmonics, which sometimes happens to shift in response to the APL impact.

LSSA and LS coherent analysis with and without the APL corrections based on positions and residuals were done for all IGS stations under study. The spectral peaks were thereafter extracted from their respective spectra and compared (before and after APL corrections) and tabulated in Tables A1 and A2 in appendix A. Based on the comparisons, we have summarized the qualitative relative impacts of the APL corrections in percent (%), at first to fourth harmonic on vertical positions and residuals using Figures 4.27 and 4.28 respectively. The relative impacts in the horizontal positions

have presented in Figures 4.29 whereas the relative impacts in horizontal residuals are in Figure 4.30. In all four figures, the blue color indicates a reduction of the strength of the spectral peaks (improvement) after APL correction. Red color means negative impact upon application of APL correction (increase in the strength of the spectral peaks).
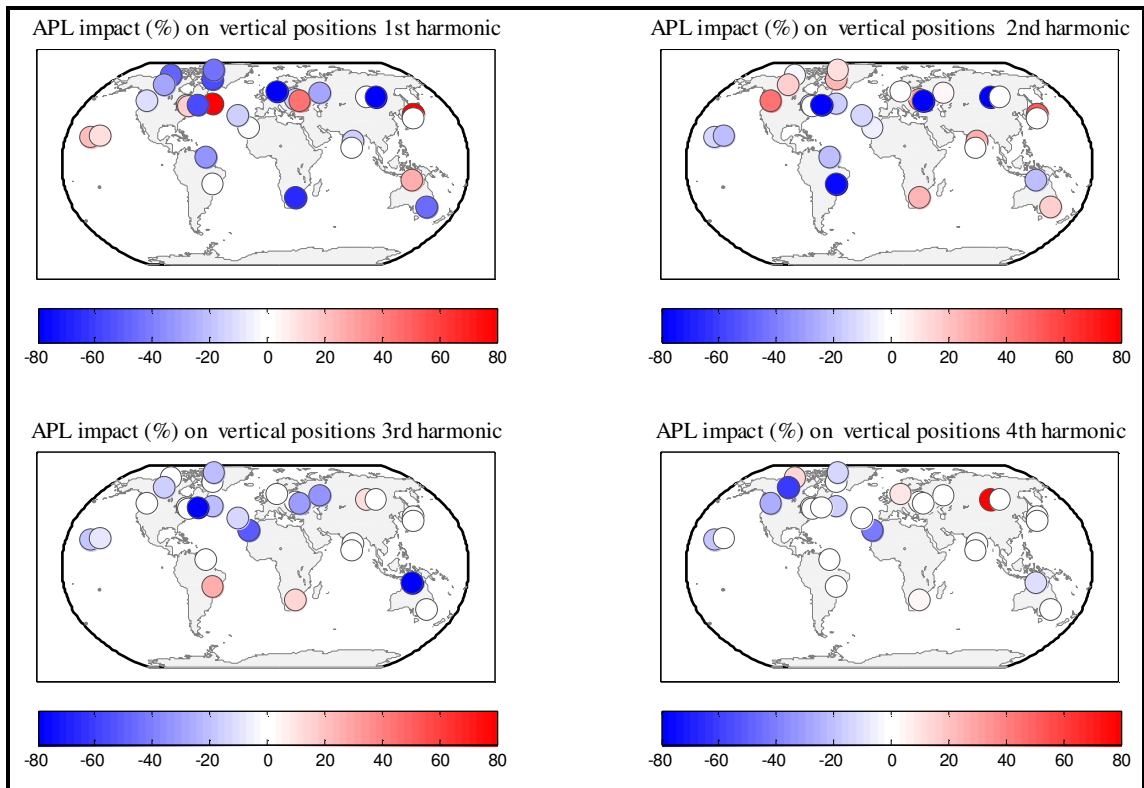

Figure 4.27 Impact of APL corrections on vertical positions. Top left shows the impact at first harmonic, top right shows the impact at second harmonic, bottom left shows the impact at third harmonic and bottom right is the impact at fourth harmonic. Blue color implies improvement and red color means that the APL corrections had negative impact.
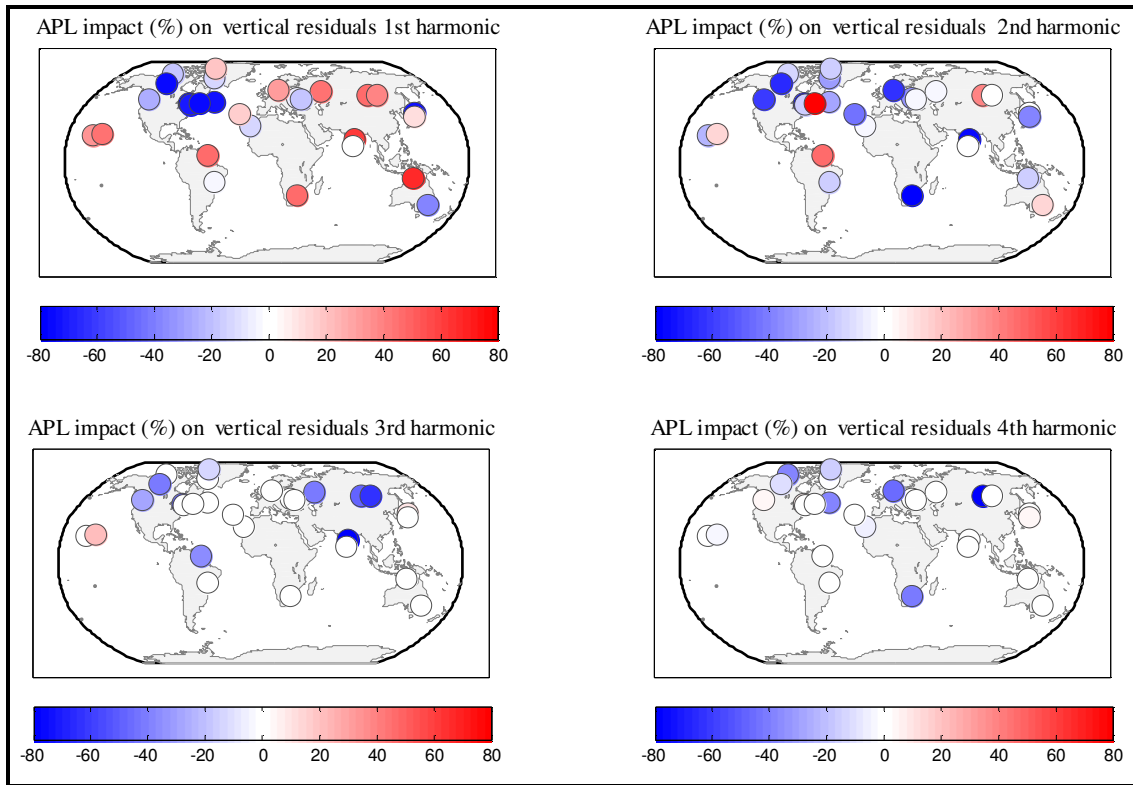
Figure 4.28 Impact of APL corrections on vertical residuals. Top left shows the impact at first harmonic, top right shows the impact at second harmonic, bottom left shows the impact at third harmonic and bottom right is the impact at fourth harmonic. Blue color implies improvement and red color means that the APL corrections had negative impact.
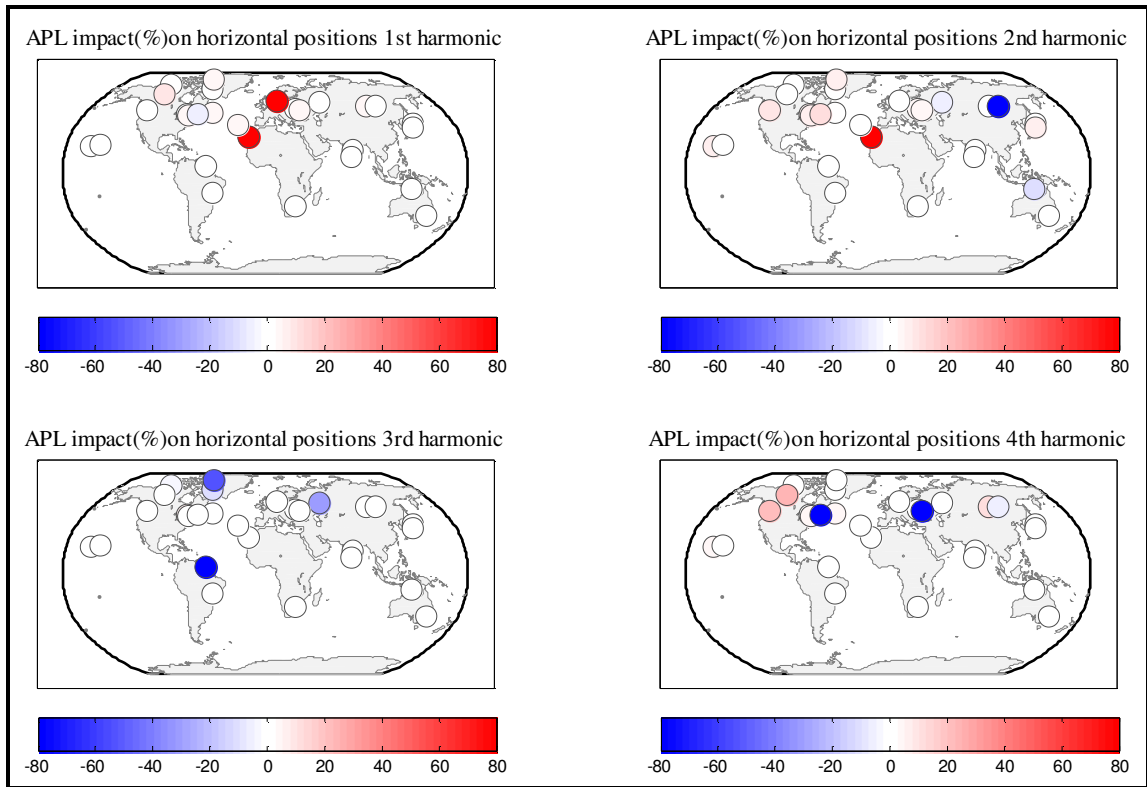
Figure 4.29 Impact of APL corrections on horizontal positions. Top left and right shows the impact at first harmonic and second harmonic respectively. Bottom left shows the impact at third harmonic and bottom right is the impact at fourth harmonic. Blue color implies improvement and red color means that the APL corrections had negative impact.
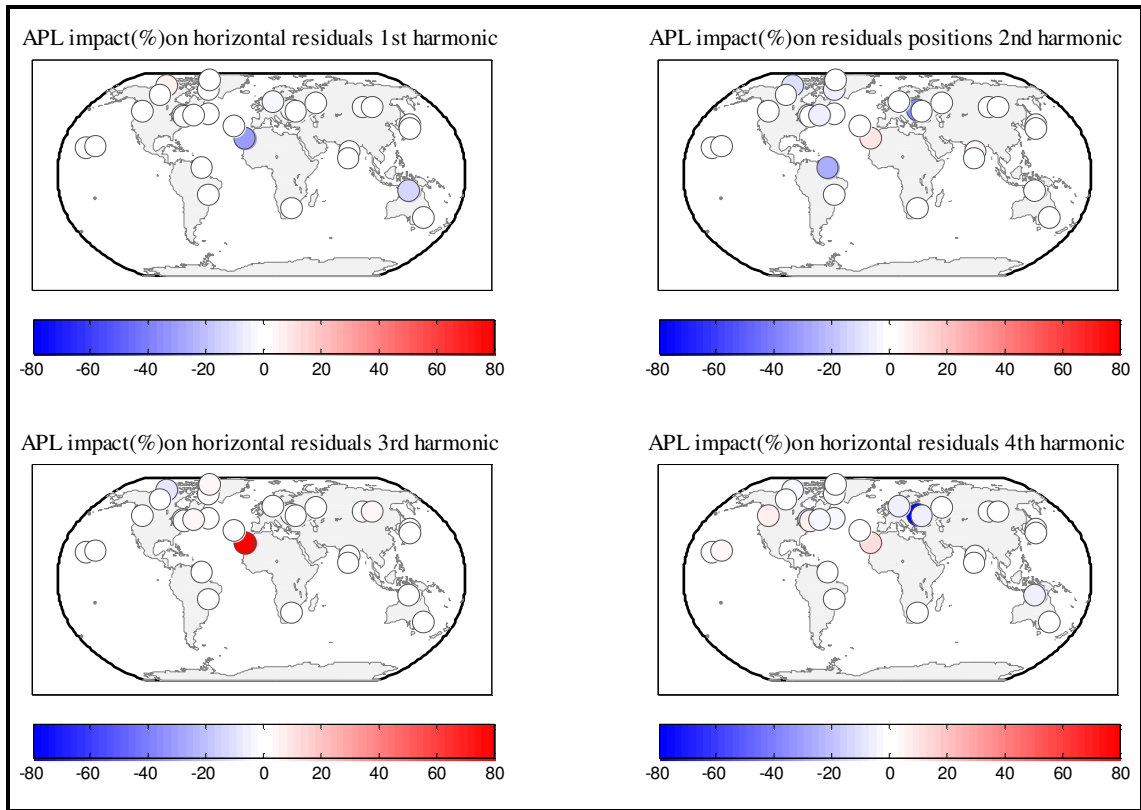
Figure 4.30 Impact of APL corrections on horizontal residuals. Top left and right shows the impact at first harmonic and second harmonic respectively. Bottom left shows the impact at third harmonic and bottom right is the impact at fourth harmonic. Blue color implies improvement and red color means that the APL corrections had negative impact.

4. 3.1 Observations on the APL impact on REPRO1 solutions

In the context of this study, improvement means the relative reduction in size of the spectral peaks and the metric used to quantify is the percentage decrease, in a qualitative sense. Following the modelling with atmospheric pressure loading from we have observed improvement in the spectral results for most of the stations under study. This improvement may to some extent improve the coordinate repeatability if APL is taken into consideration; a similar observation was made by Dach et al. [2011]. However, this improvement is not significant enough to account for the most of the remaining peaks which could be as well attributed to different factors such as the ones discussed in part 4.1.1. Other related observations are as follows:

a) Periodic signal in the LSSA Spectra at the first to the fourth harmonic level of most stations (~70%) were reduced in size upon modelling with the APL and they have been presented in the plots using blue color. The sizes of reduction of the signals were different from one station to another ranging from 0-80% and they are more significant in the vertical components positions than in the horizontal components.

b) APL impact on close by stations such as ALGO and NRC1, KOKB and HLNC, HYDE and IISC, MIZU and MTKA, IRKT and IRKJ, GSLV and POLV are not similar at all harmonics level and the reasons for that have not yet established. That is no clear pattern of the APL impact could be established based on the results.

Possible reasons could be limitations in APL models or significant different in the ratios between continental and ocean masses at those particular stations.

c) Significant improvements were observed in mid to high latitudes stations for the first, second and fourth harmonic peaks of most of the positional spectra. The APL impact at first harmonic of vertical residual peaks is worse in most part of Europe whereas the APL impact on second harmonic spectral peaks of positions tends to get worse in high latitudes.

d) The magnitude of the impact was more significant in the GPS vertical position and residuals spectral peaks as compared to the impact on the horizontal spectral peaks.

e) Periodic signal in the LSSA Spectra of one third of the stations (~30%) had no improvement such that, the size of the signals at different harmonic levels was increased upon modelling with the APL, and they have been illustrated using red color. The increase was different from one station to another ranging from 0-80% based on the qualitative comparison approach that has been adopted in this study.

4. 3.2 Limitations of the APL Impact on REPRO1 Solutions

Based on the spectral results on REPRO1 solutions presented in section 4.3, there is a lack of significant improvement in the resulting spectral peaks after modelling with APL. Furthermore, the improvements are not very consistent and no clear pattern can be established. This lack of significant improvements and consistency at different harmonic levels could be attributed to a number of factors but three of them are crucial.

a)   Oversimplifications in the present procedures to compute APL corrections. Presently there exist a number of simplifications that are adopted to make the computations quicker, through the use of coarse pressure field grid sizes and the approaches of dealing with the effects of topographic variations within the standard pressure grid cells [Ray, 2011]. It follows that, if the topography in the grid cell exhibits large variability, the surface pressure within the cell will also vary significantly over the area of the grid cell because the atmosphere is in hydrostatic equilibrium. Consequently, the estimates of loading effects derived for stations in regions of high topographic variability will be insufficient. Furthermore, the accuracy aspect of all the ingredient parts of the APL calculation has not been widely addressed. Such effects could be quite significant for select areas as they do not describe the regional and local effects properly, though it is not major for most of the Earth's crust.

b)   The sampling rate of the APL solutions. The weekly mean APL values used in this study are based on six hours corrections. In principle, they do not have the exact

impacts at the time when the GPS data were observed since the APL does not behave in a similar way on weekly basis. Therefore, using weekly mean APL might have an aliasing effects in some of stations and affect the resulting spectral peaks. Furthermore, the present APL corrections computations procedures are based on diurnal (S_1) and semi-diurnal (S_2) tides. Based on Ray [2011], these tides are not adequately sampled in the standard 6hours atmospheric pressure data sets. Moreover, the S_2 tide (which is larger particularly near the equator) is resonant with the GPS orbital period, it follows that any errors in it tend to go into the GPS orbit parameters if they are adjusted.

c)   Uncertainties in the final combined weekly REPRO1 solutions. Like past IGS solutions, the weekly REPRO1 solutions are based on internally self-consistent and rigorous combination of the on the terrestrial reference frame parameters and the Earth rotational parameters methods as discussed on part 3.3. However, this procedure is separated from the orbit and clock combination, which is not rigorous [Ray, 2009] and may therefore impact the quality of the final solutions. Furthermore, it is known that, some of the effects that cause station displacements such as non-tidal loading effects have not been included in the present solutions. All of such anomalies cause uncertainties in the present solutions as illustrated using 2 sigma error bars (based on standard deviations) in the plots of the final solutions for station HRAO and DRAO presented in Figures 4.31 to 4.38. Consequently, some of these uncertainties will (to some extent) absorb the APL corrections which are mostly at a millimeter level for most of stations understudy. In Figures 4.31 to 4.38, the vertical axis represents the coordinate values in meters and the horizontal axis represent the period in days of the year (DOY).
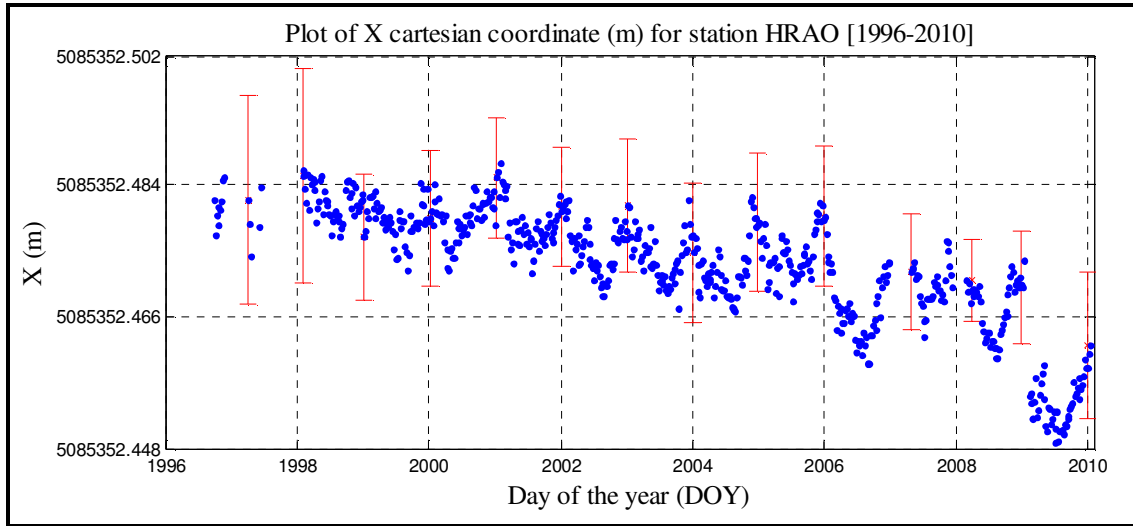
Figure 4.31 Plot of X Cartesian coordinate time series (m) for HRAO (1996-2010) with error bars. The red error bars represent the 2 sigma annual standard deviations. The mean standard deviation of the X coordinate for the 1996 to 2010 period is 4 mm (0.004m).
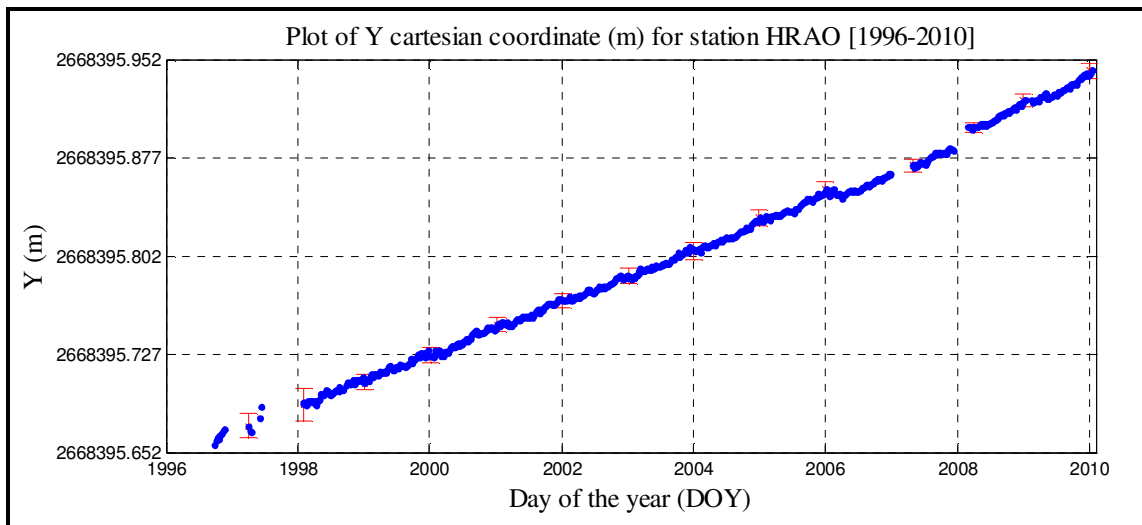

Figure 4.32 Plot of Y Cartesian coordinate time series (m) for HRAO (1996-2010) with error bars. The red error bars represent the 2 sigma annual standard deviations. The mean standard deviation of the Y coordinate for the 1996 to 2010 period is 2 mm (0.002m).
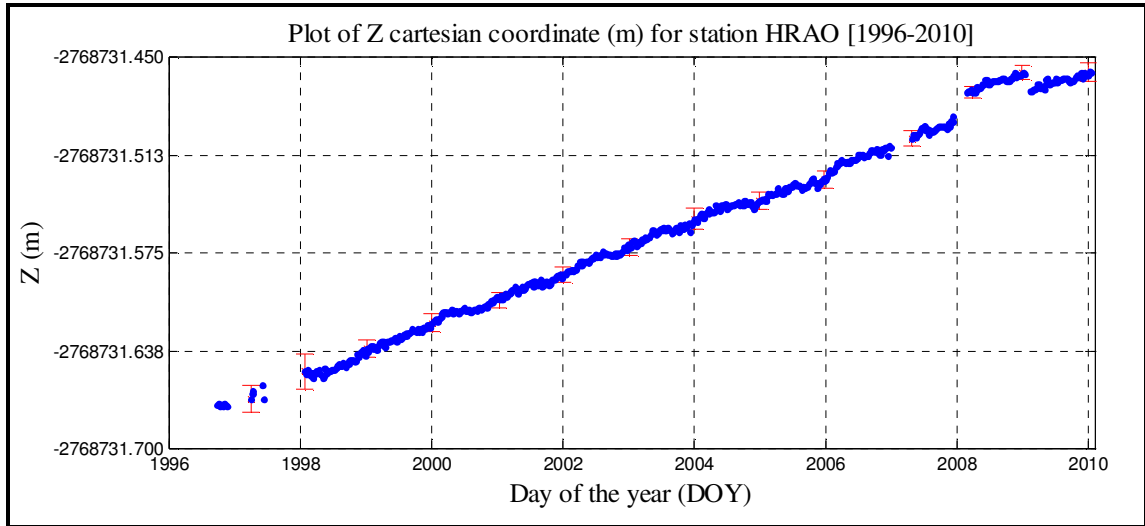
Figure 4.33 Plot of Z Cartesian coordinate time series (m) for HRAO (1996-2010) with error bars. The red error bars represent the 2 sigma annual standard deviations. The mean standard deviation of the Z coordinate for the 1996 to 2010 period is 2 mm (0.002m).
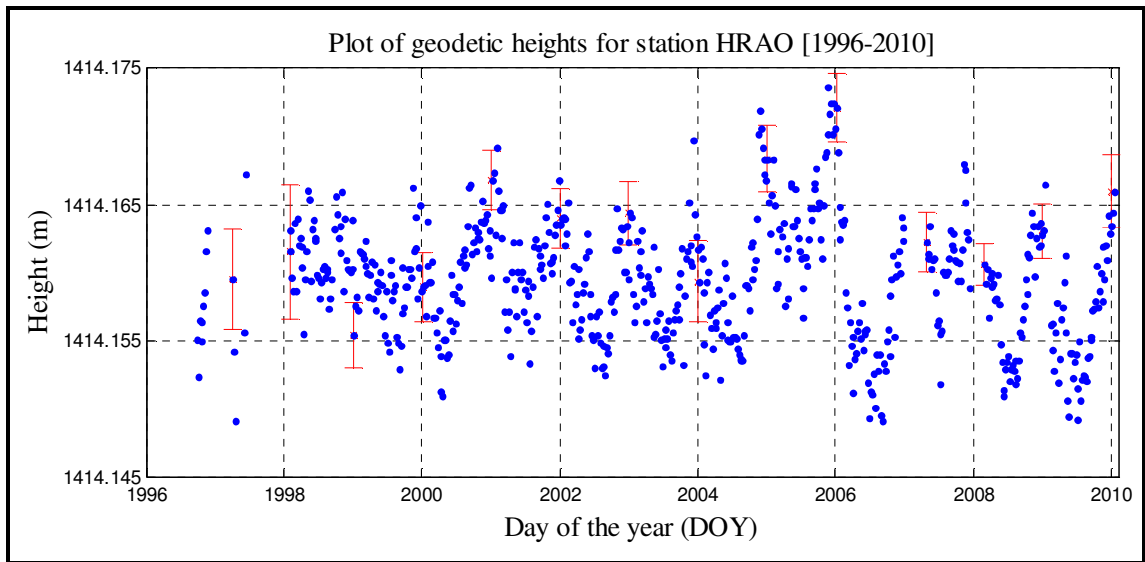

Figure 4.34 Plot of the geodetic height time series (m) for HRAO (1996-2010) with error bars. The red error bars represent the 2 sigma annual standard deviations. The mean standard deviation of the geodetic heights for the 1996 to 2010 period is 1 mm (0.001m).
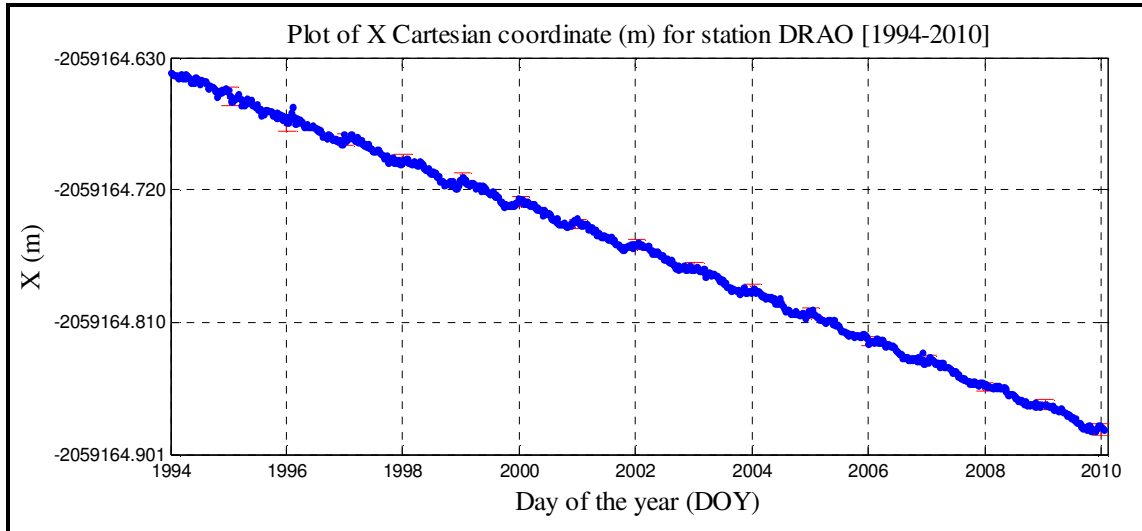
Figure 4.35 Plot of X Cartesian coordinate time series (m) for DRAO (1994-2010). The red error bars represent the 2 sigma annual standard deviations. The mean standard deviation of the X coordinate for the 1994 to 2010 period is 1.5 mm (0.0015m).

Figure 4.36 Plot of Y Cartesian coordinate time series (m) for DRAO (1994-2010). The red error bars represent the 2 sigma annual standard deviations. The mean standard deviation of the Y coordinate for the 1994 to 2010 period is 2.2 mm (0.0022m).
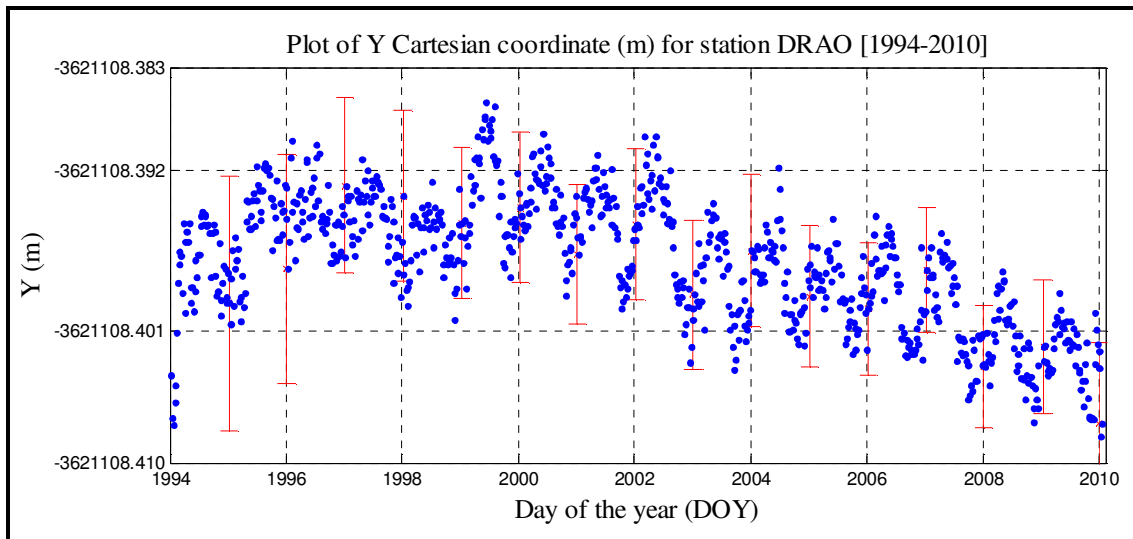
Figure 4.37 Plot of Z Cartesian coordinate time series (m) for DRAO (1994-2010). The red error bars represent the 2 sigma annual standard deviations. The mean standard deviation of the Z coordinate for the 1994 to 2010 period is 2.5 mm (0.0025m).

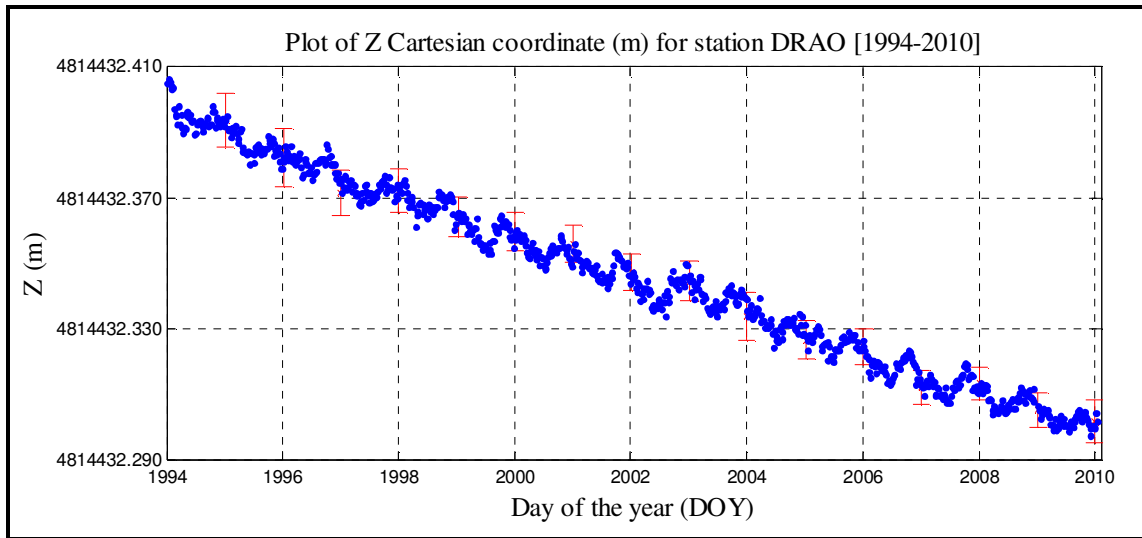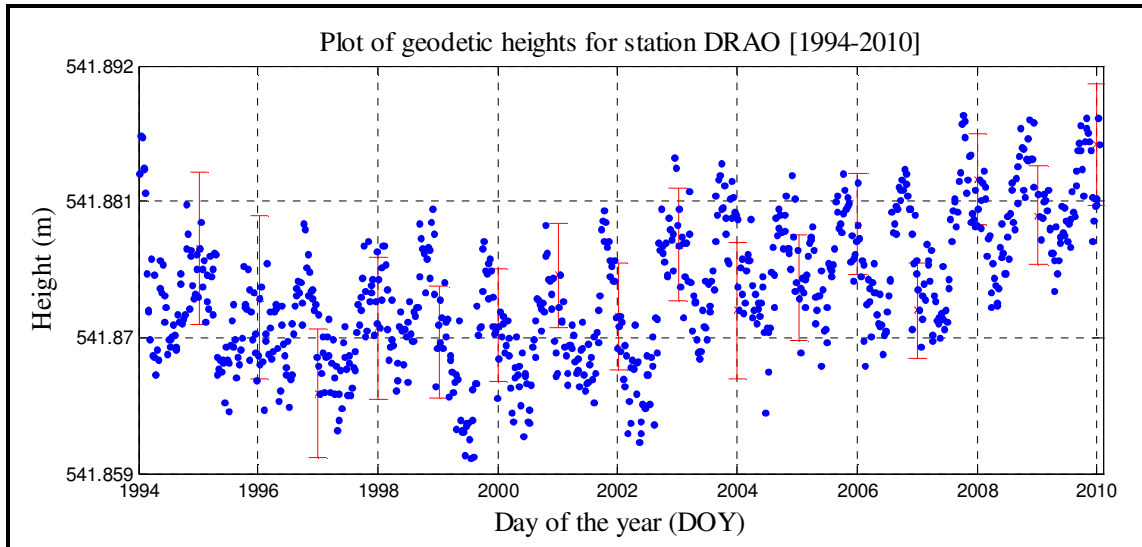
Figure 4.38 Plot of the geodetic height time series (m) for DRAO (1994-2010). The red error bars represent the 2 sigma annual standard deviations. The mean standard deviation of the geodetic height for the 1994 to 2010 period is 1.9 mm (0.0019m).

4. 4 Bernese Weekly Solution for stations NRC1 and YELL

This section presents the results of weekly coordinate solutions for the period 1995-2010 for the stations YELL and NRC1 computed using the Bernese software in baseline mode (not global network) from station STJO. The primary objective of this approach was to ensure that, the estimated solutions are solely based on site dependent effects with less contribution of global effects. The secondary objective was to validate the new model parameter [McCarthy and Petit, 2003], that have been used in the generation of REPRO1 solutions. The processing used model parameters (section 2.2.1) and data sets that are very close to those used in the generation of REPRO1 solutions. Furthermore, the baselines selection was based on the APL statistics of the Canadian IGS stations under study (Table 4.3), which found stations STJO and YELL with the lowest and highest Up APL displacements, respectively. In Table 4.3, the first column presents station names. Column two, three, four and five are the APL displacements in millimeters of the UP, North, East and horizontal components, respectively.

Table 4.3 APL statistics of the Canadian IGS stations under study (1994-2010)

Station	APL UP (mm)	APL North (mm)	APL East (mm)	Horizontal APL (mm)
ALGO	17.401310	5.722546	3.339358	6.625620
DRAO	19.372820	5.672777	2.382067	6.152613
HOLM	15.863310	4.462554	2.995857	5.374900
NRC1	17.768240	5.755916	3.135583	6.554575
QIKI	14.332740	4.414793	3.535893	5.656230
STJO	8.786647	5.382960	3.728700	6.548241
THU3	13.952880	3.836570	3.299201	5.060039
UNBJ	15.347870	5.754066	3.218410	6.592984
YELL	23.135980	5.070741	2.847493	5.815551
NB: By convention, the APL displacements are provided in six decimal places.				

The generation of the Bernese weekly solutions (1994-2010) for the said station, which are hereinafter referred to as JMB solutions, was accomplished in a two steps processing. The first step involved processing of the STJO-YELL and STJO-NRC1 baselines, involved the generation of the daily solutions in an automated procedure using the BPE_ALL.PCF (Appendix B), which is a collection (set) of standard Bernese process control files that have been selected for this purpose.

The second step involved the generation of Bernese weekly solution from the daily solutions in two steps process [Walser, 2012]. The first step is to define the user menu variable for the input parameters as shown in Table B.3, Appendix B. Examples of them are the begin and end session ranges, daily normal equation files, daily fixed coordinate solutions, orbit information and stations related information files. The second step is to compile a set of process control files and for that reason HQN_COMB.PCF was generated with the assistance of expertise from Geodetic Survey Division of Canada [Craymer, 2012]. HQN_COMB.PCF is presented in Table B.2, Appendix A.

4. 4 .1 Validation of the JMB solution

The last activity in Bernese processing, was to validate the JMB solution[37] by comparing them to the official IGS REPRO1 solutions (1995-2010), in accomplishment of the secondary objective of this Bernese processing presented in section 4.4. The two

---

[37] JMB solution is the acronym for the weekly solutions for the stations NRC1 and YELL (1995-2010), as generated using Bernese v5.0 software, based on a processing strategy developed for this research.

solutions were found to be in a close agreement, though we had a few outliers (about 1.5 percent) which were thereafter tested and removed using student statistical test. Finally, statistical information on the comparison results (differences between JMB and IGS REPRO1 solutions) were generated and they are provided in Tables 4.4. In Table 4.6, the stations names are shown in the first column and the types of coordinate differences in meters are shown in column two. Columns three and four show the respective maximum and minimum difference in meters and the respective mean and standard deviations of the differences in meters are in columns five and six.

Table 4.4 Differences between Processed and REPRO1 solutions for NRC1

Station	Category	Maximum (m)	Minimum (m)	Mean (m)	StDev (m)
NRC1	dx	0.0127	-0.0114	-0.0031	0.0032
	dy	0.0175	-0.0037	0.0056	0.0031
	dz	0.0149	-0.0192	-0.0059	0.0046
YELL	dx	0.0174	-0.0214	-0.0021	0.0051
	dy	0.0240	-0.0076	0.0072	0.0050
	dz	0.0239	-0.0246	-0.0103	0.0070

Likewise plots of the X, Y, and Z differences (m) have been plotted on the same axes for easy reference as in Figure 4.39. In Figure 4.39, the top panel correspond to the plot of the coordinate differences (m) between the processed solution and IGS REPRO1 positions for station NRC1 (1995-2010). The bottom panel corresponds to the plot of the coordinate differences (m) between the processed solution and IGS REPRO1 positions for station YELL (1995-2010). In both panels, the vertical axes represent the coordinate differences in meters and the horizontal axis presents the period in day of the year.
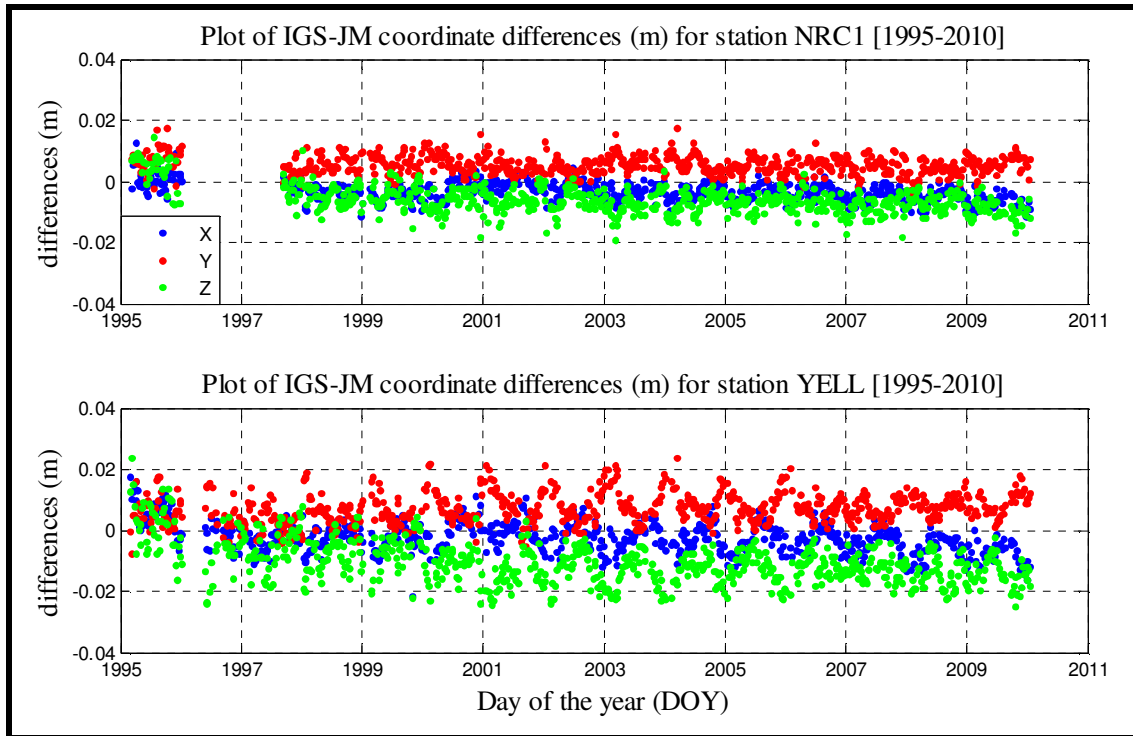
Figure 4.39 Differences in weekly solutions between Bernese processed solutions and REPRO1 solutions. Top panel are the differences for NRC1 and bottom panel are the differences for YELL. The blue dots are the X coordinate differences, red dots are the Y coordinate differences and the green dots are the Z coordinate differences.

Based on the graphical comparison on Figure 4.39, there exists a bias in the solution of few millimetres in the three components. However, such a bias will not affect the positions of the spectral peaks as it is taken care of in LSSA. Furthermore, the existence of annual signatures is evident in the differences of the two solutions.

4.4.2 LS Spectra of the weekly solutions for NRC1 and YELL

Least squares coherent spectra were generated based on the Bernese (generated) weekly solutions (JMB solutions) for both NRC1 and YELL as illustrated in Figures 4.40 and 4.42 respectively. Furthermore, their respective spectra plots based on REPRO1 solutions are presented on Figures 4.41 and 4.43. In all four figures, the top panels correspond to the vertical positions with and without APL corrections whereas the bottom panels are horizontal positions the spectra. The vertical axes are the percentage variance and the horizontal axes are the period in cycles per year. The horizontal red line corresponds to the 99 percent confidence level (99% CL) and the vertical green lines show the first to fourth harmonics.
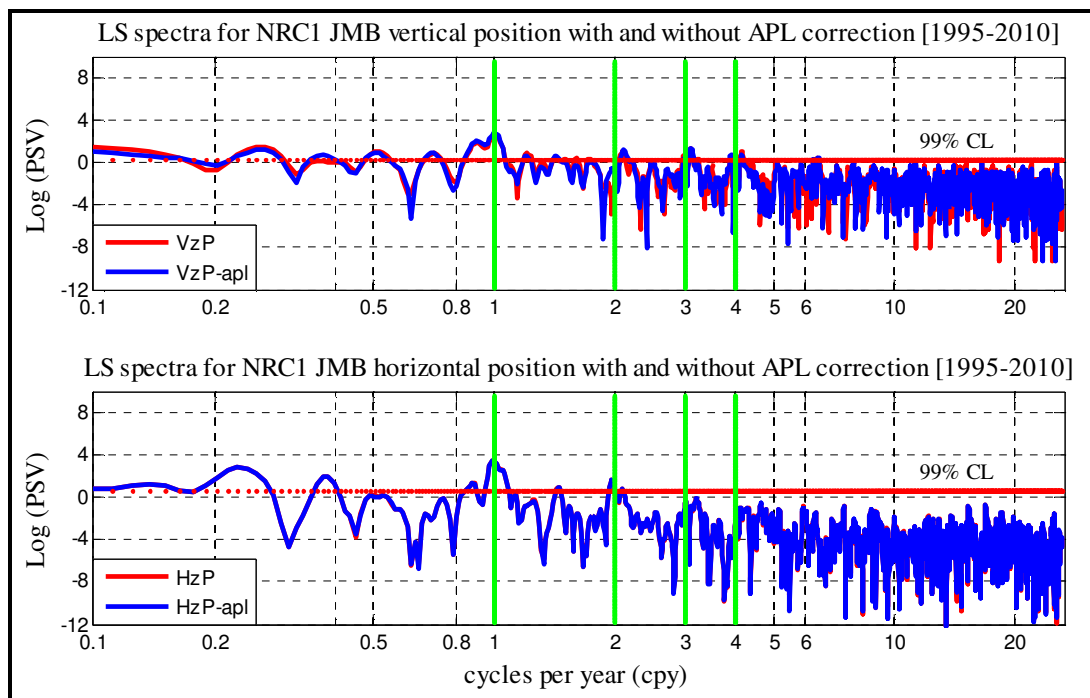

Figure 4.40 Least squares (LS) coherent spectra of the JMB (Bernese generated solution) vertical and horizontal position for station NRC1 (1995-2010).
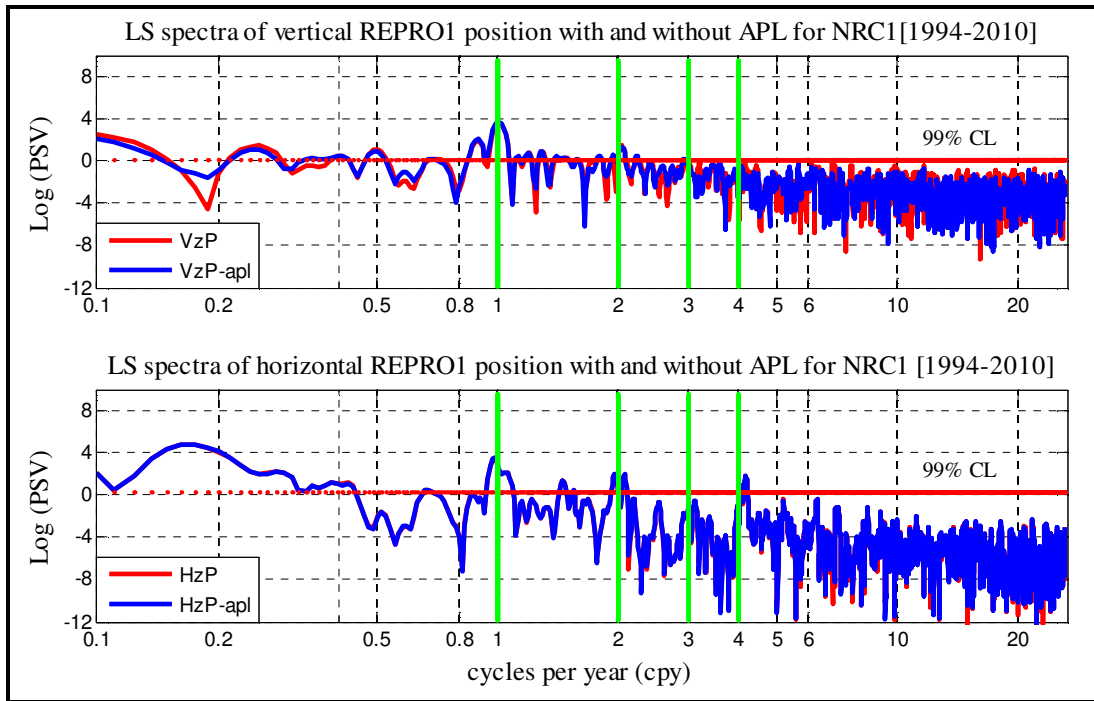
Figure 4.41 Least squares (LS) coherent spectra of the REPRO1 vertical and horizontal

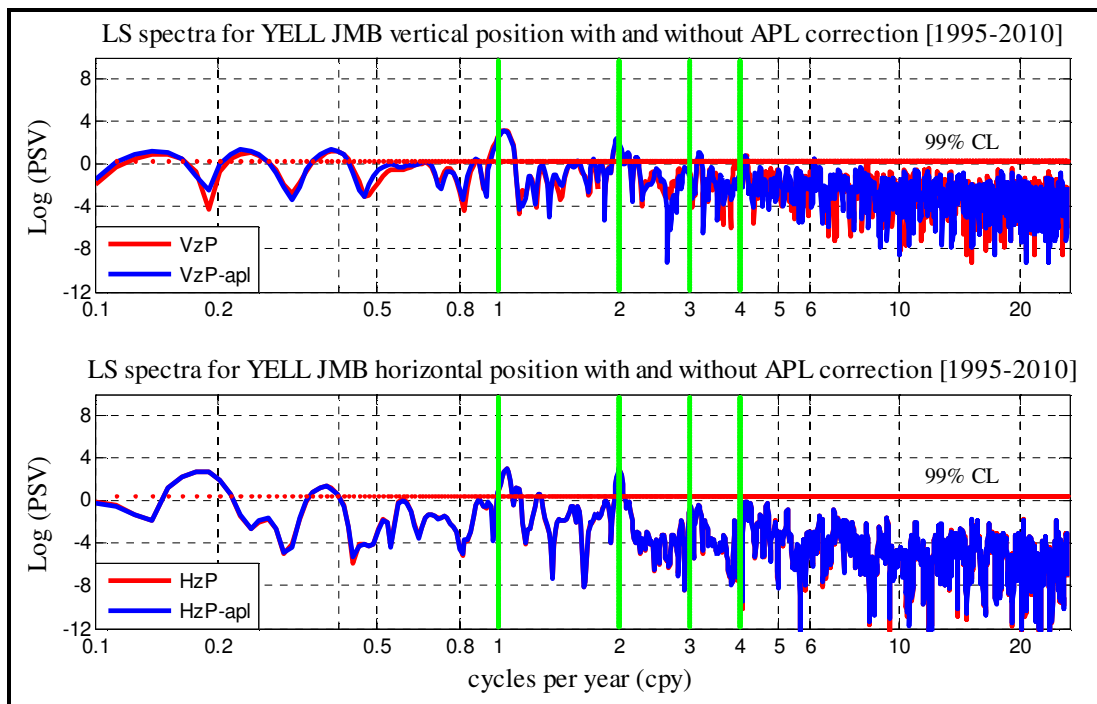position for station NRC1 (1994-2010).

Figure 4.42 Least squares (LS) coherent spectra of the JMB (Bernese generated

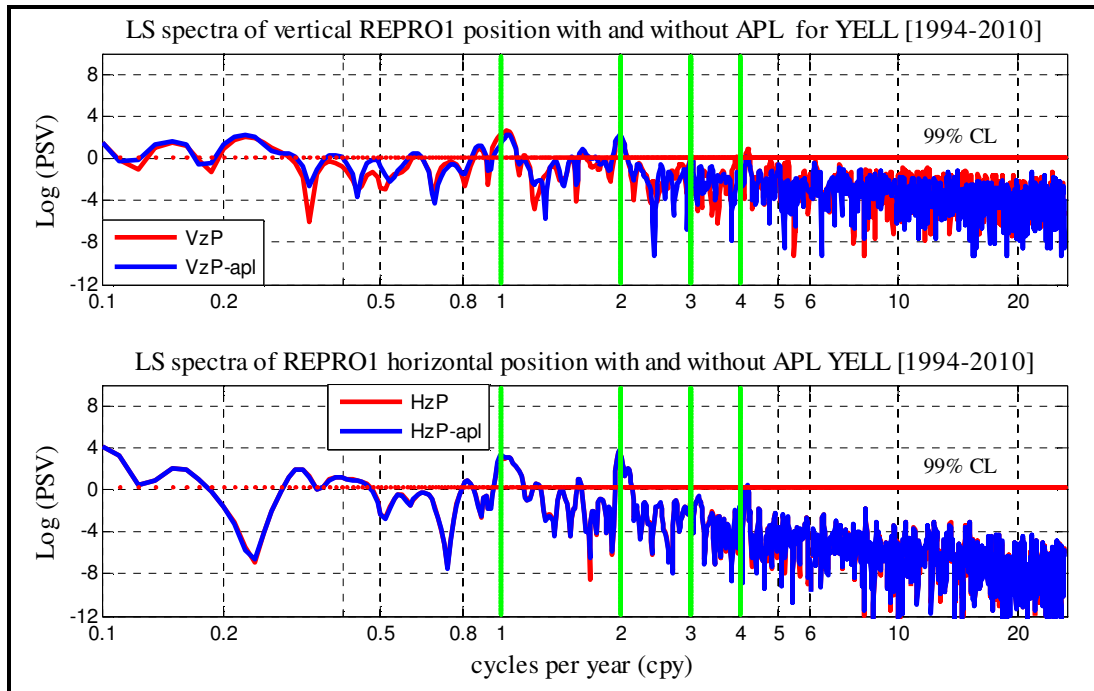solution) vertical and horizontal position for station YELL (1995-2010).

Figure 4.43 Least squares (LS) coherent spectra of the REPRO1 vertical and horizontal position for station YELL (1994-2010).

In principle, the spectra plots based on the independently Bernese generated solutions (JMB solution) show a close similarity to their counterparts from REPRO1 solutions. Furthermore, the spectral peaks of interest (at first to fourth harmonics) have approximately the same strength. However, there some minor differences in the size of some of the peaks and the impact of APL on the JMB spectra especially at the low frequencies which are not of much interest to this research. These minor differences should be expected and they could be attributed to the cumulative effect of the solution differences presented in Table 4.4 and illustration on Figure 4.39. It is also worth to remind the reader that, REPRO1 are weighted solutions based on individual solutions from eleven IGS Analysis centers. Therefore, they do contain a wide range of uncertainties which are not in JMB solutions.

5. CONCLUSION AND RECOMMENDATIONS

Operational GPS time series are known to be inconsistent and inhomogeneous for a number of reasons such as uneven distribution of observing stations, ionosphere and troposphere biases as well as biases due to EOP and increased observation noise at low elevation angles due to the then arbitrary assumption that the reference antenna is free from phase center variations. The PCV satellite-based corrections due to the separation between the GPS satellite center of mass and the phase center of its antenna. The IGS force models for modeling satellite orbit and clock products refer to the satellite center of mass whereas the orbit ephemerides in the GPS broadcast navigation message refers to the satellite antenna phase center [Kouba, 2009]. Because of that, there have been significant efforts in the last decade to improve the modeling and parameterization of global GPS solutions so as to improve the stability and homogeneity of the station positions and velocities. The latest of these improvements is the adoption of an absolute antenna phase model with non-zero PCV for both satellite and station antennas starting from November 5, 2006 [Schmid et al., 2007]. This adoption changed the processing procedures of GPS solutions and its products by the IGS Analysis Centers [Dow, 2004]. Presently, all GPS historical data from January 1994 to January, 2010 have been reprocessed and new solutions that are consistent and homogeneous based on the IGS05 reference frame, and are now available [Gendt and Ferland, 2010].

Based on the availability of the IGS REPRO1 solutions, the primary objective of this research is to identify the remaining spectral peaks in them and try to explain them

144

by correlating with known effects not modeled or modeled differently, with a specific attention to the APL displacements. APL is one of the geophysical phenomena that have not been applied in the IGS REPRO1 solutions. Others effects that have not been implemented include, for example non-tidal loading due to ocean bottom up and surface hydrology and other effects.The second objective of this study is to perform the harmonic analysis investigation of weekly time series in position and residual domain of REPRO1 solutions using LSSA and LSCA with and without APL corrections. Based on the resulting Least Squares spectra, the lack of the APL in both positional and residual domain of the REPRO1 solutions was thereafter assessed, using the APL corrections from the Global Geophysical Fluids Center model. In order to meet the research objectives, a set of twenty seven IGS stations were selected based on geometry. Thereafter a LSSA and LS Coherent spectra of their position and residuals were generated with and without APL displacements as a way to assess the lack of APL in the REPRO1 solutions. To ascertain our research findings, baselines STJO-YELL and STJO-NRC1 were selected and processed using the Bernese v5.0 software for the period 1995-2010. Amongst the Canadian IGS stations understudy, STJO and YELL has the lowest and maximum APL variation, respectively. The processing used the latest IERS error models [Petit and Luzum, 2010], most of which were very close to the ones used by the most of the IGS Analysis Centers. They include the absolute phase center variation model, adoption of the IGS05 frame and the effects due to tidal loading forces [Mtamakaya et al., 2011]. The computed solutions were compared to the IGS solutions and thereafter analyzed using LSSA and LSCA with and without APL.

5.1 Assessment of the LSSA Results

Based on discussions on part 4.1, we can conclude that, existence strong signals at first through the fourth harmonics is evident in the spectra of both position and residuals for most of the stations; and in few cases there are also present in higher and low order harmonics. The signals have different strength though most of them with periodicities beyond one cycle per year cannot be clearly explained as previously noted by Dong et al. [2002]. Different things can be learned from these observations. From the results of the position domain, this is an indication of the existence of un-quantified amount of apparent station motions, though part of the observed bias could also be attributed to the real motion of the ground. Therefore, we can study and learn more about actual station motions such as the ones due to plate tectonics, and other existing features such as periodic variations of station coordinates at first to fourth draconitic harmonics. Likewise, the results of the residual domain suggests the existence of un-quantified amount of miss modeled errors such higher order ionosphere effects as well as un-modeled errors such APL displacements in the REPRO1 solutions.

In order to establish the contribution of APL in the present solutions, we divided this task into three main parts starting with the comparison of the two APL models that are based on NCEP numerical whether model parameters. They are the GSFC model [Petrov and Boy, 2004] and the GGFC model [Van Dam et al., 2002] and all of them provide three dimensional APL displacements at six hours intervals. From the fact that the REPRO1 solutions are provided on weekly basis, we had to concatenate them into

weekly values as a way to synchronize them; followed by comparison at both six hours and weekly sampling rates. Based on the discussions on part 4.2.5, we found that mean differences, though varying depending on location they are all within a sub-millimetre level implying that there is no significant different in the choice of APL model for this study. Secondly, we generated LSSA and LS coherent spectra based on 6 hour and weekly APL, and examined the resulting harmonic signatures. Based on our discussions on part 4.2.6 we found that the spectra both the 6 hours and the weekly mean APL contain strong annual and semi-annual signatures. This observation is in agreement with a previous observation by Van Dam et al. [2001] whom suggested that the un-modeled tidal effects in diurnal and semi diurnal waves, hydrological and atmospheric loading can systematically alias into long periodic signals if left unaccounted for. Thirdly, we applied the weekly mean APL corrections to the REPRO1 positions and residuals and generated the LSSA and LS coherent spectra. We examined the results and concluded that about seventy percent (70%) of the selected stations indicate the lack of APL corrections, though the impacts vary with location as illustrated in Figures 4.27 to 4.29 and a summary of observations presented in section 4.3.1. However, the remaining thirty percent (30%) of the selected stations had either increase in the size of spectral peaks upon APL corrections and some of them had no impact at all. Based on the discussion on section 4.3.2, these anomalies could be attributed to deficiency in the APL models, weekly means averaging procedures and the un-modeled miss modeled uncertainties in the REPRO1 solutions which may absorb some of the APL impacts. Furthermore, we have observed that the amount of improvements and increase in the spectral peaks is not

consistent without a clear pattern at different harmonic levels of the same station as well as different station; and the reasons for that could not be well established. Therefore, based on the observations in our study we can conclude that, the results suggests an indication of improvement of coordinate repeatability if the next exercise similar to the REPRO1 will take APL into account. Better results may be expected with observation level corrections as previously observed in a study by Dach et al. [2011]. However, it is evident that the observed improvements are not significant enough to account for the most of the remaining peaks because of the APL model limitations and other uncertainties as per our discussions on part 4.3.2.

5.2 Assessment of the Reprocessed Baselines Results

Daily and weekly solutions based on fifteen years of data (1995-2010) have been generated using the Bernese v5.0 software and the procedures explained part 4.4. Thereafter the weekly Bernese generated positions were compared to the official IGS REPRO1 solutions. The comparison results show a close and consistent agreement for both stations YELL and NRC1. Based on the comparison results as presented on Table 4.3 and illustrations on Figure 4.30, the maximum and minimum differences between the compared solutions are below ±2.5 cm for both stations in all three components. Likewise the differences between in the mean positions were less than ±1.5 cm whereas the standard deviations were less than 1 cm in all three components.

LSSA and LS coherent spectra of the positions with and without APL corrections were thereafter generated and have been illustrated in Figures 4.31 and 4.33. The spectra were analyzed and two things were observed:

a) The spectral peaks are still present in the Bernese generated weekly solutions. They are predominant at the first through the fourth harmonics and have close similarities to the spectral peaks of the official IGS REPRO1 solutions.

b) The spectral peaks in the Bernese weekly generated solutions (JMB solutions) show a close similarity to their corresponding spectra from REPRO1 solutions. This indicates that, the impacts of APL displacements can be fairly assed at the positions level using spectral studies.

5.3 Recommendation and Future Work

Based on the research findings it is evident that the correction for APL displacements would have slight improvements in the final solutions especially in the vertical components. It is strongly suggest that the generation of the next reprocessed solutions should include APL. However, it is worth mentioning that beside APL there are other types of positional displacements that have not been included in the present REPRO1 solutions and have not been addressed in this research. Examples of them are the surface hydrological loading, ocean bottom up loading effects as well as the thermal expansion of station markers near bedrocks. Likewise, there exist limitations in some of the model parameters used to generate REPRO1 solutions such as exclusion of high order ionosphere models (2nd and 3rd) effects as well usage of the new geopotential models (new C_{20}, C_{21} and S_{21} values with their time derivatives etc). These effects could be attributed to the remaining peaks that are not well explained.

We also strongly recommend that the impact of the remaining types of un-modeled station displacements and mismodeled effects should be researched as a basis of future IGS reprocessing as soon as new IERS models are available. Lastly, the impact of the present GPS attitude models that has been adopted in generation of the present solutions should also be assessed. Based on the discussions on section 4.1.1, there exists a strong correlation between the periodicities of the observed spectral peaks and the draconitic periods at first to sixth harmonics. Therefore a proper satellite attitude model will help to explain some of the observed peaks in future similar reprocessing activities.

References

Altamimi, Z., Collilieux, X., Legrand, J., Garayt, B., Boucher C (2007). ITRF2005 A new release of the International Terrestrial Reference Frame based on time series of station positions and Earth Orientation Parameters. *JG Research,* 112, B09401.

Agnew, D., and K Larson (2007). Finding the repeat times of the GPS constellation *GPS Solutions vol. 11, pp.71–76,* doi: 10.1007/s10291-006-0038-4.

Beutler, G., E. Brockmann, W. Gurtner, U. Hugentobler, L. Mervart, and M. Rothacher (1994), Extended Orbit Modeling Techniques at the CODE Processing Center of the International GPS Service for Geodynamics (IGS): Theory and Initial Results, Manuscripta Geodaetica, 19, 367-386, April 1994.

Beutler, G., J. Kouba, and T. Springer (1995). "Combining the orbits of the IGS Analysis Centers", *Bulletin Geodesique*, 69, pp 200-222.

Blewitt, G., D. Lavall´ee, P. Clarke, and K. Nurutdinov (2001). "A new global mode of the Earth deformation: Seasonal cycle detected," *Science*, 294, pp. 2342–2345.

Blewitt, G., and D. Lavellee (2002). Effect of annual signals on geodetic velocity. *Journal of Geophysical Research,* Vol. 107, No. B7.

Bock, Y., P. Fang, P. Jamason and L. Prawirodirdjo (2005). "Scripps Orbit and Permanent Array Center (SOPAC) Analysis Strategy Summary". [Online 15 January, 2012]. http://igscb.jpl.nasa.gov/igscb/center/analysis/sio.acn.

Boehm, J., B., Werl and H., Schuh (2006)a. "Troposphere mapping functions for GPS and very long baseline interferometry from European Centre for Medium-Range

Weather Forecasts operational analysis data," *J. Geophysical. Res.,* 111, B02406, doi: 10.1029/2005JB003629.

Boehm, J., E.Niell, P. Tregoning, and H. Schuh, 2006b, "Global Mapping Function (GMF): A new empirical mapping function based on numerical weather model data," *Geophysical. Res. Letters, 33, L07304*, doi: 10.1029/2005GL025546.

Bouin, M., G. Woppelmann, and A. Gomez (2007). " University of La Rochelle (URL) IGS Analysis Strategy Summary".[Online 15 January, 2012]. http://igscb.jpl.nasa.gov/igscb/center/analysis/ulr.acn.

Claudius, P (2009). "International GNSS Service Data Reprocessing Campaign" http://acc.igs.org/reprocess.html.

Collilieux, X., Z. Altamimi, D. Coulot, J. Ray, and P. Sillard (2007). Comparison of very long baseline interferometry, GPS, and satellite laser ranging height residuals from ITRF2005 using spectral and correlation methods. *Journal of Geophysical Research,* Vol. 112, B12403.

Craymer, M., (2012)."Personal communications". Geodetic Survey Division of Canada

Craymer, M., M. Piraszewski, and J. Henton (2007). The North American Reference Frame (NAREF) project to densify the ITRF in North America. *ION GNSS 2007,* Fort Worth, Texas, September 25-28, 2007

Dach, R., U. Hugentobler, P. Fridez, and M. Meindl (2007). "User Manual Bernese GPS Software Version 5.0." Astronomical Institute University of Berne

Dach,R., J. Böhm, S. Lutz, P. Steigenberger and G. Beutler (2011). "Evaluation of the impact of atmospheric pressure loading modeling on GNSS data analysis". *Journal of Geodesy (2011)* 85:75–91DOI 10.1007/s00190-010-0417-z.

Darwin, G. H. (1882). On variations in the vertical due to elasticity of the Earth's surface, *Philosophical Magazine* , Ser. 5, 14(90), 409– 427.

Davis, J. L., T.Herring, I. Shapiro, E.Rogers, and G. Elgered (1985). "Geodesy by radio interferometry": effects of atmospheric modeling errors on estimates of baseline length," Radio Sci., 20(6), pp. 1593-1607.

Dong D, P. Fang, Y. Bock, M.Cheng and S. Miyazaki (2002). Anatomy of apparent seasonal variations from GPS-derived site position time series. *Journal of Geophysical Research* 107(B4):2075.doi:10.doi:10.1029/2001JB00573

Dow, J.M., R. Neilan and C. Rizos (2009). The International GNSS Service in a changing landscape of Global Navigation Satellite Systems, *Journal of Geodesy (2009)* 83:191–198, DOI: 10.1007/s00190-008-0300-3

Desai, S., W. Bertiger, B. Haines, A. Sibthorpe and J.Weiss (2008)." Jet Propulsion Laboratory (JPL) Analysis Strategy Summary". [Online 15 January, 2012]. http://igscb.jpl.nasa.gov/igscb/center/analysis/jpl.acn.

Donahue, B., P. Tetreault and Y. Mireault (2008). "Natural Resources Canada (EMR) Analysis Strategy Summary". [Online 15 January, 2012]. http://igscb.jpl.nasa.gov/igscb/center/analysis/emr.acn.

Dow, J.M., R. Neilan and G. Gendt (2005). The International GPS Service (IGS): Celebrating the 10th anniversary and looking to the next decade. *Adv Space Res 36(3):* 320-326 DOI: 10.1016/j.asr.2005.05.125

Dulaney, R., J. Griffiths, S. Hilla, J. Ray, J. Rohde, K. Choi and G. Mader (2006). "National Geodetic Survey (NGS) Analysis Strategy Summary". [Online 15 January, 2012]. http://igscb.jpl.nasa.gov/igscb/center/analysis/noaa.acn.

Enderle, W., and T. Springer (2011). "European Space Operation Center (ESOC) IGS Analysis Strategy Summary ". [Online 15 January, 2012]. http://igscb.jpl.nasa.gov/igscb/center/analysis/esa.acn.

Feltens, J., (2003). The activities of the Ionosphere working group of the International GPS Service. *GPS Solutions (2003)7*:41–46, DOI 10.1007/s10291-003-0051-9

Ferland, R., and M. Piraszewski (2009). The IGS-combined station coordinates, earth rotation parameters and apparent geocenter. *Journal Geodesy (2009)* 83:385–392DOI 10.1007/s00190-008-0295-9

Fritsche, M., R. Dietrich, A. Rülke, M. Rothacher and P. Steigenberger (2009). Low-degree earth deformation from reprocessed GPS observations. *GPS Solutions* DOI 10.1007/s10291-009-0130-7

Gendt, G., and A. Brandt (2011). "German Research Centre for Geosciences (GFZ)". IGS Analysis Strategy Summary". [Online 15 January, 2012]. http://igscb.jpl.nasa.gov/igscb/center/analysis/gfz.acn.

Gendt, G., and R. Ferland (2010). "Availability of "repro1" products**."** IGS Electronic Mail 6136, IGNSS, http://igscb.jpl.nasa.gov/mail/igsmail/2010/msg00084.html

Georgiadou, Y., and A. Kleusberg (1988). "On carrier signal multipath effects in relative GPS positioning". *Manuscript Geodesy,* 13(3), 172–179.

Griffiths J, G. Gendt, T. Nischan and J. Ray (2009). "Assessment of the orbits from the 1st IGS reprocessing campaign (Invited)". AGU Fall Meeting Abstracts

Herring,T., R. King and S. McClusky (2008). "Massachusetts Institute of Technology (MIT) IGS Analysis Strategy Summary". [Online 15 January, 2012]. http://igscb.jpl.nasa.gov/igscb/center/analysis/MIT_acn.html.

Hugentobler, U. (2005). "Models in GNSS data analysis". Presentation at COMET – Advances in GPS Data Processing and Modeling for Geodynamics, University College London.

King, A., C. Watson, N. Penna and P. Clarke (2008)." Subdaily signals in GPS observations and their effect at semiannual and annual periods". *Geophysical Research Letters*, 35, L03302, doi: 10.1029/2007GL032252.

King, A., and S. Williams (2009). "Apparent stability of GPS monumentation from short-baseline time series." *Journal of Geophysical Research*, 114, B10403, doi: 10.1029/2009JB006319

King, M. A. and C. S. Watson (2010). "Long GPS coordinate time series: Multipath and geometry effects." *JGR*, Vol. 115, B04403, pp. doi: 10.1029/2009JB006543. King_Watson_2010_JGR_long_series_multipath_geometry.pdf

Kouba, J., (2009). "A Guide to using International GNSS Service (IGS) Products". *IGS publications, 2009.*

Lemoine, F. G., S. Kenyon, K. Factor, G. Trimmer, K. Pavlis, S. Chinn, M. Cox M. Klosko, B. Luthke, H. Torrance, M. Wang, G. Williamson, C. Pavlis, H. Rapp, and R. Olson (1998). "The Development of the Joint NASA GSFC and National Imagery and Mapping Agency (NIMA) Geopotential Model EGM96," NASA/TP-1998-206861, Goddard Space Flight Center, Greenbelt, Maryland.

Langley, R., (2007). "Class notes for Extraterrestrial Positioning". Department of Geodesy and Geomatics Engineering, University of New Brunswick.

Letellier, T., 2004, "Etude des ondes de mar´ee sur les plateaux continentaux," Th`ese doctorale, Universit´e de Toulouse III, 237pp.

Lyard, F., F. Lefèvre, T. Letellier and O. Francis. Modelling the global ocean tides: a modern insight from FES2004, *Ocean Dynamics*, 56, 394-415, 2006

Manabe, S., T. Sato, S. Sakai, and K. Yokoyama (1991), Atmospheric load effect on VLBI observations, in Chapman Conference on Geodetic VLBI: Monitoring Global Change, Washington, D. C.; April 22 – 26, 1991, *NOAA Tech. Rep. NOS 137 NGS 49*, pp. 111– 122, U.S. Dep. of Comm., Silver Spring, Md.

McCarthy, D., and G. Petit (2003). "International Earth Rotation and Reference Systems (IERS) Technical Note No.32", IERS Conventions Centre.

Melchior, P (1983). *The tides of the planet Earth*, pp 1-34.

Montenbruck, O., and E. Gill (2000). *Satellite Orbits, Models, Methods Applications*. Springer, Berlin, Heidelberg, New York. NovAtel Inc. (1997).

Mtamakaya, J., M. C. Santos, and M. Craymer (2011). "Assessment of Temporal Behavior of IGS Stations in Canada Using Least Squares Spectral Analysis." *IAG Symposia*, IAG General Assembly, Buenos Aires, Argentina, Aug 31-Sep, 2009.

Pavlis, N. K., A.S. Holmes, C.S. Kenyon, and K.J. Factor (2008). "An Earth gravitational model to degree 2160: EGM2008," presented *at the 2008 General Assembly of the European Geosciences Union*, Vienna, Austria, April 13-18, 2008.

Pagiatakis, S. (1999). "Stochastic significance of peaks in the least-squares spectrum". *Journal of Geodesy, vol. 73, issue 2, pp. 67-78*

Pagiatakis, S.D., H. Yin, and M. Abd El-Gelil (2007). Least-squares self-coherency analysis of superconducting gravimeter records in search for the Slichter triplet. *Physics of the Earth and Planetary Interiors, 160* (2): 108-123.

Penna, N. T., and M. P. Stewart (2003), Aliased tidal signatures in continuous GPS height time series, *Geophysical Research Letters*, *30(23), 2184.*

Penna, T., M. King, and M. Stewart (2007). "GPS height time series: Short-period origins of spurious long-period signals", *Journal of Geophysical Research*, 112, B02402, doi: 10.1029/2005JB004047.

Petit, G., and B. Luzum (2010). "International Earth Rotation and Reference Systems (IERS) Technical Note No.36".

Petrov, L., and J. Boy (2004). "Study of the atmospheric pressure loading signal in VLBI observations". *JGR,* 10.1029/2003JB002500, Vol. 109, No. B03405, 2004.

Ponte, R. M., and R. D. Ray (2002), Atmospheric pressure correction in geodesy and oceanography: A strategy for handling air tides, *Geophysical Research Letters*, 29(24), 2153, doi: 10.1029/2002GL016340.

Ray, R., D., (1999). "A Global Ocean Tide Model From TOPEX/POSEIDON Altimetry: GOT99.2". *NASA Technical Memorandum 209478*, National Aeronautics and Space Administration, Goddard Space Flight Center, Greenbelt, MD.GOT99.2b/GOT00.2

Ray, R. D. and R. M. Ponte, 2003, "Barometric tides from ECMWF operational analyses," *Annales Geophysicae*., 21(8), pp. 1897–1910, doi: 10.5194.

Ray, J. R., Z. Altamimi, X. Collilieux, and T. van Dam (2008). "Anomalous harmonics in the spectra of GPS position estimates". *GPS Solutions* (2008) 12:55–64, DOI: 10.1007/s10291-007-0067-7

Ray, J., and J. Griffiths (2008). "Overview of IGS products and Analysis Center Modeling". *IGS 2008 Workshop,* Miami Beach, 2 June 2008. http://igscb.jpl.nasa.gov/overview/pubs/IGSWorkshop2008/prog.html.

Ray, J. (2009). *"*Preparations for the 2nd IGS Reprocessing Campaign." *Eos Trans. AGU, 90*(52), *Fall Meeting Suppl.*, Abstract G11B-0642.

Ray, J., (2011). "Personal communications". National Oceanic and Atmospheric Administration.

Rabbel, W., and H. Schuh (1986). The influence of atmospheric loading on VLBI-experiments. *Journal of Geophysics* 59:164–170

Rabbel, W., and J. Zschau (1985) Static deformations and gravity changes at the earth's surface due to atmospheric loading. Journal of Geophysics 56:81– 99

Rudenko, S., G. Gendt and M. Daehnn (2008). "German Research Centre for Geosciences (GTZ) IGS Analysis Strategy Summary". [Online 15 January, 2012]. http://igscb.jpl.nasa.gov/igscb/center/analysis/gtz.acn.

Rülke, A., R. Dietrich, M. Fritsche, M. Rothacher, P.Steigenberger (2008). Realization of the Terrestrial Reference System by a reprocessed global GPS network. *Journal of Geophysical Research, Vol. 113.*

Santos, M.C (2008)." Class notes for Quantitative Analysis-GGE6102". Department of Geodesy and Geomatics Engineering, University of New Brunswick.

Schmid, R., G. Mader, T. Herring (2005). "From relative to absolute antenna phase center corrections". *In: MeindlM (ed) Proc IGS Workshop and Symposium*, Bern, March 2004, pp 209-219.

Schmid, R., P.Steigenberger, G.Gendt and M. Rothacher M (2007). Generation of a consistent absolute phase center correction model for GPS receiver and satellite antennas. *Journal of Geodesy,* Vol. 81, No. 12, pp. 781-798.

Segall, P., and J. L. Davis (1997). GPS applications for geodynamics and earthquake studies. *Annual Revision Earth Planetary Science, 23, 201– 336, 1997.*

Schaer, S., R. Dach, M. Meindl, H. Bock, A. Jaeggi and L. Ostini (2008). "Center for Orbit Determination in Europe (CODE) IGS Analysis Strategy Summary". [Online January, 2012].   http://igscb.jpl.nasa.gov/igscb/center/analysis/code.acn.

Steigenberger, P., M. Fritsche and A. Ruelke (2006). " GeoForschungsZentrum (GFZ) IGS Analysis Strategy Summary". [Online 15 January, 2012]. http://igscb.jpl.nasa.gov/igscb/center/analysis/pdr.acn.

Tregoning, P., and C. Watson (2009). "Atmospheric effects and spurious signals in GPS analyses." *JGR*, 114, B09403, doi:10.1029/2009JB006344

Tregoning, P., G. Ramillien, H. McQueen, and D. Zwartz (2009). "Glacial isostatic adjustment and nonstationary signals observed by GRACE." *Journal of Geophysical Research*, 114, B06406, doi: 10.1029/2008JB006161

van Dam, T., G. Blewitt, and M. B. Heflin (1994), Atmospheric pressure loading effects on Global Positioning System coordinate determinations, *Journal of Geophysical Research*, 99, 23,939–23,950.

van Dam, T., J. Wahr, P. Milly, A. Shmakin, G. Blewitt, D. Lavallee, and K. Larson (2001). Crustal displacements due to continental water loading, *Geophysical Research Letters,* 28, 651– 654.

van Dam, T., J. Wahr, and D. Lavalle´e (2007), A comparison of annual vertical crustal displacements from GPS and Gravity Recovery and Climate Experiment (GRACE) over Europe, *Journal of Geophysical Research*, 112, B03404, doi: 10.1029/2006JB004335.

van Dam, T., H. Plag, O. Francis, P. Gegout (2002). "GGFC Special Bureau for Loading: Current Status and Plans." Proceedings of the IERS Workshop on Combination Research and Global Geophysical Fluids. Bavarian Academy of Sciences, Munich, Germany, 18 - 21 November 2002.

van Dam, T., 2010, Updated October 2010. NCEP Derived 6-hourly, global surface displacements at 2.5 x 2.5 degree spacing. Data set accessed on 2011-01-17 at http://geophy.uni.lu/ncep-loading.html.

van Dam, T., Z. Altamimi, X. Collilieux, and J. Ray (2010). "Topographically Induced Height Errors in Predicted Atmospheric Loading Effects." *Journal of Geophysical Research,* Vol. 115, B07415, doi: 10.1029/2009JB006810

Vaníček, P., (1969). Approximate spectral analysis by least-squares fit. *Astrophysical Space Science 4:387-391*

Vaníček, P., (1971). Further development and properties of the spectral analysis by least squares. *Astrophysical Space Science 12:10-33*

Walser, P., (2012). Personal communications

Weber R, (2001). [IGSMAIL-3229]: *IGP Products / Closing date*. [Online 20 March 2011] http://igscb.jpl.nasa.gov/mail/igsmail/2001/msg00077.html.

Wells, D., P.Vaníček and S. Pagiatakis (1985). Least squares spectral analysis revisited. Tech Report 84, Department of Survey Engineering, University of New Brunswick, Fredericton.

Willis, K., D. Chambers, and R. Nerem (2008). "Assessing the globally averaged sea level budget on seasonal to inter annual timescales", *Journal of Geophysical Research,* Vol. 113, C06015, doi: 10.1029/2007JC004517.

Wijaya, D., J. Böhm, M. Schindelegger, M. Karbon, and H. Schuh (2010). "Determination and comparison of atmospheric pressure loading corrections." WG1/WG2 Workshop of COST Action ES0701, Nov., 2010–TU Vienna, Austria. http://ggosatm.hg.tuwien.ac.at/LOADING/COSTES0701/05_2010_COST_Vienna_Wijaya.pdf

Appendix A: Summary of LS Spectra Results with and Without APL

Appendix A provides a summary of the LSSA and LS Coherent Analysis with and without the corrections for APL displacements and is provided by mean of Figures A1 to A52. All the Figures have the following common characteristics:

a) All plots have been produced using logarithmic scale for the purpose of having a better presentation of the results in a single plot.

b) The top panels correspond to the vertical components (positions and residuals) and the bottom panels present the horizontal components (positions and residuals).

c) The blue red spectral plots correspond to spectral plots without APL corrections whereas the plots in red have been corrected for APL.

d) The vertical axes are the percentage variance and the horizontal axes are the period in cycles per year

e) The vertical green lines indicate the first through fourth harmonics in the spectra.
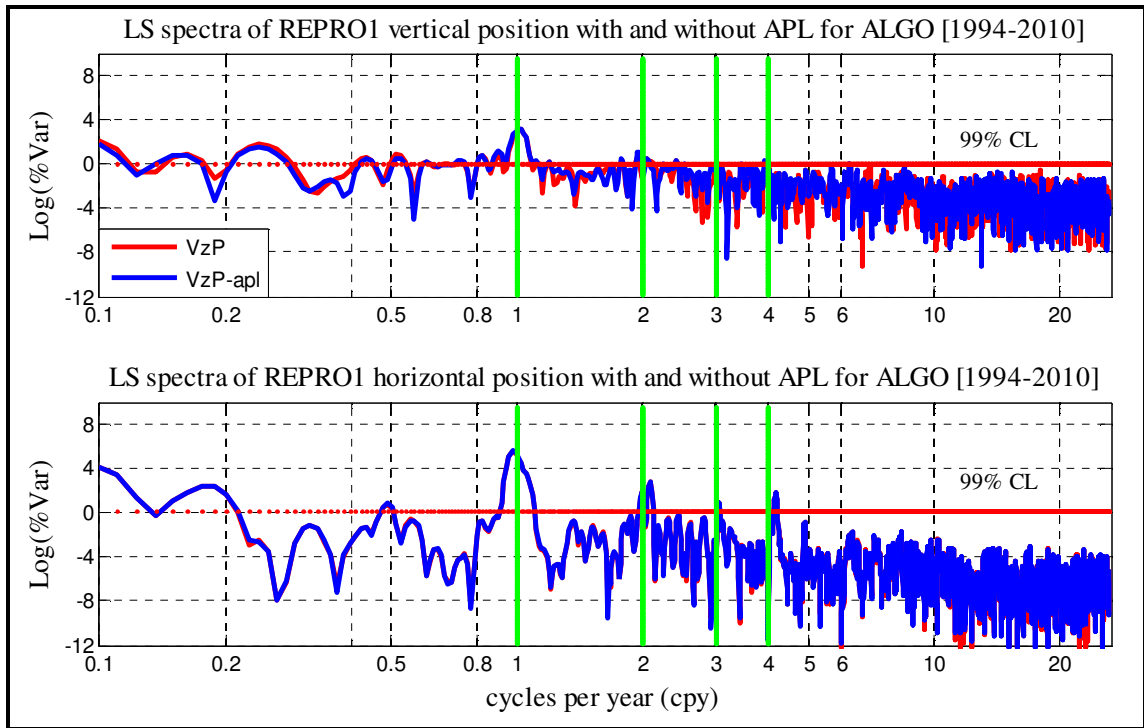
Figure A1 Least squares coherent spectra of REPRO1 positions for ALGO (1994-2010)
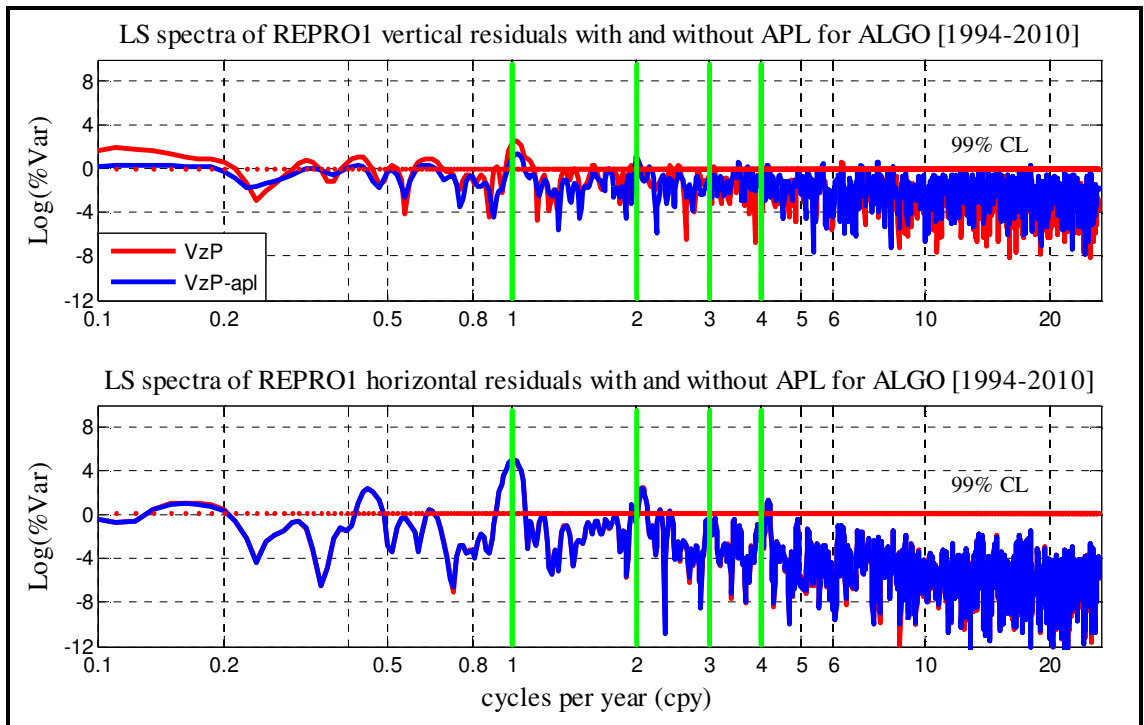

Figure A2 Least squares coherent spectra of REPRO1 residuals for ALGO (1994-2010)
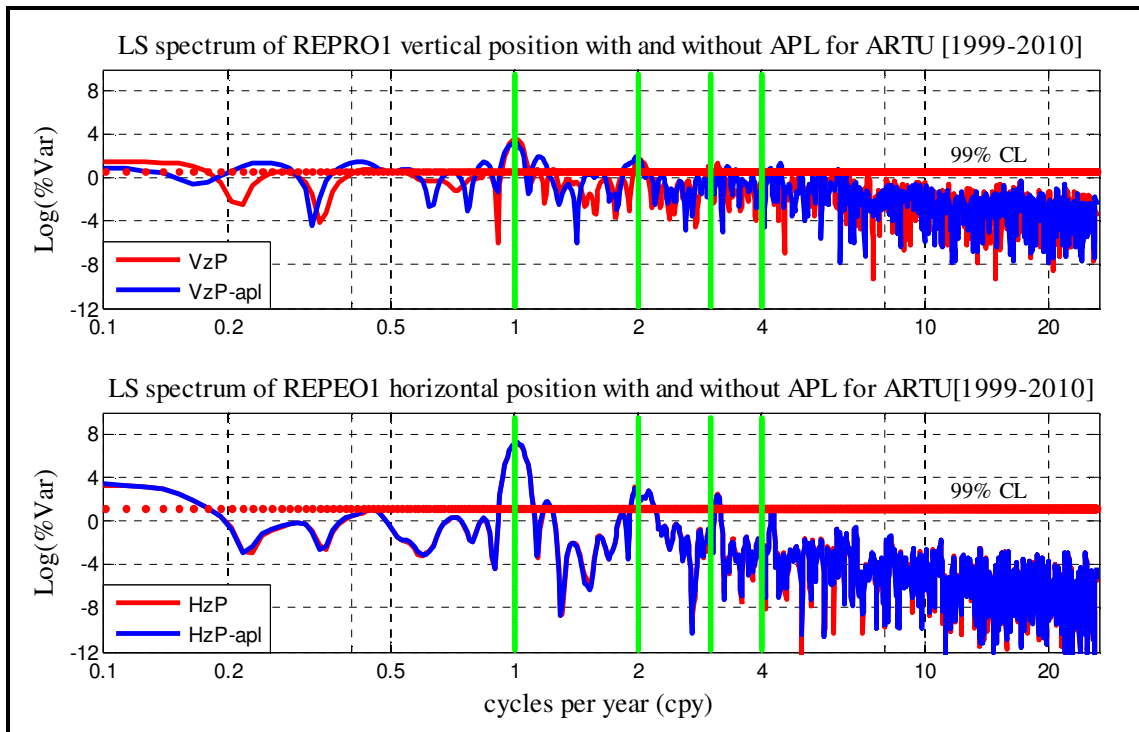
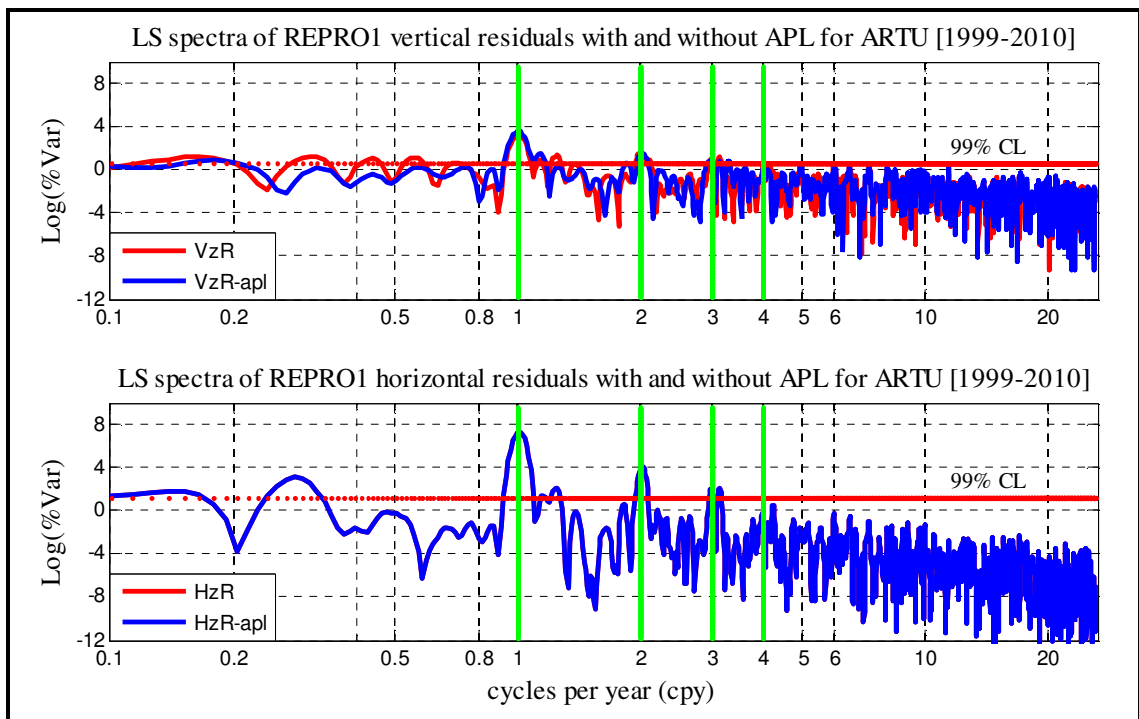Figure A3 Least squares coherent spectra of REPRO1 positions for ARTU (1999-2010)

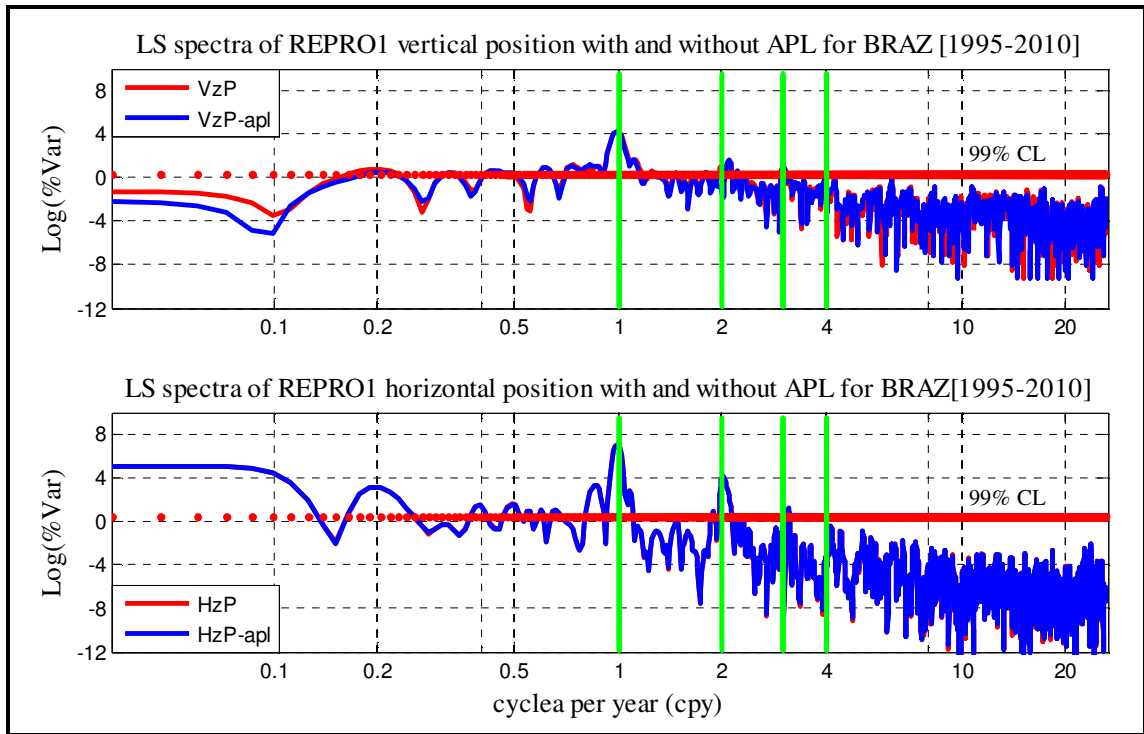Figure A4 Least squares coherent spectra of REPRO1 residuals for ARTU (1999-2010)

Figure A5 Least squares coherent spectra of REPRO1 positions for BRAZ (1995-2010)
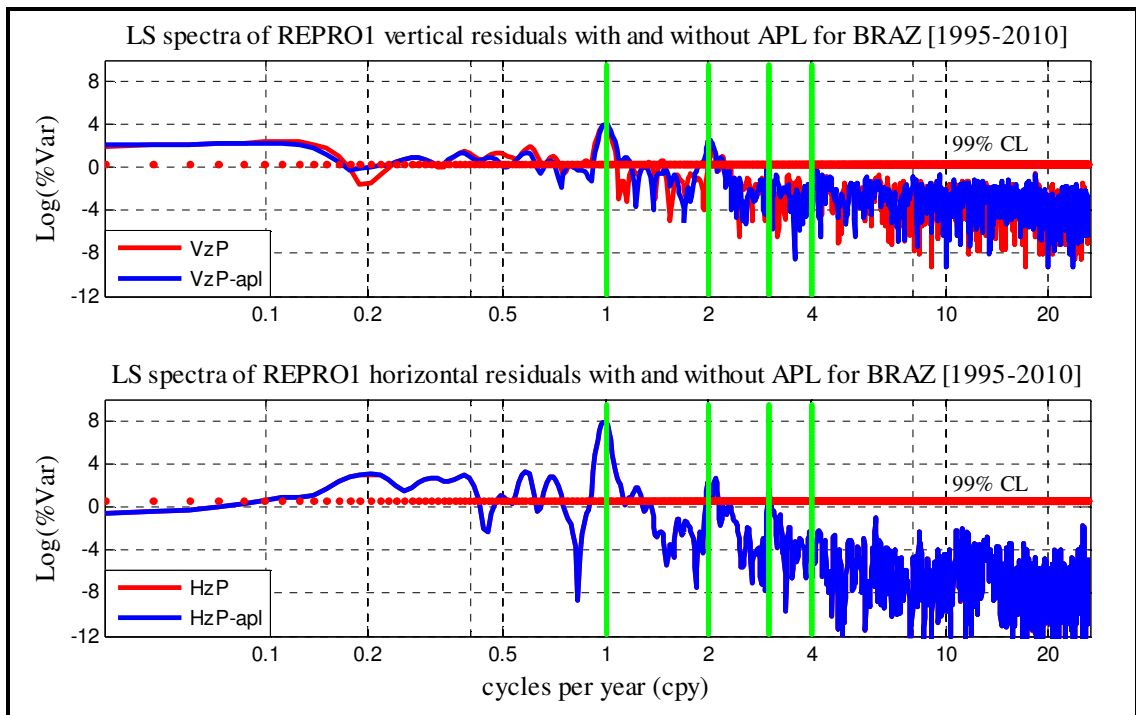

Figure A6 Least squares coherent spectra of REPRO1 residuals for BRAZ (1995-2010)
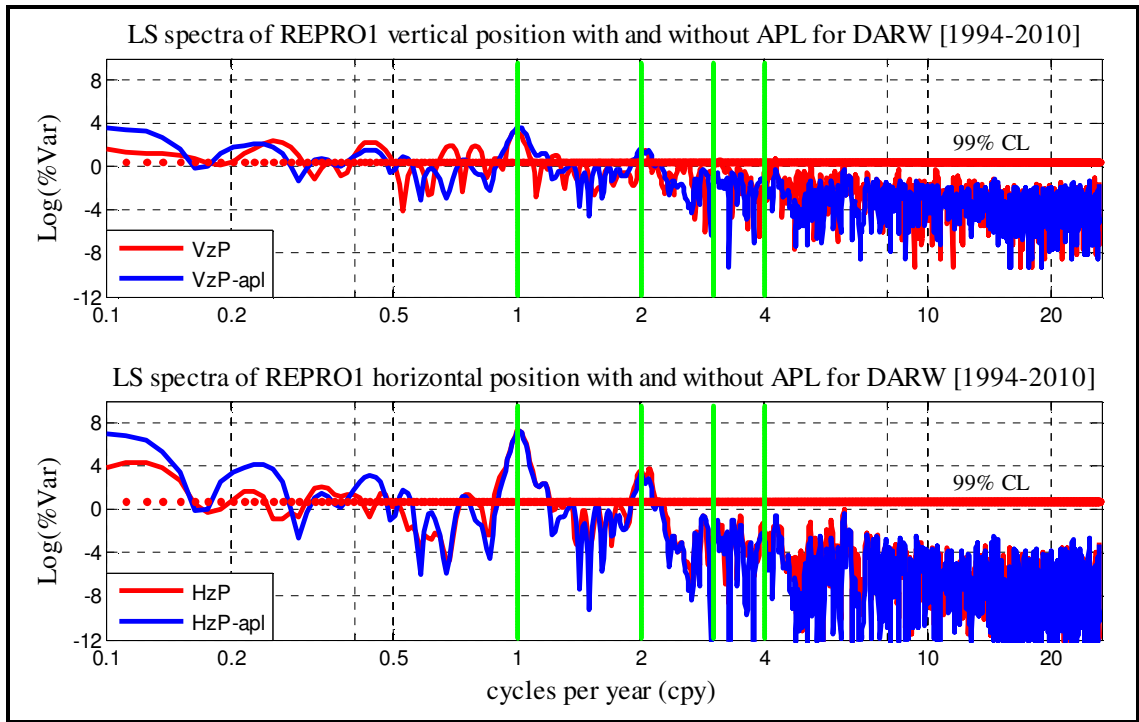
Figure A7 Least squares coherent spectra of REPRO1 positions for DARW (1994-2010)
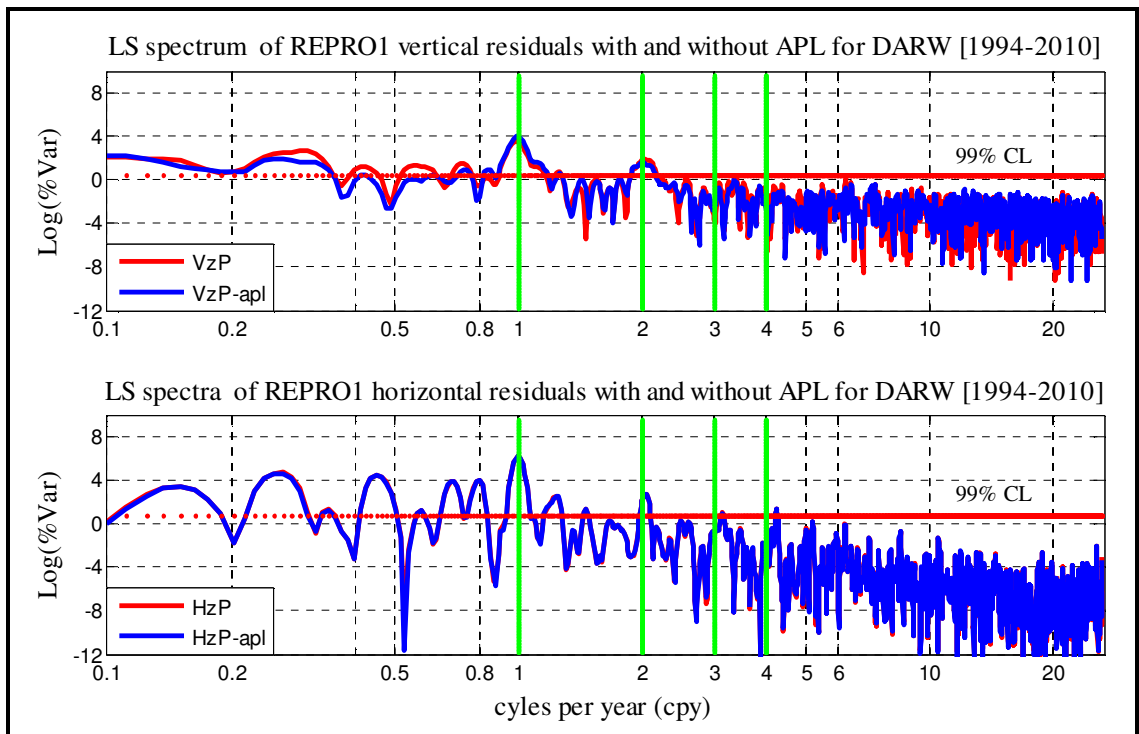

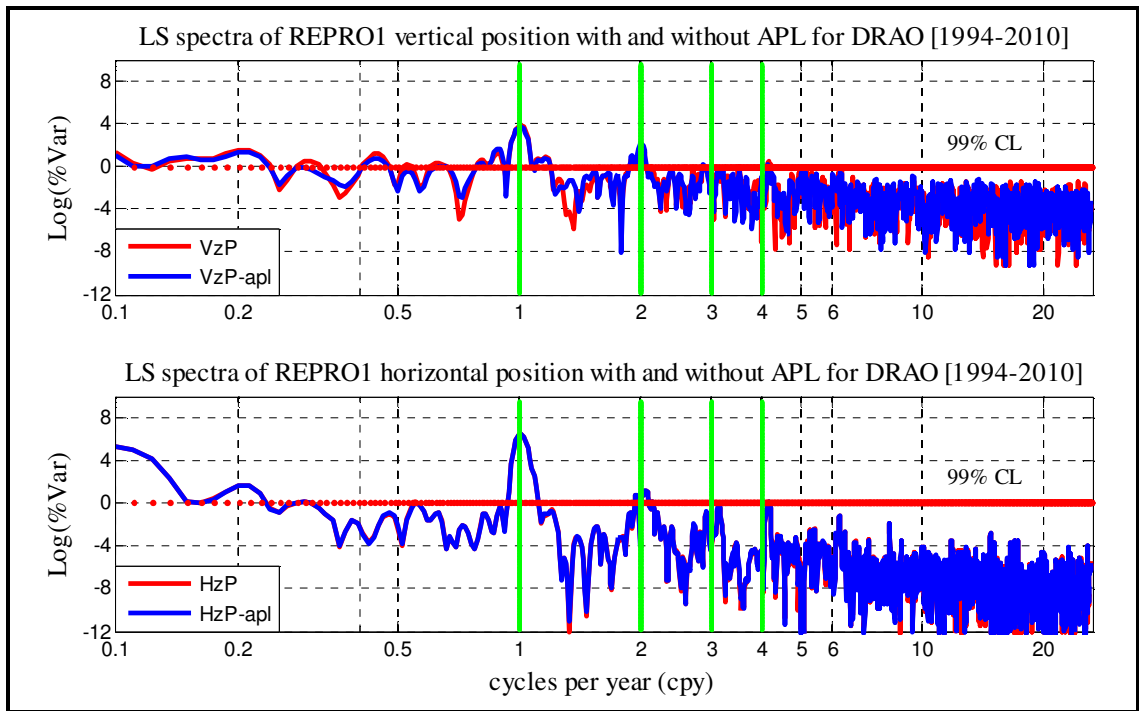Figure A8 Least squares coherent spectra of REPRO1 residuals for DARW (1994-2010)

Figure A9 Least squares coherent spectra of REPRO1 positions for DRAO (1994-2010)

Figure A10 Least squares coherent spectra of REPRO1 residuals for DRAO (1994-2010)

167

Figure A11 Least squares coherent spectra of REPRO1 positions for GSLV (1998-2010)

Figure A12 Least squares coherent spectra of REPRO1 residuals for GSLV (1998-2010)

168

Figure A13 Least squares coherent spectra of REPRO1 positions for HLNC (1997-2010)
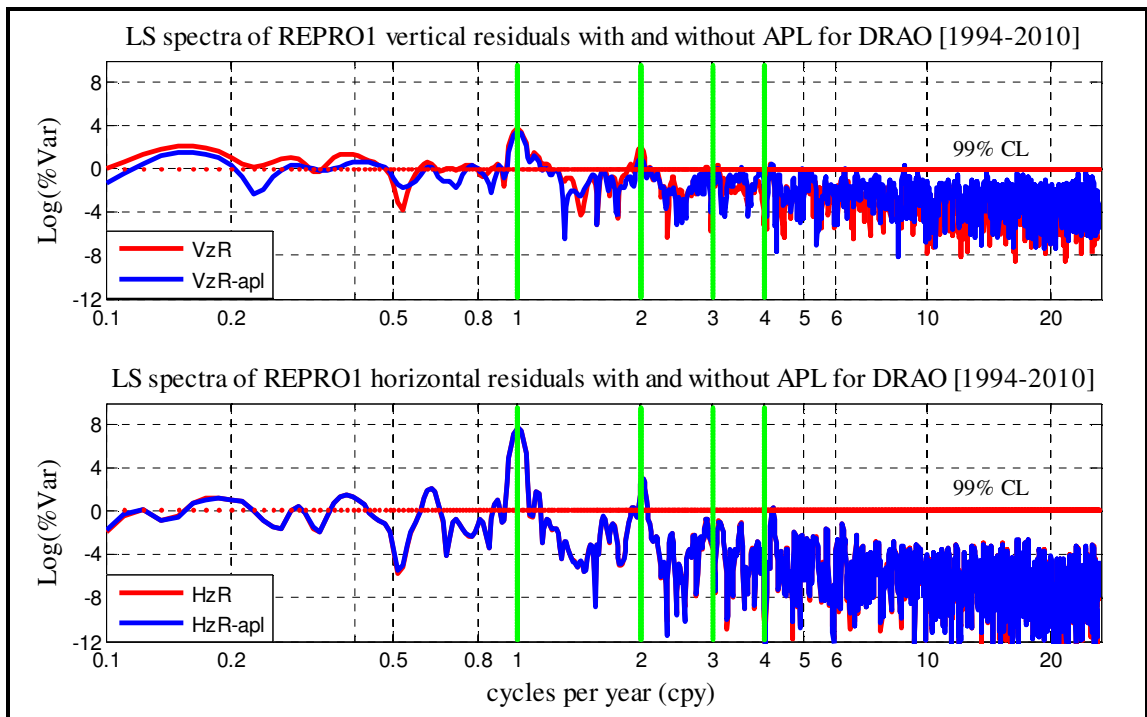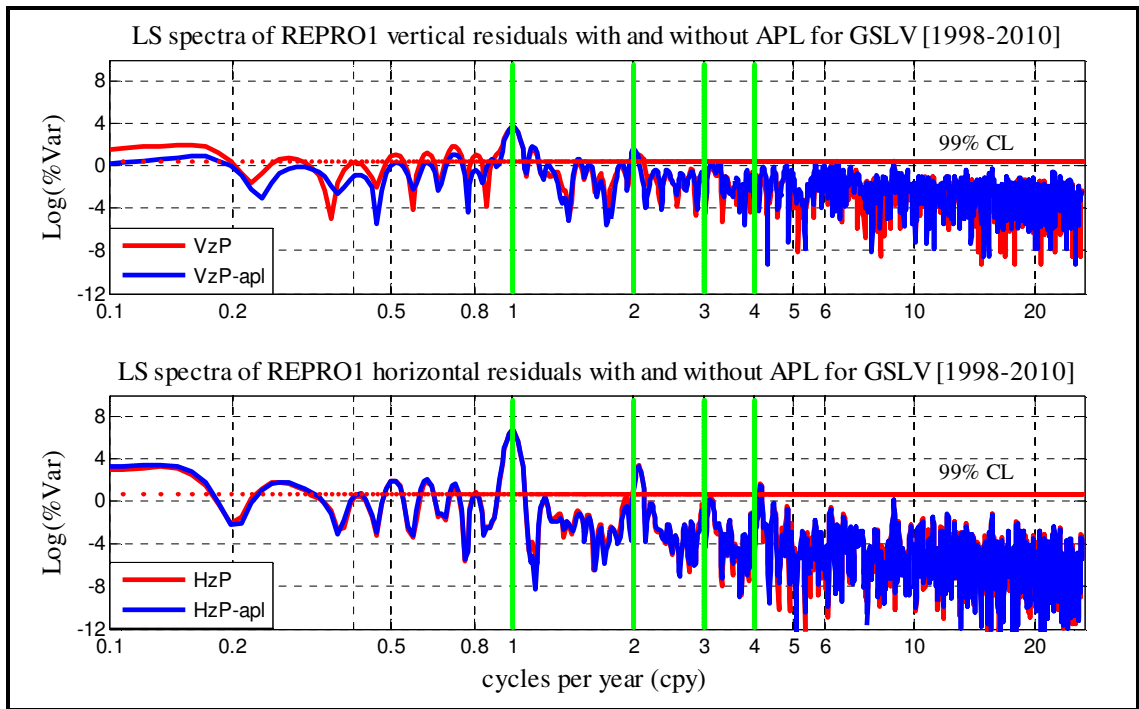

Figure A14 Least squares coherent spectra of REPRO1 residuals for HLNC (1997-2010)

Figure A15 Least squares coherent spectra of REPRO1 positions for HOLM (2001-2010)

Figure A16 Least squares coherent spectra of REPRO1 residuals for HOLM (2001-2010)

170

Figure A17 Least squares coherent spectra of REPRO1 positions for HYDE (2002-2010)

Figure A18 Least squares coherent spectra of REPRO1 residuals for HYDE (2002-2010)

171

Figure A19 Least squares coherent spectra of REPRO1 positions for IISC (1994-2010)
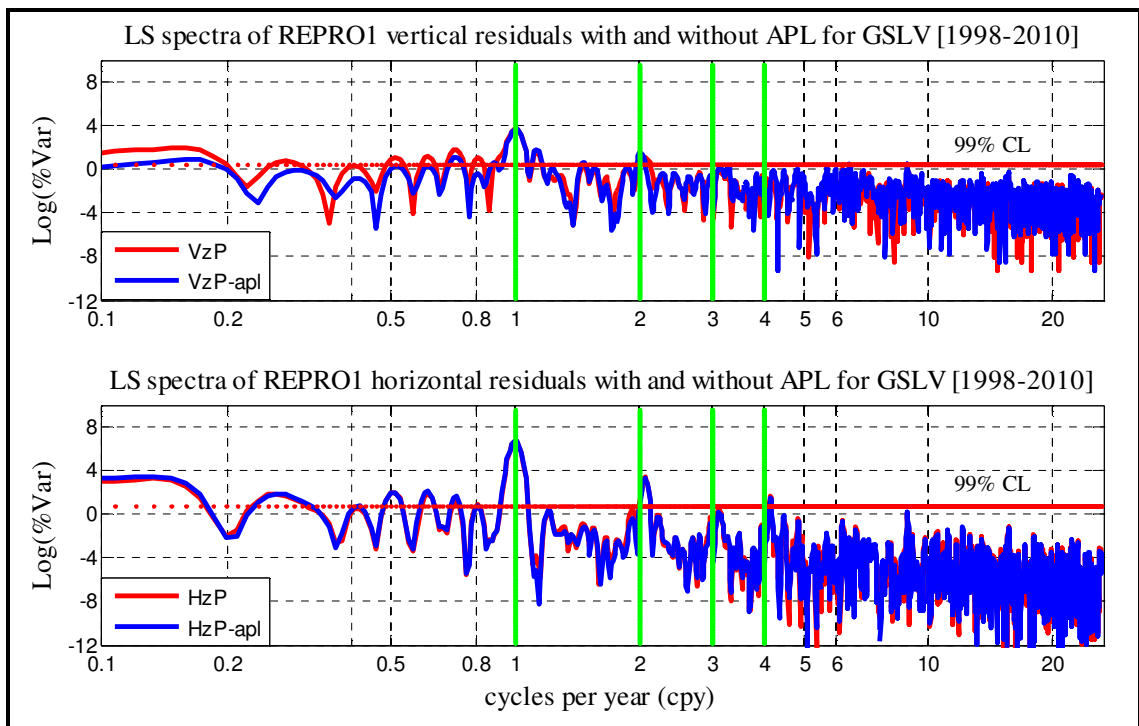

Figure A20 Least squares coherent spectra of REPRO1 residuals for IISC (1994-2010)

Figure A21 Least squares coherent spectra of REPRO1 positions for IRKJ (2002-2010)

Figure A22 Least squares coherent spectra of REPRO1 residuals for IRKJ (2002-2010)

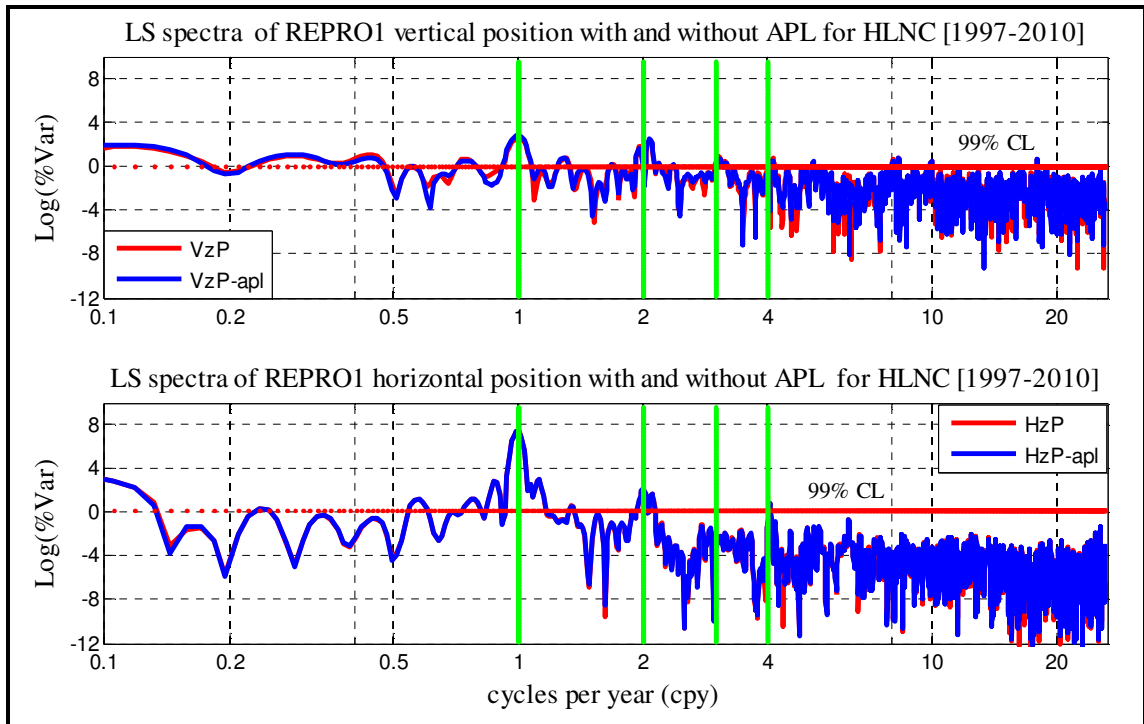Figure A23 Least squares coherent spectra of REPRO1 positions for IRKT (1995-2010)

Figure A24 Least squares coherent spectra of REPRO1 residuals for IRKT (1995-2010)

174

Figure A25 Least squares coherent spectra of REPRO1 positions for KOKB (1994-2010)
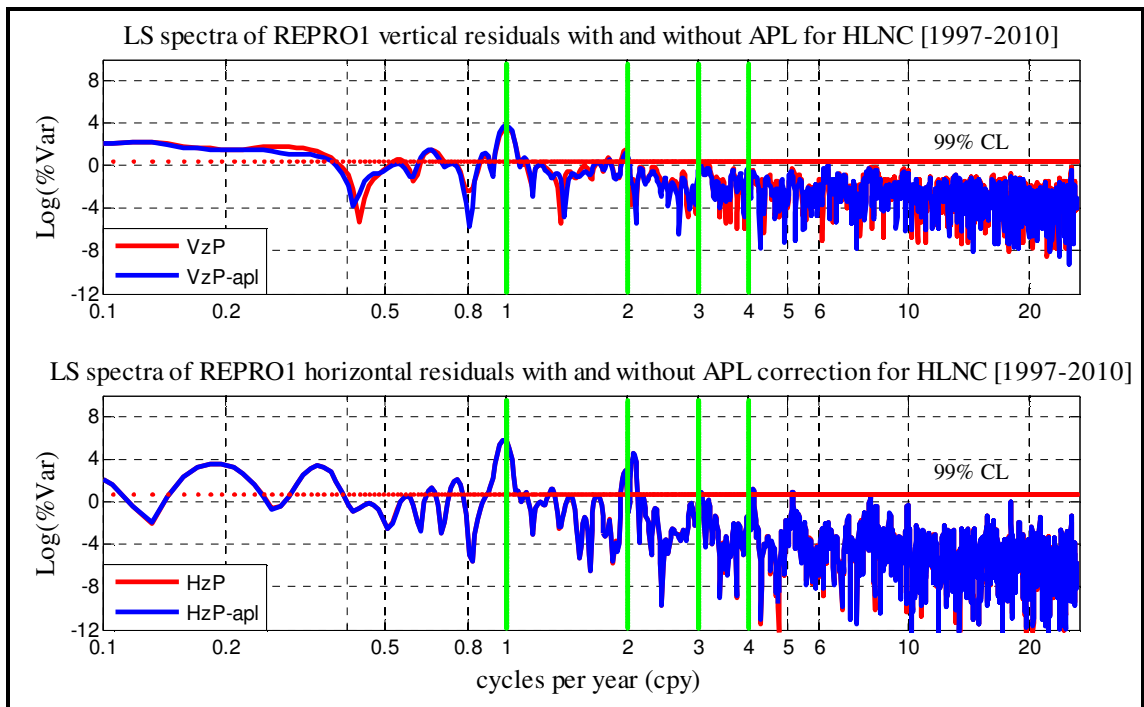

Figure A26 Least squares coherent spectra of REPRO1 residuals for KOKB (1994-2010)

Figure A27 Least squares coherent spectra of REPRO1 positions for KOUR (1994-2010)

Figure A28 Least squares coherent spectra of REPRO1 residuals for KOUR (1994-2010)

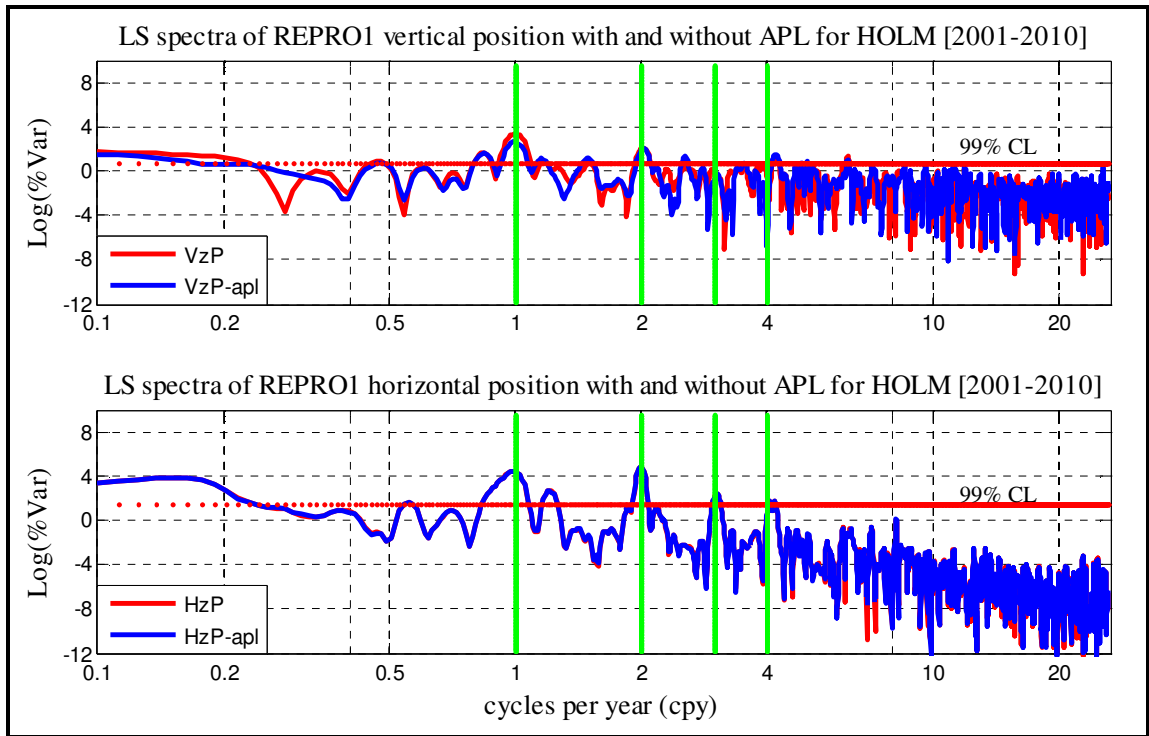Figure A29 Least squares coherent spectra of REPRO1 positions for MAS1 (1994-2010)

Figure A30 Least squares coherent spectra of REPRO1 residuals for MAS1 (1994-2010)

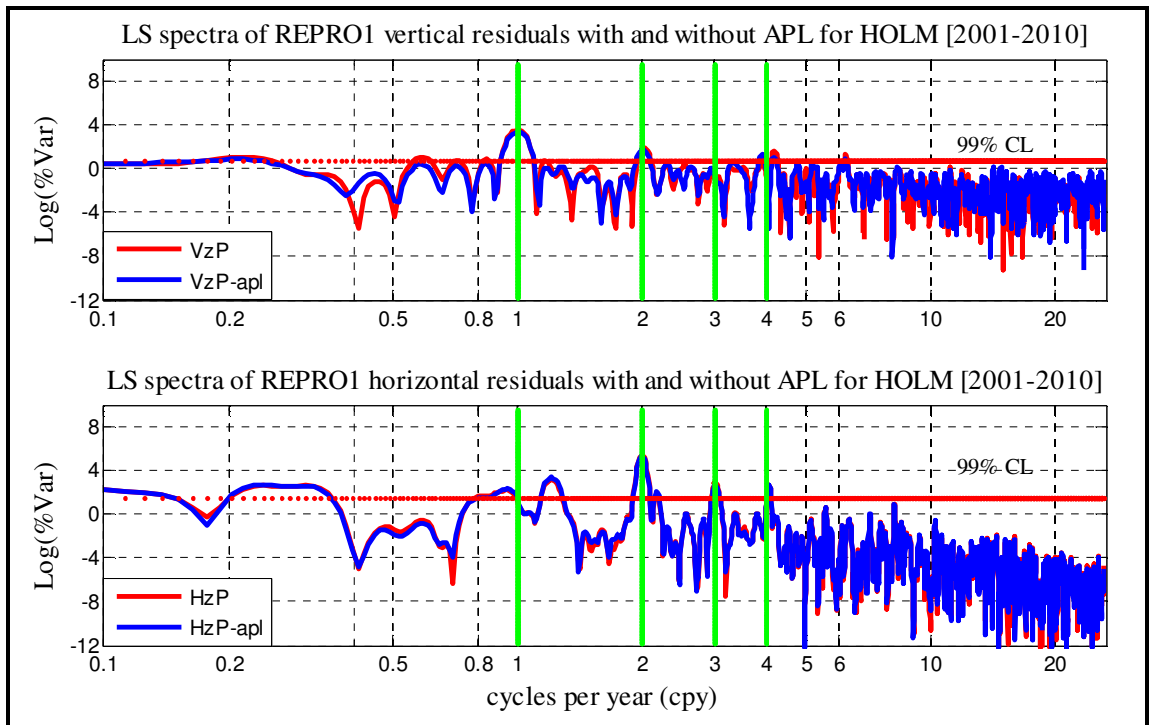Figure A31 LSSA and LS coherent spectra of positions for MIZU (2002-2010)
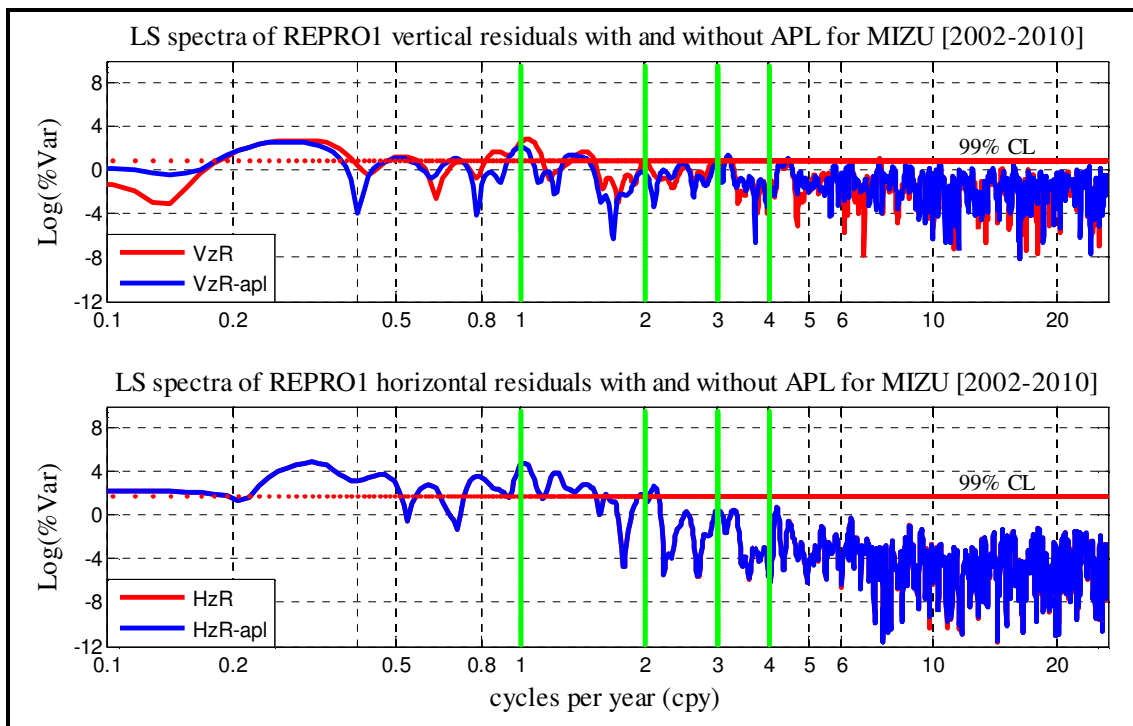
Figure A32 Least squares coherent spectra of REPRO1 residuals for MIZU (2002-2010)
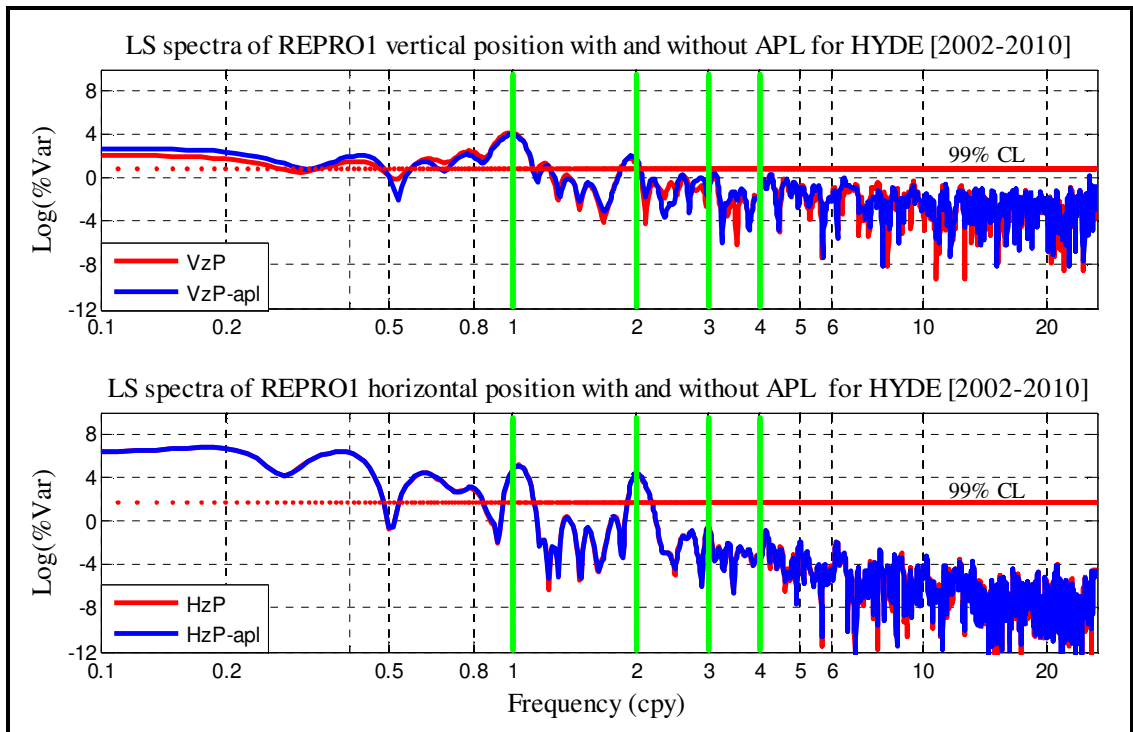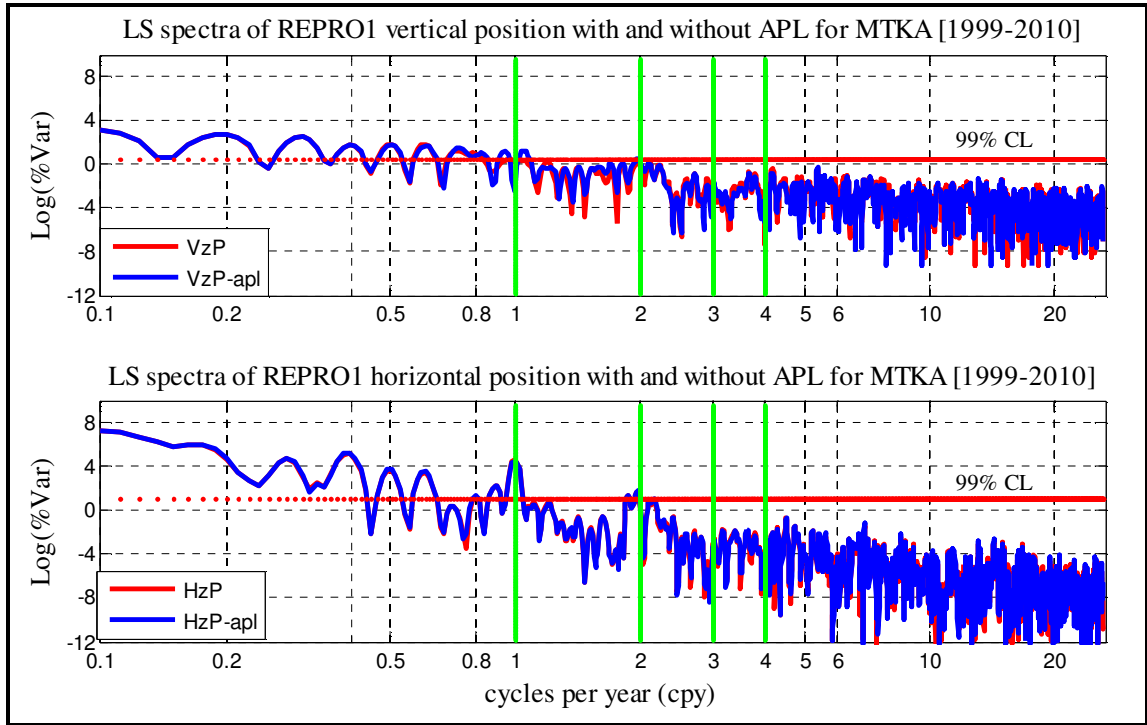
Figure A33 Least squares coherent spectra of REPRO1 positions for MTKA (1999-2010)
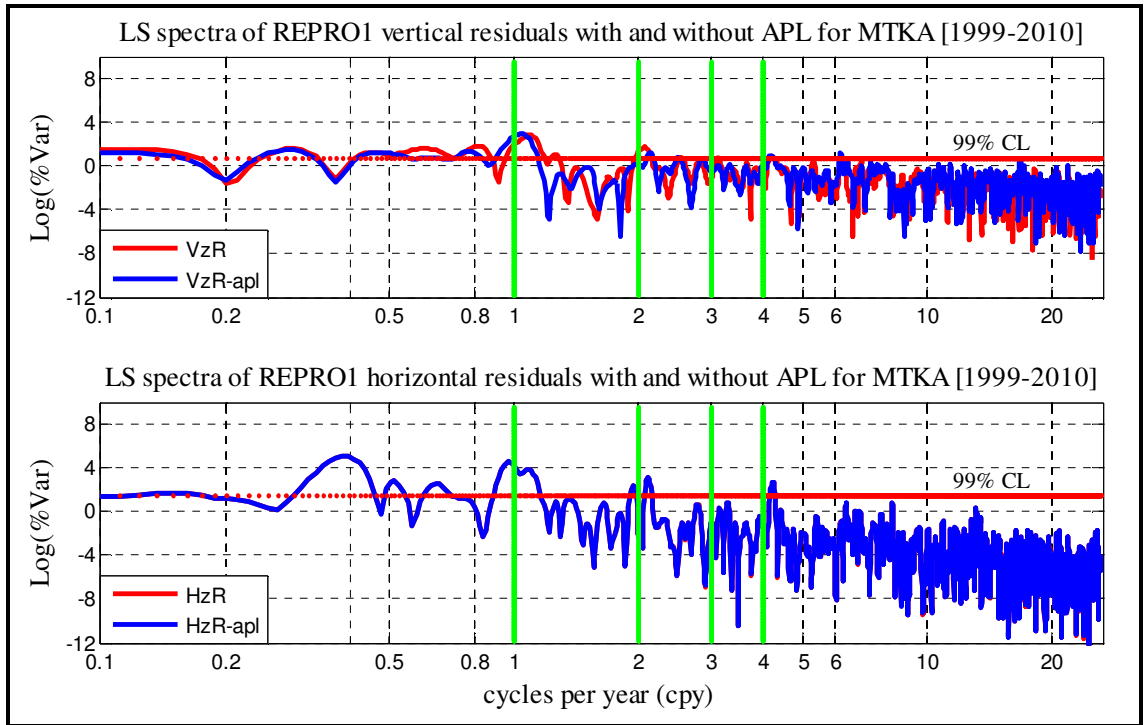
Figure A34 Least squares coherent spectra of REPRO1 residuals for MTKA (1999-2010)
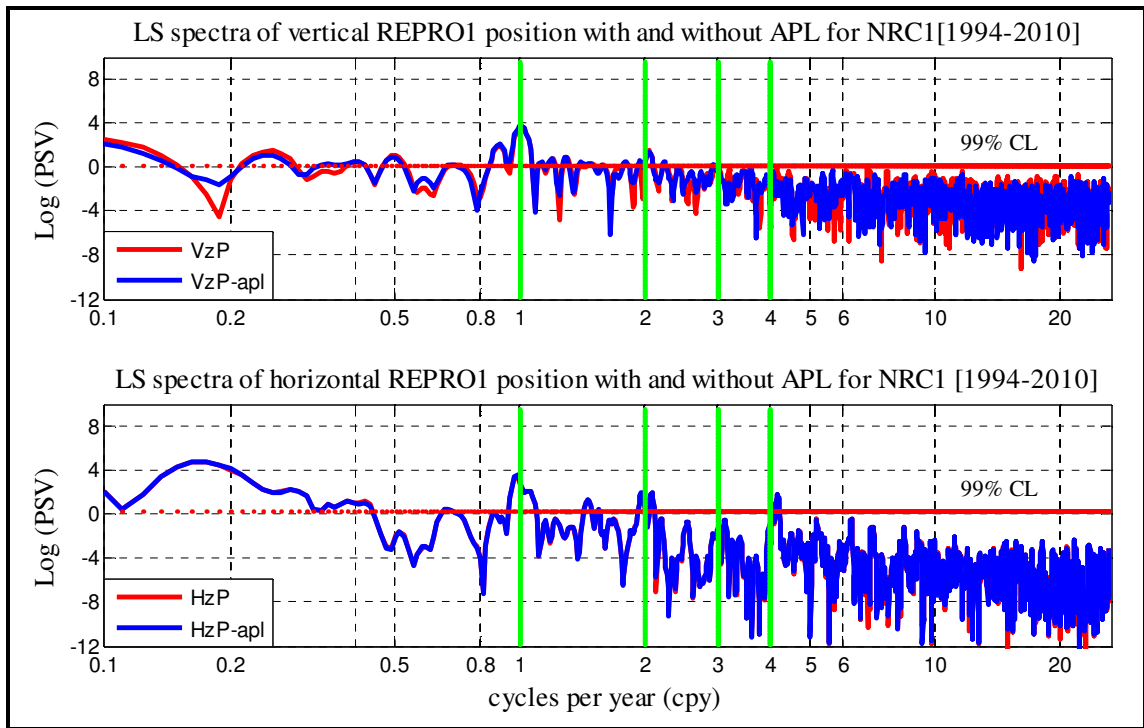
Figure A35 Least squares coherent spectra of REPRO1 positions for NRC1 (1994-2010)
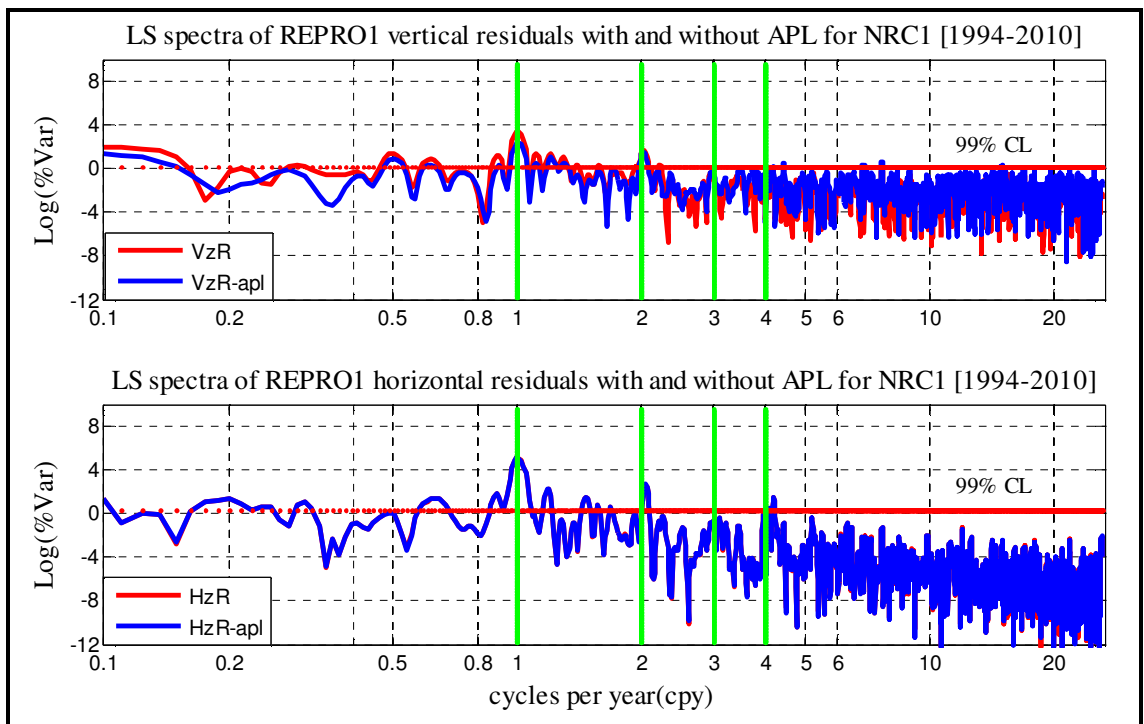
Figure A36 Least squares coherent spectra of REPRO1 residuals for NRC1 (1994-2010)

180
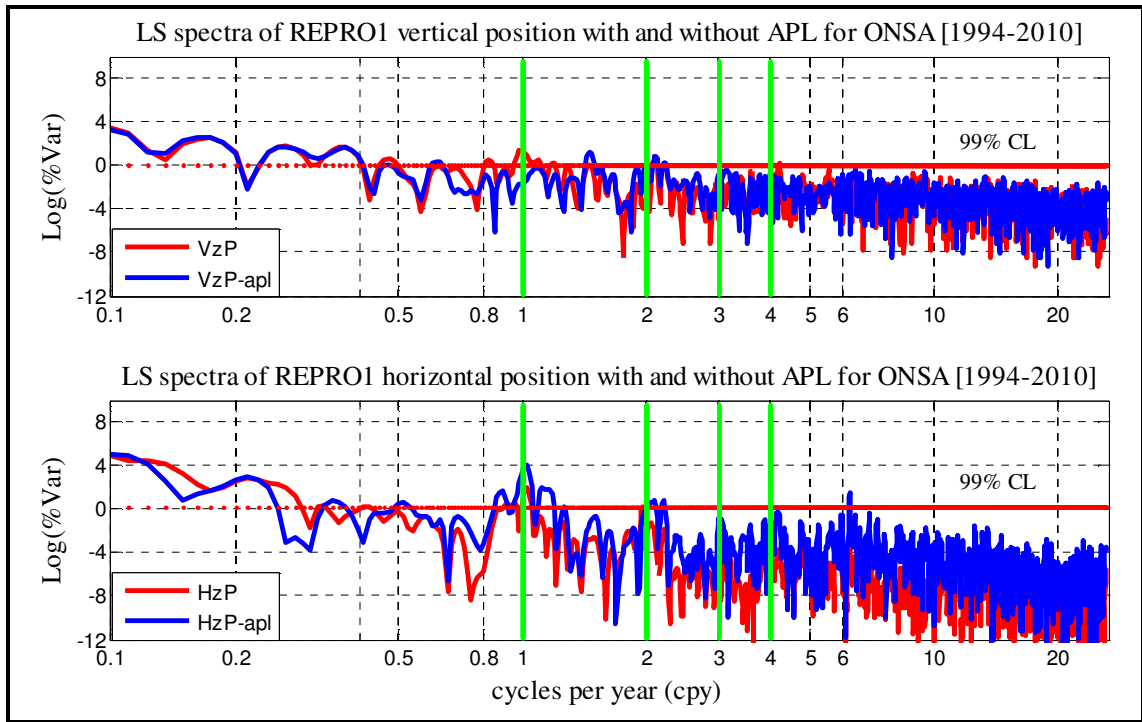
Figure A37 Least squares coherent spectra of REPRO1 positions for ONSA (1994-2010)
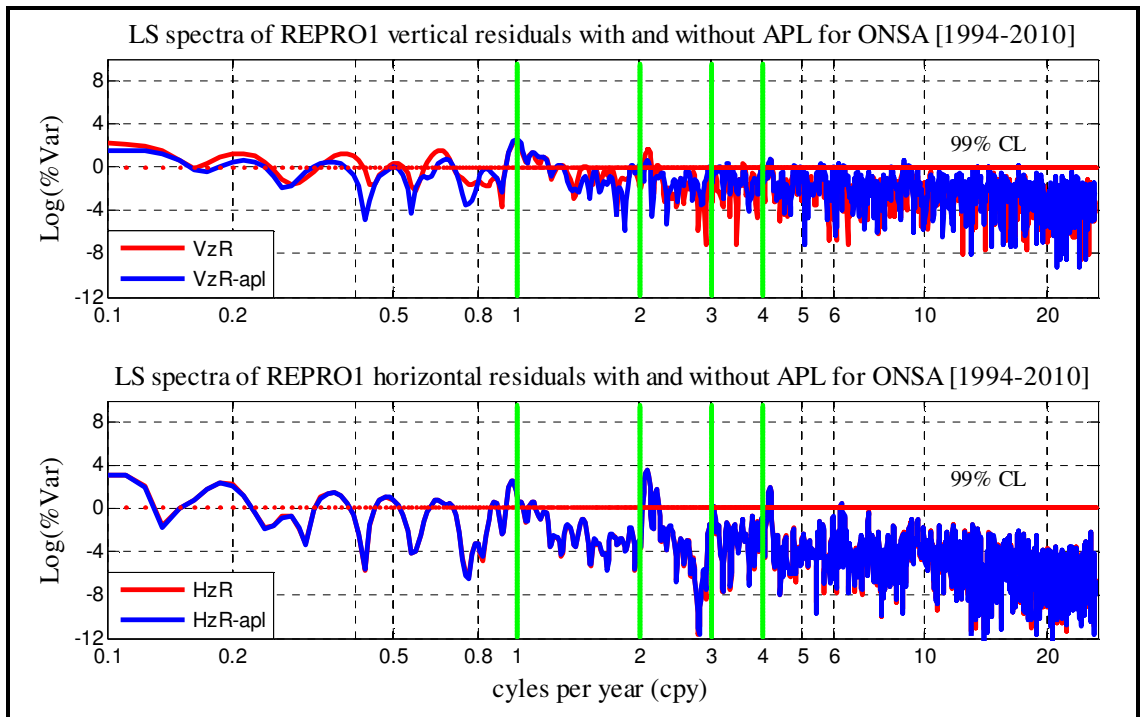
Figure A38 Least squares coherent spectra of REPRO1 residuals for ONSA (1994-2010)
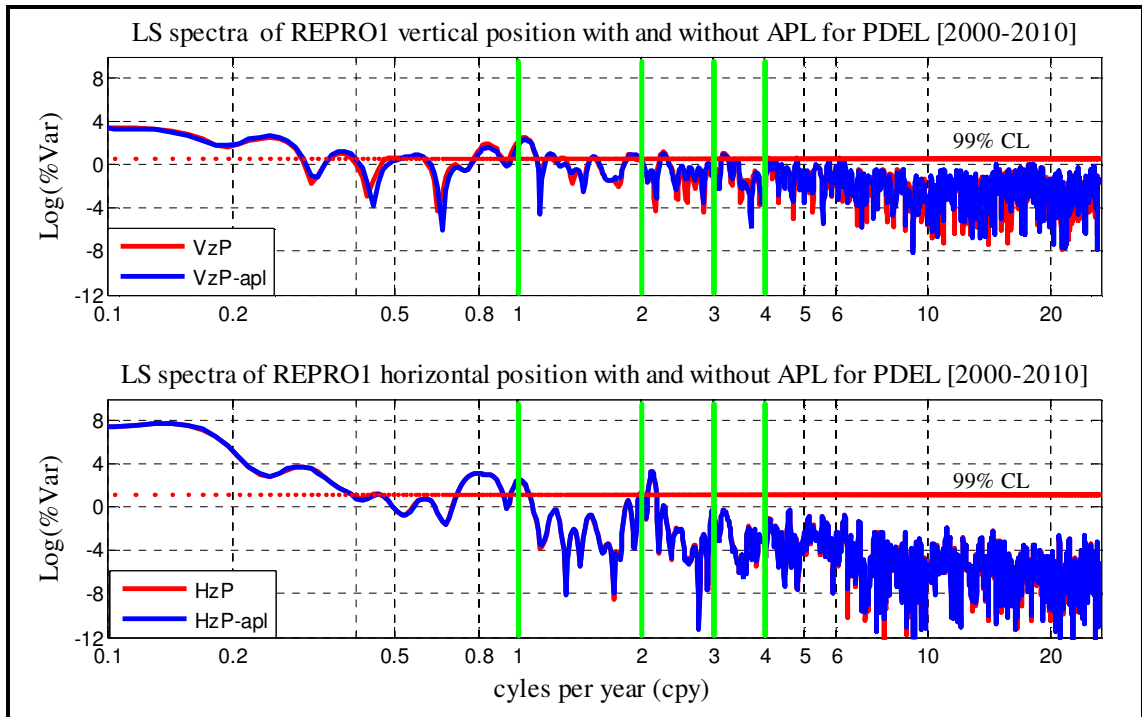
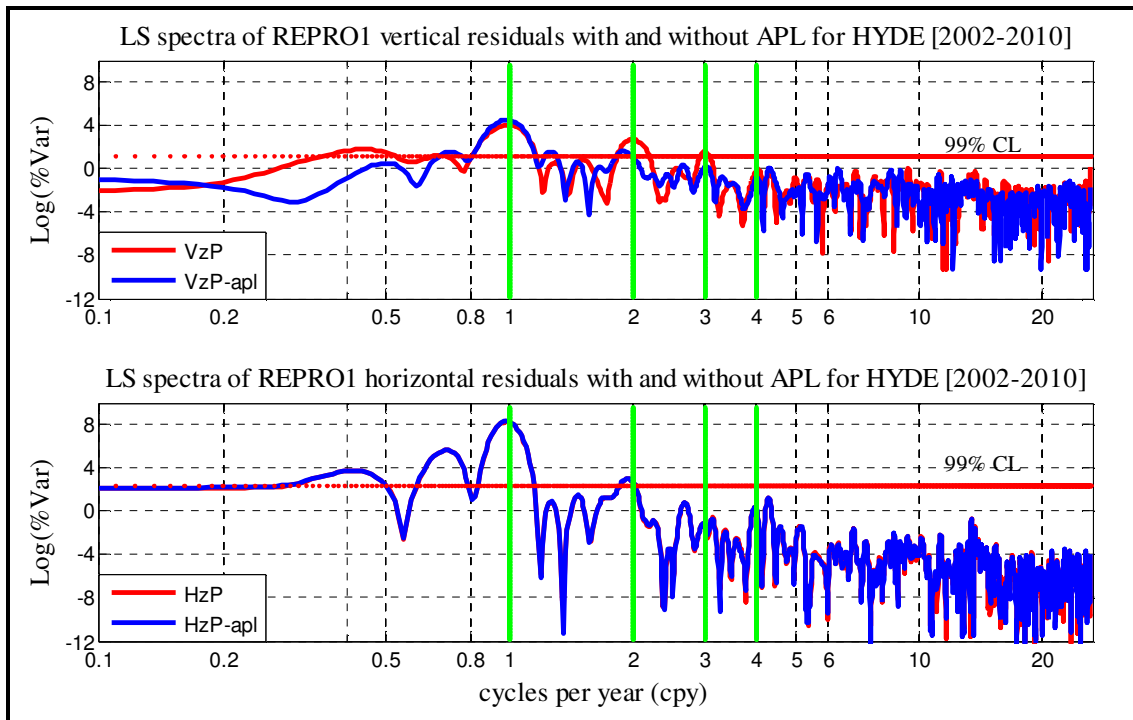Figure A39 Least squares coherent spectra of REPRO1 positions for PDEL (2000-2010)
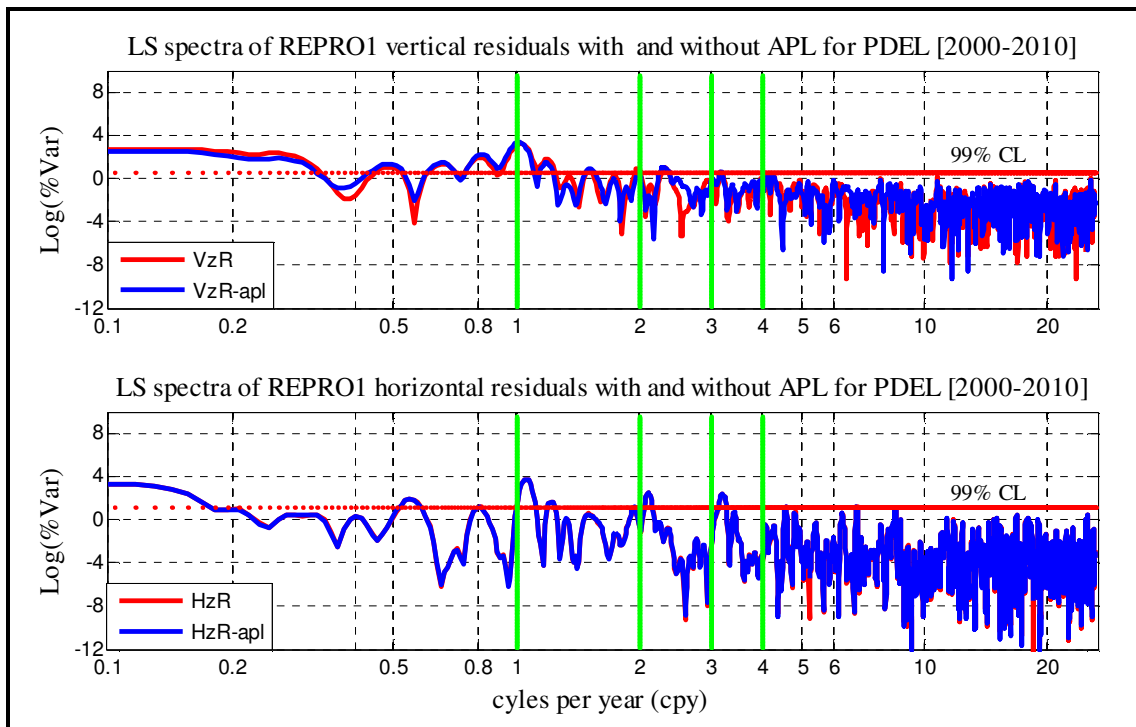
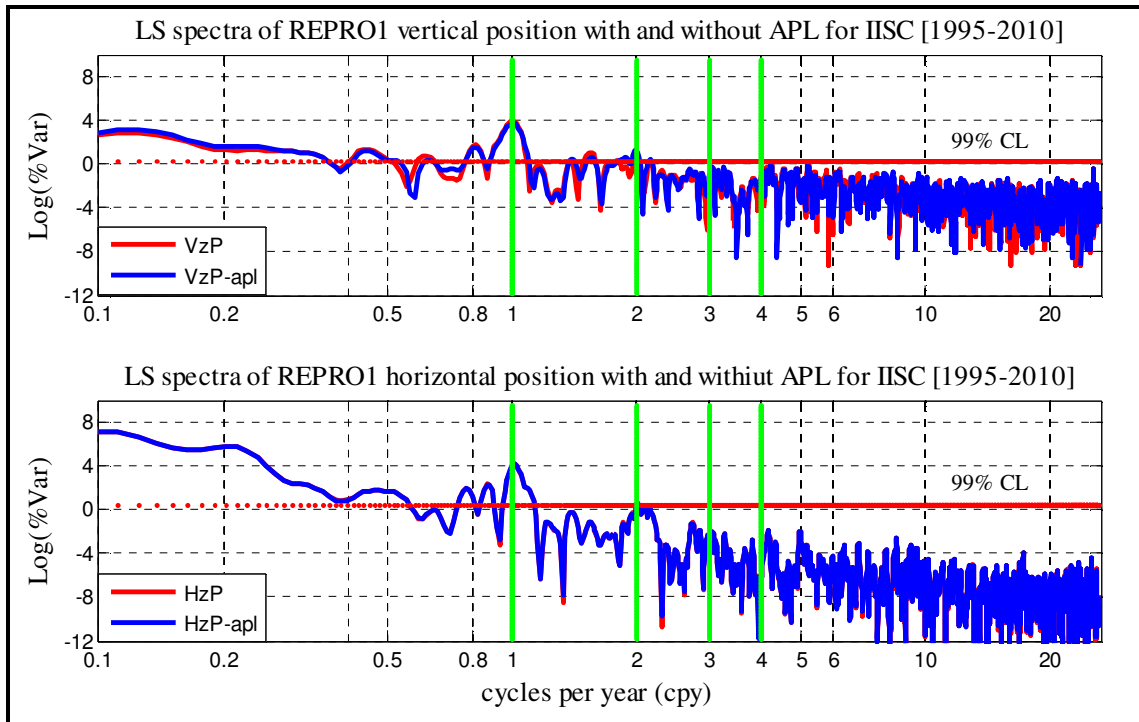Figure A40 Least squares coherent spectra of REPRO1 residuals for PDEL (2000-2010)
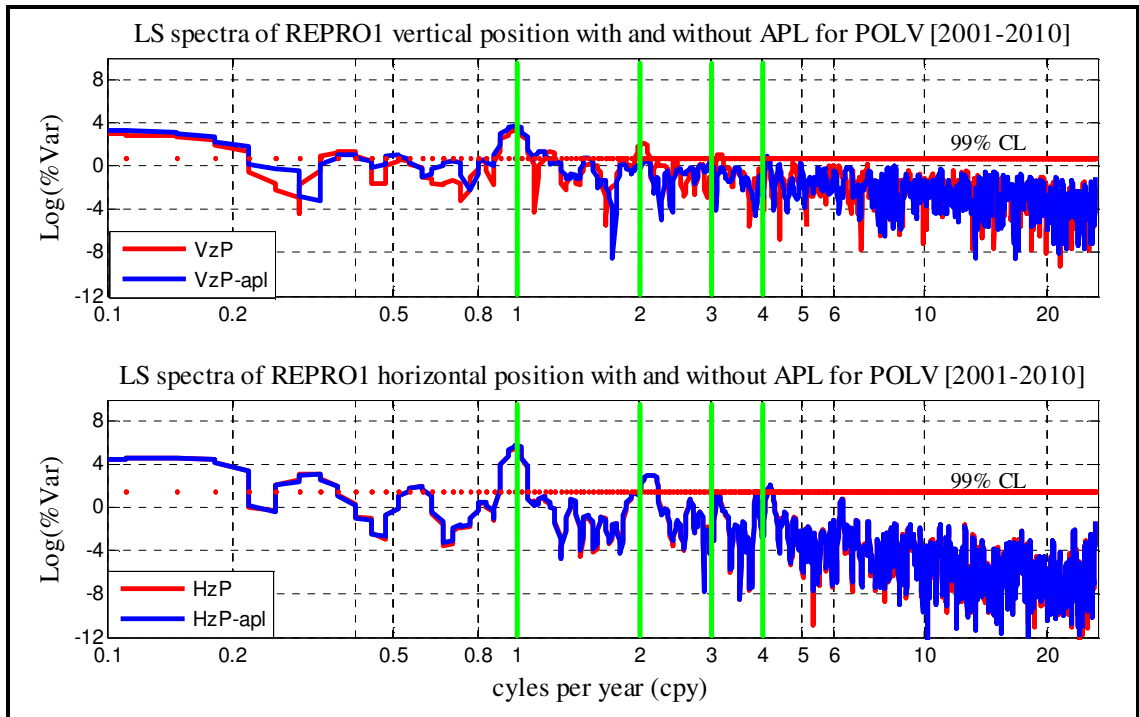
Figure A41 Least squares coherent spectra of REPRO1 positions for POLV (2001-2010)
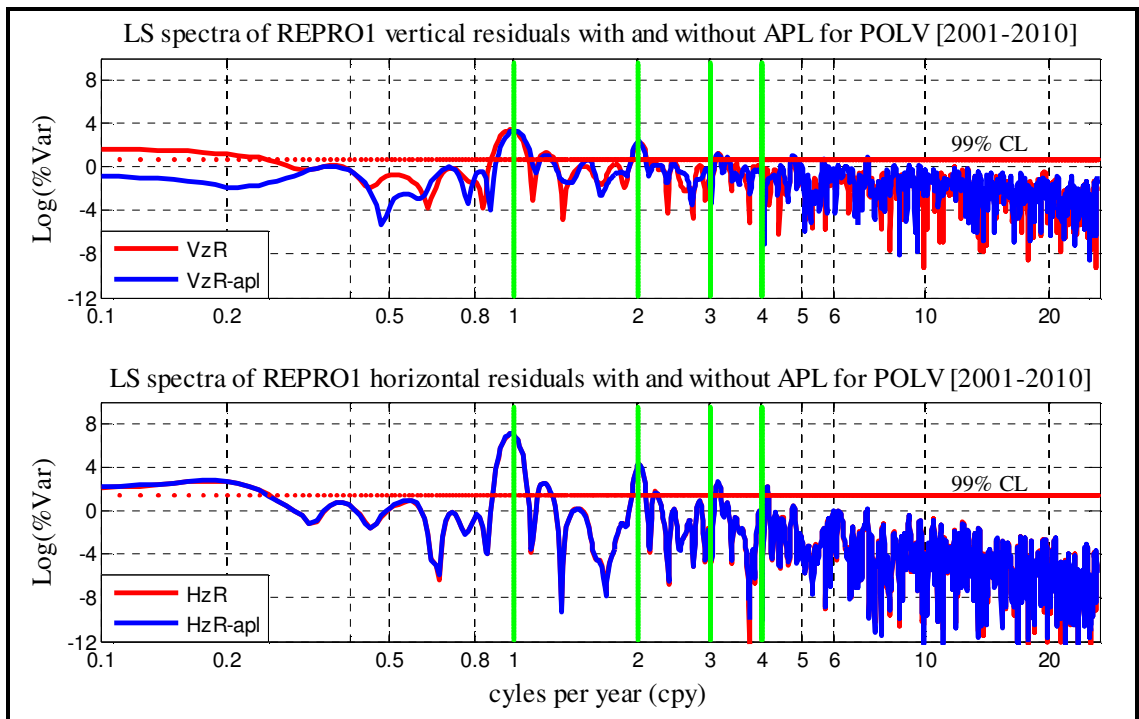
Figure A42 Least squares coherent spectra of REPRO1 residual for POLV (2001-2010)
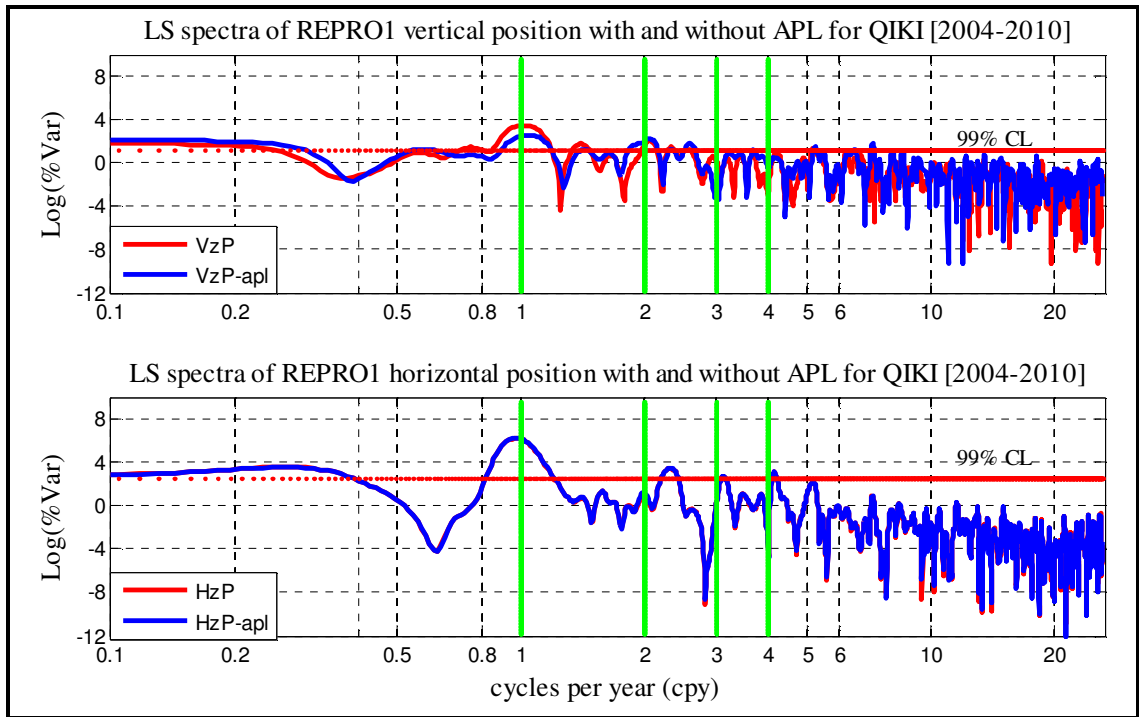
Figure A43 Least squares coherent spectra of REPRO1 positions for QIKI (2004-2010)
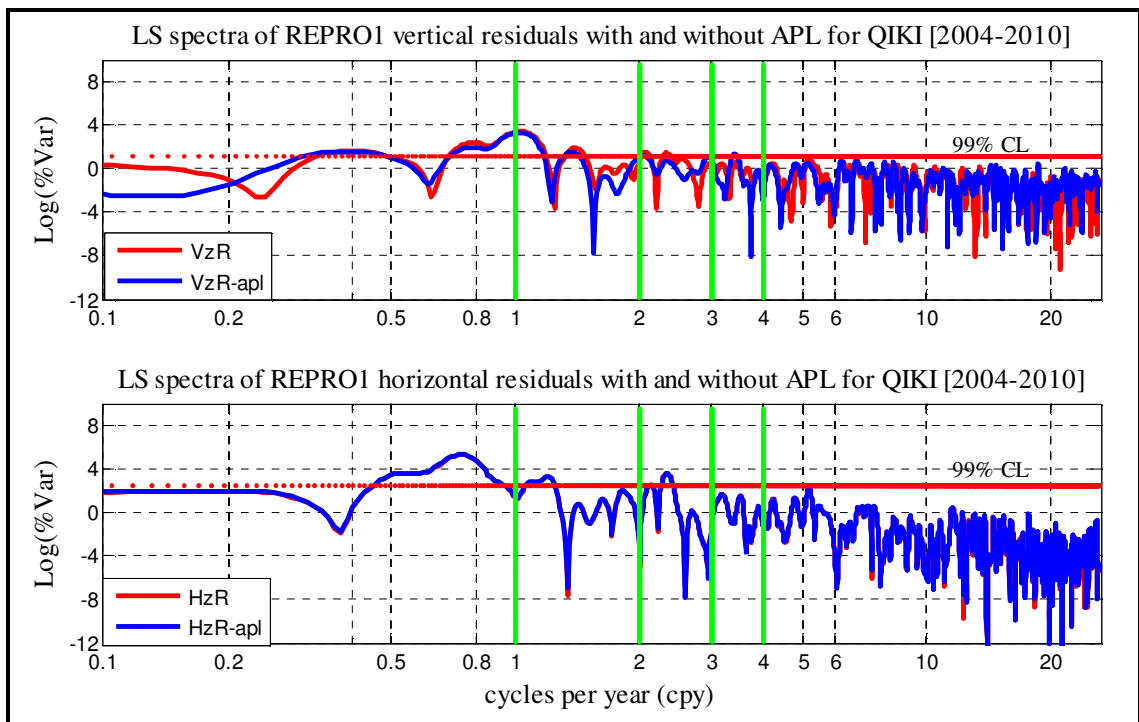
Figure A44 Least squares coherent spectra of REPRO1 residuals for QIKI (2004-2010)
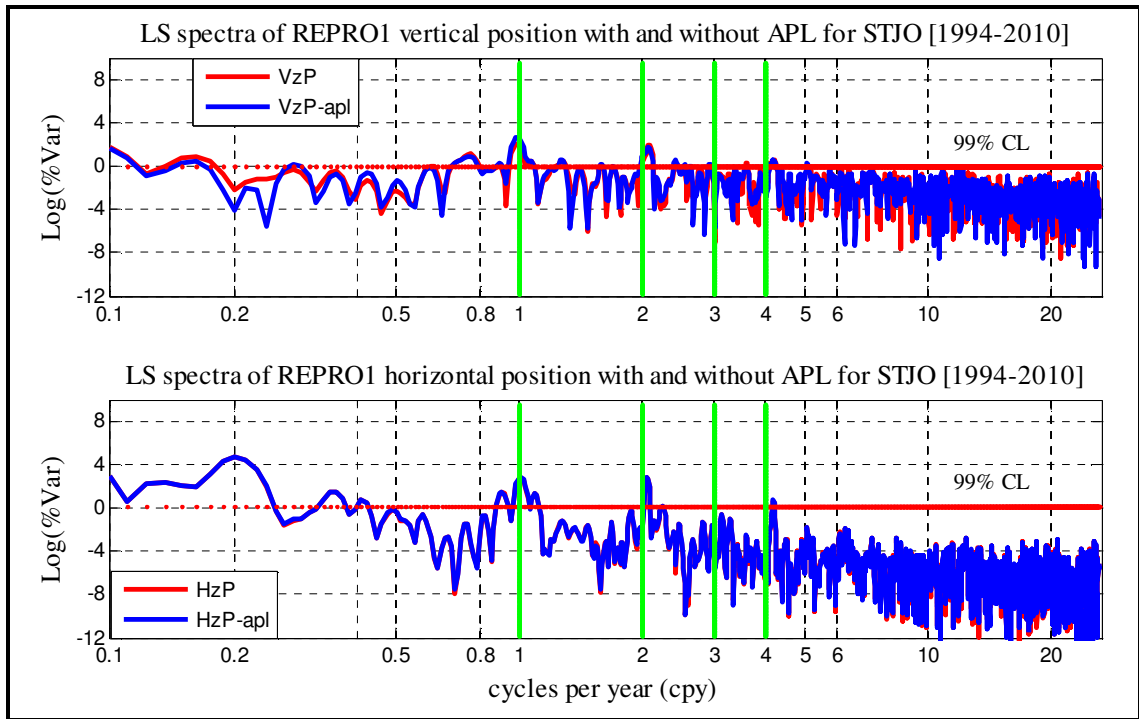
Figure A45 Least squares coherent spectra of REPRO1 positions for STJO (1994-2010)
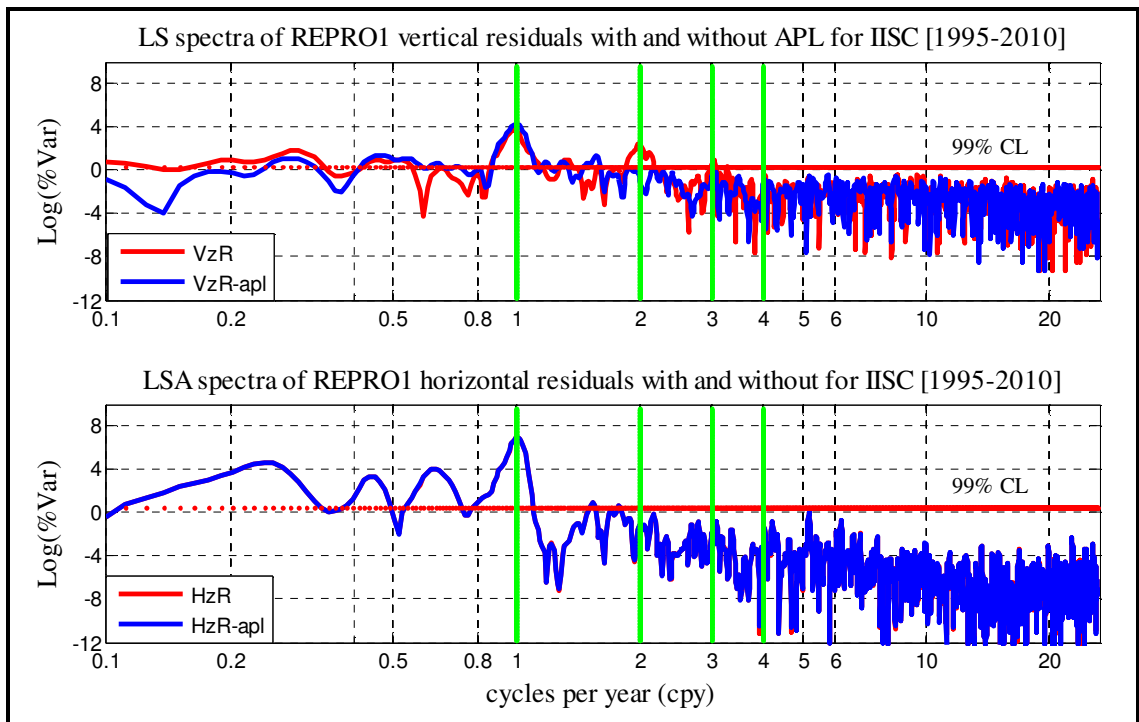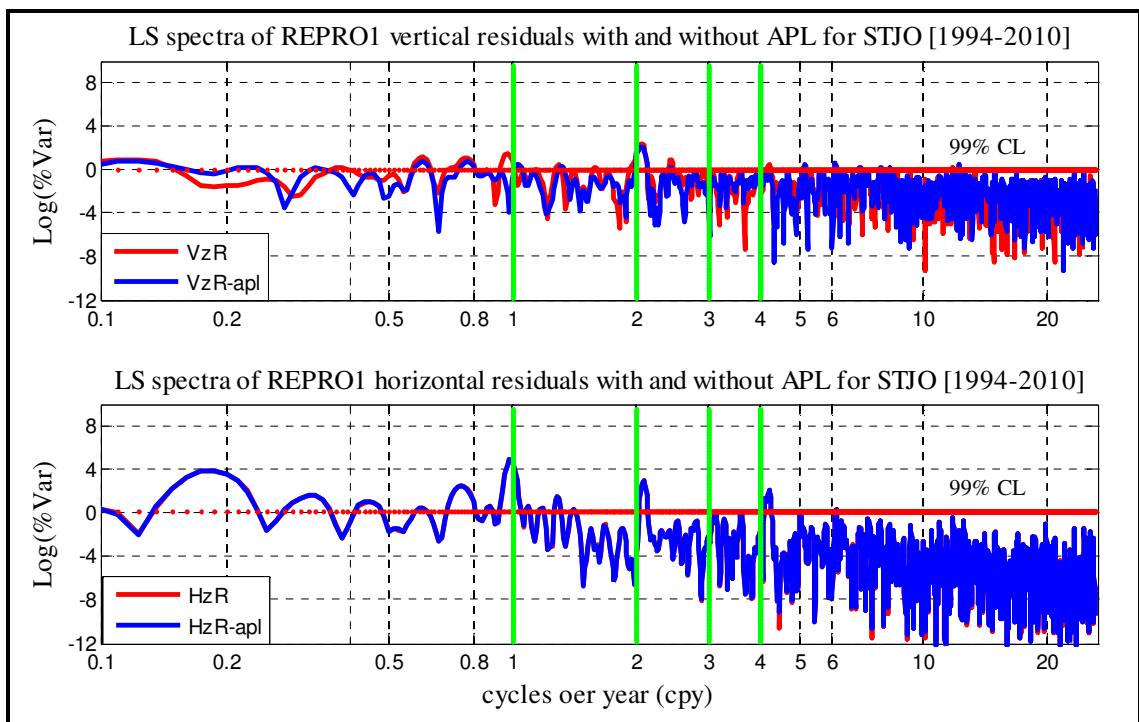

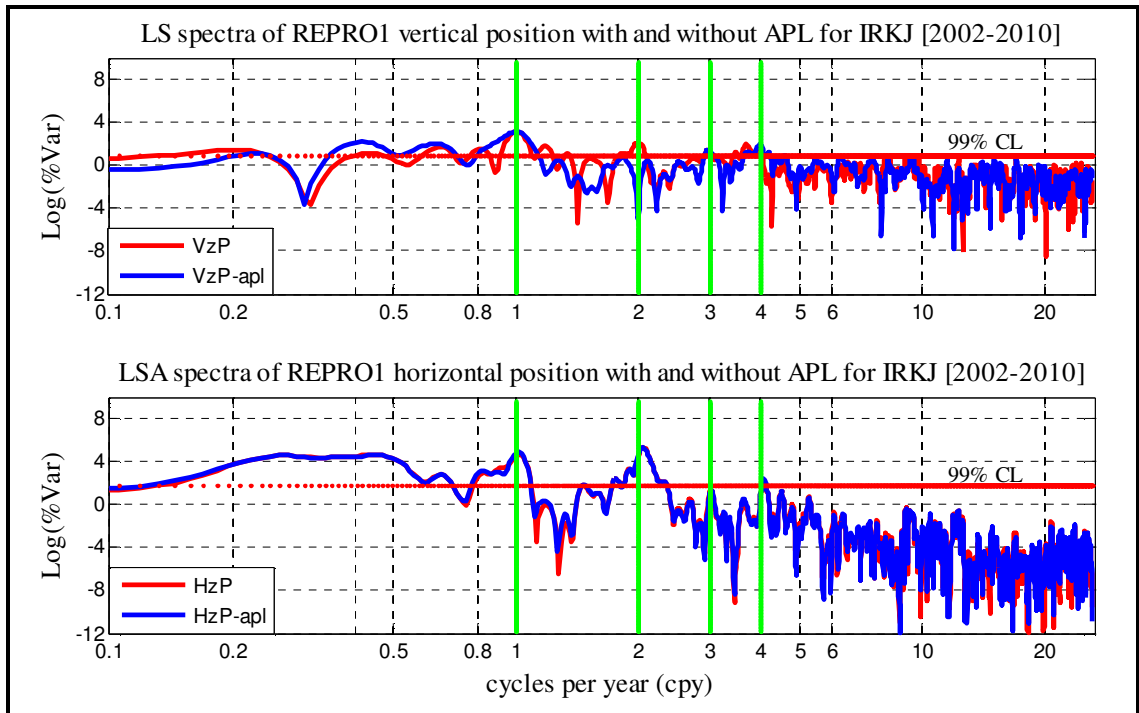Figure A46 Least squares coherent spectra of REPRO1 residuals for STJO (1994-2010)
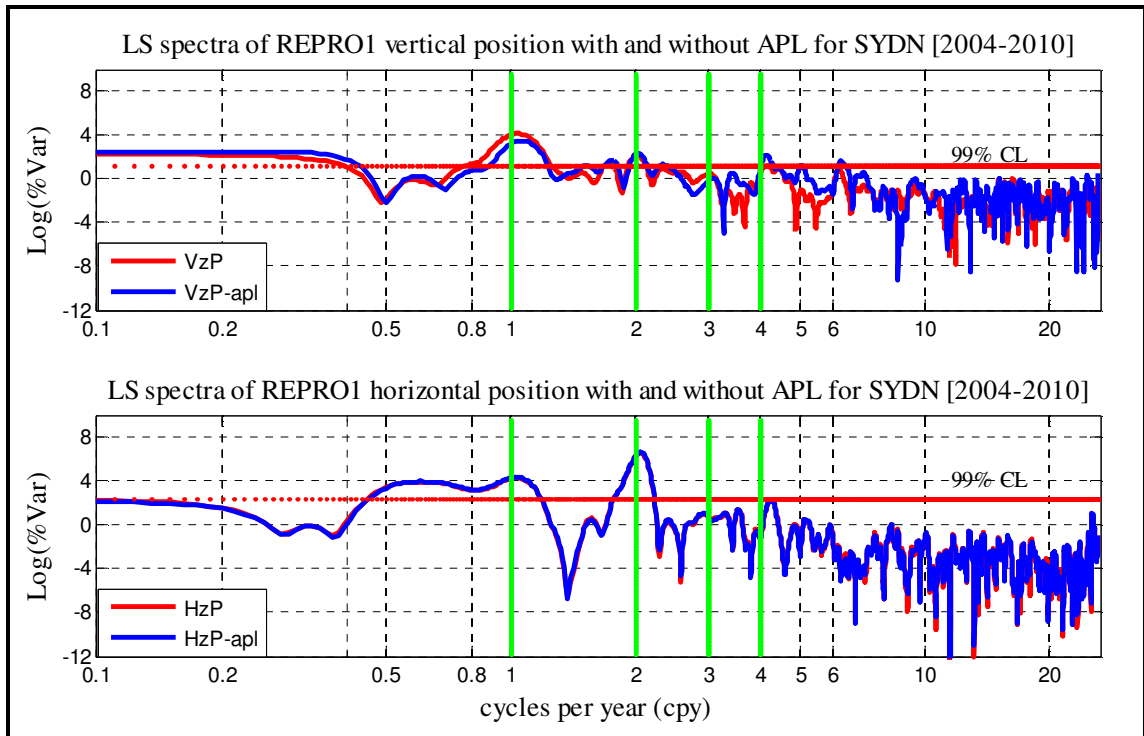
Figure A47 Least squares coherent spectra of REPRO1 positions for SYDN (2004-2010)
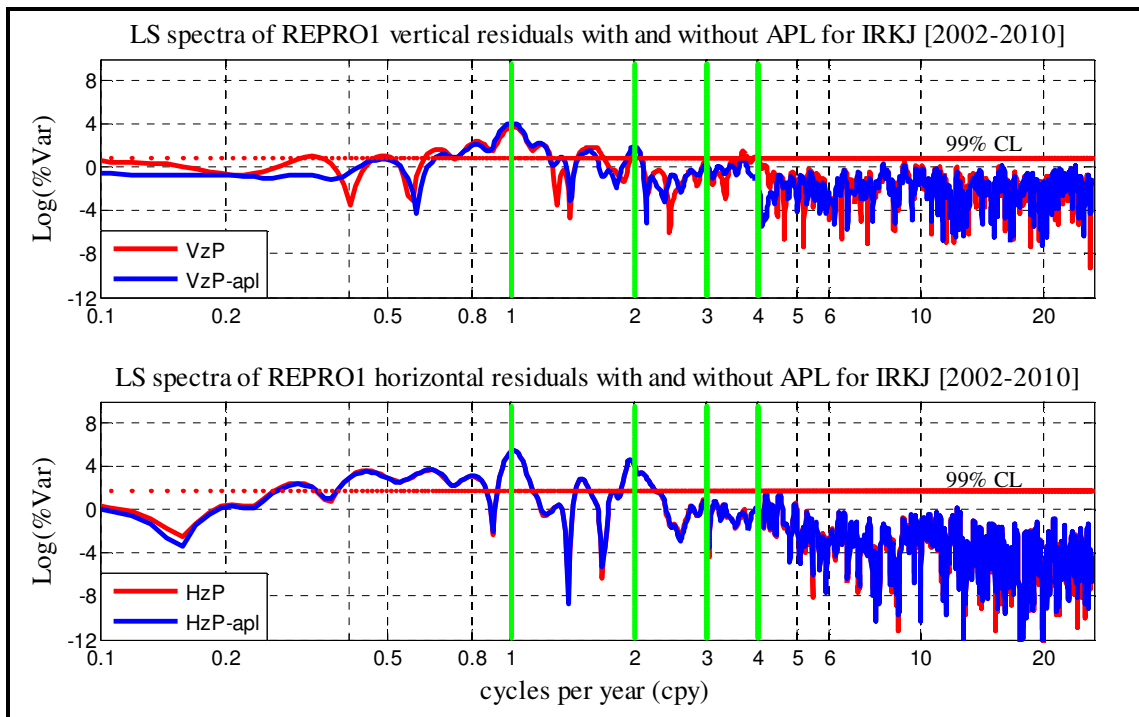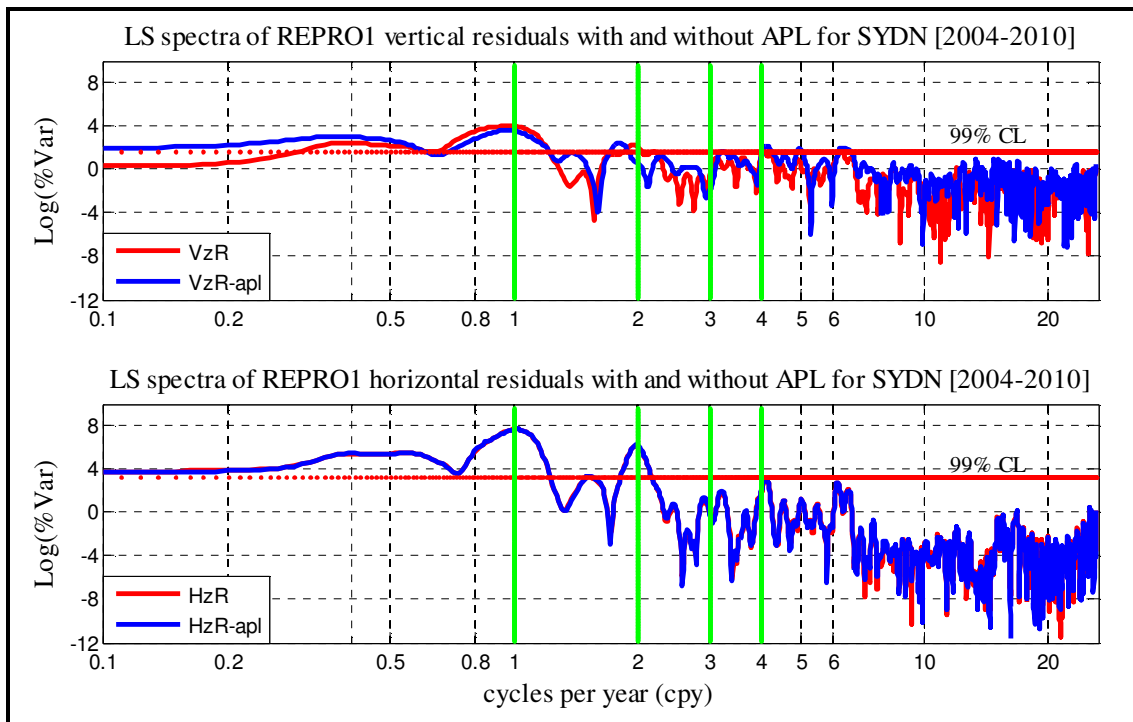

Figure A48 Least squares coherent spectra of REPRO1 residuals for SYDN (2004-2010)
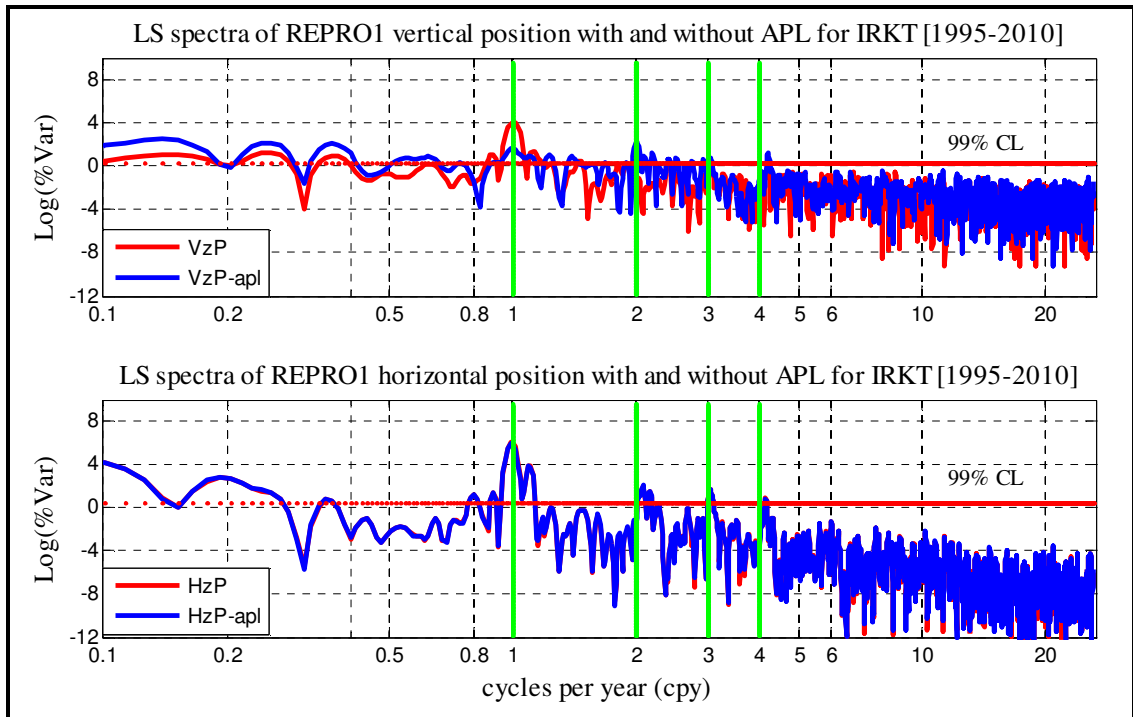
186
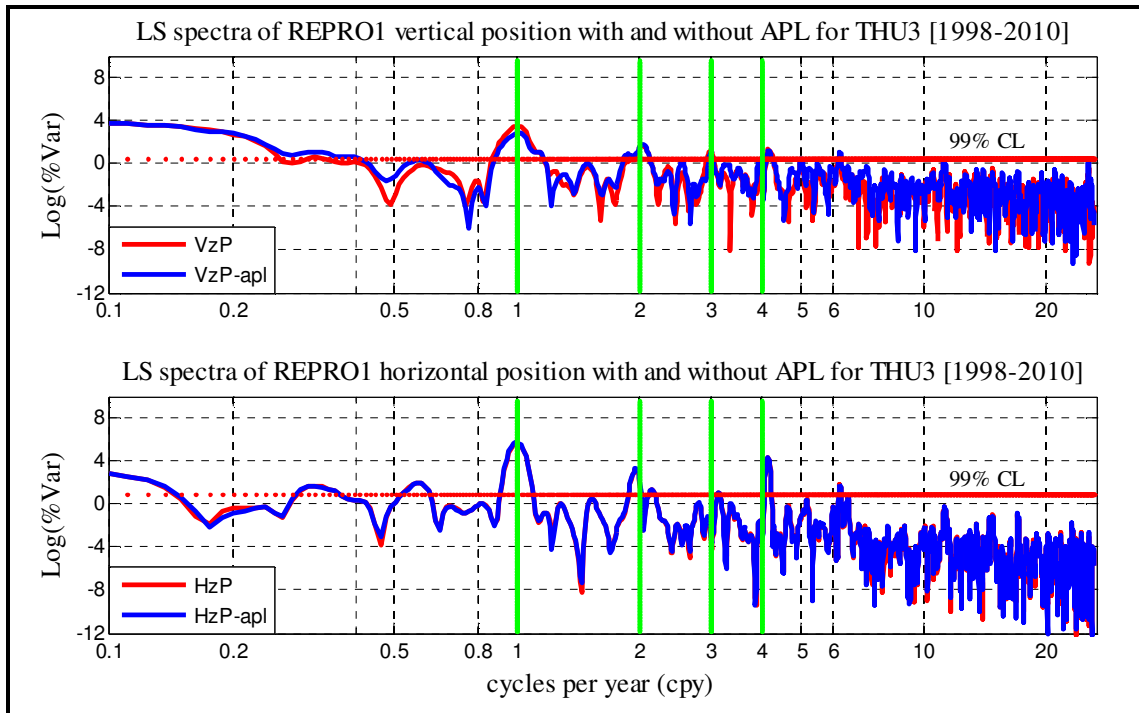
Figure A49 Least squares coherent spectra of REPRO1 positions for THU3 (1998-2010)
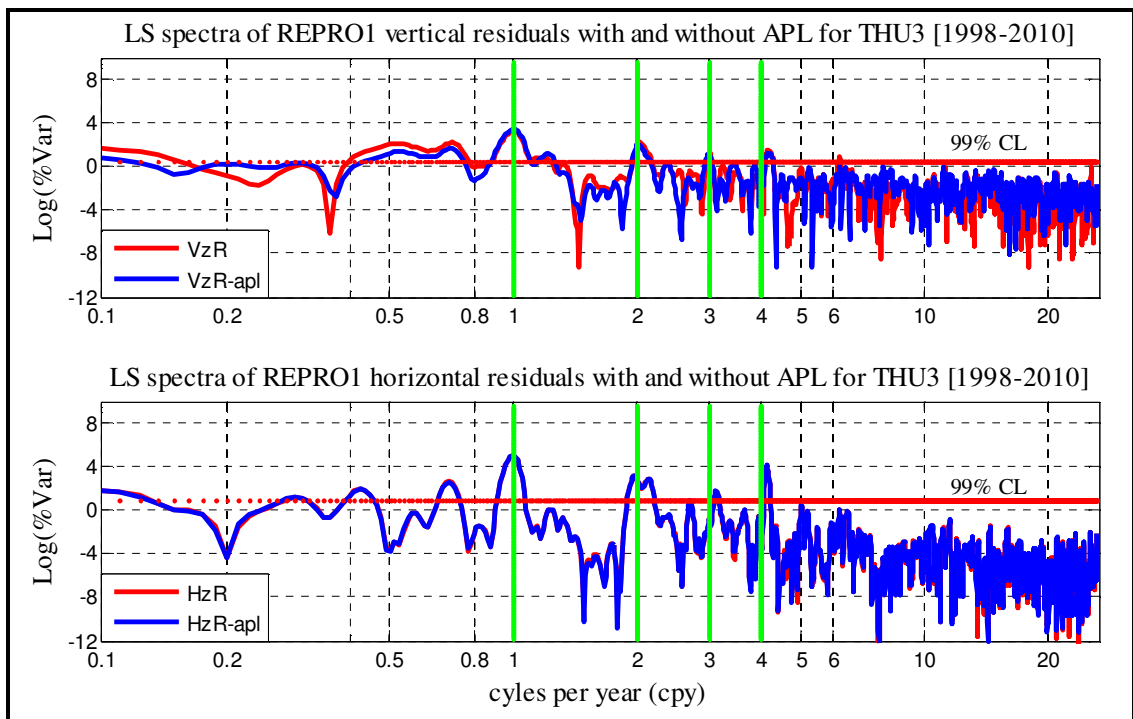
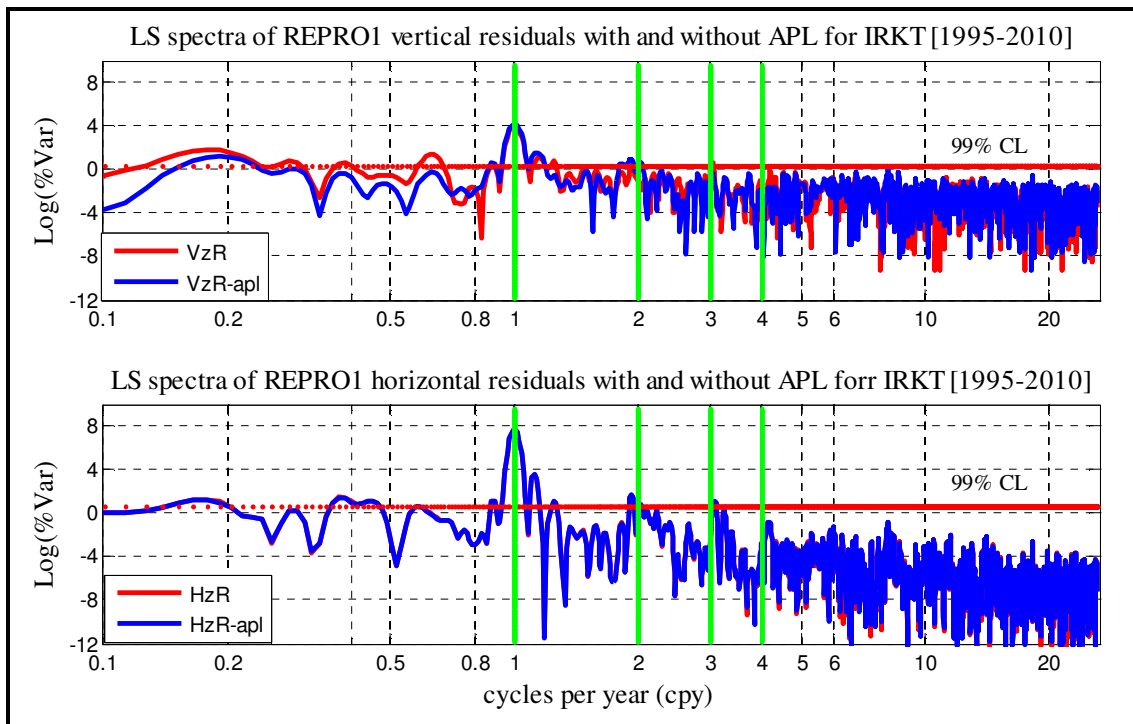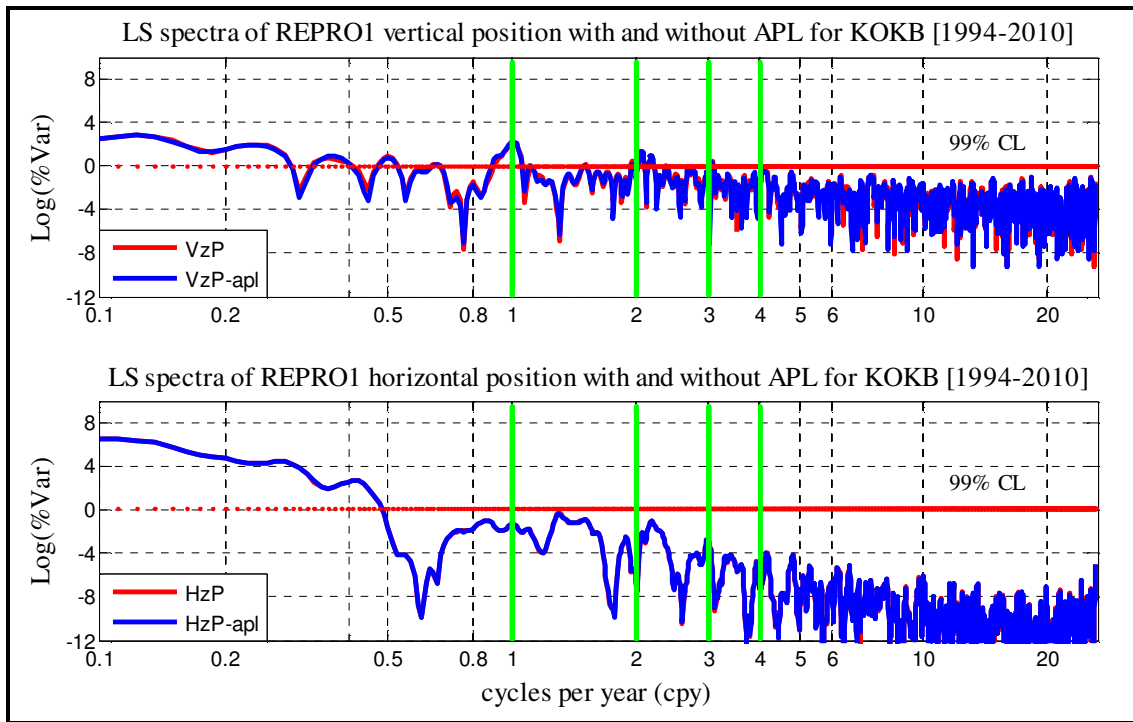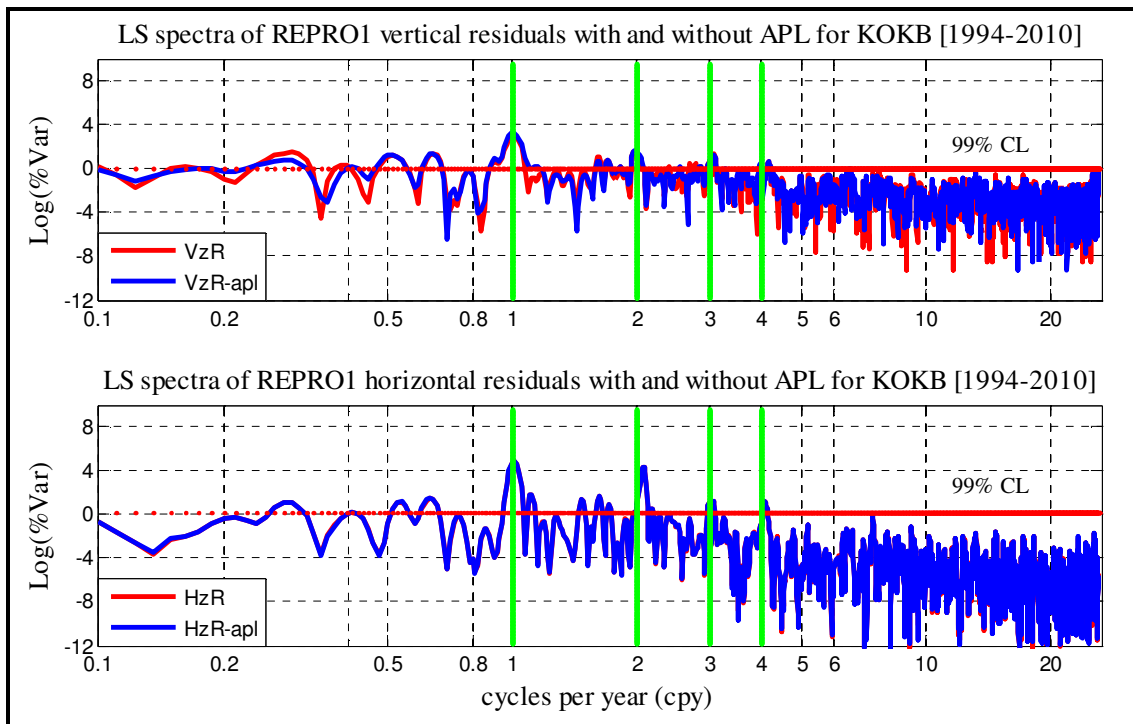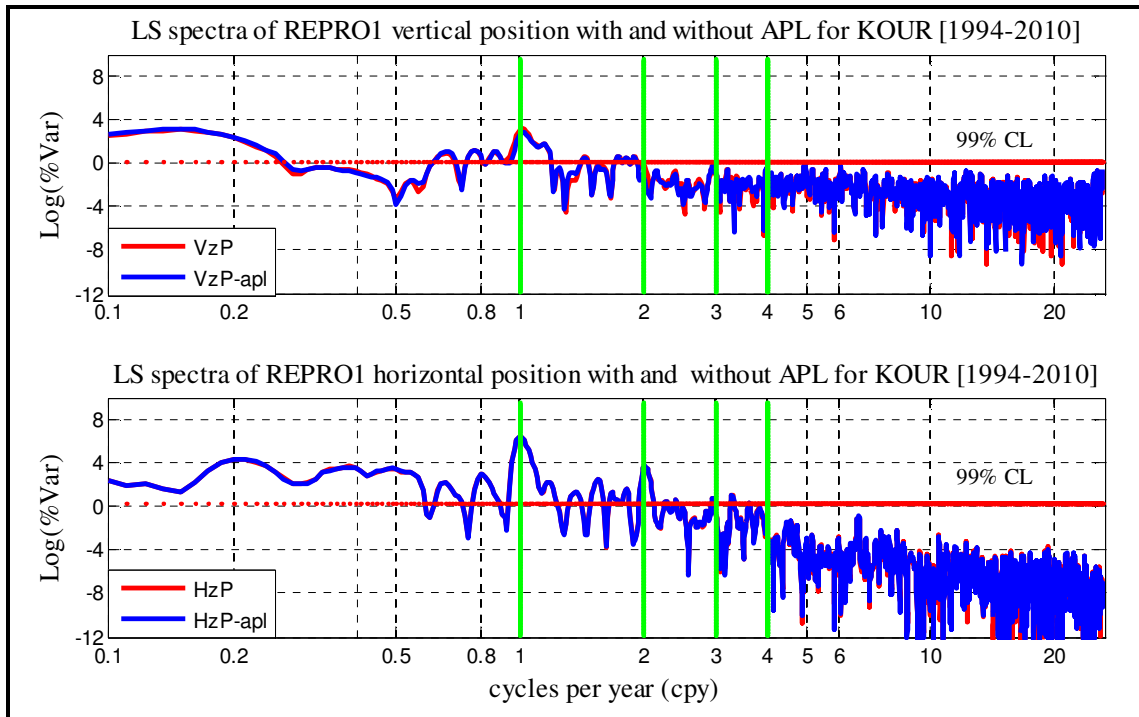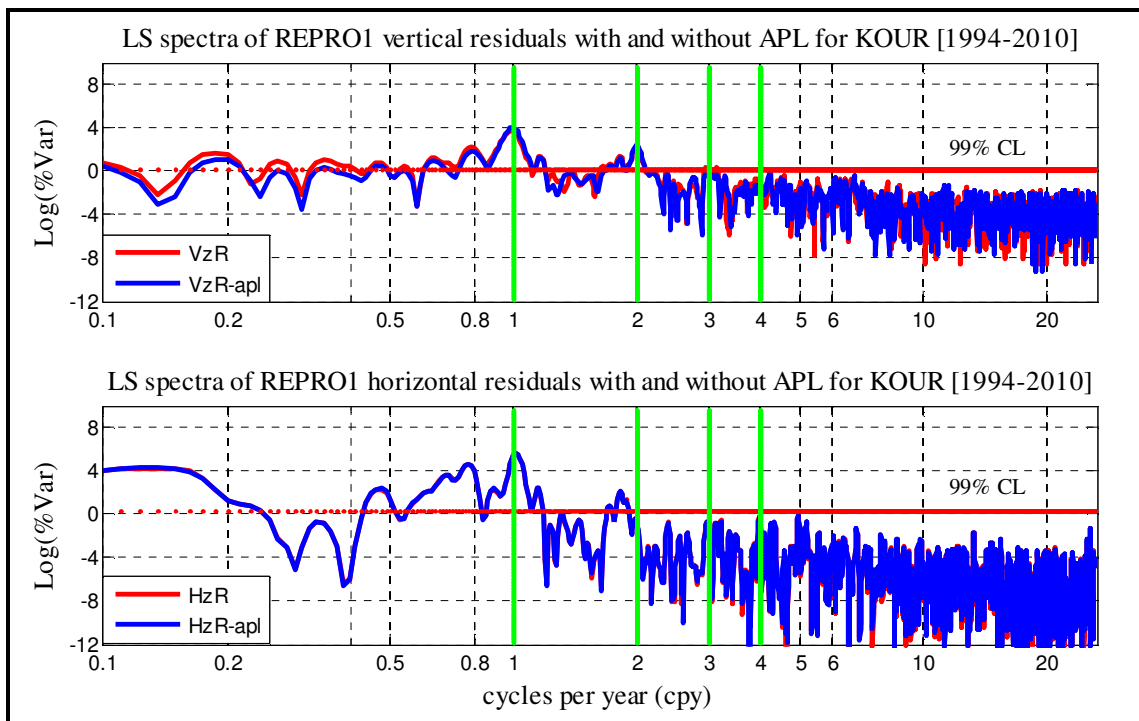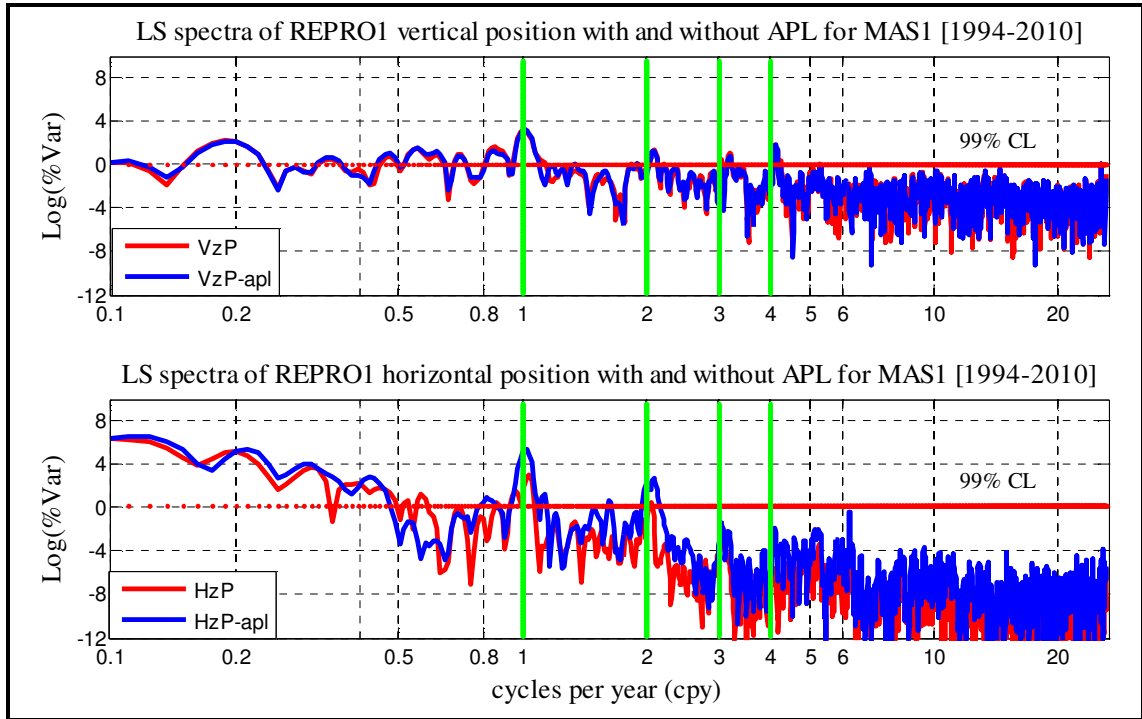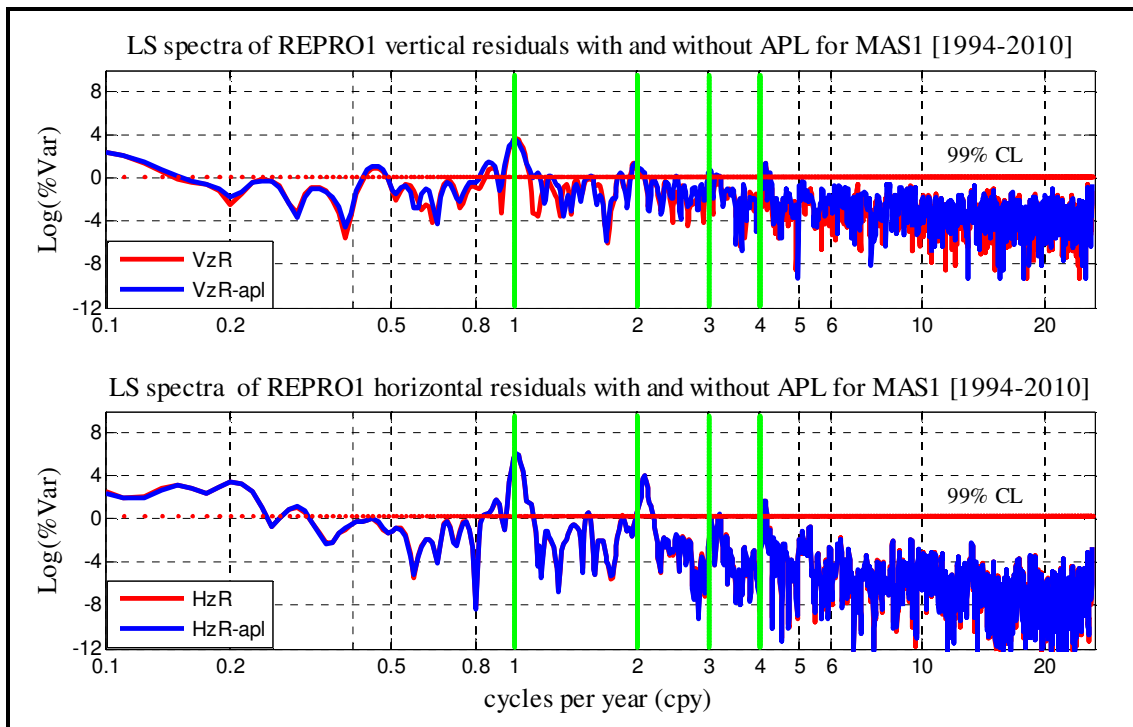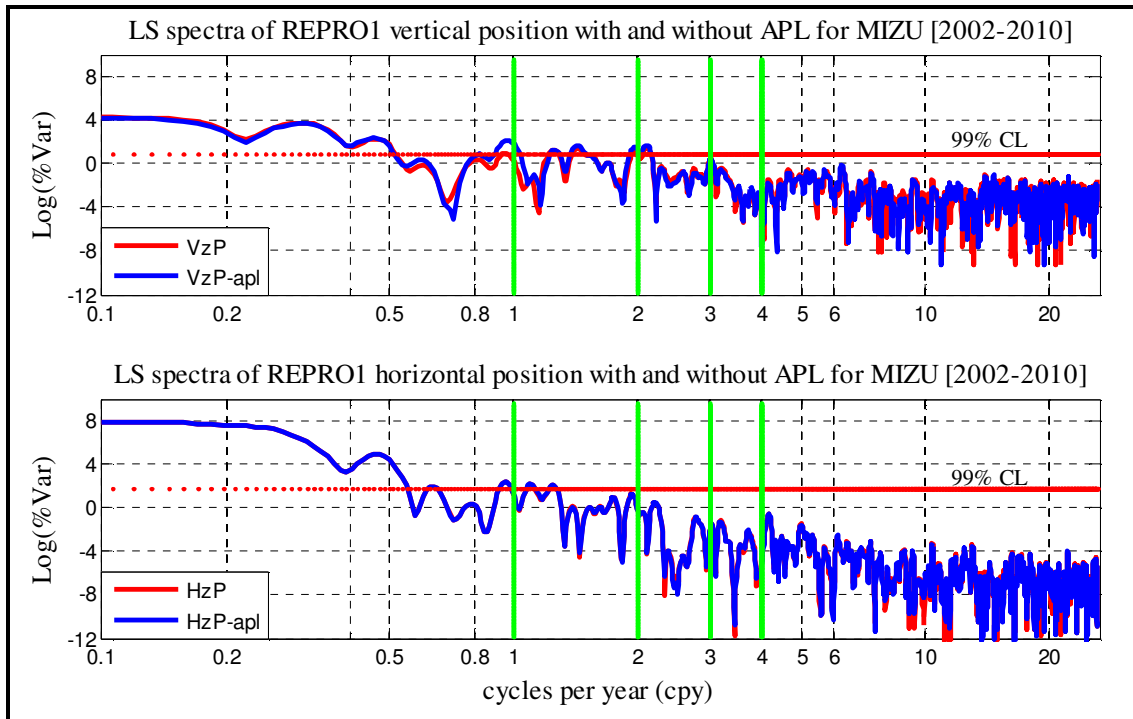Figure A50 Least squares coherent spectra of REPRO1 residuals for THU3 (1998-2010)

187
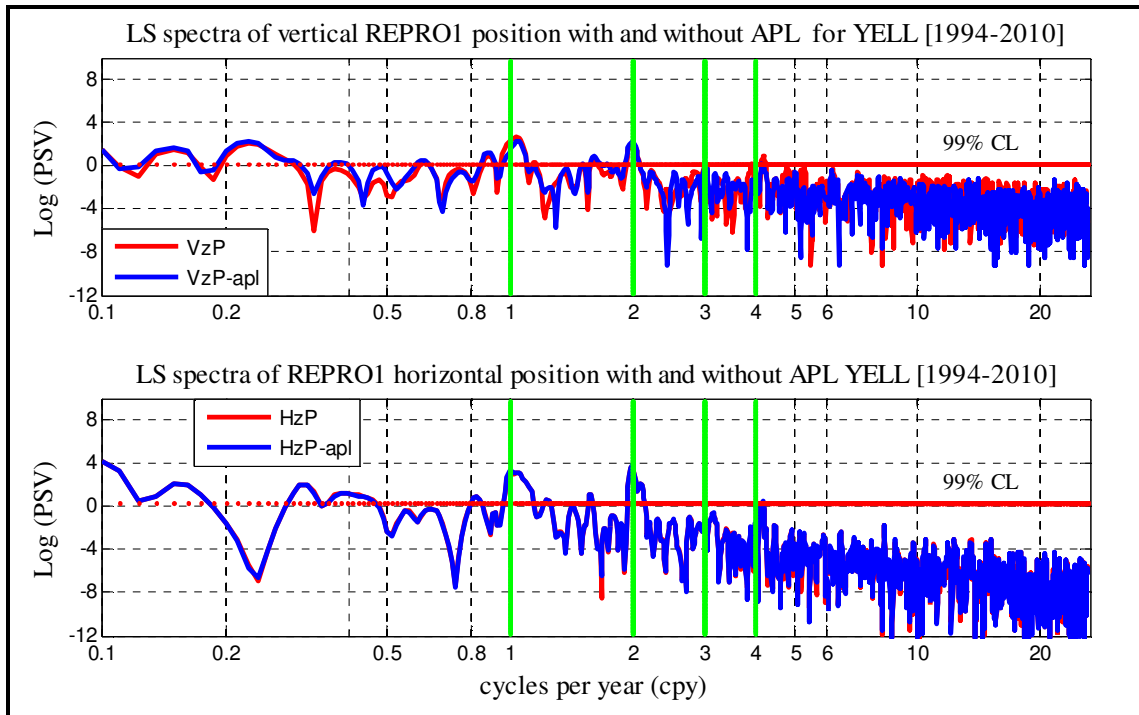
Figure A51 LSSA and LS coherent spectra of positions for YELL (1994-2010)
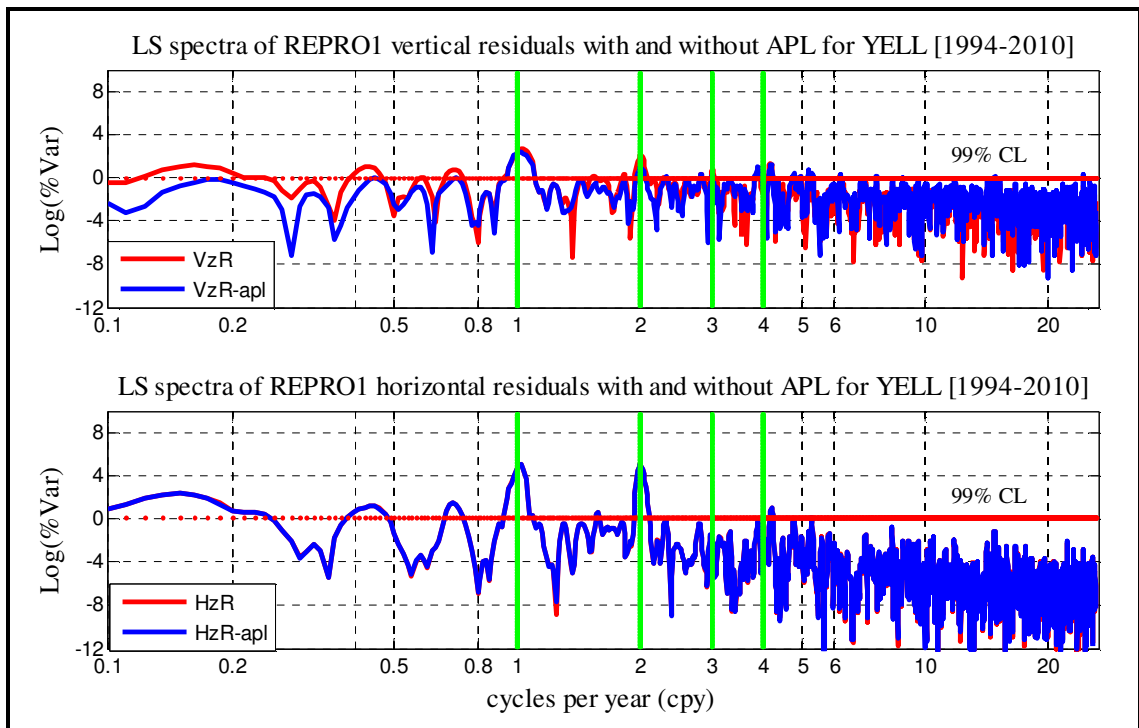
Figure A52 Least squares coherent spectra of REPRO1 residuals for YELL (1994-2010)

Table A1 and A2 below presents the statistical summary of the different spectral peaks in the REPRO1 vertical positions and residuals presented in Figures A1 to A52. The tabulation of the vertical positions spectral peaks are in Table A1 whereas Table A2 presents equivalent summary for the vertical residuals. In both Tables, the first column presents the station names and column two shows the harmonic levels. Columns three and four are the respective period of the spectral peaks in days and cycles per year (CPY). Columns five and six are the respective percentage variances (PSV) before and after the APL corrections. Column six present the percentage change in the spectral peaks after the APL corrections.

Table A1 Statistics of the vertical positional spectral peaks with and without APL

Station	Harmonic level	Period in days	CPY	PSV before APL	PSV after APL	Percentage Change in PSV
ALGO	1	361.93	1 ± 0.009	21.41	23.43	9.45
	2	179.13	2 ± 0.010	1.64	1.46	-11.10
ARTU	1	365.63	1 ± 0.001	34.50	24.34	-29.44
	2	181.26	2 ± 0.004	5.67	5.85	3.18
	3	122.60	3 ± 0.002	2.90	1.89	-34.87
BRAZ	1	365.92	1 ± 0.002	4.25	4.21	-0.85
	2	183.65	2 ± 0.003	2.47	0.52	-78.81
	3	121.00	3 ± 0.002	3.15	3.94	24.77
DARW	1	366.20	1 ± 0.003	27.91	35.06	25.61
	2	177.89	2 ± 0.013	4.43	3.42	-22.65
	3	117.48	3 ± 0.012	1.98	0.49	-75.30
	4	86.08	4 ± 0.014	0.70	0.64	-9.50
DRAO	1	362.04	1 ± 0.009	45.31	39.59	-12.61
	2	182.66	2 ± 0.000	6.42	9.21	43.37
	4	87.73	4 ± 0.010	1.56	1.24	-20.87
GSLV	1	367.72	1 ± 0.007	47.82	40.32	-15.70
	2	176.04	2 ± 0.018	5.33	7.02	31.62
HLNC	1	363.77	1 ± 0.004	13.26	15.91	20.03
	2	185.56	2 ± 0.008	5.87	5.03	-14.35
	3	119.75	3 ± 0.005	2.38	1.92	-19.63
	4	88.68	4 ± 0.007	2.05	1.72	-16.17

Table A1 Statistics of the vertical positional spectral peaks- continued

HOLM	1	366.26	1 ± 0.003	29.31	14.42	-50.78
	2	180.29	2 ± 0.006	8.35	8.05	-3.50
	4	87.22	4 ± 0.011	4.13	4.60	11.18
HRAO	1	364.53	1 ± 0.002	24.97	8.21	-67.10
	2	179.79	2 ± 0.008	5.13	6.28	22.44
	3	119.83	3 ± 0.005	1.90	2.15	13.19
	4	91.03	4 ± 0.001	1.71	1.73	1.02
HYDE	1	372.44	1 ± 0.020	66.74	54.70	-18.03
	2	189.16	2 ± 0.018	6.09	7.59	24.60
IISC	1	366.06	1 ± 0.002	52.12	43.03	-19.37
IRKJ	1	364.10	1 ± 0.003	22.13	22.42	1.29
	2	183.31	2 ± 0.002	7.83	1.61	-79.47
	3	123.57	3 ± 0.005	3.82	4.18	9.39
	4	91.67	4 ± 0.001	4.27	6.97	63.11
IRKT	1	365.50	1 ± 0.001	56.78	15.13	-73.36
KOKB	1	362.04	1 ± 0.009	8.67	9.58	10.46
	2	186.31	2 ± 0.010	1.60	1.27	-20.74
	3	119.03	3 ± 0.007	1.61	1.48	-8.23
KOUR	1	362.04	1 ± 0.009	25.11	16.33	-34.96
	2	192.71	2 ± 0.028	1.84	1.46	-20.65
MAS1	1	361.75	1 ± 0.010	25.17	25.46	1.17
	2	175.72	2 ± 0.019	3.82	3.62	-5.24
	3	120.54	3 ± 0.003	1.69	0.78	-53.91
	4	86.36	4 ± 0.014	1.40	0.94	-33.01
MIZU	1	383.70	1 ± 0.051	2.54	4.11	61.84
	2	186.90	2 ± 0.012	2.99	4.50	50.65
NRC1	1	361.74	1 ± 0.010	36.68	42.37	15.54
	2	179.09	2 ± 0.010	4.24	4.18	-1.42
ONSA	1	366.78	1 ± 0.004	4.09	0.87	-78.68
	2	174.69	2 ± 0.022	2.26	2.28	0.71
	4	87.18	4 ± 0.011	1.19	1.26	6.11
PDEL	1	355.21	1 ± 0.027	12.55	10.38	-17.31
	2	161.21	2 ± 0.059	3.42	2.92	-14.80
	3	114.48	3 ± 0.020	3.11	2.69	-13.53
POLV	1	371.60	1 ± 0.017	29.06	41.65	43.31
	2	180.40	2 ± 0.006	8.58	1.75	-79.58
	3	116.15	3 ± 0.015	3.23	2.15	-33.40
QIKI	1	360.07	1 ± 0.014	32.08	13.07	-59.25
	2	176.63	2 ± 0.016	7.86	9.69	23.25

Table A1 Statistics of the vertical positional spectral peaks- continued

STJO	1	371.52	1 ± 0.017	7.75	12.47	60.91
	2	175.76	2 ± 0.019	7.32	6.14	-16.15
	3	101.74	3 ± 0.055	1.40	1.09	-22.08
	4	88.83	4 ± 0.007	1.32	1.14	-13.95
SYDN	1	353.67	1 ± 0.032	61.61	32.73	-46.87
	2	181.90	2 ± 0.002	8.78	10.05	14.52
THU3	1	361.93	1 ± 0.009	32.17	17.46	-45.71
	2	179.18	2 ± 0.009	5.55	6.13	10.48
	3	122.18	3 ± 0.001	3.50	2.74	-21.63
	4	87.76	4 ± 0.010	3.70	3.29	-11.13
UNBJ	1	366.53	1 ± 0.004	34.87	14.83	-57.49
	2	182.70	2 ± 0.000	11.07	0.94	-91.47
	3	113.78	3 ± 0.022	5.49	0.11	-97.93
YELL	1	352.91	1 ± 0.034	13.78	9.60	-30.35
	2	183.86	2 ± 0.003	7.99	9.23	15.54
	3	121.62	3 ± 0.000	1.27	1.06	-16.28
	4	88.00	4 ± 0.009	2.37	1.17	-50.46

Table A2 Statistics of the vertical residuals spectral peaks with and without APL

Station	Harmonic level	Period in days	CPY	PSV before APL	PSV after APL	Percentage Change in PSV
ALGO	1	357.43	1 ± 0.021	12.82	4.13	-67.79
	2	188.82	2 ± 0.017	1.48	0.34	-77.26
	3	118.53	3 ± 0.009	1.17	0.60	-48.42
	4	87.73	4 ± 0.010	1.38	1.46	5.68
ARTU	1	365.63	1 ± 0.001	25.48	34.84	36.72
	2	182.44	2 ± 0.001	4.86	4.63	-4.69
	3	122.60	3 ± 0.002	2.93	1.76	-39.93
BRAZ	1	370.76	1 ± 0.015	49.62	48.23	-2.81
	2	181.35	2 ± 0.004	6.72	5.54	-17.51
DARW	1	371.05	1 ± 0.016	33.95	53.06	56.30
	2	181.35	2 ± 0.004	6.72	5.54	-17.51
DRAO	1	362.04	1 ± 0.009	40.11	31.31	-21.95
	2	182.66	2 ± 0.000	8.11	2.92	-63.95
	3	118.03	3± 0.010	1.44	1.03	-28.85
	4	87.73	4 ± 0.010	1.63	1.67	2.29
GSLV	1	362.96	1 ± 0.006	41.08	38.63	-5.97
	2	177.16	2 ± 0.015	2.92	1.88	-35.79
HLNC	1	363.77	1 ± 0.004	34.14	44.16	29.34
	2	185.56	2 ± 0.008	4.37	3.28	-25.06
HOLM	1	366.26	1 ± 0.003	34.68	28.86	-16.80
	2	180.29	2 ± 0.006	6.78	5.84	-13.76
	4	87.22	4 ± 0.011	5.08	3.04	-40.22
HRAO	1	374.26	1 ± 0.025	15.25	21.27	39.47
	2	178.64	2 ± 0.011	2.14	0.79	-63.12
	4	88.44	4 ± 0.008	3.20	1.81	-43.35
HYDE	1	367.56	1 ± 0.006	55.93	85.17	52.28
	2	184.20	2 ± 0.004	14.80	3.29	-77.74
	3	121.82	3 ± 0.000	5.02	1.17	-76.79
IISC	1	370.91	1 ± 0.015	39.95	62.74	57.05
	2	183.69	2 ± 0.003	11.48	2.98	-74.03
	3	121.02	3 ± 0.002	2.52	1.04	-58.91
IRKJ	1	359.44	1 ± 0.016	41.71	57.91	38.83
	2	180.95	2 ± 0.005	4.84	6.75	39.58
	3	99.12	3 ± 0.062	4.67	2.41	-48.43
	4	91.97	4 ± 0.002	2.71	0.80	-70.38
IRKT	1	365.45	1 ± 0.001	47.81	63.04	31.86
	3	120.96	3 ± 0.002	1.95	0.73	-62.48
KOKB	1	362.04	1 ± 0.009	18.19	24.82	36.47
	2	185.08	2 ± 0.007	4.70	5.25	11.69
	3	122.68	3 ± 0.003	1.87	2.26	20.81

Table A2 Continued Statistics of the vertical residuals spectral peaks

KOKB	4	87.73	4 ± 0.010	1.82	1.74	-4.59
KOUR	1	366.78	1 ± 0.004	40.08	56.11	39.97
	2	183.86	2 ± 0.003	7.45	10.96	47.14
	3	124.31	3 ± 0.007	1.36	0.89	-35.00
MAS1	1	361.75	1 ± 0.010	39.05	34.21	-12.40
	2	186.24	2 ± 0.010	3.86	3.71	-3.85
	4	88.54	4 ± 0.008	4.02	3.73	-7.13
MIZU	1	351.20	1 ± 0.038	16.89	5.96	-64.73
	3	114.56	3 ± 0.020	3.39	3.64	7.39
MTKA	1	335.82	1 ± 0.081	16.44	17.86	8.60
	2	176.90	2 ± 0.016	5.72	3.44	-39.84
	4	87.21	4 ± 0.011	2.56	2.66	3.80
NRC1	1	361.74	1 ± 0.010	29.39	11.04	-62.45
	2	180.24	2 ± 0.007	5.64	4.69	-16.87
ONSA	1	366.78	1 ± 0.004	10.47	13.29	26.97
	2	174.69	2 ± 0.022	5.57	1.92	-65.47
	4	91.45	4 ± 0.000	1.18	0.61	-48.16
PDEL	1	359.77	1 ± 0.015	25.76	29.28	13.69
	2	184.55	2 ± 0.005	2.56	1.40	-45.52
	3	115.42	3 ± 0.017	1.98	1.94	-2.11
POLV	1	371.60	1 ± 0.017	29.73	24.97	-16.03
	2	180.40	2 ± 0.006	10.00	9.73	-2.63
	3	116.15	3 ± 0.015	3.53	3.45	-2.21
QIKI	1	355.51	1 ± 0.027	30.45	26.68	-12.40
	2	176.63	2 ± 0.016	4.83	3.28	-32.11
STJO	1	376.78	1 ± 0.032	4.62	1.67	-63.84
	2	176.93	2 ± 0.016	11.33	7.95	-29.84
	4	86.92	4 ± 0.012	1.52	0.92	-39.35
SYDN	1	377.43	1 ± 0.033	55.77	37.31	-33.11
	2	186.74	2 ± 0.011	9.79	10.99	12.30
THU3	1	366.67	1 ± 0.004	25.77	29.68	15.19
	2	180.33	2 ± 0.006	8.99	7.49	-16.66
	3	122.18	3 ± 0.001	3.58	3.05	-14.82
	4	87.76	4 ± 0.010	4.42	3.62	-18.06
UNBJ	1	361.80	1 ± 0.009	39.36	13.31	-66.19
	2	180.35	2 ± 0.006	4.77	7.88	65.38
	3	113.78	3 ± 0.022	3.43	3.36	-2.04
YELL	1	361.80	1 ± 0.009	39.36	13.31	-66.19
	2	181.48	2 ± 0.003	8.07	2.61	-67.63
	3	121.62	3 ± 0.000	2.01	1.21	-40.09
	4	87.45	4 ± 0.011	3.74	3.31	-11.33

Appendix B: BPE_ALL and HQN_COMB Bernese PCFs

Appendix C present two sets of process control files used for data processing. They are BEE_ALL.PCF used for generating daily solutions and HQN_COMB.PCF used to generate weekly solutions. BPE_ALL.PCF is illustrated on Table B.1 in which the first column shows the PCF identification number and the second column shows the script name. The third column is the directory where the script is located and the fourth column is type of CPU in use. The number of scripts executed in parallel is presented column five whereas column six shows a sequence in which the scripts are executed.

HQN_COMB.PCF is illustrated in Table B.2 comprised of two standard scripts and four user-made scripts. The standard scripts are COMPAR for checking daily coordinate repeatability and the ADDNEQ2 for stacking normal equation files to be used in the weekly combination and based on models discussed in section 2.2.4. The HQN_COMB script is designed to copy the daily solutions and normal equations of a week of interest to a separate directory before the computations. The HQN_SUMC script generates the computation summaries before saving them using HQN_SAVC. Scripts HQN_DELC and HQN_CLNC are meant for respective deleting and cleaning files in the BPE directory after the completion of each week processing activities. Table B.2 presents the HQN_COMB.PCF, in which the first column shows the scripts (PCF) identification number and the second column shows the script name. The third column is the directory where the script is located and the fourth column is type of CPU with which the script could be handled. The number of scripts executed in parallel is in column five whereas column six shows a sequence in which the scripts are executed.

Table B.1 Bernese PCF for generating for daily solutions (BPE_ALL)

#Author	: James Mtamakaya- (20 October, 2011)				
PID	SCRIPT	OPT_DIR	CPU	P	WAIT FOR...
# Create a priori CRD file and prepare pole, orbit, and clock information					
002	COOVEL	R2S_GEN	ANY	1	
101	POLUPD	BPE_PRE	ANY	1	002
111	PRETAB	BPE_PRE	ANY	1	101
112	ORBGEN	BPE_PRE	ANY	1	111
# Convert and synchronize observation data into Bernese system/formats					
201	RNXGRA	BPE_PRE	ANY	1	112
211	RXOBV3BP	BPE_PRE	ANY	1	201
212	RXOBV3_Q	BPE_PRE	ANY	1	211
#Preprocessing					
221	CODSPPAP	BPE_PRE	ANY	1	212
222	CODSPP_P	BPE_PRE	ANY	1	221
223	CODXTR	BPE_PRE	ANY	1	222
301	SNGDIF	BPE_PRE	ANY	1	223
311	MAUPRPAP	BPE_PRE	ANY	1	301
312	MAUPRP_P	BPE_PRE	ANY	1	311
313	MPRXTR	BPE_PRE	ANY	1	312
#Data processing I-compute ambiguity-float network solution, screen phase data					
321	GPSEST	BPE_PRE	ANY	1	313
322	RESRMS	BPE_PRE	ANY	1	321
323	SATMRK	BPE_PRE	ANY	1	322
324	GPSXTR	BPE_PRE	ANY	1	323
331	GPSEST	BPE_EDT	ANY	1	324
332	RESRMS	BPE_EDT	ANY	1	331
333	SATMRK	BPE_EDT	ANY	1	332
334	GPSXTR	BPE_EDT	ANY	1	333
# Data processing II-Resolve phase ambiguities → fixed CRD/COV/NEQ/TRO files					
401	GPSQIFAP	BPE_QIF	ANY	1	334
402	GPSQIF_P	BPE_QIF	ANY	1	401
403	GPSXTR	BPE_QIF	ANY	1	402
501	GPSEST	BPE_FIX	ANY	1	403
502	GPSXTR	BPE_FIX	ANY	1	501
# Data processing II - final daily normal equations, SINEX and summary files					
511	ADDNEQ2	BPE_FIX	ANY	1	502
901	NET_SUM	BPE_PRE	ANY	1	511
# End of BPE					

Table B.2 Bernese PCF for generating weekly solutions (HQN_COMB.PCF)

PID	SCRIPT	OPT_DIR	CPU	P	WAIT FOR...
# Copy required files and create a priori CRD file					
515	HQN_COMB	HQN_COM	ANY	1	
516	COMPAR	HQN_COM	ANY	1	515
521	ADDNEQ2	HQN_COM	ANY	1	516
# Create summary file, save results, and delete files in BPE directory					
901	HQN_SUMC	HQN_CM1	ANY	1	521
902	HQN_SAVC	HQN_CM1	ANY	1	901
904	HQN_DELC	HQN_CM1	ANY	1	902
905	BPE_CLNC	HQN_CM1	ANY	1	904

Table B.3 presents the different types of predefined user variables which presented in column one. The variable descriptions are presented in column two whereas column three present their default abbreviations in the input Bernese files.

Table B.3 Predefined user variables for weekly solutions generation

Variable	Variable Description	Default
V_A	A priori information	APR
V_B	Orbit/ERP, DCB, ION information	IG1
V_C	Preliminary (ambiguity-float) results	FL1
V_E	Final (ambiguity-fixed) results	FL2
V_F	Size-reduced NEQ information	FIN
V_I	Ionosphere regional model results	I1_
V_K	Daily Addneq2 solution	FIX_
V_PC	Absolute/Relative phase center	I05
V_MINUS	Session range begin (for COMPAR)	-6
V_PLUS	Session range end	+0
V_STAINF	Station information file name	EXAMPLE_STA
V_PLDINF	Tectonic plate definition file name	EXAMPLE_PLD
V_BLQINF	Ocean loading correction file name	FES2004_BLQ
V_ABBINF	Station name abbreviation file name	EXAMPLE_ABB
V_CRDREF	Master/reference CRD/VEL file name	IGS_05_R
V_CRDMRG	Merged CRD/VEL file name	IGS_05

Appendix C Matlab codes

C.1 Cartesian coordinates to geodetic

```
%James Mtamakaya #3206337
%PhD research matlab code 1
%Computation of Geodetic coordinates from "Repro1 cartesisan coordinates"
%---------------STEP (1) and its INPUTS:   ----------------------------
%1- Input the REPRO1 Cartesian coordinates (8 columns):
% MJD, GPSWeek, X,Y,Z,StD_X, StD_Y and StD_Z,
%2- It convert XYZ to plh
%3- It converts the XYZ Standard deviations to geodetic standard deviations
diary
diary ('c:\PhDrsh\repro1\coords\plh_yell')% storing coordinates in a %specified path
diary on
 dt1= [];
a = 6378137; b = 6356752.3141; es = 1-b^2/a^2; % Parameter of GS80 ellipsoid
Format long g
gps_stn=load ('repro1_yell.txt'); % input station coordinates/residuals
 ns = size(gps_stn,1)% obtain the size/length of coordinates
X    = gps_stn(:,3); Y   =gps_stn(:,4); Z   =gps_stn(:,5);% XYZ coordinates
std_x=gps_stn(:,6);std_y=gps_stn(:,7);std_z=gps_stn(:,8);% standard deviations
 [fi,lambda,h,std_plh] = cart2geo(X,Y,Z,std_x,std_y,std_z,ns); %  geodetic positions in
radians
 dt1 (:,1)=gps_stn(:,1);%MJD
dt1 (:, 2)=fi*180./pi; % converted geodetic latitude in decimal degrees
dt1 (:, 3)=lambda*180./pi;%converted geodetic longitude in decimal degrees
dt1(:,4)=h;% height
% the geodetic (plh) standard deviations
dt1(:,5)=std_plh(:,1); %geodetic latitude standard deviations
dt1(:,6)=std_plh(:,2);% geodetic longitude standard deviations
dt1(:,7)=std_plh(:,3);% geodetic height standard deviations
 plh=dt1
diary off
```

C.2 Transformation of residuals from Cartesian to geodetic (PLH)

```
%James Mtamakaya S#3206337; %PhD research matlab code 2
%-------------------------------------- INPUTS: ----------------------------------------------------
%1- REPRO1 XYZ coordinates [MJD, GPSWK, X, Y, Z, sigX, sigY and sigZ]
%2- REPRO1 XYZ residuals    [GPSWK, Xrsd, Yrsd, Zrsd, sigXr, sigYr and sigZr]
diary
diary('b:\PhDrsh\mfiles\rp1study\propagation\rsdplh_nrc1') % saving of output files
diary on; format long g
gps_crd=load ('repro1_nrc1.txt'); % input XYZ station coordinates
gps_rsd=load ('rsdxyz_nrc1.txt'); % input XYZ station residuals
 %  --------------Part 1 rearranging the input file--------------------
gps_rm=[];dlt1=[];% initializing result/output  files
k = size (gps_crd, 1); % size of the input coordinate file
ns = size(gps_rsd,1); % size of the input residual file
gps_rse=zeros (ns, 10); % initializing the working file
 for i=1:ns
   for j=1:k
     if  gps_rsd(i,1)==gps_crd(j,2)% matching the GPS week numbers in the 2 arrays
         gps_rse(i,1)=gps_crd(j,1); %modified Julian date
            gps_rse(i,2)=gps_crd(j,3); % the X coordinates
               gps_rse(i,3)=gps_crd(j,4); % the Y coordinates
                  gps_rse(i,4)=gps_crd(j,5); % the Z coordinates
                     gps_rse(i,5)=gps_rsd(i,3); % the X residuals
                     gps_rse(i,6)=gps_rsd(i,4); % the Y residuals
                  gps_rse(i,7)=gps_rsd(i,5); % the Z residuals
               gps_rse(i,8)=gps_rsd(i,6); % the X residuals standard deviation in mm
            gps_rse(i,9)=gps_rsd(i,7); % the Y residuals standard deviation in mm
         gps_rse(i,10)=gps_rsd(i,8);% the Z residuals standard deviation in mm
    end
   end
end
gps_rsm1=gps_rse;
% filtering the columns with zeros
nv = size (gps_rsm1,1);m=1;
for i=1:nv
   if (gps_rsm1(i,1)~=0)
     pk(m,:)=gps_rsm1(i,:);
     m=m+1;
   end
```

```
end
gps_rsm=pk;
 % extracting the modified residual file with daily coordinates + respective residuals
gps_rm (:,1)= gps_rsm(:,1); %modified Julian date
gps_rm (:,2)= gps_rsm(:,2)+gps_rsm(:,5)/1000;% X coordinate + X residuals
gps_rm (:,3)= gps_rsm(:,3)+gps_rsm(:,6)/1000;% Y coordinate + Y residuals
gps_rm (:,4)= gps_rsm(:,4)+gps_rsm(:,7)/1000;% Z coordinate +  Z residuals
gps_rm (:,5)= gps_rsm(:,8)/1000;%  the X residuals standard deviation in m
gps_rm (:,6)= gps_rsm(:,9)/1000;%  the Y residuals standard deviation in m
gps_rm (:,7)=gps_rsm(:,10)/1000;% the Z residuals standard deviation in m
 gps_rsf=gps_rm; % final and extracted working file
nc=size(gps_rsf,1) % size of the extracted working file
% 3. --------------Part 3 compute the geodetic residual coordinates----------
a = 6378137;b = 6356752.3141; %  axes of the GRS80 ellipsoid
data=[];dt1=[];
Xcrd=gps_rsm (:,2);  Ycrd=gps_rsm (:, 3); Zcrd=gps_rsm (:,4); % X, Y and Z coords
p1xyz=[Xcrd, Ycrd, Zcrd]; % extract the XYZ coordinates for the matching dates
[fi_c,lambda_c,h_c] = cart2geod (Xcrd,Ycrd,Zcrd);%compute the PLH for the XYZ
p1llh=[fi_c,lambda_c,h_c];%rearranging the PLH coordinates residual vectors
 X=gps_rsf(:,2);% X coordinate + the X rsd
Y=gps_rsf(:,3);% Y coordinate + the Y rsd
Z=gps_rsf(:,4);% Z coordinate + the Z rsd
std_x=gps_rsf(:,5); % extracted  X residuals standard deviation in m
std_y=gps_rsf(:,6); % extracted  Y residuals standard deviation in m
std_z=gps_rsf(:,7); % extracted  Z residuals standard deviation in m
 p2xyz=[X, Y, Z];%rearranging the XYZ values with residuals added to them
 [fi,lambda,h,std_plh] = cart2geo(X,Y,Z,std_x,std_y,std_z,nc);
 [dllh] = distllh(p1xyz,p2xyz,p1llh);
 dlt1(:,1)=gps_rsf(:,1);%MJD
 % converted geodetic residuals
dlt1 (:,2)=dllh(:,1); %latitude residuals
dlt1 (:,3)=dllh(:,2); %longitude residuals
dlt1 (:,4)=dllh(:,3); %height residuals
dlt1 (:,5)=std_plh(:,1); %converted geodetic latitude standard deviations
dlt1 (:,6)=std_plh(:,2); %converted geodetic longitude standard deviations
dlt1 (:,7)=std_plh(:,3); %converted geodetic heights standard deviations
 rsd_geo=dlt1
diary off
```

C.3 XYZ residuals Standard Deviations to Geodetic

```matlab
% PhD research matlab code ;
function dllh = distllh(p1xyz,p2xyz,p1llh)
% Inputs:   p1xyz -> 3x1 vectors XYZ residuals and   p2xyz -> 3x1 vectors XYZ coords
% Outputs:    dllh -> 3x1 vector with the distances (in m) in lat, long and   height
rG = p2xyz-p1xyz; nl=size(rG,1);
 % defines the rotation matrices:
 P2 = [1 0 0 , 0 -1  0,   0  0  1];
dlts=zeros(nl,3);
 for i=1:nl
        lat = p1llh(i,1);    long= p1llh(i,2);
       R2 = [cos (lat - pi/2)               0            -sin (lat - pi/2)
                     0                        1                  0
              Sin (lat - pi/2)               0           cos (lat - pi/2)];
       R3 = [cos (long - pi)        sin (long - pi)            0
               -sin (long - pi)       cos (long - pi)            0
                     0                       0                  1];
     J_inv = (P2*R2*R3)';
     rGm = rG (i,:)';
     dlts(i,:) = (J_inv*rGm)';
 end
dllh = dlts;
```

C.4 Plotting the LS coherent spectrum

```
%James Mtamakaya S#3206337
%PhD research matlab code 5
Diary; diary on
diary('B:\PhDrsh\lssa\rp1study\rp1results\peaks\Pos_APL_drao')
%1.0---------------STEP (1) and its INPUTS:  ----------------------------
ts=5853;% time span for which data is represented 1994-2010
format long g;
 pk_h1 = load('drao_pks_H.txt');%heights-LS spectrum for (DRAO)
pk_l1  = load('drao_pks_L.txt');% longitude-LS  spectrum for (DRAO)
pk_f1  = load('drao_pks_F.txt');% latitude-LS spectrum (DRAO)
ns=size(pk_f1,1);
pk_h2  = load('drao_pks_HapUsub.txt');%(heights +APL correction) lssa spectrum
pk_l2  = load('drao_pks_LapEsub.txt');%(longitude+ APL correction)lssa spectrum
pk_f2  = load('drao_pks_FapNsub.txt');% (latitude + APL correction)lssa spectrum
 % 2.rearranging longitude and latitude LSSA analysis stages 1
cpy_h1=pk_h1 (:,2)*365.25;
psv_h1=log (pk_h1 (:,3));% natural log of the  height  percentage variance
psv_l1= pk_l1 (:,3); % natural log of the  longitude  percentage variance
psv_f1= pk_f1 (:,3); % natural log of the  latitude  percentage variance
psv_l2=pk_l2(:,3); % natural log of the  height  (+APL) percentage variance
psv_f2=pk_f2(:,3); % natural log of the  longitude (+APL) percentage variance
psv_h2=log (pk_h2(:,3));% % natural log of the  latitude (+APL)  percentage variance
%2. 0 Initial processing-rearranging the inputs of the Product spectrums
ps_algo1=zeros (ns,4);  % initializing the output matrix
ps_algo1(:,1)=pk_f1(:,1);% col1 = period in days
ps_algo1(:,2)=cpy_h1;    % col2 = frequency in cycles per day
ps_algo1a=zeros (ns,2);ps_algo1b=zeros (ns,2);
ps_algo1a(:,1)=psv_l1;% percentage variance of 1st longitude input (Position)
ps_algo1a(:,2)=psv_f1;% percentage variance of 1st latitude input  (Position)
 ps_algo1b(:,1)=psv_l2;%percentage variance of Position longitude +APL
ps_algo1b(:,2)=psv_f2;% percentage variance of Position latitude  + APL

For i=1: ns
    ps_algo1(i,3)=log(ps_algo1a(i,1))+log(ps_algo1a(i,2));% Add Hz PSV
    ps_algo1(i,4)=log(ps_algo1b(i,1))+log(ps_algo1b(i,2));% Add Vz PSV
End
pds_algo1=ps_algo1;
```

```matlab
% 2.1. Extract the significant peaks in the product spectrum
cl1=1.1;cf1=1.1;clh1=1.1; %critical level of longitudes, latitude & height from LSSA
cl1n=log(cl1); cf1n=log(cf1); lns1=log(clh1);% LN of critical variance in vertical
positions
lns2=cl1n+cf1n;% critical level of the horizontal positions

% initial arrangement of peaks matrix
 pds1=pds_algo1 (:,1);% period in days
pds2=pds_algo1 (:,2);% frequency in cycles per year
pds3=pds_algo1 (:,3);% natural logs of PSV from uncorrected HZ position
pds4=psv_h1; % natural logs of PSV from uncorrected VZ position
pds5=pds_algo1 (:,4);% LN of PSV from  HZ position +APL corrections
pds6=psv_h2; % LN of PSV from vertical positions +APL corrections
pds7a=pk_h1 (:,5);% power spectral density of H1 without APL correction
pds7b=pk_h2 (:,5);% power spectral density of H2 (H+ APL correction)

[peaks_hz]=pds2peaks (pds1, pds2, pds3, ns, ts, lns2); % HZ peaks without APL
[peaks_vt]=pds2peaksV (pds1, pds2, pds4, pds7a, ns, ts, lns1); % VZ peaks without
APL
[pks_hzAp]=pds2peaks (pds1, pds2, pds5, ns, ts, lns2); % HZ peaks + APL
[pks_vzAp]=pds2peaksV (pds1, pds2, pds6, pds7b, ns, ts, lns1); % VZ peaks + APL


%3.-----------------Plotting of the product spectrum----------------------
figure('position',[100 100 850 450])
subplot(2,1,1)
semilogx (pds2,pds3,'-r','LineWidth',2.5)
hold on ; semilogx (pds2,lns2,'LineStyle','-','Color','r','LineWidth',1.5)
axis ([0.1   26.5  -12   10]); % defining plot ranges
set (gca,'ytick',[-12  -8  -4   0    4    8]) % defining X ticks label
set (gca,'xtick',[0.1  0.2  0.5   1   2   3    4    5    6  10   20 ]) % defining Y ticks label
text (11.5,2.5,'99% CL','FontSize',10,'FontName','Times New Roman')
title ('Horizontal position LSSA spectrum (LN) for  DRAO [1994-2010]','FontSize',12,
'FontName', 'Times New Roman')
ylabel ('Log(%Var)','FontSize',12,'FontName','Times New Roman')
 grid on, box on, hold off
```

```
subplot (2,1,2)
semilogx (pds2,pds4,'-b','LineWidth',2.5)
hold on; semilogx(pds2,lns1,'LineStyle','-','Color','r','LineWidth',1.5)
axis([0.1  26.5  -12  10]);
set(gca,'ytick',[-12  -8  -4  0  4  8])
set(gca,'xtick',[0.1 0.2 0.5  1  2  3  4  5  6  10  20 ])
text(11.5,2.2,'99% CL','FontSize',10,'FontName','Times New Roman')
title('Vertical position LSSA spectrum (LN)for  DRAO [1994-2010]',' FontSize',12,
'FontName', 'Times New Roman')
ylabel ('Log(%Var)','Fontsize',12,'FontName','Times New Roman')
xlabel ('cycles per year (cpy)','FontSize',12,'FontName','Times New Roman')
grid on, box on, hold off

% superimposed plots of positions uncorrected and APL corrected spectra
figure('position',[100 100 850 450])
subplot(2,1,1)
semilogx (pds2,pds3,'-r','LineWidth',2.5)
hold on; semilogx(pds2,pds5,'-b','LineWidth',2.5)
hold on; semilogx(pds2,lns2,'LineStyle','-','Color','r','LineWidth',1.0)
axis([0.1  26.5  -12  10]); legend('HzP','HzP-apl',3);
set(gca,'ytick',[-12  -8  -4  0  4  8]); set(gca,'xtick',[0.1  0.2  0.5 1  2  3  4  5  6  10  20])
text (11.5,2.5,'99% CL','FontSize',10,'FontName','Times New Roman')
title ('LSSA specta(LN) of Hor position and Hor position-APL correction for DRAO
[1994-2010]','FontSize',12,'FontName','Times New Roman')
ylabel('Log(%Var)','FontSize',12,'FontName','Times New Roman')
grid on, box on, hold off

subplot(2,1,2)
semilogx(pds2,pds4,'-r','LineWidth',2.5)
hold on; semilogx(pds2,pds6,'-b','LineWidth',2.5)
hold on; semilogx(pds2,lns1,'LineStyle','-','Color','r','LineWidth',1.0)
axis ([0.1  26.5  -12  10]); legend ('VzP','VzP-apl',3);%,'HzP-apl');
set(gca,'ytick',[-12  -8  -4  0  4  8]); set(gca, 'xtick',[0.1  0.2  0.5  1  2  3  4  5  6  10  20 ])
text (11.5,2.2,'99% CL','FontSize',10,'FontName','Times New Roman')
title ('LSSA spectrum (LN) of VZ position and VZ position-APL correction for DRAO
[1994-2010]', 'FontSize',12, 'FontName', 'Times New Roman')
ylabel ('Log(%Var)','Fontsize',12,'FontName','Times New Roman')
xlabel ('ycles per year (cpy)','FontSize',12,'FontName','Times New Roman')
grid on, box on, hold off;  diary off
```

C.5 Extraction Significant Peaks in LS Coherent Spectrum

```matlab
function [peaks]=pds2peaks (pds1,pds2,pds3,ns,ts,lns);
%James Mtamakaya S#3206337; %PhD research matlab function 2
pks=zeros(ns,5); % Initializing output matrix
pks (:,1)=pds1;pks(:,2)=pds2;pks(:,4)=pds3; pk=[];pp=[];
for i=2:ns-1
   nl = i-1;nu=i+1; % Initializing upper and lower counters
   if (pds3(i)>pds3(nl)& pds3(i)>pds3(nu)) & pds3(i) > lns;
      pks(i,3)=pks(i,1);  pks(i,5)=pks(i,1).*pks(i,1)/(2*ts);
   end
end
pks1=pks;
 j=1;
for i=1:ns
    if (pks(i,3)~=0)
      pk(j,:)=pks(i,:);
     j=j+1;
   end
end
 peaks1 (:,1)=pk(:,1); (:,2)=pk(:,2);% respective  period in days  and frequency in cycles
per day
peaks1 (:,3)=pk(:,5); peaks1 (:,4)=pk(:,4); %fidelity  and the sum of LN in HZ positions
PSV
peaks = peaks1;
```

C.6 Plotting the XYZ residuals

```matlab
%PhD  matlab files 7;   Plotting the XYZ residuals
%1- Input the REPRO1 XYZ coordinates [MJD,GPSWK,X,Y,Z,sigX,sigY,sigZ]
%2- Input the XYZ residuals [GPSWK, Xrsd, Yrsd, Zrsd, sigXr, sigYr and sigZr]
%3- Matches the two values using the GPSWK number and produce final plots
diary
diary('b:\PhDrsh\mfiles\rp1study\propagation\rsdplh_drao')%saving the results
diary on; format long g
gps_crd=load('repro1_drao.txt'); % input station coordinates/residuals
gps_rsd=load('rsdxyz_drao.txt'); % input station coordinates/residuals
% ---------------rearranging the input file--------------------
 gps_rm=[];dlt1=[];
k = size (gps_crd, 1);  ns = size(gps_rsd,1);% sizes of the input  files
gps_rse=zeros (ns, 10); % initializing the working file
 for i=1:ns
   for j=1:k
     if  gps_rsd(i,1)==gps_crd(j,2)% match the GPS week #s in the 2 arrays
         gps_rse(i,1)=gps_crd(j,1); %modfied julian date
               gps_rse(i,2)=gps_rsd(i,3); % the X residual
                  gps_rse(i,3)=gps_rsd(i,4); % the Y residual
                  gps_rse(i,4)=gps_rsd(i,5); % the Z residual
                gps_rse(i,5)=gps_rsd(i,6); % the X residual standard deviation in mm
              gps_rse(i,6)=gps_rsd(i,7); % the Y residual standard deviation in mm
         gps_rse(i,7)=gps_rsd(i,8);% the  Z residual standard deviation in mm
     end
   end
end
gps_rsm=gps_rse;
jd= gps_rsm (:,1)+ 2400000.5;% computing Julian days from MJD
[doy,yr]=jd2doy (jd); % convert JD to day of the year and year
yd1 (:,1)=doy; yd1(:,2)=yr; yd2= yd1;mc=size(yd2,1);
yd3=zeros (mc, 3); yd3(:,1)=yd2(:,1); yd3(:,2)=yd2(:,2);

 for i=1:mc
     if {yd3(i,2)/4}-{fix(yd3(i,2)/4)}==0; ;% establishing leap and short year
          yd3 (i,3)= yd3 (i,2)+yd3 (i,1)/366;% leap year
        else
           yd3 (i,3)= yd3 (i,2)+yd3 (i,1)/365;% short year
        end
```

```matlab
end
yd3a=yd3;
rsd_xyz1=zeros (mc, 4);
rsd_xyz1(:,1)=yd3a (:,3); % period in decimal days of the year
rsd_xyz1(:,2)= gps_rsm (:,2);% X residual
rsd_xyz1(:,3)= gps_rsm (:,3);% Y residual
rsd_xyz1(:,4)= gps_rsm (:,4);% Z residual
rsd_xyz= rsd_xyz1;

figure ('Position',[100 100 900 650])
subplot (3,1,1)
hold on;plot( rsd_xyz(:,1),rsd_xyz (:,2),'.b','LineWidth',2.5);  % plotting X residual
axis([1994   2010.1   -6   12]); set(gca,'ytick',[-6   0   6    12])
line([1994   2010.1]  ,[0   0],'LineStyle','-.','LineWidth',2,'Color','r')
title('Plot of X residuals  for station DRAO [1994-
2010]','FontSize',12,'FontName','Times New Roman')
ylabel('X Rsd (mm)','FontSize',12,'FontName','Times New Roman')
 grid on, box on, hold off

subplot(3,1,2)
hold on ;plot( rsd_xyz(:,1),rsd_xyz (:,3),'.b','LineWidth',2.5); %plotting Y residual
axis([1994   2010.1   -8   8]); set(gca,'ytick',[-8  -4   0   4    8]); % X and Y tick locations
line([1994   2010.1]  ,[0   0],'LineStyle','-.','LineWidth',2,'Color','r')
title('Plot of Y residuals  for station DRAO [1994-
2010]','FontSize',12,'FontName','Times New Roman')
ylabel('Y Rsd (mm)','FontSize',12,'FontName','Times New Roman')
grid on, box on, hold off

subplot (3,1,3)
hold on;plot( rsd_xyz(:,1),rsd_xyz (:,4),'.b','LineWidth',2.5); %plotting Z residual
axis ([1994   2010.1   -14   14]); % specifying plotting range
set (gca,'ytick',[-14  -7    0   7    14]) % specifying Y tick locations
line ([1994   2010.1]  ,[0   0],'LineStyle','-.','LineWidth',2,'Color','r')
title ('Plot of Z residuals  for station DRAO [1994-
2010]','FontSize',12,'FontName','Times New Roman')
xlabel ('Day of the year (DOY)','FontSize',12,'FontName','Times New Roman')
ylabel ('Z Rsd (mm)','FontSize',12,'FontName','Times New Roman')
grid on, box on, hold off; diary off
```

C.7 Plotting the geodetic positions (latitude, longitude and height)

```matlab
%James Mtamakaya S#3206337
%PhD proposal matlab files 8;   plotting the geodetic positions
%Transformation of REPRO1 XYZ to Geodetic coordinates
%--------------- INPUTS:   ----------------------------
%REPRO1 XYZ coordinates: MJD;GPSWK; X, Y, Z, StD_X, StD_Y & StD_Z.
Diary;diary('c:\PhDrsh\repro1\coords\plh_yell')% saving the results
diary on
dt1=[];yd1=[];
a = 6378137;b = 6356752.3141;es = 1-b^2/a^2; % Parameter of GS80 ellipsoid
format long g
gps_stn=load ('repro1_drao.txt'); % input station coordinates
ns = size(gps_stn,1);% obtain the size/lenght of coordinates
X   =gps_stn(:,3);Y   =gps_stn(:,4);Z   =gps_stn(:,5);% XYZ coordinates
std_x=gps_stn(:,6);std_y=gps_stn(:,7);std_z=gps_stn(:,8);% XYZ sigmas
[fi,lambda,h,std_plh] = cart2geo(X,Y,Z,std_x,std_y,std_z,ns); % Pos PLH in radians
 dt1(:,1)=gps_stn(:,1);%MJD
dt1(:,2)=fi*180./pi; % converted geodetic latitude in decimal degrees
dt1(:,3)=lambda*180./pi;%converted geodetic longitude in decimal degrees
dt1(:,4)=h;% height
dt1(:,5)=std_plh(:,1); %geodetic latitude standard deviations
dt1(:,6)=std_plh(:,2);% geodetic longitude standard deviations
dt1(:,7)=std_plh(:,3);% geodetic height standard deviations
gps_rsm=dt1;
jd= dt1 (:,1)+ 2400000.5;% computing Julian days from MJD
[doy,yr]=jd2doy (jd);% convert JD to day of the year and year
yd1(:,1)=doy; yd1(:,2)=yr;
yd2= yd1;
mc=size(yd2,1);
yd3=zeros (mc,3);yd3(:,1)=yd2(:,1); yd3(:,2)=yd2(:,2);
 for i=1:mc
     xx=yd3(i,2)/4;% establishing leap and short year
       if xx-fix(xx)==0;
          yd3 (i,3)= yd3 (i,2)+yd3 (i,1)/366;% day of the leap year
        else
          yd3 (i,3)= yd3 (i,2)+yd3 (i,1)/365;% day of the short year
        end
end
```

```matlab
yd3a=yd3;
pos_plh1=zeros (mc,4);
pos_plh1(:,1)=yd3a (:,3);% period in decimal days of the year
pos_plh1(:,2)= dt1 (:,2);% geodetic latitude
pos_plh1(:,3)= dt1 (:,3);% geodetic longitude
pos_plh1(:,4)= dt1 (:,4);% geodetic height
pos_plh= pos_plh1;
as=max(pos_plh(:,2));av=min(pos_plh(:,2));

figure ('Position',[100 50 900 750])
subplot (3,1,1)
hold on
plot( pos_plh(:,1),pos_plh (:,2),'.b','LineWidth',2.5)
axis([1994   2010.1   49.322618   49.3226199999999999]);
set(gca,'YTickLabel','49:19:21.4248N|49:19:21.4266N|49:19:21.4284N|49:19:21.4302N
|49:19:21.4320N|')
title('Plot of geodetic latitude for station DRAO [1994-
2010]','FontSize',12,'FontName','Times New Roman')
ylabel ('Latitude (dms)','FontSize',12,'FontName','Times New Roman')
 grid on, box on, hold off

subplot(3,1,2)
hold on ;plot( pos_plh(:,1),pos_plh (:,3),'.b','LineWidth',2.5)
axis ([1994   2010.1   240.3750159   240.375019]);
set(gca,'YTickLabel','240:22:30.0576|240:22:30.0612|240:22:30.0648|240:22:30.0684|2
40:22:30.0720|')
title('Plot of geodetic longitude for station DRAO [1994-
2010]','FontSize',12,'FontName','Times New Roman')
ylabel('Longitude (dms)','FontSize',12,'FontName','Times New Roman')
grid on, box on, hold off

subplot(3,1,3)
hold on ;plot( pos_plh(:,1),pos_plh (:,4),'.b','LineWidth',2.5)
axis([1994   2010.1   541.857  541.890]);
set(gca,'ytick',[541.857  541.865  541.873  541.881  541.889])
title('Plot of geodetic heights for station DRAO [1994-
2010]','FontSize',12,'FontName','Times New Roman')
xlabel('Day of the year (DOY)','FontSize',12,'FontName','Times New Roman')
ylabel('Height (m)','FontSize',12,'FontName','Times New Roman')
grid on, box on, hold off;diary off
```

VITA

Candidate's Full Name : James Daniel Mtamakaya

Place of Birth   : Songea, Tanzania

Permanent address   : Survey and Mapping Division of Tanzania

Ardhi House Kivukoni Front,

P.O Box 9201, Dar Es Salaam, Tanzania .

Marital status   : Married

Nationality   : Tanzanian

Profession   : Geomatics Engineer

EDUCATION BACKGROUND

2009-2012   : Doctor of Philosophy in Geomatics Engineering.

University of New Brunswick, Fredericton, Canada.

2006-2008   : Master of Science in Geodesy and Geomatics Engineering.

University of New Brunswick, Fredericton, Canada.

1989-1990   : Post-Graduate Diploma in Geographic Information Systems

for Cadastral Applications.

University of Twenty, Faculty of Geo-Information Science

and Earth Observation (ITC) Enschede, The Netherlands.

1980-1983   : Advanced Diploma in Land Surveying.

University College of Lands and Architectural Studies.

Professional Affiliation : Full Registered Surveyor of the National Council of

Professional Surveyors of Tanzania (NCPS)

Publications

Mtamakaya, J., M. Santos and M. Craymer (2012). "Assessment of Temporal Behavior of IGS Stations in Canada Using Least Squares Spectral Analysis." *International Association of Geodesy Symposia*, Volume 136, Geodesy for Planet Earth, Part 3, Pages 705-712, Springer.

Posters presentations

Mtamakaya, J., and M. Santos (2009). "Harmonic Analysis of Temporal Behavior of IGS Stations in Canada." *Eos Trans. AGU, 90(22), Joint Assembly Supplement, Abstract G11B-03*, 2009, Toronto, Canada.

Mtamakaya, J., M. Santos, M. Craymer (2009). "Harmonic analysis of IGS stations time series". *Eos Transactions, AGU, 90(52), Fall Meeting Supplement, Abstract G11B-0634*, 2009.

Mtamakaya, J., M. Santos, and M. Craymer (2010). "In search of periodic signatures in IGS REPRO1 solution". *Eos Transactions, AGU, 91(51), Fall Meeting Supplement, Abstract G51B-0665*, 2010, San Francisco, USA.

Mtamakaya, J., M. Santos, and M. Craymer (2011). "Periodic Effects on IGS REPRO1 *Solutions". The International Union of Geodesy and Geophysics (IUGG) XXV General Assembly,* Melbourne, Australia 27 June - 8 July 2011.